| VOLUMEN 45 | NUMBER 2 | **MAY - AUGUST 2024**

ib

Una publicación de:
SOMIB
Sociedad Mexicana
de Ingeniería Biomédica

Revista Mexicana de Ingeniería Biomédica

Modalidad de publicación

***Publicación continua*:**
una vez que se acepta y prepara un manuscrito, se publicará en línea

Publication Modality

Continuous publication:
once a manuscript is accepted and prepared, it will be released online

http://www.rmib.mx

ISSN 2395-9126

SOMIB
Sociedad Mexicana
de Ingeniería Biomédica

Sociedad Mexicana de Ingeniería Biomédica

La Mesa Directiva de la Sociedad Mexicana de Ingeniería Biomédica hace una extensa invitación a las personas interesadas en participar, colaborar y pertenecer como Socio Activo de la SOMIB. La SOMIB reúne a profesionistas que se desarrollan en áreas de Ingeniería Biomédica, principalmente ingenieros biomédicos, así como otros profesionistas afines con el desarrollo de tecnología para la salud.

Membresía Estudiante
***$1,400.00* PESOS MXN**
15% de descuento para grupos de 5 o más personas.

Membresía Profesionista
***$2,400.00* PESOS MXN**
15% de descuento para grupos de 5 o más personas.

Membresía Institucional
***$11,600.00* PESOS MXN**
No aplica descuento.

Membresía Empresarial
***$20,000.00* PESOS MXN**
No aplica descuento.

EL PAGO CUBRE UN AÑO DE CUOTA. EN CASO DE REQUERIR FACTURA FAVOR DE SOLICITARLA, ADJUNTANDO COMPROBANTE DE PAGO Y ESPECIFICANDO CONCEPTO, AL CORREO ELECTRÓNICO: ***gerencia@somib.org.mx***

ib Revista Mexicana de
Ingeniería Biomédica

AUTORES

Los trabajos a publicar en la RMIB, deben ser originales, inéditos y de excelencia. Los costos de publicación para autores son los siguientes:

NO SOCIOS:	***$5,000* PESOS MEXICANOS**
SOCIOS:	***$4,000* PESOS MEXICANOS**

PUBLICIDAD

A las empresas e instituciones interesadas en publicitar su marca o productos en la RMIB, los costos por número son los siguientes:

MEDIA PLANA:	***$4,999.00* PESOS MXN** *(INCLUYE I.V.A.)*
UNA PLANA:	***$6,799.00* PESOS MXN** *(INCLUYE I.V.A.)*
CONTRAPORTADA:	***$7,799.00* PESOS MXN** *(INCLUYE I.V.A.)*
FORROS INTERIORES:	***$7,799.00* PESOS MXN** *(INCLUYE I.V.A.)*

DESCUENTO DEL **20%** AL CONTRATAR PUBLICIDAD EN DOS O MÁS NÚMEROS.

Para ser socio

- Realiza el pago de derechos, de acuerdo a la categoría que te corresponde.
- Ingresa a *www.somib.org.mx/membresias* y elige el tipo de membresía por el cual realizaste el pago de derechos.
- Completa el formulario correspondiente y envíalo.
- Se emitirá carta de aceptación y número de socio por parte de la mesa directiva (aprobada la solicitud).
- Para mayor información sobre beneficios, ingresa a *www.somib.org.mx*; o escribe a *gerencia@somib.org.mx.*

Datos bancarios

- **Beneficiario:** *Sociedad Mexicana de Ingeniería Biomédica A. C.*
- **Banco:** *Scotiabank*
- **Referencia:** *1000000333*
- **Cuenta:** *11006665861*
- **CLABE Interbancaria:** *044770110066658614*

INFORMES

Juan Vázquez de Mella #481,
Polanco I Sección,
Alc. Miguel Hidalgo, C. P. 11510,
Ciudad de México, México,
(555) 574-4505
rib.somib@gmail.com

Revista Mexicana de
Ingeniería Biomédica

Índices
La Revista Mexicana de Ingeniería Biomédica aparece en los siguientes índices científicos:
Sistema de Clasificación de Revistas Científicas y Tecnologías del CONACYT - Q4, SCOPUS, SciELO, EBSCO, LATINDEX, Medigraphic Literatura Biomedica, Sociedad Iberoamericana de Información Científica - SIIC.

www.rmib.mx
ISSN 2395-9126

Editor técnico
Carla Ivonne Guerrero Robles

Maquetadores editoriales
Sandra Sánchez Jáuregui
Marco Guerrero

Sociedad Mexicana de Ingeniería Biomédica
Juan Vázquez de Mella #481, Polanco I Sección, Alc. Miguel Hidalgo, C. P. 11510, Ciudad de México, México, (555) 574-4505

SOMIB
Sociedad Mexicana
de Ingeniería Biomédica

Afiliada a:
International Federation of Medical and Biological Engineering (IFMB-IUPSM-ICSU)
Federación de Sociedades Científicas de México, A.C. (FESOCIME)
Consejo Regional de Ingeniería Biomédica para América Latina (CORAL)

SOMIB
Juan Vázquez de Mella #481, Polanco I Sección, Alc. Miguel Hidalgo, C. P. 11510, Ciudad de México, México (555) 574-4505
www.somib.org.mx

REVISTA MEXICANA DE INGENIERÍA BIOMÉDICA, Vol. 45, No. 2, Mayo-Agostol 2024, es una publicación cuatrimestral editada por la Sociedad Mexicana de Ingeniería Biomédica A.C., Juan Vázquez de Mella #481, Polanco I Sección, Alc. Miguel Hidalgo, C. P. 11510, Ciudad de México, México, (555) 574-4505, www.somib.org.mx, rib.somib@gmail.com. Editora responsable: Dra. Dora-Luz Flores. Reserva de Derechos al Uso Exclusivo No. 04-2015-041310063800-203, ISSN (impreso) 0188-9532; ISSN (electrónico) 2395-9126, ambos otorgados por el Instituto Nacional del Derecho de Autor. Responsable de la última actualización de este número: Lic. Sandra Sánchez Jáuregui, Juan Vázquez de Mella #481, Polanco I Sección, Alc. Miguel Hidalgo, C. P. 11510, Ciudad de México, México, (555) 574-4505, fecha de última modificación, 31 de agosto del 2023.

Disponible en línea:
www.rmib.mx

CONTENTS
CONTENIDO

RESEARCH ARTICLE
VOL. 45 | NO. 2 | **MAY-AUGUST 2024** | PP 6-22

Revista Mexicana de Ingeniería Biomédica

https://dx.doi.org/10.17488/RMIB.45.2.1

E-LOCATION ID: 1408

Gammatone-Frequency Cepstral Coefficients Based Fear Emotion Level Recognition System

Sistema de Reconocimiento de Nivel de Emoción Basado en Coeficientes Cepstrales de Frecuencia Gammatone

Barlian Henryranu Prasetio [1], *La Ode Adriyan Hazmar* [2], *Dahnial Syauqy* [1], *Edita Rosana Widasari* [1]

[1] Universitas Brawijaya, Faculty of Computer Science - Indonesia

[2] Universitas Brawijaya, Computer Engineering- Indonesia

ABSTRACT

Emotions represent affective states that induce alterations in behavior and interactions within one's environment. An avenue for discerning human emotions lies in the realm of speech analysis. Empirical evidence indicates that 1.6 million Indonesian teenagers grapple with mental anxiety disorders, characterized by sensations of fear or ambiguous vigilance. This work endeavors to devise a tool for discerning an individual's emotional state through voice processing, focusing particularly on fear emotions stratified into three levels of intensity: low, medium, and high. The proposed system employs Gammatone-Frequency Cepstral Coefficients (GFCC) for feature extraction, leveraging the efficacy of its gamma filter in reducing noise. Furthermore, a Random Forest (RF) Classifier is integrated to facilitate the recognition of fear's emotional intensity in speech signals. The system is deployed on a Raspberry Pi 4B and establishes a Bluetooth connection using the RFCOMM communication protocol to an Android application, presenting the classification results. The outcomes reveal that the Signal-to-Noise Reduction achieved through GFCC extraction surpasses that of Mel-Frequency Cepstral Coefficients (MFCC). In terms of accuracy, the implemented recognition system for fear emotion levels, employing GFCC extraction and Random Forest Classifier, attains a commendable accuracy of 73.33 %.

KEYWORDS: fear emotion, gammatone-frequency cepstral coefficients, Mel-frequency cepstral coefficients, signal-to-noise reduction, speech sound

RESUMEN

Las emociones representan estados afectivos que inducen alteraciones en el comportamiento e interacciones dentro del entorno de un individuo. Un enfoque para discernir las emociones humanas se encuentra en el análisis del habla. La evidencia empírica indica que 1.6 millones de adolescentes indonesios enfrentan trastornos de ansiedad mental, caracterizados por sensaciones de miedo o vigilancia ambigua. Esta investigación se propone diseñar una herramienta para discernir el estado emocional de una persona mediante el procesamiento de la voz, centrándose especialmente en las emociones de miedo estratificadas en tres niveles de intensidad: bajo, medio y alto. La metodología propuesta emplea los Coeficientes Cepstrales de Frecuencia Gammatone (GFCC) para la extracción de características, aprovechando la eficacia de su filtro gamma para combatir el ruido. Además, se incorpora un Clasificador Random Forest (RF) para facilitar el reconocimiento de la intensidad emocional del miedo en las señales de voz. El sistema se implementa en una Raspberry Pi 4B y establece una conexión Bluetooth utilizando el protocolo de comunicación RFCOMM con una aplicación Android, presentando los resultados de la clasificación. Los resultados revelan que la Reducción de Señal a Ruido lograda mediante la extracción de GFCC supera a la de los Coeficientes Cepstrales de Frecuencia Mel (MFCC). En términos de precisión, el sistema de reconocimiento implementado para los niveles de emoción de miedo, utilizando la extracción de GFCC y el Clasificador Random Forest, alcanza una precisión destacada del 73.33 %

PALABRAS CLAVE: emoción de miedo, coeficientes cepstrales de frecuencia gammatone, coeficientes cepstrales de frecuencia Mel, reducción de señal a ruido, sonido del habla

Corresponding author

TO: **Barlian Henryranu Prasetio**

INSTITUTION: **Universitas Brawijaya, Faculty of Computer Science - Indonesia**

ADDRESS: **Jl. Veteran, Ketawanggede, Kec. Lowokwaru, Kota Malang, Jawa Timur 65113, Indonesia**

CORREO ELECTRÓNICO: **barlian@ub.ac.id**

Received:

27 November 2023

Accepted:

3 April 2024

INTRODUCTION

Speech serves as a communicative medium for conveying information in a manner comprehensible to others [1]. It is shaped by a signal influenced by both time and frequency. Speech possesses distinct characteristics, including pitch, voice type, timbre, and volume [2]. Speech encompasses two content components: verbal and nonverbal. Verbal content comprises words interpreted by listeners, while nonverbal content encapsulates information conveyed through the way these words are expressed. Within the speech, nonverbal content holds the potential to communicate an individual's emotional state [3].

Nowadays, being aware of our emotions is crucial for personal well-being and effective navigation through life's complexities [4], a principle that holds true in Indonesia. It serves as the cornerstone of self-understanding, enabling individuals to discern the intricacies of their feelings, identify patterns, and foster personal growth. Emotional awareness enhances communication skills, allowing for clear expression of thoughts and feelings, minimizing the likelihood of misunderstandings in relationships [5]. In conflicts, this awareness facilitates empathetic resolution and constructive problem-solving. Moreover, it plays a pivotal role in stress management, as recognizing emotional triggers empowers individuals to implement coping strategies and maintain mental health. By embracing emotional awareness, we bolster decision-making processes, navigate challenges with resilience, and cultivate empathy and compassion for others. Ultimately, fostering emotional awareness is integral to creating a positive emotional climate, promoting overall well-being, and building meaningful connections our self to others.

Emotion awareness, as illuminated by Robert Plutchik's emotional wheel, holds profound significance in the realm of stress management, especially considering survey results revealing that 1.6 million Indonesian teenagers grapple with mental anxiety disorders marked by feelings of fear or ambiguous vigilance [6]. Emotion, as an intrinsic human experience and a reciprocal reaction to actions, situations, or events, frequently gives rise to behavioral and interactive changes within the surrounding environment. Plutchik's model, categorizing basic emotions into eight distinct parts and further delineating them into three intensity levels: low, medium, and high [7], serves as a valuable tool for comprehending the intricate emotional landscape associated with anxiety disorders. Integrating these perspectives emphasizes the interconnected nature of emotions, stress, and mental health, highlighting the importance of emotion awareness in crafting tailored stress management strategies that acknowledge the nuanced levels of fear and vigilance experienced by individuals in specific contexts.

The correlation between high levels of fear emotion and stress is a well-established aspect of psychological and physiological responses to challenging situations. Fear, as a primal and adaptive emotion, triggers the body's "fight or flight" response, releasing stress hormones such as cortisol and adrenaline. In situations where fear is elevated, the body perceives a potential threat, leading to heightened physiological arousal and increased stress levels [8]. Chronic or intense fear can contribute to sustained stress, negatively impacting both mental and physical well-being. Recognizing and understanding this connection between fear and stress is crucial in developing effective stress management strategies. Emotion awareness, particularly concerning fear at varying intensity levels, becomes instrumental in tailoring interventions and coping mechanisms to address the specific emotional challenges contributing to elevated stress levels in individuals.

In general, apart from being expressed verbally, emotions are intricately tied to physiological. Physical responses, including changes in muscle tension, especially head and neck area. For instance, heightened emotions, such as stress or fear, may result in increased tension in the neck muscles, significantly impacting speech characteristics. Speech stands out as a preeminent method for recognizing and comprehending human emotions due to its rich and diverse set of communicative elements. The nuances in pitch, rhythm, intonation, and various vocal cues embedded in speech offer profound insights into an individual's emotional state [9]. This comprehensive spectrum of prosodic features, coupled with the tone, timbre, and non-verbal vocal cues, provides a multifaceted tapestry of emotional expression.

Emotions can undergo sudden changes in response to various circumstances, posing significant challenges when measuring them, especially unconscious emotions such as fear. This unpredictability can lead to discomfort in individuals, resulting in inaccurate measurements. Hence, non-invasive methods, particularly speech analysis [10], play a crucial role in accurately assessing emotional levels. non-invasive approach allows for emotion measurement without the need for physical contact or potentially disruptive procedures. Not only does this non-intrusive method uphold individual privacy, but it also establishes a more comfortable environment, enhancing the accuracy of emotion measurement, particularly in the face of abrupt emotional shifts.

Therefore, in this work, we propose to develop a system for recognizing the level of fear emotion condition through speech analysis. The proposed system identifies the emotion of fear in three intensity levels: Apprehension (low), Fear (medium), and Terror (high). Previous research on a similar topic utilized the Mel-Frequency Cepstral Coefficients (MFCC) extraction method [11]. While MFCC proves efficient in quiet surroundings, its adaptability to noisy environments is limited. Consequently, we propose to employ the Gammatone Frequency Cepstral Coefficients extraction method, featuring an effective gamma filter tailored for sounds with high noise levels [12]. Additionally, the study's findings can offer insights into the performance of the Random Forest Classifier in recognizing the emotional intensity of fear in sound signals.

Related research

In 2020, Wang proposed the application of Gammatone Frequency Cepstral Coefficients (GFCC) for Forensic Automatic Speaker Recognition (FASR) in comparison under noisy conditions. The system uses GFCC and integrated with Principal Component Analysis (PCA) algorithm applied on mandarin voice datasets with different levels of white noise. Based on the result, it showed that overall system based on GFCC has improvement over baseline Mel Frequency Cepstral Coefficients (MFCC) on the same conditions [13].

Previously, similar research related to Speech Emotion Recognition (SER) using GFCC has been proposed by Bharti, *et al*. in 2020 [14]. The authors introduced the use of GFCC, ALO (Ant Lion Optimization), and Multi-Class Support Vector Machine (MSVM) classification in developing Speech Emotion Recognition (SER) system. They used RAVDESS Ryerson Audiovisual data set of expression voice and song dataset that contains 7356 records, comprises 24 speech samples, and happy-sad-angry emotions. The experimental system was simulated and executed using MATLAB with GUI tool. The evaluation parameters consisted of AUC, MSE, SNR, FAR and FRR to be compared with MFCC and SVM. The result showed that GFCC+ALO+MSVM achieved 97 % accuracy, while MFCC+SVM only achieved 79.48 % accuracy.

Patni, *et al*. proposed Speech Emotion Recognition using several features including MFCC, GFCC, Chromagram and RMSE features. Those 42 extracted features (16 MFCC, 12 GFCC, 13 Chromagram, 1 RMSE) from Ryerson Audio-

Visual Database of Emotional Speech and Song (RAVDESS) were then classified using 2D-CNN which achieved overall accuracy of more than 92 % [15].

The research proposed by Choudhary in 2021 used Gammatone cepstral coefficients for automatic speaker verification. To validate the system, they used different voices from different speakers then the system decided whether the voice comes from the same or different person. The result showed that the system can effectively recognize the speaker with high accuracy. In addition, they found out that by using Gammatone cepstral coefficients, speaker verification achieved significant improvement compared to other methods based on cepstral coefficients [16].

Zheng proposed another speech emotion recognition system based on the combination of convolutional neural network and random forest in 2018. CNN was used to extract speech emotion features from spectrogram and RF was then used to classify the emotion. The result showed the combination of using random forest boost the performance result compared to only traditional CNN model [17].

Another research by Hamsa in 2020 proposed an approach and framework for emotion recognition based on voice in noisy conditions. They used Wavelet Packet Transform (WPT) based on cochlear filter bank instead of gammatone filter bank and short-time Fourier transform. The features were then classified using Random Forest (RF) algorithm. The result showed the performance on three speech corpora in two languages in noisy conditions was better than other algorithms [18].

Fear Emotion

Emotions are categorized into basic emotions and advanced emotions. Basic emotions include joy, resignation, surprise, sadness, disgust, anger, anticipation, and fear.

Emotions are interconnected in various ways, influencing each other, and contributing to the overall emotional landscape. For example, fear is intricately connected to the experience of stress, forming a complex relationship between psychological and physiological responses. Fear, as an adaptive and primal emotion, triggers the body's stress response commonly known as the "fight or flight" reaction. When confronted with a perceived threat or danger, the body releases stress hormones [19], including cortisol and adrenaline, preparing the individual to respond to the imminent challenge. In situations where fear is prolonged or intense, it can contribute significantly to chronic stress. The persistent activation of the stress response system can lead to various physiological and psychological consequences, impacting overall well-being. Physiologically, prolonged stress linked to fear can result in heightened blood pressure, increased heart rate, and tension in muscles. Psychologically, the continuous experience of fear-related stress can contribute to anxiety disorders, sleep disturbances, and other mental health challenges. Moreover, individuals may adopt coping mechanisms that, while initially helpful in managing fear, can contribute to ongoing stress if not addressed effectively.

The intensity level of fear is a crucial dimension that enhances our comprehension of this intricate emotion. Fear, a complex emotional state, spans a spectrum of intensities, encompassing mild apprehension, moderate fear, and intense terror. At the lower end of the spectrum, individuals may experience a subtle sense of unease or concern, reflecting cautious responses to potential threats without feeling overwhelmed. Moving to the middle intensity level, fear becomes more pronounced, marked by heightened alertness and a palpable sense of anxiety. Individuals at this stage exhibit more discernible physical and emotional reactions indicative of a moderate fear state. At the highest intensity level, fear transforms into terror, an overwhelming and distressing emotional experience. Here, individuals grapple with an acute sense of imminent danger, triggering intense physiological responses like increased heart rate and a heightened fight-or-flight reaction. This nuanced understanding of fear's intensity levels is invaluable across disciplines such as psychology, neuroscience, and emotion recognition research, facilitating a more precise analysis and targeted approach to managing fear across varying degrees of intensity.

Previous study entitled "Emotional Processing of Fear: Exposure to Corrective Information" conducted by Edna B. Foa and Michael J. Kozak in 1986 presents the results of research on how individuals process the emotion of fear and how they manage that fear [20]. According to the results of this study, fear is an emotion that arises when individuals feel threatened or feel insecure.

Gammatone-Frequency Cepstral Coefficients (GFCC)

Gammatone Frequency Cepstral Coefficients (GFCC) were used to perform feature extraction in this study. This method is a development of the Mel-frequency Cepstral Coefficients (MFCC). Both methods start with preprocessing and FFT, but GFCC uses a gammatone filter bank which then compresses the results using the cubic root operation. After that, it is processed using DCT [8][16]. Figure 1 depicts the flow of GFCC steps.

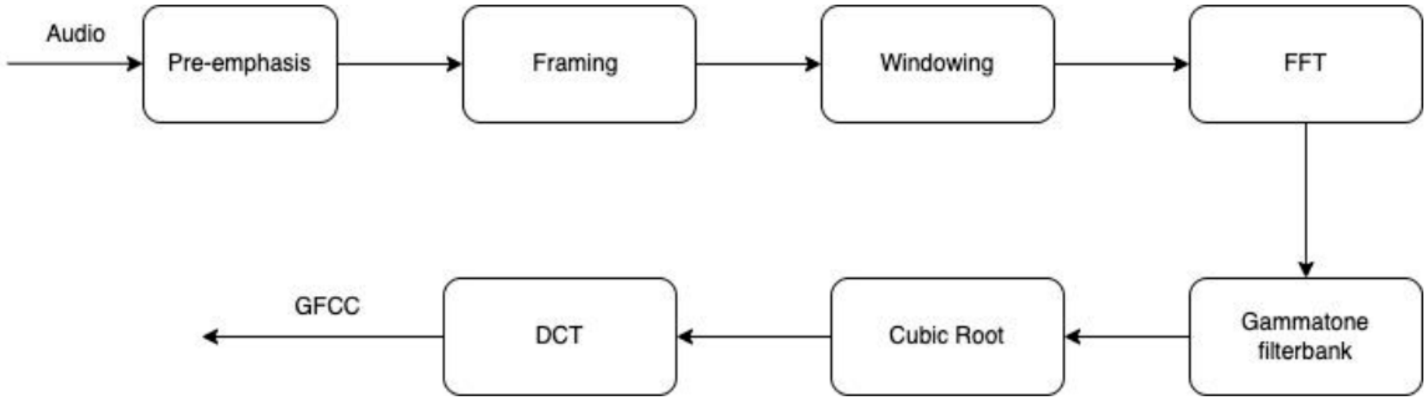

FIGURE 1. **GFCC Feature Extraction Block Diagram**

Pre-emphasis

This is the initial stage which functions to filter human speech signals. In the speech signal processing, a pre-emphasis filter is essential after the sampling process [21]. The purpose of this filtering is to achieve a smoother spectral frequency shape of the speech signal. The spectral shape is relatively high for the low-frequency region and tends to decrease sharply for frequencies above 2000 Hz. The pre-emphasis filter is grounded in the input/output relationship within the time domain, as expressed in the Equation (1).

$$y(n) = x(n) - a.x(n-1) \tag{1}$$

Where a represents the pre-emphasis filter constant, typically falling within the range of $0.9 < a < 1.0$

Framing

At this stage the signal is divided into several frames having a shorter duration because the signal in speech is always changing due to a shift in the articulation of the organs that reproduce sound. The frame size must be as long as possible, but it must also be short enough to obtain good time resolution. The frame length, often referred to as the window size, is usually chosen based on the characteristics of the speech signal and the requirements of the processing algorithm. Common frame lengths range from 20 to 30 milliseconds, but the optimal length can vary depending on the specific application. In this work, we decide frame length 30ms. This process is conducted in an overlapping manner to avoid loss of characteristics in each piece of the frame. For the overlap area, it covers 30 % and is carried out for each frame until all signals have been processed [22].

Windowing

Due to the frame blocking (framing) process, the signal to be discontinued [22]. Thus, the windowing process aims to minimize signal discontinuities at the beginning and end of each frame. Windowing is performed frame by frame, and for each frame, a specific window function is applied. If we define the window as $w(n)$, where $0 \leq n \leq N-1$, with N being the number of samples in each frame, then the result of windowing is expressed as Equation (2).

$$w(n) = 0.54 + 0.46\, cos\left(\frac{2\pi n}{N-1}\right), 0 \leq n \leq N-1 \tag{2}$$

Fast Fourier Transform (FFT)

FFT is a method for converting sound signals into spectral components which provides frequency information about the sound signal. FFT is an algorithm for efficiently computing the Discrete Fourier Transform (DFT) with the aim of reducing digital calculations to simplify the calculation of the frequency spectrum in its implementation [23]. This method implements an algorithm that operates on discrete signals. FFT formula for N samples is described in the Equation (3).

$$x(n) = \sum_{K=0}^{N-1} x_k e^{\frac{-2\pi jkn}{N}} \tag{3}$$

Where $0 \leq n \leq N-1$ and $j=\sqrt{-1}$.

Gammatone Filter banks

This method is a form of imitating the cochlea of the human ear in processing sound. In this process, the sound signal that has been processed using the FFT becomes the frequency domain into the time-frequency domain [24]. The Gammatone filter bank is a set of filters commonly used in auditory processing models to simulate the frequency analysis performed by the human auditory system. Each filter in the bank is designed to mimic the response of the human auditory nerve fibers to different frequency components of a sound signal.

The Gammatone filter response is characterized by a shape that resembles a gamma distribution. The transfer function for a single Gammatone filter can be expressed as Equation (4).

$$g(t) = a.t^{n-1} e^{-2\pi bt}\, cos\,(2\pi f_c t + \phi) \tag{4}$$

Where f (in Hz) is the center frequency, ϕ(in radians) is the phase of the carrier, a is the amplitude, n is the filter's order (set to 4), b (in Hz, set to 1.019) is the filter's bandwidth, and $t=1/(2\pi.ERB(f))$ (in seconds) is the filter time constant, and $ERB(fc)$ is the equivalent rectangular bandwidth function, expressed as Equation (5).

$$ERB(f_c) = 24.7\left(4.37\frac{f_c}{1000} + 1\right) \tag{5}$$

Cubic Root

Diverging from the logarithmic operations utilized in MFCC, the proposed GFCC employed cubic roots to compress the results of the filter bank [12]. The cubic roots better approximate the nonlinear response of the human auditory system to sound intensity variations, making them more relevant in representing auditory perception [25]. This compression technique enhances the discriminative power of the extracted features, particularly in tasks such as speech or sound classification, by capturing subtle differences in spectral characteristics [26]. The cubic root compression offers improved sensitivity to low-level details in the signal, crucial for distinguishing between similar sounds, as well as reducing the sensitivity to extreme values, leading to more robust feature extraction.

In addition, we mitigate the effects of temporal variations in the input signal by down sampling process, thereby improving the robustness of the feature representation to changes in signal duration. Finally, the equation of the operation cubic root expressed in Equation (6):

$$G_m[i] = \left|g_{downSampled}[i,m]\right|^{\frac{1}{3}}, i = 0...N-1, m = 0 \ldots M-1 \tag{6}$$

Discrete Cosine Transform (DCT)

Finally, the results of the previous stage are processed using DCT. The aim of the final stage is to do decorrelation and reduce the dimensions of the features that have been produced. Unlike the Discrete Fourier Transform (DFT), which uses complex exponentials, the DCT uses only real numbers, making it computationally more efficient [27]. The Discrete Cosine Transform for the one-dimensional DCT of a sequence $x[n]$ of length N is given in Equation (7).

$$X[k] = \sqrt{\frac{2}{N}}.C(k).\sum_{n=0}^{N-1} x[n].cos\left(\frac{\pi(2n+1)k}{2N}\right) \tag{7}$$

where $X[k]$ is the DCT coefficient at frequency index k. $C(k)$ is a scaling factor given by $C(k)=1/\sqrt{2}$ for k=0 and $C(k)=1$ for k > 0. n is the time or spatial index. k is the frequency index.

Random Forest (RF) Classifier

RF is a combination of decision tree algorithms that are considered weak in estimating, so RF combines decision trees to make stronger forecasts [28]. RF are more popular than other machine learning algorithms in over the last two decades because it can handle outliers and noisier datasets well; it also has higher accuracy and good performance with high dimensional datasets; another factor is that RF only requires two parameters ntree and mtry to be optimized [29].

MATERIALS AND METHODS

During the design stage of the system, the sound dataset was extracted using GFCC method. The extracted results then become input for Random Forest Classifier (RFC) and was divided into test data and training data. The RFC processed the sound features through 100 decision trees, which were then used as models and stored in ".pkl" format.

The mobile application design consists of use case design, flow diagram, and wireframe. The created mobile application was designed to have numbers of main functions such as connecting the application with the Raspberry Pi 4 device via Bluetooth, allowing the user to select the level of emotion to be detected, sending commands to the Raspberry Pi 4 to record sound, and receiving messages from the Raspberry Pi 4 to display the level results of the selected emotions.

The implementation of the previously designed system begins with deploying the program code and the model into Raspberry Pi 4, followed by making a Bluetooth connection by checking the Bluetooth address of the Raspberry Pi 4 and adding port 22. Furthermore, the mobile application implementation includes the steps of making block diagrams and interface design using MIT App Inventor, where block diagrams are structured using simple programming logic and application views are organized in sections Designer [30]. After all the systems have been set up, we did the preparation prototype tool by connecting microphone to Raspberry Pi 4 via port USB and connect the Raspberry Pi 4 to a power source portable form power bank.

For SNR testing, we tested the samples using both GFCC and MFCC extraction. GFCC accuracy test was done by comparing input sound received via microphone by modelling the emotional level of fear stored in the system's memory, then classifying the sound input using Random Forest Classifier to determine the appropriate emotion level of fear. Classification results were then sent to the mobile application via a Bluetooth connection and displayed on the app so that it can be seen by the user.

Design and Implementation

Sound Recording Hardware Design

In the design of subsystem for recording sound, two pieces of hardware are required, microphone and the Raspberry Pi 4B. Sound signal acquired by the USB microphone will be recorded and stored in Raspberry Pi 4B memory in wav format. Figure 2 illustrates the voice acquisition subsystem.

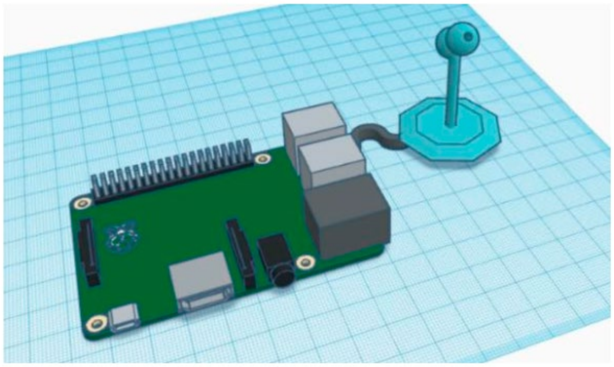

FIGURE 2. **Sound Recorder Hardware Design**

Dataset

Crowd Sourced Emotional Multimodal Actors Dataset (CREMA-D) is one of emotion dataset of 7,442 original clips featuring performances by 91 actors [31]. These actors, consisting of 48 males and 43 females spanning ages 20 to 74, represent diverse races and ethnicities, including African American, Asian, Caucasian, Hispanic, and Unspecified. The dataset includes recordings of actors delivering 12 sentences, each portraying one of six distinct emotions (Anger, Disgust, Fear, Happy, Neutral, and Sad) at four different emotion levels (Low, Medium, High, and Unspecified). In this work, we use only fear data of CREMA-D that consist of 273 utterances with 91 utterances for each class (Low, Medium, High).

Sound Extraction & Classification Design

Initially, CREMA-D dataset consist of three levels of fear emotions, HI (high), MD (medium), and LO (low). Each utterance was then extracted using the GFCC method to identify the characteristics of each sound through its amplitude, frequency, and pattern. After that, the sound extraction results become the input for classification using the Random Forest (RF) Classifier. The extraction method with the highest accuracy was the selected to be implemented into the developed system. The results of the extraction and classification produce a model in “pkl” format. Figure 3 shows the flowchart of feature extraction and classification steps.

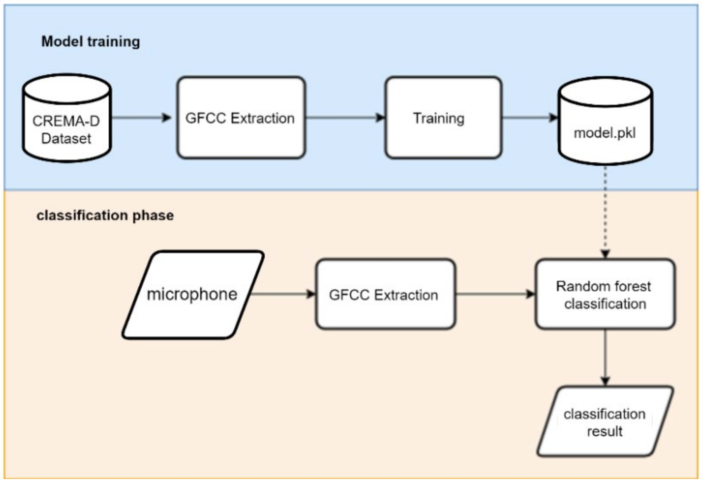

FIGURE 3. **Extraction and Classification Flowchart Design**

Bluetooth Connection Design

Based on the system requirements it was decided to use the RFCOMM Bluetooth protocol to connect Raspberry Pi 4 to smartphone. The Bluetooth RFCOMM (Radio Frequency Communications) protocol is one of the protocols used in Bluetooth technology to govern communication between Bluetooth devices. The RFCOMM protocol provides a logical channel that can be used to send and receive data between Bluetooth devices and provides several additional services such as device recognition services and authentication services. Figure 4 shows the flow diagram of Bluetooth connection between devices.

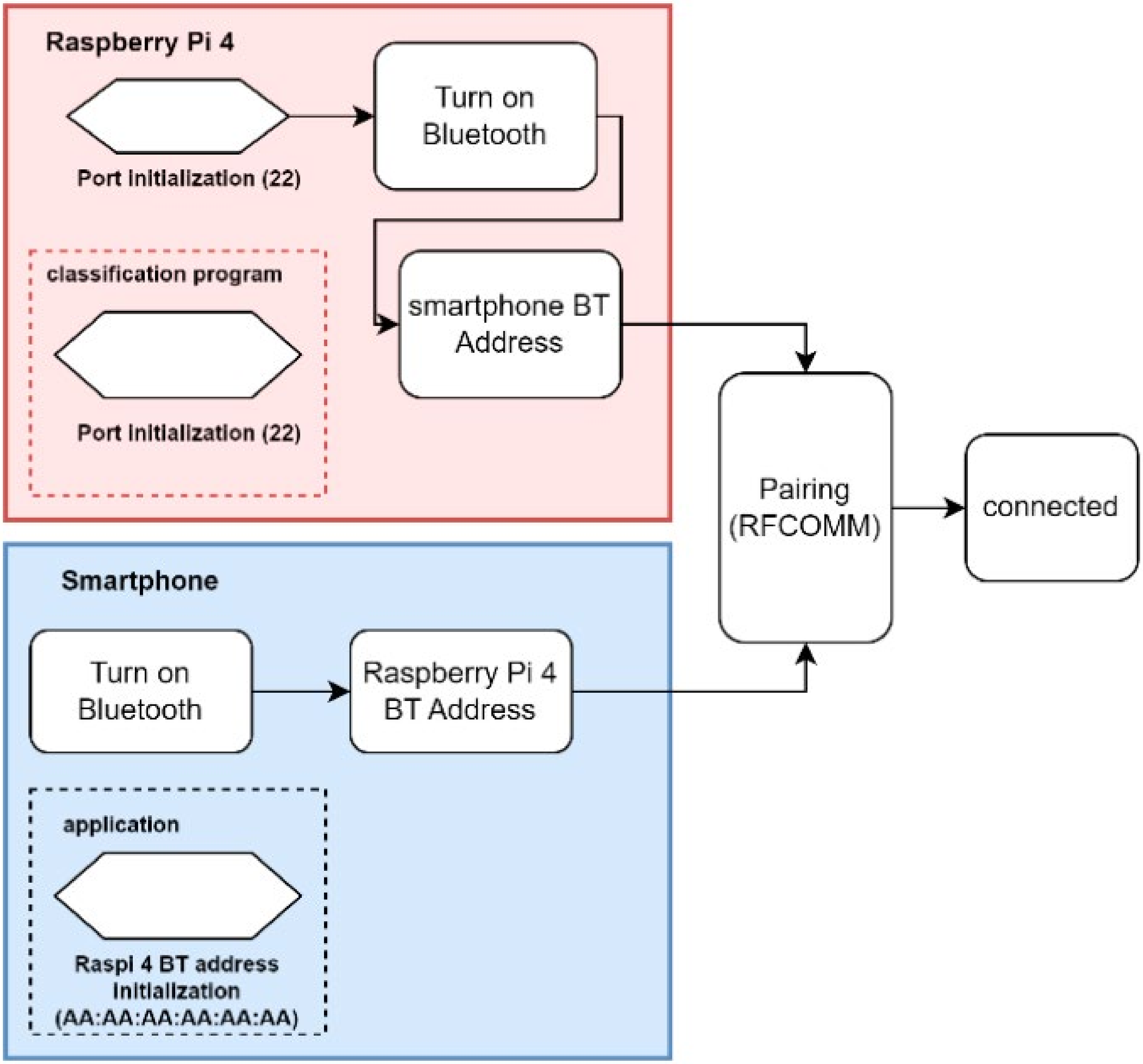

FIGURE 4. **Bluetooth Connection Flowchart**

System Implementation

The System implementation was carried out based on the previous design phase. Initially, the first step was to prepare the box as a container. The microphone was connected through the USB port of the Raspberry Pi 4. The power source used to deliver the power for the Raspberry Pi 4 was obtained from a power bank whose cable was modified by adding a switch attached to the box so that the users do not need to open the box if they want to turn on the system. Apart from that, a hole was also made at the top of the box to become a place for the microphone. After all the devices had been set up, the housing box was closed and covered so that the system became portable device. The classification algorithm was implemented in Raspberry Pi, while the smartphone was used mainly to display the result via bluetooth. Figure 5 depicts the overall implemented system as a portable device. Apart from hardware, the implementation of mobile application can be seen in Figure 6.

FIGURE 5. **Prototype of the System as portable device**

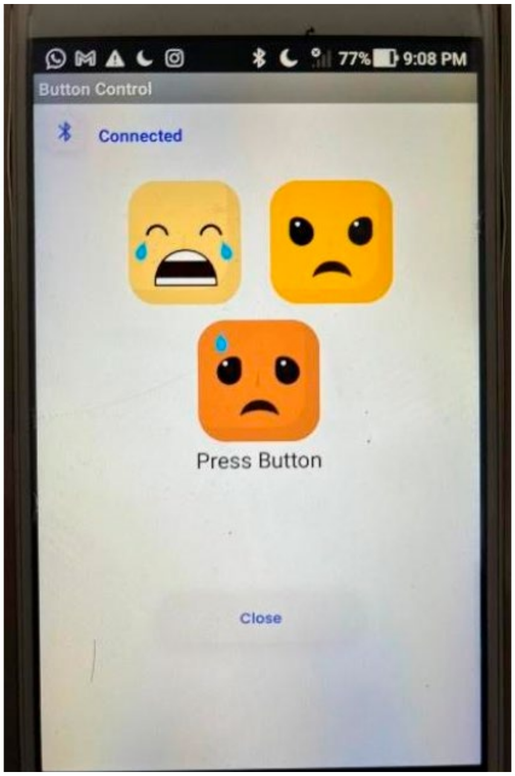

FIGURE 6. **Mobile Application User Interface**

In contrast to Mishra, *et al*. [32] and Alshamsi's, *et al*. [33] utilization of single hardware, such as Raspberry Pi or smartphones, for their emotion recognition systems, our approach involves the simultaneous integration of two hardware components - the Raspberry Pi and a smartphone. This strategic is rooted in the advantageous future utilization of both devices, facilitating the more effective incorporation of multimodal sensor inputs. The Raspberry Pi interfaces seamlessly with a diverse array of sensors, including microphones, cameras, and physiological sensors, enabling the capture of varied data modalities associated with emotions, such as speech, facial expressions, and physiological signals. This approach offers several notable benefits. Firstly, it allows for the collection of multimodal data, enriching the understanding of emotions. Secondly, the computational capabilities of the Raspberry Pi support initial data processing and feature extraction, complemented by the smartphones' enhanced processing power for advanced analysis and interaction. Additionally, the combined portability and affordability of the Raspberry Pi and smartphones enhance the system's versatility, enabling its use in diverse or multiple environments.

RESULTS AND DISCUSSION

The effectiveness of the proposed system is evaluated in term of Signal to Noise Ratio (SNR) and accuracy. In all experiments, we divide the CREMA-D dataset into around 5 % (15 utterances) as test data, 15% as data validation (40), and 80 % as training data (218 utterances). The 15-testing data are selected randomly with different subject and level of fear emotion.

Signal Testing-to-Noise Ratio (SNR)

Signal-to-noise ratio (SNR) is the ratio between the desired signal and noise in a system or signal. SNR can also be calculated by calculating the ratio between the amplitude of the desired signal to the amplitude of the noise.

$$SNR = 10\left(\frac{S}{N}\right) dB \tag{8}$$

This test aims to determine which extraction has the highest SNR value between Raw, GFCC and MFCC. The test results are shown in Table 1.

TABLE 1. SNR Test Results.

Sample*	***Signal-to-Noise Ratio (dB)***		
	Raw	**GFCC**	**MFCC**
1001-IEO-FEA-HI	52.45	174.50	78.46
1002-IEO-FEA-HI	59.18	160.69	93.90
1005-IEO-FEA-HI	52.30	74.60	106.42
1008-IEO-FEA-HI	51.14	149.82	89.07
1011-IEO-FEA-HI	52.53	96.85	89.95
1001-IEO-FEA-MD	45.00	184.36	86.32
1004-IEO-FEA-MD	61.97	238.64	92.62
1005-IEO-FEA-MD	54.42	101.56	97.04
1007-IEO-FEA-MD	50.84	138.47	89.17
1008-IEO-FEA-MD	48.99	125.39	91.36
1001-IEO-FEA-LO	49.68	124.94	85.42
1002-IEO-FEA-LO	58.02	69.44	101.27
1003-IEO-FEA-LO	60.47	75.20	97.71
1036-IEO-FEA-LO	50.67	165.56	102.25
1039-IEO-FEA-LO	60.64	128.06	106.39

*** Sample code: the first number indicate subject number**

Based on the test results, 12 out of 15 or 80 % of the data samples had a higher SNR using GFCC extraction. From the table of SNR test results, the average SNR results for each label are presented in Table 2. It can be seen in the table that the highest SNR was obtained for sound data samples labelled "MID" using GFCC extraction with an average of 133.85 dB.

TABLE 2. Average SNR Test Results for Each Label.

Label	***Signal-to-Noise Ratio (dB)***		
	Raw	**GFCC**	**MFCC**
HIGH	53.52	131.29	91.56
MEDIUM	52.24	157.64	91.30
LOW	55.89	112.64	98.60
Average	**53.88**	**133.85**	**93.82**

Accuracy

The aim of this test is to determine the accuracy of using GFCC extracted features as input and RFC classification in the emotion level detection system of fear. To obtain these results Equation (9) was used. The test results can be seen in Table 3. Based on these data it is known that the system succeeds in predicting correctly 11 out of 15 data samples so that the obtained accuracy was 73.33 %.

$$accuracy(\%) = \frac{Total\ data\ is\ correct}{Total\ data} x\ 100 \tag{9}$$

TABLE 3. **Results of the Detection Accuracy of Fear Emotional Levels.**

Sample*	Label	Detection Results	Information
1008-IEO-FEA-HI	*HIGH*	*HIGH*	Correct
1034-IEO-FEA-HI	*HIGH*	*HIGH*	Correct
1048-IEO-FEA-HI	*HIGH*	*HIGH*	Correct
1025-IEO-FEA-HI	*HIGH*	*MID*	Wrong
1039-IEO-FEA-HI	*HIGH*	*HIGH*	Correct
1006-IEO-FEA-MD	*MID*	*MID*	Correct
1009-IEO-FEA-MD	*MID*	*MID*	Correct
1007-IEO-FEA-MD	*MID*	*MID*	Correct
1018-IEO-FEA-MD	*MID*	*MID*	Correct
1024-IEO-FEA-MD	*MID*	*MID*	Correct
1005-IEO-FEA-LO	*LOW*	*LOW*	Correct
1016-IEO-FEA-LO	*LOW*	*LOW*	Correct
1018-IEO-FEA-LO	*LOW*	*MID*	Wrong
1026-IEO-FEA-LO	*LOW*	*MID*	Wrong
1037-IEO-FEA-LO	*LOW*	*MID*	Wrong

*** Sample code: the first number indicate subject number**

In addition, to ensure the effectiveness of the proposed system, we compare the proposed system with baseline system in term of SNR and accuracy. The comparison results show in Table 4.

TABLE 4. **Results of the Detection Accuracy of Fear Emotional Levels.**

Reference	Number of Classes	Number of Features	Accuracy
Chebbi, *et al.*[34]	3 classes (fear, neutral, other emotions)	11 (based on FDR and ANOVA)	78 %
		10 (based on Scatter measure)	77 %
		23 (based on divergence)	83 %
		8 (based on FDR, ANOVA, Scatter measure, Divergence)	86 %
Clavel, *et al.* [35]	2 classes (fear and neutral)	-	70 %
This work	3 classes (high fear, medium fear, and low fear)	GFCC	73 %

Table 4 demonstrates the result performance of the proposed system compared baseline system. Chebbi, *et al*. [34] and Clavel, *et al*. [35] explored a range of features and achieved accuracies up to 86 % in a three-class fear classification task, while our work focuses on a more nuanced fear analysis, classifying fear into high, medium, and low levels. Despite achieving an accuracy of 73 %, which may be lower than the maximum reported by Chebbi, *et al*., the multiclass approach adds granularity to the classification, providing valuable insights into different fear intensities. The use of GFCC as features in this work offers a distinct representation of the data, potentially capturing nuanced aspects of fear expression. Furthermore, the decomposition of fear levels allows for a more detailed understanding of emotional states, catering to specific applications where finer distinctions in fear intensity are essential. Overall, the advantages of this work lie in its multiclass approach, detailed fear level analysis, and the potential relevance of GFCC features in capturing the nuances of fear expressions.

CONCLUSION

GFCC (Gamma Frequency Cepstral Coefficients) are better than MFCC (Mel-Frequency Cepstral Coefficients) in reducing noise in feature extraction of sound. This is due to the use of the gamma filter on the GFCC which can reduce noise. In the developed system, the fear emotion labelled with the "MID" label has the highest SNR (Signal-to-Noise Ratio) value by using GFCC. The GFCC extraction method and the Random Forest Classifier are quite effective for detecting the moderate emotional level of fear (MID) with an accuracy of around 73 %.

For future research directions, several areas have been identified. First, further optimization of the fear emotion recognition model can be pursued by considering various neural network architectures, activation functions, and training parameters to enhance accuracy and system responsiveness. Second, expanding the dataset by collecting additional data from diverse sources could improve the diversity and representation of fear expression variations. Exploring other frequency features to deepen the understanding and detection of fear emotion levels is another avenue for research. The selection and comparison with alternative machine learning techniques, such as Support Vector Machines (SVM) or Decision Trees, can also be a focus for future research. The integration of multimodal data, such as audio and visual information, and the addition of sentiment and context analysis elements can enrich the understanding of emotions. Furthermore, evaluating the system's effectiveness in real-world scenarios can provide richer insights and test the system's performance in complex and variable situations. Developments in these various aspects are expected to enhance the performance and usability of the fear emotion level recognition system based on GFCC.

ACKNOWLEDGMENTS

We thank our colleagues from Embedded System and Robotics Laboratory Universitas Brawijaya that has supported us in this work.

AUTHOR CONTRIBUTIONS

B. H. P. Conceptualization, methodology, validation, supervision, project administration, funding acquisition. L. O. A. H. Software, formal analysis, investigation, resources, data curation, writing original draft. D. S. Validation, formal analysis, data curation, writing review and editing, visualization. E. R. W. Methodology, validation, formal analysis, investigation, data curation, writing review and editing.

REFERENCES

[1] M. Gupta, S. S. Bharti, and S. Agarwal, "Gender-based speaker recognition from speech signals using GMM model," Mod. Phys. Lett. B, vol. 33, no. 35, 2019, doi: https://doi.org/10.1142/S0217984919504384

[2] J. Otašević and B. Otašević, "Voice-based identification and contribution to the efficiency of criminal proceedings," J. Crim. Crim. Law, vol. 59, no. 2, pp. 61-72, Nov. 2021, doi: . https://doi.org/10.47152/rkkp.59.2.4

[3] S. A. Kotz, R. Dengler, and M. Wittfoth, "Valence-specific conflict moderation in the dorso-medial PFC and the caudate head in emotional speech," Soc. Cogn. Affect Neurosci., vol. 10, no. 2, 2015, doi: https://doi.org/10.1093/scan/nsu021

[4] S. J. Gomez, "Self-Management Skills of Management Graduates," Int. J. Res. Manag. Bus. Stud., vol. 4, no. 3, pp. 40-44, 2017.

[5] S. A. Saddiqui, M. Jawad, M. Naz, and G. S. Khan Niazi, "Emotional intelligence and managerial effectiveness," RIC, vol. 4, no. 1, pp. 99-130, 2018, doi: https://doi.org/10.32728/RIC.2018.41%2F5

[6] H. E. Erskine, S. J. Blondell, M. E. Enright, J. Shadid, et al., "Measuring the Prevalence of Mental Disorders in Adolescents in Kenya, Indonesia, and Vietnam: Study Protocol for the National Adolescent Mental Health Surveys," J. Adolesc. Health, vol. 72, no. 1, pp. S71-S78, 2023, doi: https://doi.org/10.1016/j.jadohealth.2021.05.012

[7] K. Cherry, "What Are Emotions and the Types of Emotional Responses?" Verywell Health. https://www.verywellhealth.com/what-are-emotions-279517807 (accessed 2023).

[8] S. Sharma, A. Mamata, Deepak, "Psychological Impacts, Hand Hygeine Practices & and Its Correlates in View of Covid-19 among Health Care Professionals in Northern States of India," Indian J. Forensic Med. Toxicol., vol. 15, no. 2, pp. 3691-3698, 2021, doi: https://doi.org/10.37506/ijfmt.v15i2.14947

[9] S. A. Mahar, M. H. Mahar, J. A. Mahar, M. Masud, M. Ahmad, N. Z. Jhanhi, and M. A. Razzaq, "Superposition of functional contours based prosodic feature extraction for speech processing," Intell. Autom. Soft Comput., vol. 29, no. 1, pp. 183-197, 2021, doi: https://doi.org/10.32604/iasc.2021.015755

[10] S. Sondhi, M. Khan, R. Vijay, A. K. Salhan, and S. Chouhan, "Acoustic analysis of speech under stress," Int. J. Bioinform. Res. Appl., vol. 11, no. 5, pp. 417-432, 2015, doi: https://doi.org/10.1504/ijbra.2015.071942

[11] M. S. Likitha, S. R. R. Gupta, K. Hasitha, and A. U. Raju, "Speech based human emotion recognition using MFCC," in 2017 International Conference on Wireless Communications, Signal Processing and Networking (WiSPNET), Chennai, India, 2017, pp. 2257-2260, doi: https://doi.org/10.1109/WiSPNET.2017.8300161

[12] M. Jeevan, A. Dhingra, M. Hanmandlu, and B. K. Panigrahi, "Robust speaker verification using GFCC based i-vectors," in Proceedings of the International Conference on Signal, Networks, Computing, and Systems. Lecture Notes in Electrical Engineering, vol 395. New Delhi, India, pp. 85-91, 2017, doi: https://doi.org/10.1007/978-81-322-3592-7_9

[13] H. Wang and C. Zhang, "The application of Gammatone frequency cepstral coefficients for forensic voice comparison under noisy conditions," Aust. J. Forensic Sci., vol. 52, no. 5, pp. 553-568, 2020, doi: https://doi.org/10.1080/00450618.2019.1584830

[14] D. Bharti and P. Kukana, "A Hybrid Machine Learning Model for Emotion Recognition from Speech Signals," in 2020 International Conference on Smart Electronics and Communication (ICOSEC), Trichy, India, 2020, pp. 491-496, doi: https://doi.org/10.1109/ICOSEC49089.2020.9215376

[15] H. Patni, A. Jagtap, V. Bhoyar, and A. Gupta, "Speech Emotion Recognition using MFCC, GFCC, Chromagram and RMSE features," in 2021 8th International Conference on Signal Processing and Integrated Networks (SPIN), Noida, India, 2021, pp. 892-897, doi: https://doi.org/10.1109/SPIN52536.2021.9566046

[16] H. Choudhary, D. Sadhya, and V. Patel, "Automatic Speaker Verification using Gammatone Frequency Cepstral Coefficients," in 2021 8th International Conference on Signal Processing and Integrated Networks (SPIN), Noida, India, 2021, pp. 424-428, doi: https://doi.org/10.1109/SPIN52536.2021.9566150

[17] L. Zheng, Q. Li, H. Ban, and S. Liu, "Speech emotion recognition based on convolution neural network combined with random forest," in 2018 Chinese Control And Decision Conference (CCDC), Shenyang, China, 2018, pp. 4143-4147, doi: https://doi.org/10.1109/CCDC.2018.8407844

[18] S. Hamsa, I. Shahin, Y. Iraqi, and N. Werghi, "Emotion Recognition from Speech Using Wavelet Packet Transform Cochlear Filter Bank and Random Forest Classifier," IEEE Access, vol. 8, pp. 96994-97006, 2020, doi: https://doi.org/10.1109/ACCESS.2020.2991811

[19] A. Cuncic, "Amygdala Hijack and the Fight or Flight Response," Very Well Mind. https://www.verywellmind.com/what-happens-during-an-amygdala-hijack-4165944 (accessed 2023).

[20] E. B. Foa and M. J. Kozak, "Emotional Processing of Fear. Exposure to Corrective Information," Psychol. Bull., vol. 99, no. 1, pp. 20-35, 1986, doi: https://psycnet.apa.org/doi/10.1037/0033-2909.99.1.20

[21] S. M. Qaisar, "Isolated speech recognition and its transformation in visual signs," J. Electr. Eng. Technol., vol. 14, no. 2, pp. 955-964, 2019, doi: https://doi.org/10.1007/s42835-018-00071-z

[22] S. Lokesh and M. R. Devi, "Speech recognition system using enhanced mel frequency cepstral coefficient with windowing and framing method," Cluster Comput., vol. 22, pp. 11669-11679, 2019, doi: https://doi.org/10.1007/s10586-017-1447-6

[23] J. D. Schmidt, "Simple Computations Using Fourier Transforms," in Numerical Simulation of Optical Wave Propagation with Examples in MATLAB, Bellingham, WA, USA: SPIE Press, 2010, doi: https://doi.org/10.1117/3.866274.ch3

[24] A. Krobba, M. Debyeche, and S. A. Selouani, "Mixture linear prediction Gammatone Cepstral features for robust speaker verification under transmission channel noise," Multimed. Tools Appl., vol. 79, no. 25-26, pp. 18679-18693, 2020, doi: https://doi.org/10.1007/s11042-020-08748-2

[25] A. Revathi, N. Sasikaladevi, R. Nagakrishnan, and C. Jeyalakshmi, "Robust emotion recognition from speech: Gamma tone features and models," Int. J. Speech Technol., vol. 21, no. 3, pp. 723-739, 2018, doi: https://doi.org/10.1007/s10772-018-9546-1

[26] U. Kumaran, S. Radha Rammohan, S. M. Nagarajan, and A. Prathik, "Fusion of mel and gammatone frequency cepstral coefficients for speech emotion recognition using deep C-RNN," Int. J. Speech Technol., vol. 24, no. 2, pp. 303-314, 2021, doi: https://doi.org/10.1007/s10772-020-09792-x

[27] S. Rhee, M. G. Kang, "Discrete cosine transform based regularized high-resolution image reconstruction algorithm," Opt. Eng., vol. 38, no. 8, pp. 1348-1356, 1999, doi: https://doi.org/10.1117/1.602177

[28] A. Subudhi, M. Dash, and S. Sabut, "Automated segmentation and classification of brain stroke using expectation-maximization and random forest classifier," Biocybern. Biomed. Eng., vol. 40, no. 1, pp. 277-289, 2020, doi: https://doi.org/10.1016/j.bbe.2019.04.004

[29] T. N. Phan, V. Kuch, and L. W. Lehnert, "Land cover classification using google earth engine and random forest classifier-the role of image composition," Remote Sens., vol. 12, no. 15, art. no. 2411, 2020, doi: https://doi.org/10.3390/rs12152411

[30] T. Adiono, S. F. Anindya, S. Fuada, K. Afifah, and I. G. Purwanda, "Efficient Android Software Development Using MIT App Inventor 2 for Bluetooth-Based Smart Home," Wireless Pers. Commun., vol. 105, pp. 233-256, 2019, doi: https://doi.org/10.1007/s11277-018-6110-x

[31] H. Cao, D. G. Cooper, M. K. Keutmann, R. C. Gur, A. Nenkova, and R. Verma, "CREMA-D: Crowd-sourced Emotional Multimodal Actors Dataset," IEEE Trans. Affect. Comput., vol. 5, no. 4, pp. 377-390, 2014, doi: https://doi.org/10.1109/taffc.2014.2336244

[32] A. Mishra, D. Patil, N. Karkhanis, V. Gaikar, and K. Wani, "Real time emotion detection from speech using Raspberry Pi 3," in 2017 International Conference on Wireless Communications, Signal Processing and Networking (WiSPNET), Chennai, India, 2017, pp. 2300-2303, doi: https://doi.org/10.1109/WiSPNET.2017.8300170

[33] H. Alshamsi, V. Kepuska, H. Alshamsi, and H. Meng, "Automated Speech Emotion Recognition on Smart Phones," in 2018 9th IEEE Annual Ubiquitous Computing, Electronics and Mobile Communication Conference (UEMCON), New York, NY, USA, 2018, pp. 44-50, doi: https://doi.org/10.1109/UEMCON.2018.8796594

[34] S. Chebbi and S. Ben Jebara, "On the Selection of Relevant Features for Fear Emotion Detection from Speech," in 2018 9th International Symposium on Signal, Image, Video and Communications (ISIVC), Rabat, Morocco, 2018, pp. 82-86, doi: https://doi.org/10.1109/ISIVC.2018.8709233

[35] C. Clavel, I. Vasilescu, L. Devillers, G. Richard, and T. Ehrette, "Fear-type emotion recognition for future audio-based surveillance systems," Speech Commun., vol. 50, no. 6, pp. 487-503, 2008, doi: https://doi.org/10.1016/j.specom.2008.03.012

RESEARCH ARTICLE

VOL. 45 | NO. 2 | **MAY-AUGUST 2024** | PP 23-34

Revista Mexicana de Ingeniería Biomédica

dx.doi.org/10.17488/RMIB.45.2.2

E-LOCATION ID: 1409

Involvement of the Lung Parenchyma Analyzed by Frequency Components of the Tidal Volume Assessed by Electrical Bioimpedance

Afectación del Parénquima Pulmonar Analizada por Medio de las Componentes de Frecuencia del Volumen Tidal Evaluado por Bioimpedancia Eléctrica

Francisco Miguel Vargas Luna[1], *María Isabel Delgadillo Cano*[1], *Pere Joan Riu Costa*[2], *Svetlana Kashina*[1]
José Marco Balleza Ordaz[1]

[1] Universidad de Guanajuato - México

[2] Universitat Politécnica de Catalunya, Electronics and Biomedical Instrumentation Department, Barcelona - Spain

ABSTRACT

Pulmonary function tests are vital for detecting pathologies, especially chronic obstructive pulmonary diseases (COPD), emphasizing the importance of assessing lung parenchyma involvement in maintaining proper gas exchange. Electrical impedance tomography (EIT) offers a non-invasive alternative for respiratory function evaluation while preserving natural breathing. We propose using EIT to detect lung parenchyma conditions by analyzing tidal volume patterns (by averaging the impedance image) in the frequency domain. Twenty COPD patients underwent simultaneous evaluation with a pneumotachometer and an EIT device, performing three 30-second respiratory maneuvers. FFT spectra analysis yielded parameters, including the area under the curve and quartiles (25 %, 50 %, 75 %) of power values in six frequency regions. Correlations between these parameters and clinical test results (pulmonary diffusing capacity and arterial blood gas analysis) revealed significant associations, particularly with PCO2. Multiple linear regression analysis predicted PCO2 with an R2adj = 0.827, suggesting the potential for non-invasively detecting lung parenchyma affectation by correlating FFT bioimpedance ventilatory patterns with gas exchange performance in COPD patients.

KEYWORDS: **COPD, electrical impedance tomography, lungs, pulmonary function testing**

RESUMEN

Las pruebas de función pulmonar son fundamentales para detectar patologías, especialmente enfermedades pulmonares obstructivas crónicas (EPOC), destacando la importancia de evaluar la participación del parénquima pulmonar en el mantenimiento adecuado del intercambio gaseoso. La tomografía por la bioimpedancia eléctrica (TIE) ofrece una alternativa no invasiva para la evaluación de la función respiratoria mientras se conserva la respiración natural. Proponemos utilizar la TIE para detectar condiciones del parénquima pulmonar mediante el análisis de patrones de volumen tidal en el dominio de frecuencia. Veinte pacientes con EPOC fueron evaluados simultáneamente con un neumotacómetro y un dispositivo de TIE, realizando tres maniobras respiratorias de 30 segundos cada una. El análisis de espectros FFT proporcionó parámetros, incluyendo el área bajo la curva y los cuartiles (25 %, 50 %, 75 %) de los valores de potencia en seis regiones de frecuencia. Las correlaciones entre estos parámetros y los resultados de pruebas clínicas (capacidad de difusión pulmonar y análisis de gases en sangre arterial) revelaron asociaciones significativas, especialmente con PCO2. El análisis de regresión lineal múltiple predijo PCO2 con un R2adj = 0.827, sugiriendo la posibilidad de detectar de manera no invasiva la afectación del parénquima pulmonar al correlacionar los patrones ventilatorios de bioimpedancia FFT con el rendimiento del intercambio gaseoso en pacientes con EPOC.

PALABRAS CLAVE: EPOC, pulmón, test de funciones pulmonares, tomografía por impedancia eléctrica

Corresponding author

TO: **José Marco Balleza-Ordaz**
INSTITUTION: **Universidad de Guanajuato - México**
ADDRESS: **Loma del Bosque #103, Lomas del Campestre,**
37150 León de los Aldama, Guanajuato, Mexico.
EMAIL: **jm.balleza@ugto.mx**

Received:

22 November 2023

Accepted:

7 April 2024

INTRODUCTION

The importance of diagnosing lung function lies in determining whether patients exhibit a restrictive, obstructive, or restrictive-obstructive respiratory pattern through the interpretation of measurements depicting dynamic or static lung performance [1]. There are four clinical trials to diagnose respiratory patterns in patients: a) spirometry, b) static lung volumes, c) lung's ability to diffuse carbon monoxide, and d) 4 examination of blood gas [1]. All of these are used to diagnose and monitor the severity level of pulmonary diseases such as chronic obstructive pulmonary disease (COPD). COPD is a prevalent, avoidable, and manageable condition marked by persistent respiratory symptoms and restricted airflow resulting from abnormalities in the airways and/or alveoli, typically stemming from substantial exposure to harmful particles or gases [2][3][4]. Since the appearance of SARS-CoV-2 (COVID-19), the performance of the four clinical trials has become a complicated routine not only for COPD diagnosis but also for COPD patients with SARS-CoV-2. Nowadays, the main risk of conducting these tests is COVID-19 transmission due to contamination of materials used during each procedure [4][5][6], increasing the probability of developing severe lung disease or death.

Electrical Impedance Tomography (EIT) is a radiation-free and non-invasive method employed for visualizing the distribution of impedance in specific regions across the cross-sectional human body [7][8]. EIT frames are reconstructed from a set of impedance measurements obtained by an arrangement of 16 electrodes placed around the thorax at the level of the sixth intercostal space [9][10][11], registering impedance changes that allow the characterization of internal movements produced by the human body. Some EIT applications in pneumology include: 1) estimation of regional lung perfusion [12][13], 2) regional lung ventilation characterization in patients with pulmonary fibrosis [14] and pulmonary hypertension [15], 3) detection of bronchopulmonary dysplasia in neonates at early stages [16], 4) ventilatory pattern monitoring in patients diagnosed with sudden onset of respiratory distress syndrome (ARDS) [17], 5) evaluation of an effect of pleural effusion drainage in patients submitted to mechanical ventilation [18], among others.

EIT applications in COPD patients aim to monitor parameters that describe temporal changes in pulmonary airflow limitation. For example, Milne *et al.* (2019) proposed using EIT to characterize ventilatory heterogeneity (VH) using lung tidal volume changes. In this case, EIT determinations were compared with the forced oscillation technique (FOT) in COPD patients compared with a control group. Three parameters from bioimpedance changes corresponding to each voxel of the EIT image were calculated. The first one was the mean expiratory time. The second measure involved calculating the average time gap between the impedance alterations in individual voxels and the overall impedance variation in the entire EIT image or phase shift. The third one was the mean amplitude of impedance signals determined by each EIT voxel. The coefficient of variation (VC) and index of heterogeneity (HI) for each parameter were calculated to quantify lung impedance distribution: the coefficient of variation (CV) and the heterogeneity index (HI). A HI is the CV of the region defined by the 28 near neighboring voxels of the point considered. The HI is defined as the mean value of all local HI for the whole EIT image. From the obtained results, both CV and HI evidenced a significant increase in COPD patients compared with the control. All assessments were linked to spirometry parameters and measurements of resistance and reactance in the Forced Oscillation Technique (FOT), revealing statistically significant distinctions between the groups [19].

Karagiannidis *et al.* (2018) suggested employing EIT to ascertain regional expiratory time constants in intubated patients with COPD and ARDS. These time constants were calculated based on the overall impedance signal obtained from EIT. These parameters were compared with lung volume signals obtained by a pneumotachograph. Authors evidenced a significant correlation, roughly 80 %, between EIT-derived time constants and those obtained by a pneumotachometer [20].

Vogt *et al*. (2016) suggested utilizing EIT to observe the spatial and temporal distribution of ventilation (VD) in COPD patients while under the influence of an inhaled bronchodilator. In this study, spirometry served as the gold standard. The EIT image values corresponding to various spirometry parameters were identified, including FEV1, FVC, FEV1/FVC, tidal volume, peak flow, and mean forced expiratory flow between 25 and 75 % of FVC (FEF25-75 %). The FEV1/FVC ratio was used to assess the bronchodilator's impact on spatial ventilation distribution. A significant bronchodilator response was evidenced in most of the patients assessed by these EIT parameters [21].

In the above-mentioned studies, authors used EIT as an alternative method to monitor parameters that describe lung function. These parameters were compared with those obtained by different clinical trials. EIT utilizes frequency analysis to interpret signals, but correlating FFT frequencies with respiratory parameters remains challenging. EIT captures impedance variations within a body, offering insights into lung function. However, the exact correspondence between FFT peaks and specific respiratory metrics remains elusive. Despite advancements, establishing a direct correlation remains complex due to the multifactorial nature of physiological processes and signal intricacies. New research is needed to fully unveil these connections, enabling precise respiratory parameter estimations. Bridging this gap promises enhanced diagnostic capabilities and refined monitoring techniques, driving EIT towards more accurate and insightful clinical applications in respiratory care.

This study proposes to analyze the frequency of electrical bioimpedance changes in the ventilation pattern with those parameters corresponding to clinical procedures, mainly diffusing lung capacity trials and arterial blood gas tests in a group of COPD patients. We hypothesize that EIT supplies information about lung airflow limitation through the frequency analysis of tidal-volume respiration signals. The main objective of this research is to identify frequency components of the tidal volume lung signal obtained by EIT and correlate them with parameters of the pulmonary trials in a group of COPD patients to detect lung parenchyma involvement.

MATERIALS AND METHODS

Instrumentation

The TIE4-sys represents the fourth iteration of an EIT prototype developed at the Department of Electronic Engineering, Universitat Politècnica de Catalunya, Barcelona, Spain. This system features 16 electrodes positioned around the thoracic box at the sixth intercostal space, aligning with the established protocol of our research group [22]. The process involves injecting a 1 mA electrical current at 48 kHz through a pair of adjacent electrodes, with the resulting differential voltage recorded at the rest of the adjacent electrode pairs. Following the completion of potentials for a specific injection pair, the injection point is shifted to the next adjacent electrode pair, initiating a new cycle of measurements [23]. The entire procedure concludes when all adjacent electrode pairs have been employed as injectors. EIT determinations are redundant, enabling the estimation of the reciprocity error [24]. This parameter characterizes systematic errors and malfunctions that may arise during the procedure, such as inadequate contact between electrodes and the skin [25][26].

The TIE4-sys reconstruction algorithm utilized for image generation is a weighted back-projection algorithm. The software incorporates a weight matrix that considers the spatial sensitivity of each pixel in the EIT image [27][28]. The TIE4-sys scan rate is 17 images/s [25]. Dynamic images are relative impedance changes calculated using a baseline (BL) as a reference. The BL of TIE4-sys is composed of averaging 204 images corresponding to 12 seconds of acquisition [25].

Following the recording of the breathing pattern and the generation of dynamic images, an impedance signal (ΔZ) is obtained by determining the variance between the average impedance of an Electrical Impedance Tomography (EIT) image and the baseline (BL). The parameter ΔZ is computed for each of the 510 EIT images, corresponding to a 30-second monitoring period with TIE4sys.

For monitoring lung tidal volume, the pneumatometer employed was a Med Graphics preVentTM Pneumotach provided by Medical Graphics Corporation (St. Paul, MN, USA). The device is controlled by software supplied by the manufacturer, recording measurements displayed graphically on the screen and numerically downloadable as a text file. Calibration of the pneumotachometer was performed using a 3-L syringe following standard laboratory protocols, establishing it as the gold standard for measurements [29].

Participants

A group of 20 male patients (Caucasic, age 67±9), all diagnosed with COPD at the Pneumology Department of Hospital de la Santa Creu I Sant Pau, Barcelona, Spain, was analyzed. In general, all patients showed an intense obstructive ventilatory alteration (FEV1/FVC roughly 45 % ± 11 %) and a moderate level of air trapping (RV/TLC roughly 1.4) [30]. The prevalence of COPD in the countries of the European Union is higher in men than in women by approximately 30 % [31]. Due to this fact, this study was conducted on male subjects. All clinical procedures were performed between 9 am and noon in a quiet room at sea level with an ambient temperature of 25 °C and a relative humidity of 60 %. All patients voluntarily consented to participate in the study, which had been previously approved by the institutional ethics committee. A written informed consent was read and signed by all participants. This research was conducted according to the guidelines outlined in the Declaration of Helsinki [32].

Clinical Tests

The medical history of the COPD patients included at least one of the four clinical procedures of interest for our study: 1) spirometry, 2) static lung volumes, 3) carbon monoxide diffusing capacity in the lungs, 4) analysis of blood gases. Spirometry is used to screen for abnormalities of airflow or lung volume [33][34]. The variables obtained from this test are forced vital capacity (FVC), forced expiratory volume in the first second (FEV1), and the FEV1/FVC ratio. All patients had spirometry test parameters. Static lung volume test assesses air trapping in the lungs. The parameters from this test are residual volume (RV) and total lung capacity (TLC) [35]. Out of the 20 COPD patients, only 15 participants had this test available. Pulmonary diffusing capacity for carbon monoxide test measures gas transferred from the alveoli to the capillary blood per unit time [36]. The variables obtained from this test are pulmonary diffusing capacity for carbon monoxide (DLCO), pulmonary diffusing capacity adjusted to hemoglobin (DLCOAdj), and the ratio DLCO/Av (Av: alveolar volume). In this case, out of the 20 patients, only 16 had results from this procedure available. Finally, the arterial blood gas analysis gives information about the partial pressures of gas in blood and acid-base content [37]. The parameters measured in this test include the partial pressure of oxygen in arterial blood (PO2) and the partial pressure of carbon dioxide in arterial blood (PCO2). From the group of patients, only 14 had results from this analysis.

Procedure

All determinations analyzed in this study were previously used to obtain and assess a set of calibration equations to convert EIT signals into measurable volume signals [38][39]. In this study, two devices were used: the pneumotachometer and TIE4-sys. Both devices were simultaneously connected to each patient; the pneumotachometer through a mouthpiece and clip nose and TIE4-sys through 16 electrodes (Red Dot 2560-3M, London, Ontario, Canada) placed at the level of the sixth intercostal space, making a 224 pixel mesh. At this level of the thorax, the bioimpedance changes corresponding to lung tidal volume are not affected [40][41]. The pneumotachometer is used to quantify pulmonary airflow, meanwhile, TIE4-sys monitors bioimpedance changes corresponding to lung volume variations. Three respiratory exercises under tidal volume conditions were recorded for each patient. Each respiratory maneuver was performed by each volunteer adopting a sitting position and lasted 30 seconds with three minutes of rest between measurements. The sitting position contributes to reducing strain on the body during respiration and reduces the wear and tear on the joints, muscles, and ligaments [42]. Figure 1 shows the electrodes´ placement and a typical image obtained by EIT.

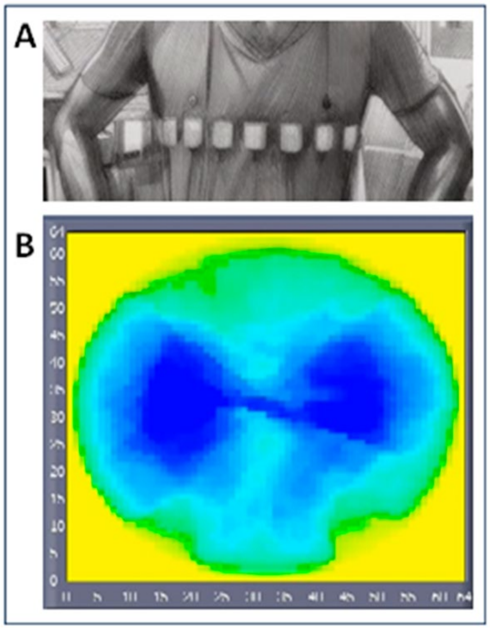

FIGURE 1. **A) Electrodes´ placement on the thorax; B) Typical EIT image**

Signal Processing

The three bioimpedance signals include 30 seconds with a scan rate of 17 samples/s, which is 510 points for each one. Each pneumotachometer signal data encompasses 30 seconds with a scan rate of 50 samples/s, that is 1500 points. The tidal volume determinations and bioimpedance changes corresponding to each respiratory maneuver were estimated using the differences between each maximum and the following minimum values of each signal. MatLab software was used to perform the signal processing and statistical analysis. From the analysis of FFT graphs, six regions from the signal spectrum (R1 - R6) are considered for analysis: R1 is defined from 0 to 200 mHz, R2 from 200 mHz to 400 mHz, R3 from 400 mHz to 600 mHz, R4 from 600 mHz to 800 mHz, R5 is between 800 mHz and 1 Hz, and R6 covers the frequencies higher than 1 Hz. Four parameters were estimated from each frequency region and for each patient: the mean area under the curve (Ri-A from the three maneuvers), and the quartile at 25 %, 50 %, and 75 % of FFT-Spectrum data (Ri-Q1, Ri-Q2, and Ri-Q3 respectively by merging the three data sets).

Statistical Analysis

The utilization of quartile analysis was implemented due to the non-normal distribution observed in the majority of frequency segment data, as indicated by the Shapiro-Wilk test (p-value < 0.05). Following this, these parameters were correlated with the results from clinical tests, primarily focusing on pulmonary diffusing capacity for carbon monoxide and arterial blood gas analysis, but also including spirometry and static lung volumes [43][44].

The tidal volumes obtained by the pneumotachometer technique, and those volumes estimated by EIT data show normal distribution; therefore, the correlation between tidal volumes and bioimpedance changes was performed by parametric Pearson correlation. However, the correlations between the parameters (areas under the curve and quartiles) estimated in each segment of FFT spectrums and those obtained by clinical tests were performed by a Spearman correlation because most of the FFT parameters do not have a normal distribution.

RESULTS AND DISCUSSION

It is known that bioimpedance changes due to respiration vary greatly between persons. Even one person may present different results due to, for example, hydration status. For that reason, in the present study, we have not chosen a study-control group approach, but the frequency variations were directly correlated with the parameters obtained in clinical tests. The correlation between tidal volume measurements obtained by the pneumotachometer and electrical bioimpedance change determinations for all the participants was over 95 % (Pearson r, p-value < 0.05).

Most of the data parameters corresponding to segmented FFT-Spectrum (Parameters from regions 1, 3, 5, 6, and R4-Q1 and R4-Q2) did not follow a normal distribution in the electrical bioimpedance spectrum (S-W, p-value < 0.05). The correlations between these parameters and clinical evaluations are performed by the Spearman rank correlation test (ρ, p-values < 0.05). The parameter PCO2 shows significant correlations with the following electrical bioimpedance FFT parameters: R3-A with a correlation $\rho = -0.564$ ($p=0.036$), R4-A with a correlation $\rho = -0.666$ ($p=0.009$), R5-A with a correlation $\rho = -0.635$ ($p=0.015$), and R6-A with a correlation $\rho = -0.586$ ($p=0.028$). Also, this parameter shows a significant correlation with quantile values of FFT data at the same regions: R3-Q3, $\rho = -0.686$ ($p=0.007$), R4-Q1, R4-Q2, R4-Q3 with $\rho = -0.533$ ($p=0.05$), $\rho = -0.560$ ($p=0.037$), $\rho = -0.648$ ($p=0.012$) respectively; R5-Q1, R5-Q2, R5-Q3 with $\rho = -0.626$ ($p=0.017$), $\rho = -0.611$ ($p=0.02$), $\rho = -0.569$ ($p=0.034$) respectively; and R6-Q3, $\rho = -0.584$ ($p=0.028$). Residual volume (RV) correlates with impedance R2-Q1 $\rho = -0.595$ ($p=0.019$). Also, DLCOadj correlates with R4-Q1 and R4-Q2, $\rho = 0.506$ ($p=0.045$) and $\rho = 0.512$ ($p=0.043$) respectively (Table 1, Table 2, Table 3).

TABLE 1. **Spearman correlations of partial areas under FFT spectrum in different frequency ranges of electrical bioimpedance signal and PCO2.**

Electrical bioimpedance region area	Correlation with PCO2: ρ (p)
R3	-0.564 (0.036)
R4	-0.666 (0.009)
R5	-0.635 (0.015)
R6	-0.586 (0.028)

TABLE 2. **Spearman correlation of PCO2, RV and DLCOadj with quantiles of power values of FFT spectrum in different frequency ranges of bioimpedance signal.**

Electrical bioimpedance region-quartile	Correlation with PCO2: ρ(p)	Correlation with RV: ρ(p)	Correlation with DLCOadj: ρ (p)
R2-Q1		-0.595 (0.019)	
R3-Q3	-0.686 (0.007)		
R4-Q1	-0.533 (0.05)		0.506 (0.045)
R4-Q2	-0.560 (0.037)		0.512 (0.043)
R4-Q3	-0.648 (0.012)		
R5-Q1	-0.626 (0.017)		
R5-Q2	-0.611 (0.02)		
R5-Q3	-0.569 (0.034)		
R6-Q3	-0.584 (0.028)		

TABLE 3. **Spearman correlation of PCO2 and PO2 with quantiles of power values of FFT spectrum in different frequency ranges of Pneumotachometer signal.**

Pneumotac region-quartile	Correlation with PCO2: ρ (p)	Correlation with PO2: ρ (p)
R2-Q1		0.682 (0.007)
R2-Q3	-0.540 (0.046)	
R4-Q1	-0.560 (0.037)	

Based on these results, multiple linear regression was calculated with PCO2 as a dependent variable and the significantly correlated areas and quartiles as predictors, obtaining an expression with the most significant coefficients (9 predictors: R3-A, R4-A, R5-A, R6-A, R3-Q3, R4-Q1, R4-Q2, R6-Q3, R5-Q2). This multiple regression has an R^2=0.947 with an R^2adj=0.827 (Figure 2).

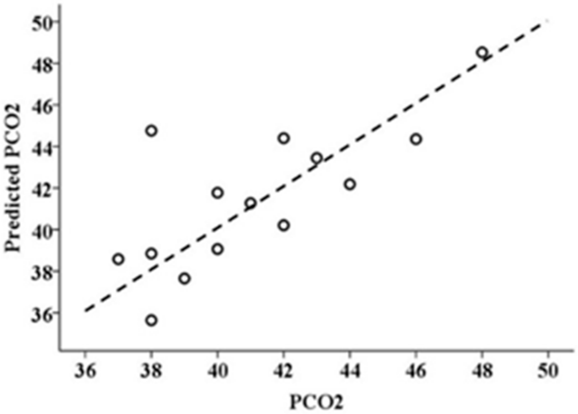

FIGURE 2. **Dispersion graph of predicted PCO2 obtained by multiple regression (R2=0.947 with an R2adj=0.827) and the value measured by arterial gas exchange analysis.**

Pneumotachometer FFT parameters correlate mainly with spirometry results, as was discussed in other investigations. PCO2 correlates with R2-Q3 and R4-Q1 with ρ = - 0.540 (p=0.046) and ρ = - 0.560 (p=0.037) respectively, and R2-Q1 correlates with PO2 with ρ = 0.682 (p=0.007).

This research aimed to detect lung parenchyma involvement by electrical impedance tomography in a group of COPD patients. To achieve this goal, it was proposed to analyze the frequency spectrum (FFT-module) of the bioimpedance signal obtained by EIT, under lung tidal volume conditions. Each FFT spectrum was segmented into six frequency ranges, in which four parameters of interest (area under each range of FFT spectrum, and quartile at 25 %, 50 %, and 75 % of FFT data in each range) were estimated. These parameters were correlated with those resulting from four clinical tests involved with the gas exchange condition, mainly with arterial blood gas parameters.

The normal respiration frequency lies in the first and sometimes second defined range frequencies (< 400 mHz). It is proposed that high-frequency ranges defined involve the noise coming from parenchyma involvement and that this is detected better with the electrical bioimpedance technique. Low frequency (< 4Hz) Forced Oscillation Lung Function Test has been related to viscoelastic properties of parenchyma [45], so our claim can be understood as a way to relate parenchyma involvement with low-frequency features of tidal volume (> 0.4 Hz corresponding to what we call high-frequency range) While the exact relationship between the involvement of lung parenchymal and bioimpedance is complex and not fully elucidated, it's clear that alterations in lung parenchymal properties can potentially affect bioimpedance measurements. This highlights the importance of considering various physiological factors when interpreting bioimpedance data in the context of lung function assessment or disease diagnosis. In this study, the highest correlations of bioimpedance areas and quartiles of the FFT spectrum at high frequencies (higher than 400 mHz) were those corresponding to the parameters of arterial blood gas technique, mainly PCO2. This correlation is negative, implying that the higher FFT values of the high-frequency region, the lower PCO2 determinations or better performance of the gas exchange. This parameter is important to determine the level of obstruction, restriction, or obstruction-restriction of the ventilatory pattern of a patient [1][2][3][4]. This could be possible because EIT detects the alteration of lung parenchyma through electrical current application and biopotential detection around the thorax. An explanation could be that during inhalation, alveoli expand to perform the gas exchange. These alveoli expansions produce high-frequency noise when this is electrically monitored. However, one COPD condition is the destruction of alveoli ramification (emphysema), including bronchioles [1][2][3][4]. We hypothesize that EIT detects the involvement of lung parenchyma (alveoli and bronchioles). The involvement of the parenchyma can be detected by the analysis of low frequencies features of the tidal volume obtained by the whole EIT image or by regions of interest.

It's crucial to emphasize that the results we've acquired are constrained to a group of 20 individuals with COPD. To enhance the robustness of future studies, it is essential to augment the size of the patient sample. As well as, to use regions of interest on EIT images and monitor the bioimpedance changes, analyzing its frequency components and correlating them with parameters of clinical tests.

CONCLUSIONS

From the frequency analysis of an electrical bioimpedance signal obtained by EIT, under lung tidal volume conditions, it is possible to detect parameters of gas exchange conditions such as PCO2 by analyzing frequency features at high frequencies from the FFT spectrum. Therefore, based on the sample of patients, it is possible to detect the level of affectation of the ventilatory pattern. Likewise, using EIT, we can predict the performance level of gas exchange in a group of COPD patients with an intense obstructive ventilatory alteration and a moderate level of air trapping.

ETHICAL STATEMENT

The clinical study in which the lung volumes and bioimpedance determinations were acquired in a group of COPD patients was approved by the Committee of Ethics of the Hospital de la Santa Creu i Sant Pau, Barcelona, Spain.

ACKNOWLEDGMENTS

All authors thank Universidad de Guanajuato, Dirección de Apoyo a la Investigación y al Posgrado (DAIP) for financial support.

S. Kashina acknowledges CONAHCyT for her postdoctoral fellowship.

DECLARATION OF INTERESTS

The authors declare that they have no known competing financial interests or personal relationships that could have appeared to influence the work reported in this paper.

AUTHOR CONTRIBUTIONS

F. M. V. L. Data acquisition, data analysis and interpretation, and writing original draft. M. I. D. C. Data analysis and interpretation, review of the manuscript. P. J. R. C. Study design, data analysis and interpretation, and review of the manuscript. S. K. Study design, data acquisition, data analysis and interpretation, review of the manuscript, and funding acquisition. J. M. B. O. Study design, data acquisition, data analysis and interpretation, review of the manuscript, and funding acquisition. All authors approved the version to be published and agree to be accountable for all aspects of the work in ensuring that questions related to the accuracy or integrity of any part of the work are appropriately investigated and resolved.

REFERENCES

[1] B. H. Culver, “Pulmonary function testing,” in Clinical Respiratory Medicine, S. G. Spiro, G. A. Silvestri, A. Agusti, Eds., Philadelphia, PA, United State: Elsevier, 2012, ch. 9, pp. 133-142.

[2] A. Virani, S. Baltaji, M. Young, T. Dumont, T. Cheema, “Chronic Obstructive Pulmonary Disease: Diagnosis and GOLD Classification,” Crit. Care Nurs. Q., vol. 44, no. 1, pp. 9-18, Mar. 2021, doi: https://doi.org/10.1097/CNQ.0000000000000335

[3] Global Initiative for Chronic Obstructive Ling Disease. “Global strategy for the diagnosis, management, and prevention of chronic obstructive pulmonary disease.” Global Initiative for Chronic Obstructive Lung Disease: https://goldcopd.org/wp-content/uploads/2019/12/GOLD-2020-FINAL-ver1.2-03Dec19_WMV.pdf (accessed Sep. 28, 2023).

[4] D. M. D. Halpin, G. J. Criner, A. Papi, D. Singh, et al., “Global Initiative for the Diagnosis, Management, and Prevention of Chronic Obstructive Lung Disease. The 2020 GOLD Science Committee Report on COVID-19 and Chronic Obstructive Pulmonary Disease,” Am. J. Resp. Crit. Care, vol. 203, no. 1, pp. 24-36, 2021, doi: https://doi.org/10.1164/rccm.202009-3533SO

[5] A. McGowan. “Recommendation from ERS Group 9.1 (Respiratory function technologists /Scientists) Lung function testing during COVID-19 pandemic and beyond.” ERS. https://ers.app.box.com/s/zs1uu88wy51monr0ewd990itoz4tsn2h

[6] M. C. McCormack, D. A. Kaminsky. “American Thoracic Society. Pulmonary function laboratories: Advice Regarding COVID-19.” American Thoracic Society. https://www.thoracic.org/professionals/clinical-resources/disease-related-resources/pulmonary-function-laboratories.php (accessed Sep. 16, 2023).

[7] F. A. Escobar Revelo, V. H. Mosquera Leyton, C. F. Rengifo, “Electrical Impedance Tomography: Hardware Fundamentals And Medical Applications,” Ing. Solidar., vol. 16, no. 3, pp. 2-29, 2020, doi: https://doi.org/10.16925/2357-6014.2020.03.02 (accessed 2023).

[8] T. A. Khan, S. H. Ling, “Review on electrical impedance tomography: Artificial intelligence methods and its applications,” Algorithms, vol. 12, no. 5, pp. 70-88, 2019, doi: https://doi.org/10.3390/a12050088

[9] P. Grasland-Mongrain, C. Lafon, “Review on Biomedical Techniques for Imaging Electrical Impedance,” IRBM, vol. 39, no. 4, pp. 243-250, 2018, doi: https://doi.org/10.1016/j.irbm.2018.06.001

[10] Z. Wang, S. Yue, H. Wang, Y. Wang, “Data preprocessing methods for electrical impedance tomography: a review,” Physiol. Meas., vol. 41, no. 9, art. no. 09TR02, 2020, doi: https://doi.org/10.1088/1361-6579/abb142

[11] Z. Zong, Y. Wang, Z. Wei, “A Review of Algorithms and Hardware Implementations in Electrical Impedance Tomography,” Prog. Electromagn. Res., vol. 169, pp. 59-71, 2020, doi: https://doi.org/10.2528/PIER20120401

[12] S. Yuan, H. He, Y. Long, Y. Chi, I. Frerichs, Z. Zhao, “Rapid dynamic bedside assessment of pulmonary perfusion defect by electrical impedance tomography in a patient with acute massive pulmonary embolism,” Pulm. Circ., vol. 11, no. 1, pp. 1-3, 2021, doi: https://doi.org/10.1177/2045894020984043

[13] H. He, Y. Long, I. Frerichs, Z. Zhao, “Detection of acute pulmonary embolism by electrical impedance tomography and saline bolus injection,” Am. J. Resp. Crit. Care., vol. 202, no. 6, pp. 881-882, 2020, doi: https://doi.org/10.1164/rccm.202003-0554IM

[14] E. Krauss, D. van der Beck, I. Schmalz, J. Wilhelm, et al., “Evaluation of Regional Pulmonary Ventilation in Spontaneously Breathing Patients with Idiopathic Pulmonary Fibrosis (IPF) Employing Electrical Impedance Tomography (EIT): A Pilot Study from the European IPF Registry (eurIPFreg),” J. Clin. Med., vol. 10, no. 2, art. no. 192, 2021, doi: https://doi.org/10.3390/jcm10020192

[15] M. Proença, F. Braun, M. Lemay, J. Solà, et al., “Non-invasive pulmonary artery pressure estimation by electrical impedance tomography in a controlled hypoxemia study in healthy subjects,” Sci. Rep., vol. 10, art. no. 21462, 2020, doi: https://doi.org/10.1038/s41598-020-78535-4

[16] W. Onland, J. Hutten, M. Miedema, L. D. Bos, P. Brinkman, A. H. Maitland-van der Zee, A. H. van Kaam, “Precision Medicine in Neonates: Future Perspectives for the Lung,” Front. Pediatr., vol. 8, pp. 732-742, 2020, doi: https://doi.org/10.3389/fped.2020.586061

[17] R. Cornejo, P. Iturrieta, T. M. Olegário, C. Kajiyama, et al., “Estimation of changes in cyclic lung strain by electrical impedance tomography: Proof-of-concept study,” Acta Anaesth. Scand., vol. 65, no. 2, pp. 228-235, 2021, doi: https://doi.org/10.1111/aas.13723

[18] A. Rara, K. Roubik, T. Tyll, “Effects of pleural effusion drainage in the mechanically ventilated patient as monitored by electrical impedance tomography and end-expiratory lung volume: A pilot study,” J. Crit. Care, vol. 59, pp. 76-80, 2020, doi: https://doi.org/10.1016/j.jcrc.2020.06.001

[19] S. Milne, J. Huvanandana, C. Nguyen, J. M. Duncan, et al., “Time-based pulmonary features from electrical impedance tomography demonstrate ventilation heterogeneity in chronic obstructive pulmonary disease,” J. Appl. Physiol., vol. 127, no. 5, pp. 1441-1452, 2019, doi: https://doi.org/10.1152/japplphysiol.00304.2019

[20] C. Karagiannidis, A. D. Waldmann, P. L. Róka, T. Schreiber, S. Strassmann, W. Windisch, S. H. Böhm, “Regional expiratory time constants in severe respiratory failure estimated by electrical impedance tomography: a feasibility study,” Crit. Care, vol. 22, no. 1, art. no. 221, 2018, doi: https://doi.org/10.1186/s13054-018-2137-3

[21] B. Vogt, Z. Zhao, P. Zabel, N. Weiler, I. Frerichs, “Regional lung response to bronchodilator reversibility testing determined by electrical impedance tomography in chronic obstructive pulmonary disease,” Am. J. Physiol Lung Cell Mol. Physiol., vol. 311, no. 1, pp. L8-L19, 2016, doi: https://doi.org/10.1152/ajplung.00463.2015

[22] B. De Lema, P. Casan, P. Riu, “Electrical impedance tomography: standardizing in the procedure in pneumology,” Arch. Bronconeumol., vol. 42, pp. 299-301, 2006, doi: https://doi.org/10.1016/s1579-2129(06)60146-8

[23] J. Fornos Herrando, “Estimació del Patró Ventilatori mitjanc¸ ant Tomografía d’Impedància Elèctrica,” Bachelors dissertation, Universitat Politècnica de Catalunya, Cataluña, Spain, 2006.

[24] D. B. Geselowitz, “An application of electrocardiographic lead theory to impedance plethysmography,” IEEE Trans. Biomed. Eng., vol. BME-18, no. 1, pp. 38-41, 1971, doi: https://doi.org/10.1109/TBME.1971.4502787

[25] O. Casas, “Contribución a la obtención de imágenes paramétricas en tomografía de impedancia eléctrica para la caracterización de tejidos biológicos,” Ph.D. dissertation, Universitat Politècnica de Catalunya, Cataluña, Spain, 1998.

[26] A. Fontova, “Desenvolupament d’un mòdul de comunicacions Ethernet per a un sistema de TIE,” Bachelors dissertation, Universitat Politècnica de Catalunya, Cataluña, Spain, 2004.

[27] R. E. Serrano, B. De Lema, O. Casas, T. Feixas, et al., “Use of electrical impedance tomography (TIE) for the assessment of unilateral pulmonary function,” Physiol. Meas., vol. 23, art. no. 211, 2002, doi: https://doi.org/10.1088/0967-3334/23/1/322

[28] O. Casas, J. Rosell, R. Bragós, A. Lozano, P. J. Riu, “A parallel broadband real-time system for electrical impedance tomography,” Physiol. Meas., vol. 17, art. no. A1, 1996, doi: https://doi.org/10.1088/0967-3334/17/4A/002

[29] MedGraphics Products. “Technical specifications.” MedGraphics Products. http://www.sanomed.ee/images/Med.Graph/CPFSDusbSpiro.pdf (accessed Sept. 7, 2023).

[30] J. Vestbo, S. S. Hurd, A. G. Agustí, P. W. Jones, et al., “Global strategy for the diagnosis, management, and prevention of chronic obstructive pulmonary disease: GOLD executive summary,” Am. J. Resp. Crit. Care, vol. 187, no. 4, pp. 347-365, 2013, doi: https://doi.org/10.1164/rccm.201204-0596PP

[31] G. Ntritsos, J. Franek, L. Belbasis, M. A. Christou, et al., “Gender-specific estimates of COPD prevalence: a systematic review and meta-analysis,” Int. J. Chronic Obstr., vol. 13, pp. 1507-1514, 2018, doi: https://doi.org/10.2147%2FCOPD.S146390

[32] P. P. Rickham, “Human experimentation. Code of ethics of the world medical association. Declaration of Helsinki,” Brit. Med. J., vol. 2, no. 5402, art. no. 177, 1964, doi: https://doi.org/10.1136/bmj.2.5402.177

[33] F. García-Río, M. Calle, F. Burgos, P. Casan, et al., “Espirometría,” Arch. Bronconeumol., vol. 49, no. 9, pp. 388-401, 2013, doi: https://doi.org/10.1016/j.arbr.2013.07.007

[34] J. M. Haynes, “Basic spirometry testing and interpretation for the primary care provider,” Can. J. Respir. Ther., vol. 54, no. 4, pp. 92-98, 2018, doi: https://doi.org/10.29390/cjrt-2018-017

[35] J. A. Neder, S. Andreoni, A. Castelo-Filho, L. E. Nery, “Reference values for lung function tests: I. Static volumes,” Braz. J. Med. Biol. Res., vol, 32, no. 6, pp. 703-717, 1999, doi: https://doi.org/10.1590/S0100-879X1999000600006

[36] N. Macintyre, R. O. Crapo, G. Viegi, D. C. Johnson, et al., “Standardization of the single breath determination of carbon monoxide uptake in the lung,” Eur. Respir. J., vol. 26, pp. 720-735, 2005, doi: https://doi.org/10.1183/09031936.05.00034905

[37] L. Gattinoni, A. Pesenti, M. Matthay, Understanding blood gas analysis, Intens. Care Med. vol. 44, no. 1, pp. 91-93, 2018, doi: https://doi.org/10.1007/s00134-017-4824-y

[38] M. Balleza-Ordaz, E. Alday-Perez, M. Vargas-Luna, S. Kashina, M. R. Huerta-Franco, L. A. Torres-González, P. J. Riu-Costa, “Tidal volume monitoring by a set of tetrapolar impedance measurements selected from the 16-electrodes arrangement used in electrical impedance tomography (EIT) technique. Calibration equations in a group of healthy males,” Biomed. Signal Process. Control, vol. 27, pp. 68-76, 2016, doi: https://doi.org/10.1016/j.bspc.2016.02.001

[39] M. Balleza-Ordaz, R. Estrella-Cerón, T. Romero-Muñiz, M. Vargas-Luna, “Lung ventilation monitoring by electrical bioimpedance technique using three different 4-electrode thoracic configurations: Variability of calibration equations,” Biomed. Signal Process. Control, vol. 47, pp. 401-412, 2019, doi: https://doi.org/10.1016/j.bspc.2018.08.032

[40] J. Karsten, T. Stueber, N. Voigt, E. Teschner, H. Heinze, “Influence of different electrode belt positions on electrical impedance tomography imaging of regional ventilation: a prospective observational study,” Crit. Care, vol. 20, art. no. 3, 2015, doi: https://doi.org/10.1186/s13054-015-1161-9

[41] S. Krueger-Ziolek, B. Schullcke, J. Kretschmer, U. Müller-Lisse, K. Möller, Z. Zhao, “Positioning of electrode plane systematically influences EIT imaging,” Physiol. Meas., vol. 36, art. no. 1109, 2015, doi: https://doi.org/10.1088/0967-3334/36/6/1109

[42] E. Szczygieł, K. Zielonka, S. Mętel, J. Golec, “Musculo-skeletal and pulmonary effects of sitting position-a systematic review,” Ann. Agric. Environ. Med., vol. 24, no. 1, pp. 8-12, 2017, https://doi.org/10.5604/12321966.1227647

[43] S. W. Smith, The Scientist and Engineer’s Guide to Digital Signal Processing, 2nd ed., San Diego, CA, USA: California Technical Publishing, 1999.

[44] M. Weeks, Digital signal processing using MATLAB and wavelets, 1st ed., Hingham, MA, USA: Infinity Science Press LLC, 2007.

[45] M. Ghita, D. Copot, M. Ghita, E. Derom, C. Ionescu, “Low Frequency Forced Oscillation Lung Function Test Can Distinguish Dynamic Tissue Non-linearity in COPD Patients,” Front. Physiol., vol. 10, art. no.1390, 2019, doi: https://doi.org/10.3389/fphys.2019.01390

REVIEW ARTICLE

VOL. 45 | NO. 2 | **MAY - AUGUST 2024** | PP 35-61

Revista Mexicana de Ingeniería Biomédica

dx.doi.org/10.17488/RMIB.45.2.3

E-LOCATION ID: **1410**

Salvia rosmarinus Spenn. Main Applications and Ultrasonic Extraction of Secondary Metabolites: a General Review

Salvia rosmarinus Spenn. Principales Aplicaciones y Extracción Ultrasónica de Metabolitos Secundarios: una Revisión General

José Juan Cedillo-Portillo[1], *Wendy Yaneth Villastrigo-López*[1], *Adali Oliva Castañeda-Facio*[1], *Sandra Cecilia Esparza-González*[2], *Elia Martha Múzquiz-Ramos*[1], *Aidé Sáenz-Galindo*[1]

[1]Universidad Autónoma de Coahuila, Facultad de Ciencias Químicas - México

[2]Universidad Autónoma de Coahuila, Facultad de Odontología - México

ABSTRACT

This paper provides an overview of the various applications of the bioactive compounds found in *S. rosmarinus*. at present. Additionally, it explores emerging technologies for its extraction, such as ultrasound, which is an effective, fast, and sustainable technology for obtaining these secondary metabolites from this millenary plant. *S. rosmarinus* has gained considerable importance due to its beneficial properties, including antimicrobial, antioxidant, hepatoprotective, anti-inflammatory, and anticarcinogenic effects. These effects result from the different metabolites, which, without the use of ultrasound, are produced in *S. rosmarinus*. The main objective of this research is to provide an overview of some of the main applications in which *S. rosmarinus* is involved and to present a viable and effective alternative for the extraction of the different metabolites it contains using a technique such as ultrasound. The literature review was performed by searching for information on digital platforms such as SciFinder, PubMed, Scopus, and ScienceDirect, using keywords such as Rosemary, *S. rosmarinus*, ultrasound, green extraction, and secondary metabolite.

KEYWORDS: *S. rosmarinus*, emerging technologies, ultrasound

RESUMEN

En el presente trabajo se muestra un panorama general de las diversas aplicaciones que se tiene hoy en día de los compuestos bioactivos encontrados en *S. rosmarinus* así mismo, se toma en cuenta las tecnologías emergentes para su extracción como el ultrasonido, la cual es una tecnología eficaz, rápida y sustentable para la obtención de estos metabolitos secundarios a partir de esta planta milenaria, dicha planta ha generado una importancia considerable debido a las buenas propiedades que presenta como el efecto antimicrobiano, antioxidante, hepatoprotectora, antiinflamatorio y anticancerígeno, las cuales son productos de los diferentes metabolitos que sintetiza entre los cuales destaca el carnosol, ácido carnósico, rosmadial o rosmanol, ácido rosmarinico entre otros; logrando posicionarla en aplicaciones que van desde el área culinaria hasta aplicaciones dentro de la biomedicina. El objetivo principal de la presente investigación es brindar un panorama general de algunas de las principales aplicaciones en las que se ve involucrado el *S. rosmarinus* y así mismo, dar a conocer una alternativa viable y eficaz para la extracción de los diferentes metabolitos contenidos en este, mediante una técnica como el ultrasonido. La revisión literaria se hizo buscando información en algunas plataformas digitales como Sicfinder, PubMed, Scopus, SiencieDirect, utilizando palabras clave: Rosemary, *S. rosmarinus*, ultrasound, green extraction, secondary metabolite.

PALABRAS CLAVE: *S. rosmarinus*, tecnologías emergentes, ultrasonido

Corresponding author

TO: **Aidé Sáens-Galindo**
INSTITUTION: **Facultad de Ciencias Químicas, Univerdad Autónoma de Coahuila**
ADDRESS: **Blvd. Venustiano Carranza S/N, República Oriente, C.P. 25280, Saltillo, Coahuila, México.**
EMAIL: aidesaenz@uadec.edu.mx

Received:

22 November 2023

Accepted:

22 April 2024

INTRODUCTION

Since prehistoric times, human beings from different cultures have used plants as medicinal sources. Until the 19th century, physicians had used them as the main source of pain relief for their patients. Today, the World Health Organization estimates that about 80 % of people in developing countries still use traditional medicine. Medicinal plants have shown numerous unique and interesting pharmacological properties, including antimicrobial properties[1][2]. Plants synthesize a wide variety of metabolites to protect themselves and maintain homeostasis in their environment. Often, these secondary metabolites differ among plant species in their quantity, diversity, and biological activities[3].

Rosemary (*Rosmarinus officinalis* L. syn *Salvia rosmarinus* Spenn.) is a plant that grows wild in the Mediterranean basin. It is a perennial and aromatic plant belonging to the Lamiaceae family and recently merged with the genus *Salvia*, so it is now known as *Salvia Rosmarinus*[2][4]. It can reach 150 cm in height and is a lush, branched, and evergreen shrub. *S. rosmarinus* is traditionally used as a culinary species to modify or improve food flavors and other organoleptic properties. It is also used in traditional and folk medicine, being a highly valued medicinal herb. About 20 types or varieties of *S. rosmarinus* can be distinguished according to morphological descriptors; however, the infraspecific systematics are confusing and uncertain[5][6].

Currently, *S. rosmarinus* is one of the most important major sources of naturally occurring biologically active compounds in the functional food industry[7][8]. However, this plant possesses many pharmacological activities such as hepatoprotective, antimicrobial, antiulcerogenic, antidiabetic, diuretic, anti-inflammatory, anticarcinogenic, and antioxidant properties. Most of these activities are related to the phenolic content in this shrub. Significantly, the potent antioxidant activity is primarily due to phenolic diterpenes, such as carnosol, carnosic acid, rosmadial, or rosmanol, among others[9].

FIGURE 1. **Specimen of *S. rosmarinus.***

Botanical description

S. rosmarinus. taxonomic series No.: 32677 (ITIS, 2023), belongs to the Lamiaceae family, formerly called Labiatae, and is known by the popular name Rosemary in English, Alecrim in Portuguese, and Romero in Spanish. It is a xeromorphic shrub that grows spontaneously in stony places, sand, cliffs, and sea fences in different parts of the world, such as Europe, Africa, America, and Asia. The shrub is fragrant, with leaves characterized by being strongly curved, linear, and aromatic. The upper part of the leaf has a very intense green hue, while the lower area tends to be gray, with a width of about 4 cm, an average size between 1.0-2.5 cm long, and a thickness ranging from 1-3 mm. The flowers are small and arranged in axillary pauciflorus whorls, light blue, or lilac, both having an intense and fragrant aroma. This aroma is due to the volatile oil accumulated in various parts of the flower, such as the glandular trichomes, petals, and capitate. In Figure 1, the plant of *S. rosmarinus* is presented[10][11].

Chemical composition

The components that confer pharmacological properties to *S. rosmarinus* are classified into flavonoids, terpenoids (sesquiterpenes, triterpenes, diterpenes, monoterpenes), and hydroxycinnamic derivatives[9]. It has been reported that *S. rosmarinus* extracts contain about 24 % of volatile molecules belonging to terpenes, while in the non-volatile fraction, flavonoids appear along with non-volatile terpenoids and phenolic acids. Phytochemical studies have indicated that the concentration of non-volatile compounds varies between 1.8 % and 2.5 %, depending on the region. The predominant constituents are α-pinene, 1,8-cineole, limonene, camphor, and borneol. These differences arise due to the form of cultivation, the growing cycle, and the aging that the plant undergoes at the time of cutting[12][13].

On the other hand, among the most reported chemical compounds in *S. rosmarinus* extracts are rosmarinic acid (RA), chlorogenic acid, caffeic acid, ρ-coumaric acid, carnosic acid (CA), oleanolic acid, betulinic acid, ursolic acid, rosmanol, and carnosol (CR), among other di- and triterpenoids. In such a way, the most involved compounds in various investigations are CA, CR, and AR. This is because these chemical compounds are the main ones responsible for the medicinal activities of the extracts[5][14][15].

The chemical composition of the essential oil of S. rosmarinus has been described in a general way by various researchers who have reported the identification of various chemical molecules such as camphene, α-pinene, and β-pinene, as well as some terpenes like camphor, 1,8-cineole, verbinol, borneol, linalool, rosmanol, terpineol, carnosol, isorosmanol, α-amyrin, β-amyrin, and β-caryophyllene. Additionally, vanillic, chlorogenic, caffeic, ursolic, rosmarinic, carnosic, butylinic, oleanolic, betulinic acids are also identified and different chemical molecules such as botulin, bornyl acetate, 3-octanone, isobanyl-acetate[16].

The different fractions, both volatile and non-volatile, vary greatly depending on the plant due to various factors such as climatic changes, age, region of procurement, and season of the year. Similarly, the concentration of these compounds is not evenly distributed throughout the plant. For example, CA and CR can be found mainly in the photosynthetic tissues of the plant, such as sepals and petals. Several fractions are also significantly affected by the type of processing for the extraction of bioactive compounds. Therefore, the conditions for obtaining these bioactive compounds are crucial, including temperature, type of solvent or extracting agent, and time[9]. Figure 2 shows the structures of some of the chemical compounds present in *S. rosmarinus*.

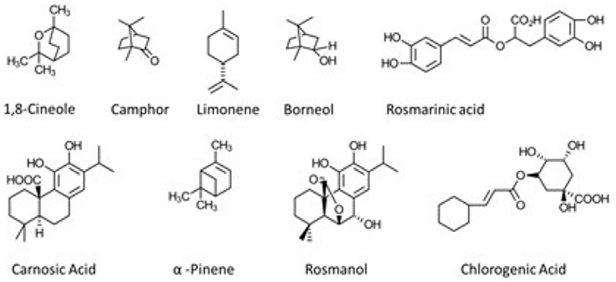

FIGURE 2. Structure of some of the chemical compounds present in *S. rosmarinus.*

Culinary uses

Generally, this plant finds use in Mediterranean cuisine as a condiment contributing flavor to food. The two fundamental ways in which fresh or dried leaves are utilized in the kitchen involve imparting a bitter, astringent, and highly aromatic flavor. Different preparations, such as pork, fish, meat, poultry, soups, stews, dressings, sauces, and various preserves, often see the addition of *S. rosmarinus*. Due to the drying of the leaves, some attributes, like the fresh aroma, are lost. However, the dried leaves gradually lose their quality of life, rendering them highly favorable for storage and transportation. This characteristic transforms them into a profitable product in the market. As a result, the *S. rosmarinus* plant has been employed in the food industry to enhance the shelf life of foods, add value, and improve their quality[14][15].

Food industry

Since ancient times, *S. rosmarinus* has maintained great popularity within the food industry because it contains several bioactive compounds that provide food with antioxidant activity. Some of the compounds responsible include rosmarinic acid, carnosic acid, carnosol, rosmariquinone, rosmanol, and rosmaridiphenol, which can undergo reactions with free radicals formed in oxidation processes. Nowadays, foods containing these types of compounds are of great interest because an increasing number of consumers are opting for foods containing natural antioxidants, considering them to be healthy or "non-chemical"[16][17].

In 2015, the extension of the shelf life and quality of refrigerated fillets of Nile tilapia (*Orechromis niloticus*) by immersing them in a methanolic extract of *S. rosmarinus* at 1.5 % was reported by Khalafalla *et al.*, The result was efficient antioxidant activity with a clear reduction in the value of TBA-RS (a reagent composed of 2-thiobarbituric acid and glacial acetic acid), prolonging the shelf life of these fillets for up to 9 days more than the control[18].

In 2016 in Portugal, a study was reported on the antimicrobial effect provided by the essential oil of *S. rosmarinus* and thyme in foods packaged using the Sous vide cook-chill (SVCC) technology. This technology is characterized by vacuum packaging of raw or partially prepared foods before pasteurization, followed by rapid cooling and storage below 3 °C. In 2016, Gouveia *et al.*, mentioned that at 2 °C, the samples containing thyme essential oil presented a reduction in the population of *L. monocytogenes*; however, it was lower than that observed in *S. rosmarinus* oil. Likewise, the latter managed to show inhibition towards *L. monocytogenes* at a temperature of 8 °C for up to a maximum of 14 days. Furthermore, they highlighted that this dangerous pathogen is found in some "Ready-to-eat" foods and depends on the number of additives present in the food, as well as the temperatures used for storage[19].

In 2016, the antimicrobial Activity against *C. perfringens* of six essential oils usually used as condiments in Brazil (rosemary, basil, marjoram, mint, thyme, and anise) was described by Radaelli. It was pointed out that the use of such oils from commonly employed spices clearly offers an alternative to chemical preservatives for the inactivation and control of pathogens in food. It was also reported that their results suggest that oxygenated compounds, especially monoterpenes and phenylpropanoids, may be responsible for carrying out the antimicrobial Activity. However, a synergistic effect of these chemical compounds with other constituents present in smaller amounts in the essential oil is also considered[20]. The main objective of this research is to provide an overview of *S. rosmarinus*, its main applications, and the implementation of ultrasound extraction for obtaining bioactive compounds present in this plant. This positions this technique as a green and alternative methodology for the extraction of phytochemical compounds.

MATERIALS AND METHODS

The present research was carried out based on a literature search in various databases such as: Scifinder, PubMed, Scopus, ScienceDirect, looking for articles related to *S. rosmarinus*. The search criteria were keywords such as: Rosemary, *S. rosmarinus*, ultrasound, green extraction, secondary metabolite.

RESULTS AND DISCUSSION

Bioactive compounds of plant origin

In nature, unlike animals, plants are stationary and are not exempt from aggressive environmental changes. They are also exposed to harmful microorganisms that become aggressive pathogens, insect pests, parasitic plants, and weeds. This is not to mention temperature changes, mineral and nutrient deficiencies, osmotic imbalance, and contamination by heavy metals. Therefore, plants have a wide range of cellular, molecular, and biochemical protective mechanisms. The metabolic pathways of plants synthesize two types of organic compounds of natural origin or metabolites: (i) primary plant metabolites (PPM), and (ii) secondary plant metabolites (SPM). PPM are produced in large quantities and are responsible for maintaining various vital processes in plants, such as photosynthesis, respiration, growth, and development. Some prominent PPMs include carbohydrates, lipids, proteins, and hormones. They also participate in the primary response by regulating these biomolecules against pathogen infection[12]

In contrast, SPM are produced in minimal quantities, however, they have fundamental functions in plant adaptation to unfavorable conditions. They include various groups of chemical compounds such as alkaloids, flavonoids, anthocyanins, lignans, quinones, peptides, phenols, terpenoids, and amines. These compounds are primarily used in some pesticides, agrochemicals, and food additives. Moreover, they are directly or indirectly related to taste, color, and aroma. Secondary metabolites are synthesized by various pathways in plants and are directly involved in the plant's defensive reaction to an external stimulus[13].

At present, about 200,000 secondary metabolites (MSPs) have been identified, which are divided into four main groups: terpenes, phenols, and nitrogen/sulfur-containing substances. The most important functions of secondary metabolites lie in plant protection[21]. In Figure 3, a classification of the four main groups of secondary metabolites in plants is presented. In Table 1. Main types of the most reported secondary metabolites in the literature for *S. rosmarinus*. as well as their biological activity are presented.

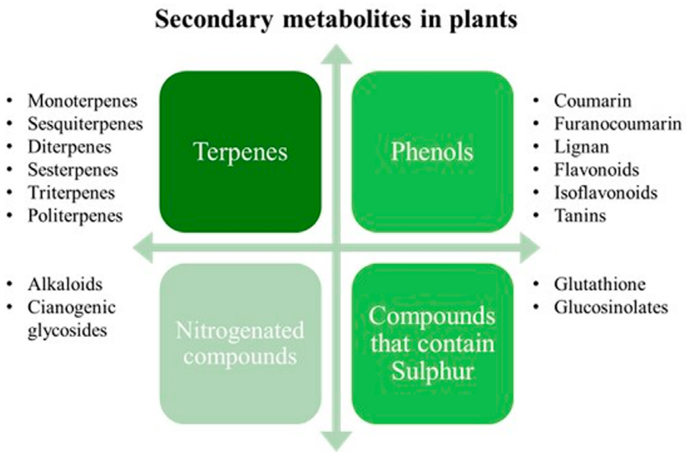

FIGURE 3. **Main types of secondary metabolites in plants.**

TABLE 1. **Secondary metabolites for *S. rosmarinus*.**

Structure	Compound	Biological Activity	Ref.
	1,8-cineole	Antimicrobial Activity, Proliferative and antioxidant activity	[22] [23] [24] [25]
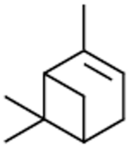	α-pinene	Antiproliferative Activity, Antimicrobial Activity, Antioxidant activity, Green pesticide and anticarcinogenic Activity	[26] [27] [23] [28] [29] [24]
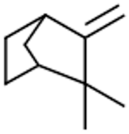	Camphene	Fumigant activity, Anticarcinogenic activity	[30] [31]
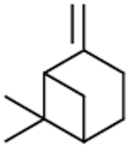	β-pinene	Antioxidant activity, Photoprotective activity, Insecticidal and repellent activity	[24] [29] [32]
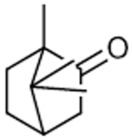	Camphor	Anticancer Activity, Antimicrobial Activity, Antimicrobial Activity, Antimicrobial Activity, Antioxidant activity, Food preservative	[33] [34]
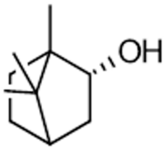	Borneo	Anticancer Activity, Antioxidant Activity, Anti-inflammatory Activity, Analgesic Activity	[35] [2]
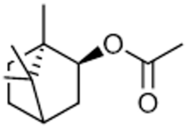	Bornyl acetate	Immunomodulatory Activity, Anti-inflammatory Activity, Sedative Activity	[36]
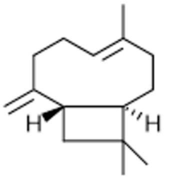	β-caryophyllene	Anticoccidial Activity, pesticide, Proliferative Activity, Activity against cardiac hypertrophy	[37] [38] [25]

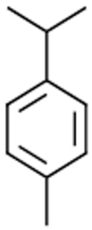	P-cymene	Antioxidant activity, Anti-inflammatory Activity, Antiparathyroid Activity, Antiproliferative Activity and Antidiabetic Activity.	[39]
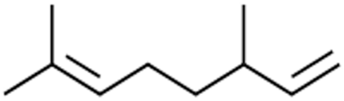	β-myrcene	Chemoprophylactic Activity	[40]
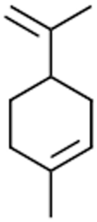	Limonene	Antiproliferative Activity, Photoprotective Activity, Anticancer activity, Anticancer activity, Antioxidant activity	[41] [32]
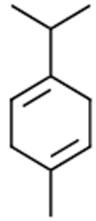	γ -terpinene	Antioxidant activity, Photoprotective Activity	[42] [32]
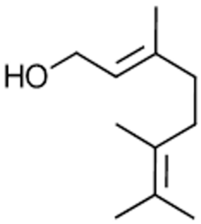	Geraniol	Bactericidal Activity, Antimicrobial Activity, Antimicrobial Activity, Fungicidal Activity, Anti-inflammatory Activity	[43]
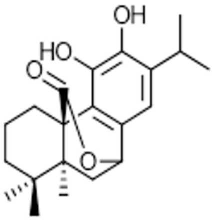	Carnosol	Anticarcinogenic, antimicrobial, antiinflammatory	[44] [45]
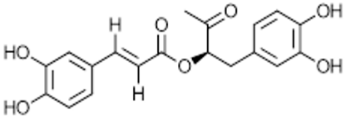	Rosmarinic Acid	Antioxidant, anti-inflammatory, anti-microbial	[46] [47] [48]
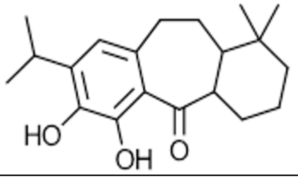	Rosmaridiphenol	Anti-tumor, anti-inflammatory, neuroprotective	[49]

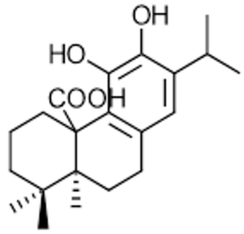	Carnosic acid	Antioxidant, anti-inflammatory, anti-microbial	[46] [47] [48] [50]
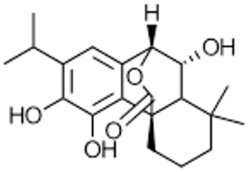	Isorosmanol	Antimicrobial, anti-inflammatory, anticarcinogenic	[51]
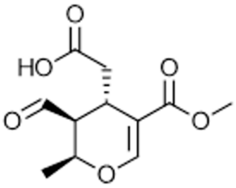	Elenolic acid	Antioxidant, anti-inflammatory, anti-microbial	[52]
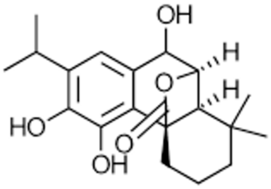	Rosmanol	Anticarcinogenic, antimicrobial, antiinflammatory	[53]
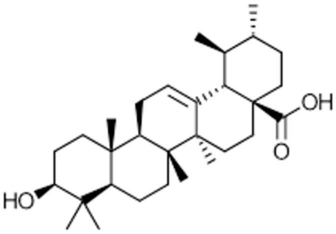	Ursolic acid	Antioxidant, anti-inflammatory, anticarcinogenic	[54]
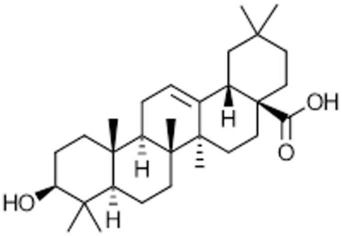	Oleanolic acid	Anti-tumor, anti-inflammatory, neuroprotective	[55]
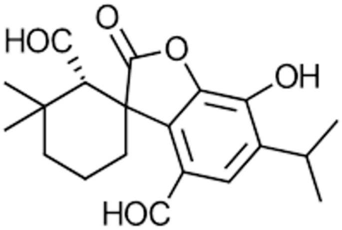	Rosmadial	Antioxidant, anti-inflammatory, anti-microbial	[56] [57] [48]
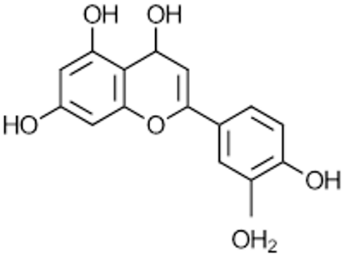	Luteolin	Antioxidant, anti-inflammatory, anticarcinogenic	[56]

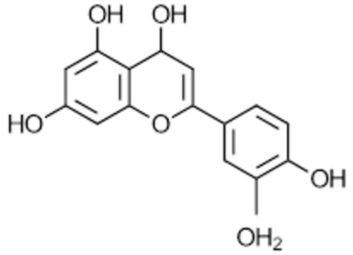	Luteolin	Antioxidant, anti-inflammatory, anticarcinogenic	[56]
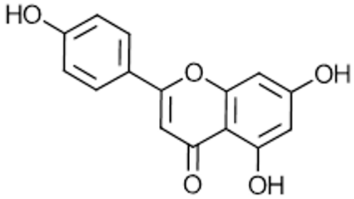	Apigenin	Anticarcinogenic, antimicrobial, antiinflammatory	[56]
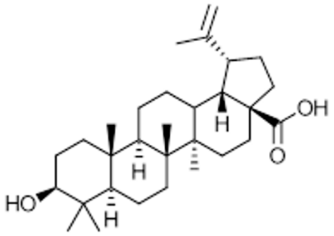	Betulinic acid	Anti-tumor, anti-inflammatory, neuroprotective	[58] [59]
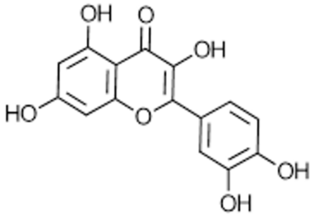	Quercetin	Anticarcinogenic, antimicrobial, antiinflammatory	[60] [61]
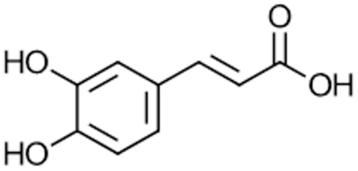	Caffeic acid	Anticarcinogenic, antimicrobial, antiinflammatory	[46] [57]
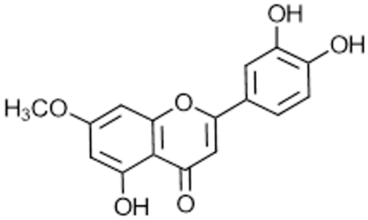	Genkwanin	Antioxidant, anti-inflammatory, anticarcinogenic	[56]
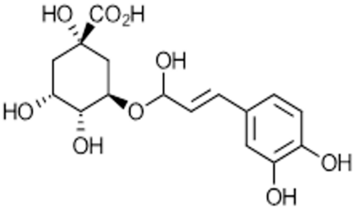	Colorogenic acid	Anticarcinogenic, antimicrobial, anti-inflammatory,	[62] [63]
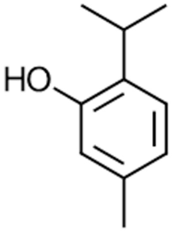	Thymol	Antioxidant, antimicrobial, anti-inflammatory, anticarcinogenic	[64]

Anticarcinogenic activity

The constitution of the human diet is one of the most substantial factors influencing the risk of developing cancer; the components of the diet can contribute either positively or negatively to the likelihood of contracting such a condition. Chemoprevention is the long-term pharmacological control of the risk of cancer, for which a myriad of plants and their components have been analyzed for their potential anticarcinogenic Activity. Around 60 % of the drugs used today in cancer treatment are derived from natural products[65][66].

As is well known, the *S. rosmarinus* plant exhibits significant antioxidant activity, inhibiting genotoxicity and providing protection against carcinogens or toxic agents. However, the side effects of therapeutic methods largely hinder their effectiveness, increasing the demand for new research on more efficient methods and treatments in the fight against cancer[67].

Polyphenols are chemical compounds capable of inducing cell differentiation and modulating growth, causing interference in tumor development and progression. Since *S. rosmarinus* is rich in various phenolic compounds, numerous studies focus on the anticarcinogenic Activity that this plant may exhibit. Some diterpenic polyphenols, such as carnosol and carnosic acid, are chemical compounds present in the dried leaves of *S. rosmarinus* at a 5 % concentration. It is reported that these compounds are largely responsible for the anticarcinogenic Activity[25][68].

Antioxidant capacity

Natural plant-derived antioxidants are becoming increasingly important, not only around food preservation and stability but also in preventive medicine. The Lamiaceae family has been highly relevant in research on antioxidant compounds, thanks to the high concentration of polyphenols. Antioxidants play a crucial role in the prevention and treatment of diseases associated with oxidative damage, such as cancer, cardiovascular diseases, and neurodegenerative diseases. Free radicals, reactive oxygen species, and hydrogen peroxide are inevitably produced by living organisms in metabolic processes. Continuous exposure to free radicals causes functional and structural damage, such as aging and cell death[69].

The antioxidant capacity of *S. rosmarinus* is due to the phenolic compounds present in the plant, which can inhibit the production of reactive species. The accumulation of these species has a negative effect on various organs and even systems of the human body[70]. Various studies have demonstrated that this property is directly related to the concentration of phenolic diterpenes. However, the content of these antioxidant molecules depends on different factors, including seasonal variations, environmental influences, species, origin, and plant growth. As mentioned earlier, antioxidants are chemical compounds that can inhibit and delay the oxidation of different lipids and biomolecules. They prevent the initiation of a chain reaction by radicals or propagation, which can cause functional damage in the human body, such as cancer or cardiovascular diseases. An antioxidant can prevent such processes due to its redox properties, such as hydrogen donation, reducing behavior, or quenching of singlet molecular oxygen[71][72].

In 2008, Wang *et al.*, examined the in vitro antioxidant activity of the essential oil of *S. rosmarinus* obtained through steam distillation, compared to three of its main components (α-pinene, 1,8-cineole, β-pinene). The oil and components were subjected to evaluation of their antioxidant activity using the 2,2-diphenyl-1-picrylhydrazyl (DPPH) assay, with ascorbic acid used as a positive control. The inhibition percentages of the radical were 62.45 %, 42.7 %, 45.61 %, and 46.21 % for the essential oil of *S. rosmarinus*, α-pinene, 1,8-cineole, and β-pinene, respectively. In general, the essential oil showed higher antioxidant activity than its components[73].

In 2015, Chen *et al.*, used the ABTS (2,2'-azino-bis-(3-ethylbenzothiazoline-6-sulfonic acid)) and FRAP (ferric ion reduction) techniques to assess the antioxidant activity of aqueous extracts of *S. rosmarinus*[72]. In 2023, Perales and collaborators demonstrated the antioxidant capacity of *S. rosmarinus* using the DPPH technique. The plant was collected from Iturbide, Nuevo León. They obtained the extracts through ultrasound-assisted maceration at 40 KHz for 60 minutes at room temperature, with a ratio of 1:12.5, solid: liquid. Antioxidant capacity was measured at 519 nm using a spectrophotometer, and ascorbic acid was used as a positive control. Subsequently, serial dilutions were performed, and the extracts were evaluated in triplicate. The authors successfully demonstrated an antioxidant capacity of 31.653 (IC50(μg/mL)), even higher than that of the ascorbic acid control[68].

Antioxidant capacity

Most plants produce secondary metabolites with antimicrobial Activity in response to the attack of pathogens or their normal course of growth and development. The increasing use of essential oils or aqueous extracts represents a new way to combat the proliferation of microorganisms. The escalating use of antibiotics in medicine, agriculture, and livestock has contributed to the growing resistance of various microorganisms to drugs. Drug resistance has been categorized as a global health problem, prompting an increasing number of researchers to delve into the investigation of new bioactive antimicrobial compounds. Several studies have examined the antimicrobial capacity of the *S. rosmarinus* plant against a broad spectrum of gram-positive bacteria (*S. aureus, S. pyogenes, S. pneumoniae*) and gram-negative bacteria (*E. coli, S. typhi*)[74][75].

Its antimicrobial Activity is primarily attributed to carnosol, carnosic acid, and rosmarinic acid. *S. rosmarinus* extracts have bioactive properties and antimicrobial Activity, stimulating anticarcinogenic Activity and phagocytosis by inactivating adhesins, enzymes, and transport proteins in bacteria. Flavonoids tend to form soluble protein complexes in the bacterial wall, which destroy it in response to microbial infection. On the other hand, essential oils exhibit antiseptic and antimicrobial capabilities attributed to bioactive compounds present in this plant, such as camphor, α-pinene, 1,8-cineole, eucalyptol, verbenone, limonene, borneol, and camphene. The mechanism of action of diterpenes involves lysing the bacterial cell membrane due to their lipophilic compounds, including some triterpene alcohols like alpha and beta-amyrin, as well as acids such as oleanolic acid and ursolic acid[76].

The *S. rosmarinus* extract acts at the cellular membrane level, increasing permeability and causing distortion of the cell wall in both Gram-positive (*S. aureus*) and Gram-negative (*E. coli*) bacteria. The following are descriptions of some in vitro studies demonstrating the antimicrobial capacity of the *S. rosmarinus* plant. In 2010, Castaño *et al.*, demonstrated the antimicrobial activity of the essential oil and ethanolic extract of *S. rosmarinus*, obtained through steam distillation and maceration, respectively, against Gram-positive and Gram-negative bacteria, including *S. aureus, E. coli, S. sonnei, S. typhimurium, P. aeruginosa,* and *L. monocytogenes,* using the minimum inhibitory concentration (MIC) technique through microdilution colorimetry in broth. For the ethanolic extract, they subjected dried *S. rosmarinus* leaves to 95 % ethanol for 48 hours, followed by preconcentration using a rotary evaporator and finally lyophilization. Meanwhile, for the oil, dehydrated leaves were used, and the oil was obtained by steam distillation. The inoculum was obtained from an exponentially growing culture, and an aliquot of the inoculum was adjusted to 0.5 McFarland (1.5 x 108 CFU/mL). The essential oil exhibited antimicrobial Activity against a wide variety of Gram-positive and Gram-negative bacteria. The growth inhibition of Escherichia coli was achieved at a concentration of 4096 ppm, while for *Shigella sonnei* and *Staphylococcus aureus*, it was at 512 ppm. On the other hand, in the ethanolic extract, concentrations of 1024 ppm were obtained for S. *sonnei, S. typhimurium,* and *L. monocytogenes*. Greater sensitivity was observed in Gram-negative bacteria compared to Gram-positive ones, and the compound with the broadest inhibition spectrum was the essential oil, attributed to increased permeability and changes in the structure of the cell membrane[77].

Solano and Zambrano, in 2016, demonstrated the inhibition of the oil and aqueous phase extracts of *S. rosmarinus* against *S. mutans*. They used dried leaves of *S. rosmarinus,* which were macerated with distilled water for three days with continuous agitation at room temperature. Subsequently, the extract was filtered, and the water was evaporated for 18 hours at 70 °C. On the other hand, the oily extract was obtained through steam distillation. To establish the concentration of the extracts, the broth dilution method was performed to obtain the minimum bactericidal concentration (MBC). They observed that the aqueous extracts showed no inhibition against *Streptococcus mutans,* while the oily extracts exhibited inhibitions of 11.93 mm[78].

Montero *et al.*, in 2017, demonstrated the antimicrobial Activity of the oily extract of the *S. rosmarinus* plant against *E. coli,* obtaining inhibition zones of 10.90 mm at a concentration of 80 %[79].

On the other hand, Karadag *et al.*, in 2019, for the antimicrobial tests, ground *S. rosmarinus* leaves with methanol for 24 hours, filtered and evaporated, to obtain subfractions. These subfractions were prepared using liquid-liquid extraction with hexane and ethyl acetate, respectively. These authors demonstrated that the hexane fractions are susceptible to *S. aureus*, obtaining a minimum bactericidal concentration of 500 µg/mL[2].

Pharmacological and therapeutic studies

Medications and plant-based treatments for the management of various diseases are complementary approaches in medicine due to their few side effects[80]. Filiptsova *et al.*, in 2018, conducted a study to observe the effects of lavender and *S. rosmarinus* essential oils, obtained through steam distillation, on short-term human memory. They obtained the oils using steam distillation. The study involved 79 high school students (34 boys and 45 girls) aged 13 to 17 years, residing in the Ukrainian metropolis. Participants were divided into 3 groups: the control group (not exposed to any oil), the group sprayed with lavender oil, and the *S. rosmarinus* group. A standard Petri dish was placed in each corner of the room, filled from the bottom with tap water at room temperature in a volume of 15 mL, and 10 drops of each essential oil were added. Statistically significant differences were found in the short-term memory productivity of participants in different groups. Therefore, *S. rosmarinus* and lavender essential oils significantly increased image memory compared to the control group. Inhalation of *S. rosmarinus* essential oil increased the memorization of numbers, while inhalation of lavender oil weakened the process[81].

El-Desouky *et al.*, in 2019, demonstrated the nephroprotective effect of green tea extract (GTE), rosmarinic acid (RA), and *S. rosmarinus* (RE) on acute renal toxicity initiated by N-nitrosodiethylamine (DEN) and promoted by ferric nitrilotriacetate (Fe-NTA) in Wistar rats. *S. rosmarinus* extract countered the initiation of diethylnitrosamine and ferric nitriloacetate-induced nephrotoxicity in rats. Rats were classified into 5 groups: Group 1 included healthy rats, Group 2 received DEN+Fe-NTA, Group 3 received 200 mg/kg body weight of RE-DEN-Fe-NTA, Group 4 received 1 g/kg of GTE-DEN-Fe-NTA, and Group 5 received 50 mg/kg of RA+DEN+Fe-NTA. RE, GTE and RA were administered orally for 14 days before a single intraperitoneal administration of DEN (160 mg/kg) until the end of the experiment. Eighteen days after DEN, a single intraperitoneal dose of Fe-NTA (5 mg Fe/kg) was administered to promote nephrotoxicity in rats. The kidneys of each group were histopathologically examined at intervals. GTE, RA, and RE exerted a protective effect against renal toxicity, with GTE showing a more pronounced effect on renal function parameters, while RA showed the best protective results[82].

Jaglanian and Tsiani, in 2020, demonstrated the inhibition of proliferation and survival of prostate cancer cells by acting on Akt (protein kinase B) and mTOR (protein). They used a methanolic extract of *S. rosmarinus* obtained using an ultrasonic probe. They found a significant inhibition of survival and proliferation of androgen-sensitive PC-3 prostate cancer cells, while normal prostatic epithelial cells PNT1A were not affected. Furthermore, treatment with *S. rosmarinus* induced apoptosis and reduced the migration of PC-3 prostate cancer cells[8].

Makaremi *et al.*, in 2021, inhibited tumor growth in mice with colorectal cancer CT-26 using alcoholic extracts of *S. rosmarinus* obtained through ultrasound-assisted extraction. These authors conducted the measurement of cell cytotoxicity through the MTT colorimetric assay, showing a concentration-dependent increase in cytotoxicity in the CT-26 cell group. Cell treatment with half the inhibitory concentration (IC50) of *S. rosmarinus*, turmeric, and the combination induced apoptosis. In vivo studies revealed that the combined treatment (*S. rosmarinus* with turmeric) inhibited tumor growth in mice transplanted with CT-26 cells without side effects, such as weight loss or renal and hepatic functional changes. Additionally, mice treated with the plant mixture exhibited a significant increase in the proportion of cytotoxic T lymphocytes. In conclusion, the results showed that the combination of *S. rosmarinus* with turmeric has the potential to inhibit the growth of the CT-26 cancer cell line, reducing tumor growth in mice with colorectal cancer[83].

Cytotoxicity of *S. rosmarinus*

It has been reported that the main bioactive compounds contained in the plant, such as rosmarinic acid (RA), chlorogenic, caffeic, and ρ-coumaric acids, carnosic acid (CA), oleanolic acid, betulinic acid, ursolic acid, rosmanol, and carnosol (CR), exhibit no toxicity. However, some individuals sensitive to the bioactive compounds in this plant may experience allergies or contact dermatitis. Similarly, the use of this plant is not recommended for individuals with conditions such as gallstones without prior consultation with a doctor. While intoxication from *S. rosmarinus* infusions is not common, an overdose could lead to consequences such as vomiting, hemorrhages, uterine gastroenteritis, renal irritation, and abdominal spasms. Regarding the essential oil of *S. rosmarinus*, in much higher concentrations, it can be toxic to the central nervous system and may induce seizures[5][84].

Extraction technologies

In recent years, a wide variety of methods have been used for obtaining bioactive compounds from different plants, such as conventional heating extraction, aqueous alkaline extraction, solid-liquid extraction, extraction with conventional or traditional solvents, extraction with vegetable oils, and extraction using emerging technologies such as microwave and ultrasound, among others. However, extraction methodologies that are more environmentally friendly and do not compromise bioactive compounds during the extraction process have been preferred[85]. To achieve this, a possible solution could involve the use of emerging techniques and the implementation of green solvents. Table 2 shows the advantages and disadvantages of conventional methods compared to ultrasound.

TABLE 2. **Advantages and disadvantages of conventional methods compared to ultrasound.**

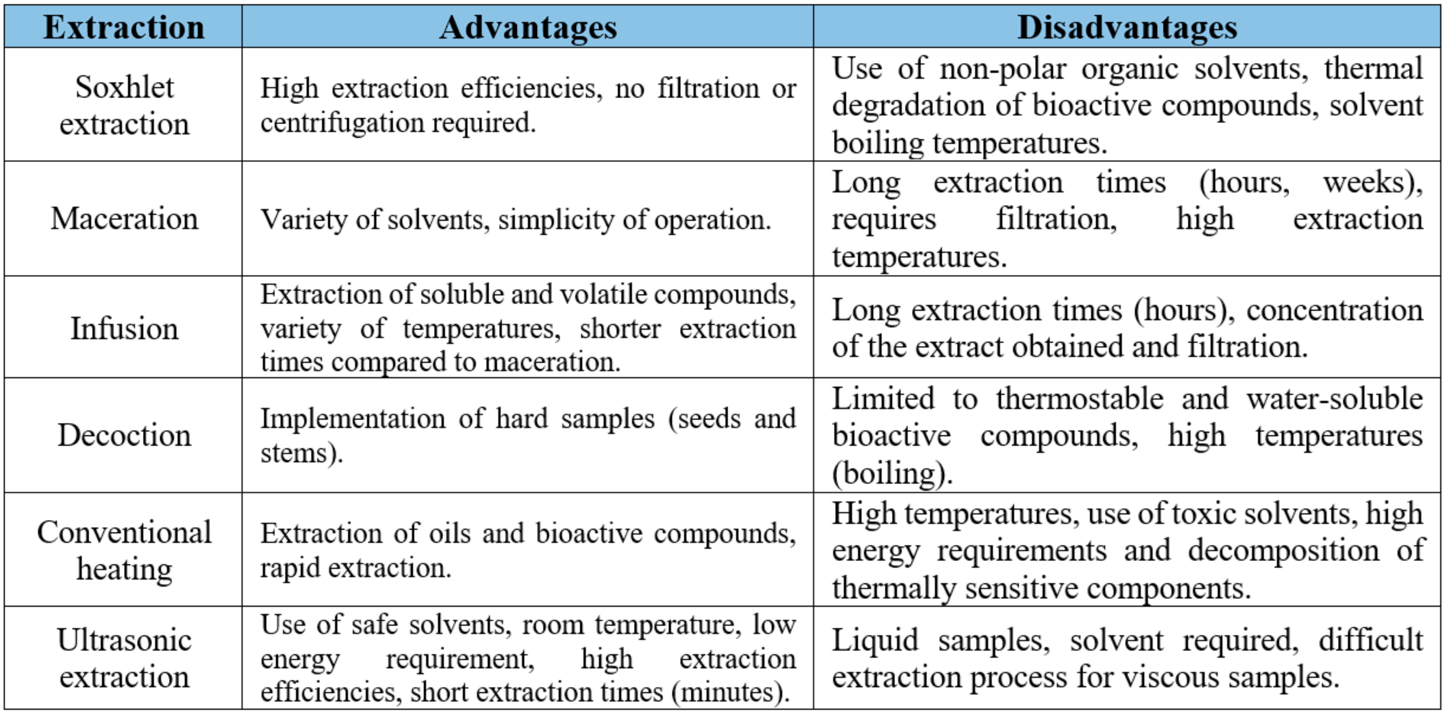

Extraction	Advantages	Disadvantages
Soxhlet extraction	High extraction efficiencies, no filtration or centrifugation required.	Use of non-polar organic solvents, thermal degradation of bioactive compounds, solvent boiling temperatures.
Maceration	Variety of solvents, simplicity of operation.	Long extraction times (hours, weeks), requires filtration, high extraction temperatures.
Infusion	Extraction of soluble and volatile compounds, variety of temperatures, shorter extraction times compared to maceration.	Long extraction times (hours), concentration of the extract obtained and filtration.
Decoction	Implementation of hard samples (seeds and stems).	Limited to thermostable and water-soluble bioactive compounds, high temperatures (boiling).
Conventional heating	Extraction of oils and bioactive compounds, rapid extraction.	High temperatures, use of toxic solvents, high energy requirements and decomposition of thermally sensitive components.
Ultrasonic extraction	Use of safe solvents, room temperature, low energy requirement, high extraction efficiencies, short extraction times (minutes).	Liquid samples, solvent required, difficult extraction process for viscous samples.

The extraction of bioactive and phytochemical compounds from plants is relevant due to the range of applications in the therapeutic, pharmaceutical, and food industries. This leads to the search for more efficient techniques that aid in the extraction of purer compounds with higher extraction yields. Several factors have been reported to limit or favor extraction techniques, such as the source or raw material, temperature, and solvent used. The current interest is in developing efficient and environmentally friendly techniques. Therefore, there is a notable focus on green or emerging techniques, including ultrasound-assisted extractions, supercritical fluids, pressurized liquids, microwaves, and cold plasma. These techniques, whether used individually or in combination, offer significant advantages over conventional methods, such as reducing high concentrations of solvents, shorter extraction times, lower temperatures, and higher quantitative and qualitative yields[86][87]. As described by Chemat, "Green extraction is based on extraction methodologies and processes that reduce energy consumption, allow the use of alternative solvents, and produce renewable natural products, ensuring a safe and high-quality extract or product."[88], Ultrasound extraction addresses some of the limitations of conventional techniques and incorporates key points of "green extraction"[89].

Ultrasound

Richards and Loomis first studied the effects of ultrasound in 1927, successfully solubilizing dimethyl sulfate in an alkaline solution. The case was forgotten for about 60 years; however, around the 1980s, sonochemistry experienced a revival and was highly implemented in different areas. Most modern devices rely on transducers (converters of electrical or mechanical energy into sound energy) for the generation of ultrasonic energy, which are made up of piezoelectric materials. If ultrasound is applied to a system, chemical changes can occur due to the generation and implosion of cavitation bubbles[90][91].

The cavitation phenomenon was first identified and reported in 1895 by Thorneycroft and Barnaby. It is based on the formation of cavitation bubbles, which grow until they collapse due to the pressure formed by their surroundings, as shown in Figure 4. Cavitation bubbles generate local heating and high pressure, known as a hot spot[92].

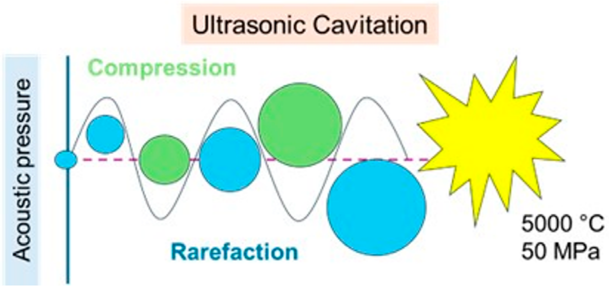

FIGURE 4. **Process of ultrasonic cavitation.**

Ultrasound is defined as sound of high frequency, which is above the limit at which the human ear can respond. The range of human hearing is generally considered to be between 16 Hz and 18 kHz, while ultrasound is typically considered to have frequencies between 20 kHz and 100 MHz. Sonochemistry usually operates in the range of around 20 to 40 kHz, although current sonochemical research explores broader ranges[93].

The ultrasound equipment was designed based on a piezoelectric transducer to treat solid materials in a liquid medium, such as ultrasound baths and ultrasound probes, as shown in Figure 5. Ultrasound baths have been widely used in industries for cleaning and extracting bioactive compounds, such as in the pharmaceutical, cosmetic, and ornamental industries. They consist of a transducer, a tank, a timer probe, and a heater. Indirect sonication is more effective as it is non-invasive, does not affect the degradation of bioactive compounds, and eliminates foam formation. On the other hand, direct sonication using an ultrasound probe is the most commonly used method, as it directly transfers ultrasound intensity to the sample, resulting in higher extraction efficiency and significantly reducing the time compared to the bath[94][95].

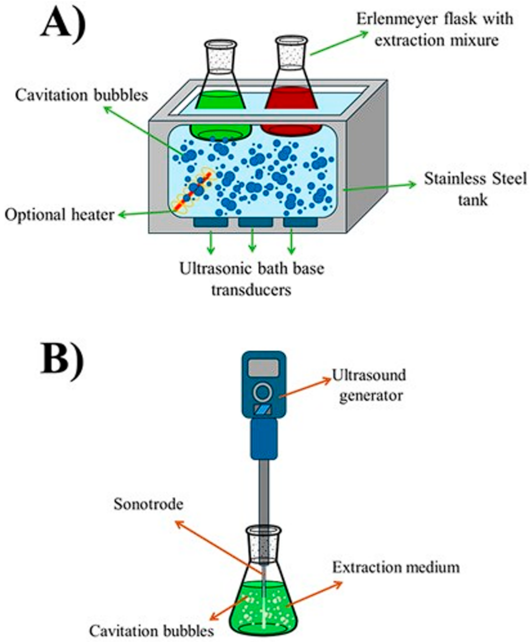

FIGURE 5. **Ultrasonic bath (A) and ultrasonic probe (B)**

Some of the most important factors to consider when implementing this technique for the extraction of bioactive compounds include considering the equipment's power, also expressed as the percentage of amplitude ranging from 0 to 100 %. This amplitude is linear to power. It has been reported that the power used for each selected plant sample depends entirely on the type of sample. However, working with powers in the range of 20 to 70 W and amplitudes of 30 to 80 %, the extraction yield increases with the increase in power and subsequently decreases after reaching a peak. This is explained by the increase in violent cavitation effects, which increases with the power. The size of the resonant bubble is directly proportional to the power, and as it increases, the size of the bubble and its implosion also intensify. This leads to greater sample fragmentation, pore formation, and higher extraction yields[96].

Other factors to consider include the equipment frequency, duty cycles, relaxation, extraction time, as well as the solvent-solid ratio and temperature. However, these factors show a trend where, as time, solvent-solid ratio, or frequency increases, the extraction percentages also increase until reaching a peak, after which they start to decrease. Therefore, optimal extraction design by varying these factors is important to obtain good extraction yields, which directly depend on the type of material used[97][98]. In addition to selecting the appropriate parameters for extraction, it is crucial to consider energy consumption. Ultrasound equipment requires electrical energy for operation. Taking this into account, it is essential to measure the energy consumption during extraction. Nowadays, some researchers use a wattmeter to calculate energy expenditure. These calculations are based on the assumption that 1 kWh of energy generates 800 g of CO_2 during the combustion of fossil fuels, which is released into the atmosphere[99].

The choice of the appropriate solvent for the extraction of bioactive compounds depends on physical properties such as surface tension, viscosity, and vapor pressure. These physical characteristics of solvents directly affect the cavitation phenomenon. Cavitation has been observed in solvents with high vapor pressure, low viscosity, and low surface tension. However, high cavitation intensity has also been observed in solvents with low vapor pressure, high viscosity, and high surface tension. Various solvents have been used for the extraction of bioactive compounds, with the most popular ones being methanol, ethanol, and different water ratios. Currently, there is an increasing focus on research into the implementation of deep eutectic solvents, particularly environmentally friendly ones[94]. Table 3 shows the main parameters governing the extraction of bioactive compounds.

The advantages derived from the use of extracts and the growing interest in research have led to the development of various technologies that can enable better extraction without compromising the final product. One emerging technology that has shown substantial advantages over traditional maceration, conventional heating, and Soxhlet extraction is the use of ultrasound-assisted extraction, which is characterized as a high-efficiency, low-cost, environmentally friendly extraction method with flexibility to integrate with other treatment processes[100].

TABLE 3. **Advantages and disadvantages of conventional methods compared to ultrasound.**

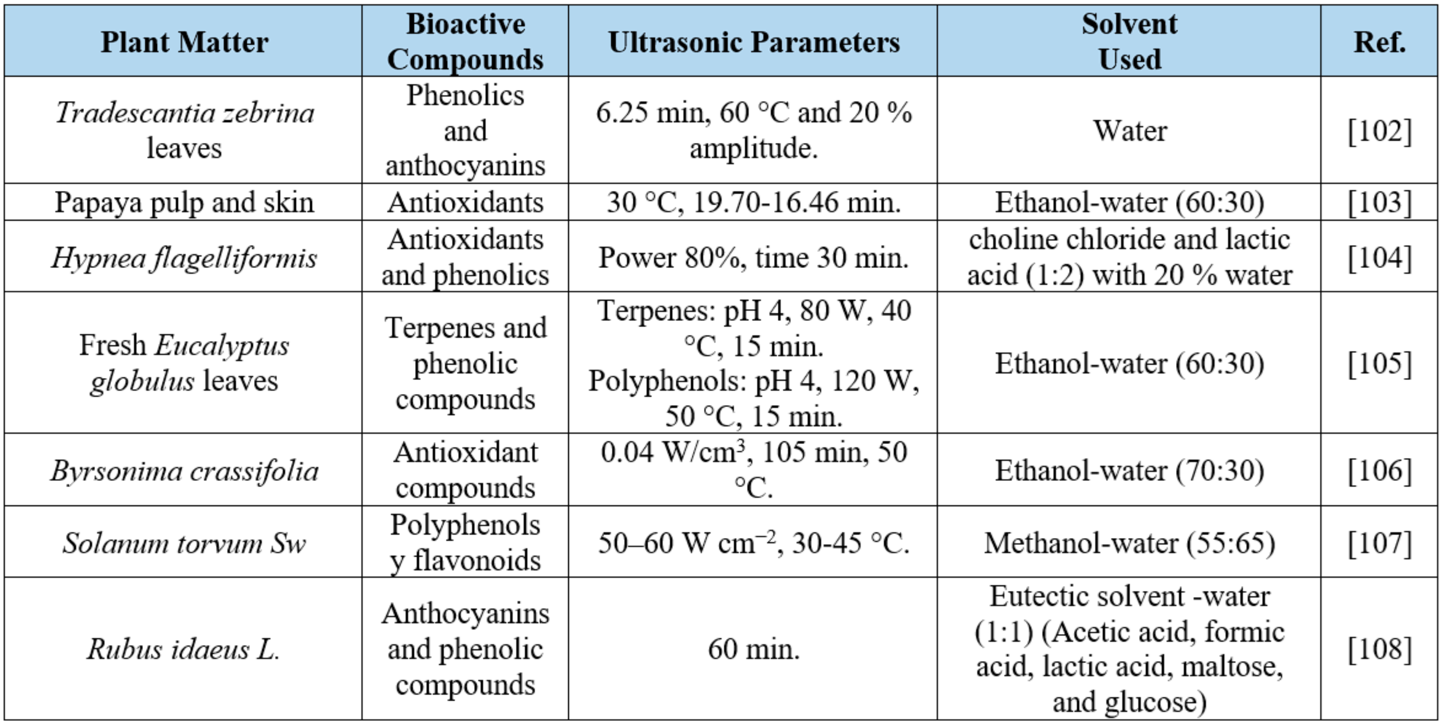

Plant Matter	Bioactive Compounds	Ultrasonic Parameters	Solvent Used	Ref.
Tradescantia zebrina leaves	Phenolics and anthocyanins	6.25 min, 60 °C and 20 % amplitude.	Water	[102]
Papaya pulp and skin	Antioxidants	30 °C, 19.70-16.46 min.	Ethanol-water (60:30)	[103]
Hypnea flagelliformis	Antioxidants and phenolics	Power 80%, time 30 min.	choline chloride and lactic acid (1:2) with 20 % water	[104]
Fresh *Eucalyptus globulus* leaves	Terpenes and phenolic compounds	Terpenes: pH 4, 80 W, 40 °C, 15 min. Polyphenols: pH 4, 120 W, 50 °C, 15 min.	Ethanol-water (60:30)	[105]
Byrsonima crassifolia	Antioxidant compounds	0.04 W/cm^3, 105 min, 50 °C.	Ethanol-water (70:30)	[106]
Solanum torvum Sw	Polyphenols y flavonoids	50–60 W cm^{-2}, 30-45 °C.	Methanol-water (55:65)	[107]
Rubus idaeus L.	Anthocyanins and phenolic compounds	60 min.	Eutectic solvent -water (1:1) (Acetic acid, formic acid, lactic acid, maltose, and glucose)	[108]

Extraction of bioactive compounds using ultrasound

Ultrasound-assisted extraction is carried out by creating cavitation bubbles that generate thermal and mechanical points within plant cells, as show in Figure 6. This leads to the rupture of the cell wall and the release of bioactive compounds into a solvent through diffusion. The extraction mechanism involves unique and combined mechanisms such as cellular alteration and mass transfer. It has been reported that the cavitation phenomenon creates pores, microchannels, and cavities in plant material, facilitating the penetration of solvent molecules and promoting extraction. Additionally, studies indicate that wet plant material is more effective. On the other hand, research suggests that 20 kHz ultrasound can break hydrogen bond and glycosidic linkages, change amide functional groups to carboxyls, and enhance extraction[101].

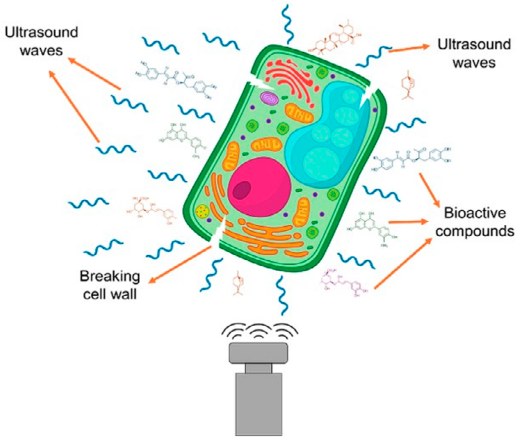

FIGURE 6. **Breaking cell wall by ultrasound waves.**

Albu *et al.*, in 2004, reported the use of ultrasound to improve the extraction processes of carnosic acid from *S. rosmarinus* using butanone, ethyl acetate, and ethanol as solvents, both from dry and fresh leaves. They found that sonication improved the yields of carnosic acid for all three solvents and shortened the extraction times. They also mentioned that sonication improved the choice of less aggressive solvents, such as ethanol, because ethanol is a poor solvent under conventional conditions (high pressures and temperatures) and achieved a similar extraction efficiency compared to the other two solvents used. Extraction from dry herb with ethanol proved to be more efficient than that from fresh material, which they attributed to the water present in fresh leaves[109].

On the other hand, Paniwnyk *et al.*, in 2009, studied the effect of ultrasound on the extraction of antioxidants from *S. rosmarinus* using solvents compared to conventional heating. They found that ultrasound provides more efficient extraction by increasing the extraction by 66 % of rosmarinic acid (mg/g) at temperatures of 35 °C and with less dependence on the extraction solvent used compared to the conventional heating method. They also reported that the application of this technique is possible for the extraction of bioactive compounds with antioxidant activity[110].

In 2016, a study was conducted on the antioxidant activity and rosmarinic acid content in ethanolic extracts of six medicinal plants (*L. angustifolia, H. perforatum, S. officinalis, M. sylvestris, M. officinalis, S. rosmarinus*) using ultrasound technique with a frequency of 35 kHz for 15 minutes. The study reported that all plants showed antioxidant activity greater than 70 % (0.1 g/ml), except for L. angustifolia and M. sylvestris. They also reported that all plants contain rosmarinic acid. In conclusion, they found that ultrasound is a fast and effective technique for preserving antioxidant activity and rosmarinic acid content in a matter of minutes[111].

Zhong *et al.*, in 2021, reported the extraction of polar extracts from *S. rosmarinus* using ethanol. They found two new compounds and six already known compounds, with most of the isolated compounds showing significant antimicrobial properties, with minimum concentration values ranging from 2 to 128 μg/mL. However, these inhibitions were weaker than those obtained with the polar fraction. Additionally, the polar fraction was reported as a promising food additive due to its higher antimicrobial activity than the essential oil[112]. Table 4 shows some references of extraction of bioactive compounds from *S. rosmarinus*. using ultrasound as an extraction method.

TABLE 4. **Advantages and disadvantages of conventional methods compared to ultrasound.**

Plant Matter	Bioactive Compounds	Extraction efficiency	Results	Ref.
S. rosmarinus	Carnosic acid and rosmarinic acid	24.0 ± 0.3 $mg_{CA}*g^{-1}_{Biomass}$ 8.4 ± 0.3 $mg_{RA}*g^{-1}_{Biomass}$	Ultrasonic extraction is more effective in only 10 min compared to 48 h of agitation.	[113]
S. rosmarinus	Rosmarinic acid	Extraction yield 6.10 %	The best extraction yield was obtained with a natural deep eutectic solvent.	[114]
S. rosmarinus	Rosmarinic acid and carnosol	C: 5.61 ± 1.96 mg/g RA: 3.61 ± 0.94 mg/g	A yield increase of 11 % was obtained with eutectic solvents compared to organic solvents.	[115]
S. rosmarinus	Rosmarinic acid and carnosol	Extraction yield 13.73 % and C+CA 17.63 mg/100g	High C+CA concentrations were obtained with short extraction times (10 min) and relatively low temperatures (30 °C).	[116]
M. officinalis	Rosmarinic acid	86.3 ± 4.1 mgRA/gplantaseca	The ultrasound technique proved to be more efficient than microwave and conventional heating, in addition to reducing the extraction temperature and time.	[117]
S. rosmarinus	Ursolic acid and carnosic acid	Extraction yield 18.8 ± 2.2 % CA: 15.4 ± 0.0 mg/grosmary UA: 35.3 ± 0.0 mg/grosmary	The ultrasound technique proves to be more efficient than Conventional Solvent Extraction, Controlled Instant Pressure Drop Deodorization, Pressurized Liquid Extraction, Microwaves, Subcritical Extraction with Water, Supercritical Fluid Extraction, and Ionic Liquids. Additionally, it is the technique with the lowest carbon emissions and the lowest energy consumption.	[118]
S. rosmarinus	Flavonoids and rosmarinic acid	Extraction yield 22 % F:10.3 mg/g RA: 4.8 mg/g	The ultrasound technique proved to be the most suitable for the extraction of bioactive compounds compared to the microwave technique and conventional methods.	[119]
P. scutellarioides	Rosmarinic Acid	118 mg/g	The best extraction conditions were obtained using ultrasound for a duration of 45 minutes and a frequency of 30 kHz.	[120]
S. rosmarinus	Carnosic acid and rosmarinic acid	Extraction yield 100 %	It was demonstrated that the proposed approach has higher efficiency, a shorter extraction time, and is a new alternative for the extraction of carnosic acid and rosmarinic acid compared to traditional reference methods, in addition to the use of ionic liquids.	[121]
S. officinalis	Carnosic acid and carnosol	CA:147.5 mg/100g C:42.7 mg/100g	They report ultrasound-assisted extraction as a green, simple, and safe technique for extracting bioactive compounds. They also report higher concentrations of analytes compared to the maceration technique.	[122]
S. rosmarinus	Carnosic and rosmarinic acids	CA: 62.19 ± 0.903 RA: 54.14 ± 0.786	The ultrasound technique shows great potential as an ecological method to obtain *S. rosmarinus*. extract rich in antioxidants with higher concentrations of polyphenolic constituents compared to the supercritical extraction method.	[123]

*** CA: Carnosic acid, RA: Rosmarinic acid, C: Carnosol, F: Flavnoides, UA: Ursolic acid.**

CONCLUSIONS

The *S. rosmarinus* plant has been used since ancient times, from home remedies to therapeutic applications. Currently, it has gained significant importance in various fields of research due to its culinary, antioxidant, antimicrobial, and therapeutic properties resulting from its secondary metabolites, such as rosmarinic acid, carnosol, and carnosic acid, among others. Although conventional methodologies used for extracting bioactive compounds from *S. rosmarinus* are widely employed today, there is still a search for more environmentally sustainable methods that allow a reduction in solvents, high temperatures, and waste generation.

The use of non-conventional technologies such as ultrasound has successfully improved extraction percentages and the selectivity of *S. rosmarinus* components compared to thermal and hydrothermal methods, with enhanced extraction yields when using poor solvents like ethanol, which is a less effective solvent in conventional extractions. Furthermore, emerging technologies enable the industrial scaling of extraction and open new possibilities for implementing various metabolites from natural resources in a wide range of applications, from culinary to therapeutic areas.

ACKNOWLEDGEMENTS

We would like to thank the Faculty of Chemical Sciences for providing the necessary facilities to carry out the Postgraduate Studies in Science and Technology of Materials, CONAHCYT for the granted scholarships 863187 and 771323, as well as the support provided by CONAHCYT through the SEP-CONACyT Basic Sciences Project 2017-2018 CB2017-2018 A1-S-44977.

DECLARATION OF CONFLICT OF INTEREST

All authors declare that there is no personal or financial relationship with other individuals or organizations that could inappropriately influence or bias the work.

CONTRIBUTIONS OF THE AUTHORS

J. J. C. P. conceptualized the project, wrote, reviewed and edited the different versions of the manuscript, carried out analysis, designed and developed the methodology. W. Y. V. L. participated in the investigation, carried out analyses, wrote, reviewed and edited different versions of the manuscript. A. O. C. F. carried out analysis and oversaw the project. S. C. E. G. carried out analyses and reviewed and edited different versions of the manuscript. E. M. M. R. carried out analyses and reviewed and edited the manuscript. A. S. G. conceptualized the project, designed and developed the methodology, wrote, reviewed and edited the different versions of the manuscript, funding acquisition, wrote, reviewed and edited the different versions of the manuscript. All authors reviewed and approved the final version of the manuscript.

REFERENCES

[1] I. Messaoudi Moussii, K. Nayme, M. Timinouni, J. Jamaleddine, H. Filali, and F. Hakkou, "Synergistic antibacterial effects of Moroccan Artemisia herba alba, Lavandula angustifolia and Rosmarinus officinalis essential oils," Synergy, vol. 10, art. no. 100057, Jun. 2020, doi: https://doi.org/10.1016/j.synres.2019.100057

[2] A. E. Karadağ, B. Demirci, A. Çaşkurlu, F. Demirci, M. E. Okur, D. Orak, H. Sipahi, K. H. C. Başer, "In vitro antibacterial, antioxidant, anti-inflammatory and analgesic evaluation of Rosmarinus officinalis L. flower extract fractions," South Afr. J. Bot., vol. 125, pp. 214-220, Sep. 2019, doi: https://doi.org/10.1016/j.sajb.2019.07.039

[3] A. Manilal, K. R. Sabu, M. Shewangizaw, A. Aklilu, M. Seid, B. Merdikios, B. Tsegaye, "In vitro antibacterial activity of medicinal plants against biofilm-forming methicillin-resistant Staphylococcus aureus: efficacy of Moringa stenopetala and Rosmarinus officinalis extracts," Heliyon, vol. 6, no. 1, art. no. e03303, Jan. 2020, doi: https://doi.org/10.1016/j.heliyon.2020.e03303

[4] L. M. de Macedo, É. M. D. Santos, L. Militão, L. L. Tundisi, J. A. Ataide, E. B. Souto, P. G. Mazzola, “Rosemary (Rosmarinus officinalis L., syn Salvia rosmarinus Spenn.) and Its Topical Applications: A Review,” Plants, vol. 9, no. 5, art. no. 651, May 2020, doi: https://doi.org/10.3390/plants9050651

[5] M. T. López Luengo, “El romero. Planta aromática con efectos antioxidantes,” Offarm, vol. 27, no. 7, pp. 60-63, Jul. 2008. [Online]. Available: https://www.elsevier.es/es-revista-offarm-4-articulo-el-romero-planta-aromatica-con-13124840

[6] D. R. Berdahl y J. McKeague, “Rosemary and sage extracts as antioxidants for food preservation,” in Handbook of Antioxidants for Food Preservation, F. Shahidi, Ed., Sawstin, United Kingdom: Elsevier, 2015, pp. 177-217, doi: https://doi.org/10.1016/B978-1-78242-089-7.00008-7

[7] J. L. Machado, A. K. Martins Assunção, M. C. Pinto da Silva, A. Silva Dos Reis, et al., “Brazilian Green Propolis: Anti-Inflammatory Property by an Immunomodulatory Activity,” Evid. Based Complement. Alternat. Med., vol. 2012, art. no. 157652, 2012, doi: https://doi.org/10.1155/2012/157652

[8] A. Jaglanian and E. Tsiani, “Rosemary Extract Inhibits Proliferation, Survival, Akt, and mTOR Signaling in Triple-Negative Breast Cancer Cells,” Int. J. Mol. Sci., vol. 21, no. 3, art. no. 810, Jan. 2020, doi: https://doi.org/10.3390/ijms21030810

[9] A. Ali, B. L. Chua, and Y. H. Chow, “An insight into the extraction and fractionation technologies of the essential oils and bioactive compounds in Rosmarinus officinalis L.: Past, present and future,” TrAC - Trends Anal. Chem., vol. 118, pp. 338-351, Sep. 2019, doi: https://doi.org/10.1016/j.trac.2019.05.040

[10] R. S. Borges, B. L. S. Ortiz, A. C. M. Pereira, H. Keita, and J. C. T. Carvalho, “Rosmarinus officinalis essential oil: A review of its phytochemistry, anti-inflammatory activity, and mechanisms of action involved,” J. Ethnopharmacol., vol. 229, pp. 29-45, Jan. 2019, doi: https://doi.org/10.1016/j.jep.2018.09.038

[11] Integrated Taxonomic Information System - Report , “Rosmarinus officinalis.” ITIS. https://www.itis.gov/servlet/SingleRpt/SingleRpt?search_topic=TSN&search_value=32677&print_version=PRT&source=to_print#null (accessed Nov. 22, 2023).

[12] Anjali, S. Kumar, T. Korra, R. Thakur, et al., “Role of plant secondary metabolites in defence and transcriptional regulation in response to biotic stress,” Plant Stress, vol. 8, art. no. 100154, Jun. 2023, doi: https://doi.org/10.1016/j.stress.2023.100154

[13] M. Lingwan, A. A. Pradhan, A. K. Kushwaha, M. A. Dar, L. Bhagavatula, and S. Datta, “Photoprotective role of plant secondary metabolites: Biosynthesis, photoregulation, and prospects of metabolic engineering for enhanced protection under excessive light,” Environ. Exp. Bot., vol. 209, art. no. 105300, May 2023, doi: https://doi.org/10.1016/j.envexpbot.2023.105300

[14] M. F. Lemos, M. F. Lemos, H. P. Pacheco, D. C. Endringer, and R. Scherer, “Seasonality modifies rosemary’s composition and biological activity,” Ind. Crops Prod., vol. 70, pp. 41-47, Aug. 2015, doi: https://doi.org/10.1016/j.indcrop.2015.02.062

[15] D. Sadeh, N. Nitzan, D. Chaimovitsh, A. Shachter, M. Ghanim, and N. Dudai, “Interactive effects of genotype, seasonality and extraction method on chemical compositions and yield of essential oil from rosemary (Rosmarinus officinalis L.),” Ind. Crops Prod., vol. 138, art. no. 111419, Oct. 2019, doi: https://doi.org/10.1016/j.indcrop.2019.05.068

[16] C. Tschiggerl, F. Bucar, “Investigation of the Volatile Fraction of Rosemary Infusion Extracts,” Sci. Pharm., vol. 78, no. 3, pp. 483-492, 2010, doi: https://doi.org/10.3797/scipharm.1004-23

[17] A.-H. Lo, Y.-C. Liang, S.-Y. Lin-Shiau, C.-T. Ho, and J.-K. Lin, “Carnosol, an antioxidant in rosemary, suppresses inducible nitric oxide synthase through down-regulating nuclear factor-κB in mouse macrophages,” Carcinogenesis, vol. 23, no. 6, pp. 983-991, Jun. 2002, doi: https://doi.org/10.1093/carcin/23.6.983

[18] F. A. Khalafalla, F. H. M. Ali, and A.-R. H. A. Hassan, “Quality improvement and shelf-life extension of refrigerated Nile tilapia (Oreochromis niloticus) fillets using natural herbs,” Beni-Suef Univ. J. Basic Appl. Sci., vol. 4, no. 1, pp. 33-40, Mar. 2015, doi: https://doi.org/10.1016/j.bjbas.2015.02.005

[19] A. R. Gouveia, M. Alves, J. A. Silva, y C. Saraiva, “The Antimicrobial Effect of Rosemary and Thyme Essential Oils Against Listeria Monocytogenes in Sous Vide Cook-chill Beef During Storage,” Procedia Food Sci., vol. 7, pp. 173-176, 2016, doi: https://doi.org/10.1016/j.profoo.2016.10.001

[20] M. Radaelli, B. P. da Silva, L. Weidlich, L. Hoehne, A. Flach, L. A. Mendonça Alves da Costa, E. M. Ethur, “Antimicrobial activities of six essential oils commonly used as condiments in Brazil against Clostridium perfringens,” Braz. J. Microbiol., vol. 47, no. 2, pp. 424-430, Apr. 2016, doi: https://doi.org/10.1016/j.bjm.2015.10.001

[21] S. Adhikary and N. Dasgupta, “Role of secondary metabolites in plant homeostasis during biotic stress,” Biocatal. Agric. Biotechnol., vol. 50, art. no. 102712, Jul. 2023, doi: https://doi.org/10.1016/j.bcab.2023.102712

[22] N. M. Vazquez, S. Moreno, and E. M. Galván, “Exposure of multidrug-resistant Klebsiella pneumoniae biofilms to 1,8-cineole leads to bacterial cell death and biomass disruption,” Biofilm, vol. 4, art. no. 100085, Dec. 2022, doi: https://doi.org/10.1016/j.bioflm.2022.100085

[23] I. Oualdi, F. Brahmi, O. Mokhtari, S. Abdellaoui, A. Tahani, and A. Oussaid, “Rosmarinus officinalis from Morocco, Italy and France: Insight into chemical compositions and biological properties,” Mater. Today Proc., vol. 45, pp. 7706-7710, 2021, doi: https://doi.org/10.1016/j.matpr.2021.03.333

[24] W. Wang, N. Wu, Y. G. Zu, and Y. J. Fu, “Antioxidative activity of Rosmarinus officinalis L. essential oil compared to its main components,” Food Chem., vol. 108, no. 3, pp. 1019-1022, Jun. 2008, doi: https://doi.org/10.1016/j.foodchem.2007.11.046

[25] C. Bai, Q. Ma, Q. Li, L. Yu, D. Zhen, M. Liu, C. Wei, “Combination of 1,8-cineole and beta-caryophyllene synergistically reverses cardiac hypertrophy in isoprenaline-induced mice and H9c2 cells,” Bioorg. Chem., vol. 124, art. no. 105823, Jul. 2022, doi: https://doi.org/10.1016/j.bioorg.2022.105823

[26] A. Kumar, K. Dev, and A. Sourirajan, "Essential Oils of Rosmarinus officinalis L., Cymbopogon citratus (DC.) Stapf., and the phyto-compounds, delta-carene and alpha-pinene mediate cell cycle arrest at G2/M transition in budding yeast Saccharomyces cerevisiae," South Afr. J. Bot., vol. 141, pp. 296-305, Sep. 2021, doi: https://doi.org/10.1016/j.sajb.2021.05.008

[27] M. Ghavam, "GC-MS analysis and antimicrobial activities of a Rosmarinus officinalis L. essential oil from Kashan Region (Iran)," Biochem. Syst. Ecol., vol. 105, art. no. 104507, Dec. 2022, doi: https://doi.org/10.1016/j.bse.2022.104507

[28] M. M. Karimkhani, M. Nasrollahzadeh, M. Maham, A. Jamshidi, M. S. Kharazmi, D. Dehnad, S. M. Jafari, "Extraction and purification of α-pinene; a comprehensive review," Crit. Rev. Food Sci. Nutr., pp. 1-26, Nov. 2022, doi: https://doi.org/10.1080/10408398.2022.2140331

[29] N. Boukraa, S. Ladjel, W. Benlamoudi, M. B. Goudjil, M. Berrekbia, and A. Eddoud, "Insecticidal and repellent activities of Artemisia herba alba Asso, Juniperus phoenicea L and Rosmarinus officinalis L essential oils in synergized combinations against adults of Tribolium castaneum (Herbst) (Coleoptera: Tenebrionidae)," Biocatal. Agric. Biotechnol., vol. 45, art. no. 102513, Oct. 2022, doi: https://doi.org/10.1016/j.bcab.2022.102513

[30] M. Ben Abada, S. Haouel Hamdi, C. Masseoud, H. Jroud, E. Bousshih, and J. Mediouni Ben Jemâa, "Variations in chemotypes patterns of Tunisian Rosmarinus officinalis essential oils and applications for controlling the date moth Ectomyelois ceratoniae (Pyralidae)," South Afr. J. Bot., vol. 128, pp. 18-27, Jan. 2020, doi: https://doi.org/10.1016/j.sajb.2019.10.010

[31] P. Satyal, T. H. Jones, E. M. Lopez, R. L. McFeeters, et al., "Chemotypic Characterization and Biological Activity of Rosmarinus officinalis," Foods, vol. 6, no. 3, art. no. 20, Mar. 2017, doi: https://doi.org/10.3390/foods6030020

[32] H. Bitterling, P. Lorenz, W. Vetter, D. R. Kammerer, and F. C. Stintzing, "Photo-protective effects of selected furocoumarins on β-pinene, R-(+)-limonene and γ-terpinene upon UV-A irradiation," J. Photochem. Photobiol. Chem., vol. 424, art. no. 113623, Feb. 2022, doi: https://doi.org/10.1016/j.jphotochem.2021.113623

[33] A. M. Eid, N. Jaradat, L. Issa, A. Abu-Hasan et al., "Evaluation of anticancer, antimicrobial, and antioxidant activities of rosemary (Rosmarinus Officinalis) essential oil and its Nanoemulgel," Eur. J. Integr. Med., vol. 55, art. no. 102175, Oct. 2022, doi: https://doi.org/10.1016/j.eujim.2022.102175

[34] B. Amina, B. Soumeya, B. Salim, B. Mahieddine, et al., "Chemical profiling, antioxidant, enzyme inhibitory and in silico modeling of Rosmarinus officinalis L. and Artemisia herba alba Asso. essential oils from Algeria," South Afr. J. Bot., vol. 147, pp. 501-510, Jul. 2022, doi: https://doi.org/10.1016/j.sajb.2022.02.012

[35] M. Saied, K. Ali, and A. Mosayeb, "Rosemary (Rosmarinus officinalis L.) essential oil alleviates testis failure induced by Etoposide in male rats," Tissue Cell, vol. 81, art. no. 102016, Apr. 2023, doi: https://doi.org/10.1016/j.tice.2023.102016

[36] Z. Zhao, Y. Sun, and X. Ruan, "Bornyl acetate: A promising agent in phytomedicine for inflammation and immune modulation," Phytomedicine, vol. 114, art. no. 154781, Jun. 2023, doi: https://doi.org/10.1016/j.phymed.2023.154781

[37] R. Aitfella Lahlou, M. Bounechada, A. Mohammedi, L. R. Silva, and G. Alves, "Dietary use of Rosmarinus officinalis and Thymus vulgaris as anticoccidial alternatives in poultry," Anim. Feed Sci. Technol., vol. 273, art. no. 114826, Mar. 2021, doi: https://doi.org/10.1016/j.anifeedsci.2021.114826

[38] E. Mahajan, S. Singh, Diksha, S. Kaur, and S. K. Sohal, "The genotoxic, cytotoxic and growth regulatory effects of plant secondary metabolite β-caryophyllene on polyphagous pest Spodoptera litura (Fabricius) (Lepidoptera: Noctuidae)," Toxicon, vol. 219, art. no. 106930, Nov. 2022, doi: https://doi.org/10.1016/j.toxicon.2022.09.016

[39] A. Balahbib, N. El Omari, N. El Hachlafi, F. Lakhdar, "Health beneficial and pharmacological properties of p-cymene," Food Chem. Toxicol., vol. 153, art. no. 112259, Jul. 2021, doi: https://doi.org/10.1016/j.fct.2021.112259

[40] J. Fabbri, M. A. Maggiore, P. E. Pensel, C. M. Albani, G. M. Denegri, and M. C. Elissondo, "Could beta-myrcene be an alternative to albendazole for the treatment of experimental cystic echinococcosis?," Acta Trop., vol. 187, pp. 5-12, Nov. 2018, doi: https://doi.org/10.1016/j.actatropica.2018.07.013

[41] T. D. Alexandrino, T. D. M. Medeiros, A. L. T. G. Ruiz, D. C. Favaro, G. M. Pastore, and J. L. Bicas, "Structural properties and evaluation of the antiproliferative activity of limonene-1,2-diol obtained by the fungal biotransformation of R -(+)- and S -(−)-limonene," Chirality, vol. 34, no. 6, pp. 887-893, Jun. 2022, doi: https://doi.org/10.1002/chir.23439

[42] Y. Guo, A. Baschieri, R. Amorati, and L. Valgimigli, "Synergic antioxidant activity of γ-terpinene with phenols and polyphenols enabled by hydroperoxyl radicals," Food Chem., vol. 345, art. no. 128468, May 2021, doi: https://doi.org/10.1016/j.foodchem.2020.128468

[43] A. Mouahid, C. Dufour, and E. Badens, "Supercritical CO2 extraction from endemic Corsican plants; comparison of oil composition and extraction yield with hydrodistillation method," J. CO2 Util., vol. 20, pp. 263-273, Jul. 2017, doi: https://doi.org/10.1016/j.jcou.2017.06.003

[44] M. Mueller, S. Hobiger, and A. Jungbauer, "Anti-inflammatory activity of extracts from fruits, herbs and spices," Food Chem., vol. 122, no. 4, pp. 987-996, Oct. 2010, doi: https://doi.org/10.1016/j.foodchem.2010.03.041

[45] D. Poeckel, C. Greiner, M. Verhoff, O. Rau et al., "Carnosic acid and carnosol potently inhibit human 5-lipoxygenase and suppress pro-inflammatory responses of stimulated human polymorphonuclear leukocytes," Biochem. Pharmacol., vol. 76, no. 1, pp. 91-97, Jul. 2008, doi: https://doi.org/10.1016/j.bcp.2008.04.013

[46] S.-Y. Yang, C.-O. Hong, G. P. Lee, C.-T. Kim, and K.-W. Lee, "The hepatoprotection of caffeic acid and rosmarinic acid, major compounds of Perilla frutescens, against t-BHP-induced oxidative liver damage," Food Chem. Toxicol., vol. 55, pp. 92-99, May 2013, doi: https://doi.org/10.1016/j.fct.2012.12.042

[47] W. Yeddes, H. Majdi, H. Gadhoumi, T. G. Affes, S. N. Mohamed, W. A. Wannes, M. Saidani-Tounsi, "Optimizing Ethanol Extraction of Rosemary Leaves and Their Biological Evaluations," J. Explor. Res. Pharmacol., vol. 7, no. 2, pp. 85-94, Jun. 2022, doi: https://dx.doi.org/10.14218/JERP.2022.00002

[48] Y. Zhang, J. P. Smuts, E. Dodbiba, R. Rangarajan, J. C. Lang, and D. W. Armstrong, "Degradation Study of Carnosic Acid, Carnosol, Rosmarinic Acid, and Rosemary Extract (Rosmarinus officinalis L.) Assessed Using HPLC," J. Agric. Food Chem., vol. 60, no. 36, pp. 9305-9314, Sep. 2012, doi: https://doi.org/10.1021/jf302179c

[49] M. S. Afonso, A. M. de o Silva, E. B. Carvalho, D. P. Rivelli, et al., "Phenolic compounds from Rosemary (Rosmarinus officinalis L.) attenuate oxidative stress and reduce blood cholesterol concentrations in diet-induced hypercholesterolemic rats," Nutr. Metab., vol. 10, no. 1, art. no. 19, Feb. 2013, doi: https://doi.org/10.1186/1743-7075-10-19

[50] J. M. Andrade, C. Faustino, C. Garcia, D. Ladeiras, C. P. Reis, and P. Rijo, "Rosmarinus officinalis L.: an update review of its phytochemistry and biological activity," Future Sci. OA, vol. 4, no. 4, art. no. FSO283, Apr. 2018, doi: https://doi.org/10.4155/fsoa-2017-0124

[51] S.-Y. Park, "Neuroprotective and Neurotrophic Effects of Isorosmanol," Z. Naturforsch. C. J. Biosci., vol. 64, no. 5-6, pp. 395-398, Jun. 2009, doi: https://doi.org/10.1515/znc-2009-5-616

[52] Y. Wang, Y. Wu, A. Wang, A. Wang, et al., "An olive-derived elenolic acid stimulates hormone release from L-cells and exerts potent beneficial metabolic effects in obese diabetic mice," Front. Nutr., vol. 9, art. no. 1051452, Nov. 2022, doi: https://doi.org/10.3389/fnut.2022.1051452

[53] L. Li, Z. Pan, D. Ning, and Y. Fu, "Rosmanol and Carnosol Synergistically Alleviate Rheumatoid Arthritis through Inhibiting TLR4/NF-κB/MAPK Pathway," Molecules, vol. 27, no. 1, art. no. 78, Dic. 2021, doi: https://doi.org/10.3390/molecules27010078

[54] F. Farhadi, V. Baradaran Rahimi, N. Mohamadi, and V. R. Askari, "Effects of rosmarinic acid, carnosic acid, rosmanol, carnosol, and ursolic acid on the pathogenesis of respiratory diseases," Biofactors, Dic. 2022, doi: https://doi.org/10.1002/biof.1929

[55] H. Feng, Y. Hu, S. Zhou, and Y. Lu, "Farnesoid X receptor contributes to oleanolic acid-induced cholestatic liver injury in mice," J. Appl. Toxicol., vol. 42, no. 8, pp. 1323-1336, Aug. 2022, doi: https://doi.org/10.1002/jat.4298

[56] H. Kheiria, A. Mounir, Q. María, J. María José, and S. Bouzid, "Total Phenolic Content and Polyphenolic Profile of Tunisian Rosemary (Rosmarinus officinalis L.) Residues," in Natural Drugs from Plants, H. A. El-Shemy, Ed., IntechOpen, 2021, ch. 9, doi: https://doi.org/10.5772/intechopen.97762

[57] M. Romo Vaquero, M.-J. Yáñez-Gascón, R. García Villalba, M. Larrrosa, et al., "Inhibition of Gastric Lipase as a Mechanism for Body Weight and Plasma Lipids Reduction in Zucker Rats Fed a Rosemary Extract Rich in Carnosic Acid," PLoS One, vol. 7, no. 6, art. no. e39773, Jun. 2012, doi: https://doi.org/10.1371/journal.pone.0039773

[58] H. Lou, H. Li, S. Zhang, H. Lu, and Q. Chen, "A Review on Preparation of Betulinic Acid and Its Biological Activities," Molecules., vol. 26, no. 18, art. no. 5583, Sep. 2021, doi: https://doi.org/10.3390/molecules26185583

[59] M. Aswathy, A. Vijayan, U. D. Daimary, S. Girisa, K. V. Radhakrishnan, and A. B. Kunnumakkara, "Betulinic acid: A natural promising anticancer drug, current situation, and future perspectives," J. Biochem. Mol. Toxicol., vol. 36, no. 12, art. no. e23206, Dec. 2022, doi: https://doi.org/10.1002/jbt.23206

[60] P. Singh, Y. Arif, A. Bajguz, and S. Hayat, "The role of quercetin in plants," Plant Physiol. Biochem., vol. 166, pp. 10-19, Sep. 2021, doi: https://doi.org/10.1016/j.plaphy.2021.05.023

[61] Z. Cui, X. Zhao, F. K. Amevor, X. Du, et al., "Therapeutic application of quercetin in aging-related diseases: SIRT1 as a potential mechanism," Front. Immunol., vol. 13, art. 943321, 2022, doi: https://doi.org/10.3389/fimmu.2022.943321

[62] A. Gupta, A. G. Atanasov, Y. Li, N. Kumar, and A. Bishayee, "Chlorogenic acid for cancer prevention and therapy: Current status on efficacy and mechanisms of action," Pharmacol. Res., vol. 186, art. no. 106505, Dec. 2022, doi: https://doi.org/10.1016/j.phrs.2022.106505

[63] L. Wang, X. Pan, L. Jiang, Y. Chu, et al., "The Biological Activity Mechanism of Chlorogenic Acid and Its Applications in Food Industry: A Review," Front. Nutr., vol. 9, art. no. 943911, Jun. 2022, doi: https://doi.org/10.3389/fnut.2022.943911

[64] F. Qoorchi Moheb Seraj, N. Heravi-Daz, A. Soltani, S. S. Ahmadi, et al., "Thymol has anticancer effects in U-87 human malignant glioblastoma cells," Mol. Biol. Rep., vol. 49, no. 10, pp. 9623-9632, Oct. 2022, doi: https://doi.org/10.1007/s11033-022-07867-3

[65] V. Sharma, D. Kumar, K. Dev, and A. Sourirajan, "Anticancer activity of essential oils: Cell cycle perspective," South Afr. J. Bot., vol. 157, pp. 641-647, Jun. 2023, doi: https://doi.org/10.1016/j.sajb.2023.04.031

[66] J. Sharifi-Rad, A. Ozleyen, T. Boyunegmez Tumer, C. Oluwaseun Adetunji, et al., "Natural Products and Synthetic Analogs as a Source of Antitumor Drugs," Biomolecules, vol. 9, no. 11, art. no. 679, Nov. 2019, doi: https://doi.org/10.3390/biom9110679

[67] M. V. Barni, M. J. Carlini, E. G. Cafferata, L. Puricelli, and S. Moreno, "Carnosic acid inhibits the proliferation and migration capacity of human colorectal cancer cells," Oncol. Rep., vol. 27, no. 4, pp. 1041-1048, Apr. 2012, doi: https://doi.org/10.3892/or.2012.1630

[68] J. D. Perales Flores M. J. Verde-Star, J. E. Viveros Valdéz, M. P. Barrón-González, R. A. Garza-Padrón, V. E. Aguirre Arzola, and R. G. Rodriguez Garza, "Actividad antioxidante, tóxica y antimicrobiana de Rosmarinus officinalis, Ruta graveolens y Juglans regia contra Helicobacter pylori," Biotecnia, vol. 25, no. 1, pp. 88-93, Nov. 2022, doi: https://doi.org/10.18633/biotecnia.v25i1.1773

[69] N. Botsoglou, I. Taitzoglou, I. Zervos, E. Botsoglou, M. Tsantarliotou, and P. S. Chatzopoulou, "Potential of long-term dietary administration of rosemary in improving the antioxidant status of rat tissues following carbon tetrachloride intoxication," Food Chem. Toxicol., vol. 48, no. 3, pp. 944-950, Mar. 2010, doi: https://doi.org/10.1016/j.fct.2010.01.004

[70] P. P. Ferrer-Gallego, R. Ferrer-Gallego, R. Roselló, J. B. Peris, A. Guillén, J. Gómez, and E. Laguna, "A new subspecies of Rosmarinus officinalis (Lamiaceae) from the eastern sector of the Iberian Peninsula," Phytotaxa, vol. 172, no. 2, art. no. 61, Jun. 2014, doi: https://doi.org/10.11646/phytotaxa.172.2.1

[71] A. I. Hopia, S.-W. Huang, K. Schwarz, J. B. German, and E. N. Frankel, “Effect of Different Lipid Systems on Antioxidant Activity of Rosemary Constituents Carnosol and Carnosic Acid with and without α-Tocopherol,” J. Agric. Food Chem., vol. 44, no. 8, pp. 2030-2036, Jan. 1996, doi: **https://doi.org/10.1021/jf950777p**

[72] A. Wollinger, É. Perrin, J. Chahboun, V. Jeannot, D. Touraud, and W. Kunz, “Antioxidant activity of hydro distillation water residues from Rosmarinus officinalis L. leaves determined by DPPH assays,” Comptes Rendus Chim., vol. 19, no. 6, pp. 754-765, Jun. 2016, doi: **https://doi.org/10.1016/j.crci.2015.12.014**

[73] W. Wang, N. Wu, Y. G. Zu, and Y. J. Fu, “Antioxidative activity of Rosmarinus officinalis L. essential oil compared to its main components,” Food Chem., vol. 108, no. 3, pp. 1019-1022, Jun. 2008, doi: **https://doi.org/10.1016/j.foodchem.2007.11.046**

[74] F. V. B. Petrolini, R. Lucarini, M. G. de Souza, R. H. Pires, W. R. Cunha, and C. H. Martins, “Evaluation of the antibacterial potential of Petroselinum crispum and Rosmarinus officinalis against bacteria that cause urinary tract infections,” Braz. J. Microbiol., vol. 44, no. 3, pp. 829-834, Sep. 2013, doi: **https://doi.org/10.1590/s1517-83822013005000061**

[75] R. Hamidpour, S. Hamidpour, and G. Elias, “Rosmarinus Officinalis (Rosemary): A Novel Therapeutic Agent for Antioxidant, Antimicrobial, Anticancer, Antidiabetic, Antidepressant, Neuroprotective, Anti-Inflammatory, and Anti-Obesity Treatment,” Biomed. J. Sci. Tech. Res., vol. 1, no. 4, Sep. 2017, doi: **http://dx.doi.org/10.26717/BJSTR.2017.01.000371**

[76] E. Flores-Villa, A. Sáenz-Galindo, A. O. Castañeda-Facio, and R. I. Narro-Céspedes, “Romero (Rosmarinus officinalis L.): su origen, importancia y generalidades de sus metabolitos secundarios,” TIP, vol. 23, art. no. e20200266, Nov. 2020, doi: **https://doi.org/10.22201/fesz.23958723e.2020.0.266**

[77] H. I. Castaño P., G. Ciro G., J. E. Zapata M., and S. L. Jiménez R., “Bactericidal activity of ethanolic leaf extract and leaf essential oil of Rosmarinus officinalis L. on some foodborne bacteria,” Vitae, vol. 17, no. 2, pp. 149-154, Jul. 2010, doi: **https://doi.org/10.17533/udea.vitae.6334**

[78] X. K. Solano Solano, M. I. Zambrano Gutiérrez, “Inhibición del Streptococcus mutans, mediante el uso de extracto acuoso y oleoso de Rosmarinus officinalis “romero”,” Rev. Odontol., vol. 19, no. 2, pp. 29-34, 2016. [Online]. Available: **https://dialnet.unirioja.es/servlet/articulo?codigo=5815882**

[79] M. A. Montero-Recalde, J. A. Martinez-Jimenéz, D. F. Avilés-Esquivel, E. L. Valle-Velástegui, and N. D. P. Pazmiño-Miranda, “Efecto antimicrobiano del extracto crudo oleoso de Rosmarinus Officinalis sobre cepa de Escherichia coli,” J. Selva Andina Biosphere, vol. 5, no. 2, pp. 168-175, Nov. 2017, doi: **https://doi.org/10.36610/j.jsab.2017.050200168**

[80] N. R. Farnsworth, O. Akerele, A. S. Bingel, D. D. Soejarto, and Z. Guo, “Medicinal plants in therapy,” Bull. World Health Organ., vol. 63, no. 6, pp. 965-981, 1985. [Online]. Available: **https://www.ncbi.nlm.nih.gov/pmc/articles/PMC2536466/pdf/bullwho00089-0002.pdf**

[81] O. V. Filiptsova, L. V. Gazzavi-Rogozina, I. A. Timoshyna, O. I. Naboka, Ye. V. Dyomina, and A. V. Ochkur, “The essential oil of rosemary and its effect on the human image and numerical short-term memory,” Egypt. J. Basic Appl. Sci., vol. 4, no. 2, pp. 107-111, Jun. 2017, doi: **https://doi.org/10.1016/j.ejbas.2017.04.002**

[82] M. A. El-Desouky, M. H. Mahmoud, B. Y. Riad, and Y. M. Taha, “Nephroprotective effect of green tea, rosmarinic acid and rosemary on N-diethylnitrosamine initiated and ferric nitrilotriacetate promoted acute renal toxicity in Wistar rats,” Interdiscip. Toxicol., vol. 12, no. 2, pp. 98-110, Oct. 2019, doi: **https://doi.org/10.2478/intox-2019-0012**

[83] S. Makaremi, A. Ganji, A. Ghazavi, and G. Mosayebi, “Inhibition of tumor growth in CT-26 colorectal cancer-bearing mice with alcoholic extracts of Curcuma longa and Rosmarinus officinalis,” Gene Rep., vol. 22, art. no. 101006, Mar. 2021, doi: **https://doi.org/10.1016/j.genrep.2020.101006**

[84] L. M. Muñoz Centeno, “Plantas medicinales españolas. Rosmarinus officinalis L. (Lamiaceae) (romero),” Stud. Bot., vol. 21, 2002. [Online]. Available: **https://revistas.usal.es/historico/index.php/0211-9714/article/view/6111**

[85] I. Borrás Linares, D. Arráez-Román, M. Herrero, E. Ibáñez, A. Segura-Carretero, and A. Fernández-Gutiérrez, “Comparison of different extraction procedures for the comprehensive characterization of bioactive phenolic compounds in Rosmarinus officinalis by reversed-phase high-performance liquid chromatography with diode array detection coupled to electrospray time-of-flight mass spectrometry,” J. Chromatogr. A, vol. 1218, no. 42, pp. 7682-7690, Oct. 2011, doi: **https://doi.org/10.1016/j.chroma.2011.07.021**

[86] M. Kumar, M. D. Barbhai, S. Puranik, Radha, et al., “Combination of green extraction techniques and smart solvents for bioactives recovery,” TrAC Trends Anal. Chem., vol. 169, art. no. 117286, Dec. 2023, doi: **https://doi.org/10.1016/j.trac.2023.117286**

[87] S. Oubannin, L. Bijla, M. N. Ahmed, M. Ibourki, et al., “Recent advances in the extraction of bioactive compounds from plant matrices and their use as potential antioxidants for vegetable oils enrichment,” J. Food Compos. Anal., vol. 128, art. no. 105995, Apr. 2024, doi: **https://doi.org/10.1016/j.jfca.2024.105995**

[88] F. Chemat, M. A. Vian, A.-S. Fabiano-Tixier, M. Nutrizio, et al., “A review of sustainable and intensified techniques for extraction of food and natural products,” Green Chem., vol. 22, no. 8, pp. 2325-2353, 2020, doi: **https://doi.org/10.1039/C9GC03878G**

[89] P. R. More, A. R. Jambrak, and S. S. Arya, “Green, environment-friendly and sustainable techniques for extraction of food bioactive compounds and waste valorization,” Trends Food Sci. Technol., vol. 128, pp. 296-315, Oct. 2022, doi: **https://doi.org/10.1016/j.tifs.2022.08.016**

[90] W. T. Richards and A. L. Loomis, “The chemical effects of high frequency sound waves I. A preliminary survey,” J. Am. Chem. Soc., vol. 49, no. 12, pp. 3086-3100, Dec. 1927, doi: **https://doi.org/10.1021/ja01411a015**

[91] K. S. Suslick, “The Chemical Effects of Ultrasound,” Sci. Am., vol. 260, no. 2, pp. 80-86, feb. 1989, doi: **https://doi.org/10.1038/scientificamerican0289-80**

[92] N. Pokhrel, P. K. Vabbina, and N. Pala, “Sonochemistry: Science and Engineering,” Ultrason. Sonochem., vol. 29, pp. 104-128, Mar. 2016, doi: **https://doi.org/10.1016/j.ultsonch.2015.07.023**

[93] L. E. Robles-Ozuna and L. A. Ochoa-Martínez, "Ultrasonido y sus aplicaciones en el procesamiento de alimentos," vol. 13, no. 2, pp. 109-122, 2012. [Online]. Available: https://www.redalyc.org/articulo.oa?id=81325441002

[94] M. Islam, S. Malakar, M. V. Rao, N. Kumar, and J. K. Sahu, "Recent advancement in ultrasound-assisted novel technologies for the extraction of bioactive compounds from herbal plants: a review," Food Sci. Biotechnol., vol. 32, no. 13, pp. 1763-1782, Nov. 2023, doi: https://doi.org/10.1007/s10068-023-01346-6

[95] D. Y. Hoo, Z. L. Low, D. Y. S. Low, S. Y. Tang, S. Manickam, K. W. Tan, Z. H. Ban, "Ultrasonic cavitation: An effective cleaner and greener intensification technology in the extraction and surface modification of nanocellulose," Ultrason. Sonochem., vol. 90, art. no. 106176, Nov. 2022, doi: https://doi.org/10.1016/j.ultsonch.2022.106176

[96] M. Ramić, S. Vidović, Z. Zeković, J. Vladić, A. Cvejin, and B. Pavlić, "Modeling and optimization of ultrasound-assisted extraction of polyphenolic compounds from Aronia melanocarpa by-products from filter-tea factory," Ultrason. Sonochem., vol. 23, pp. 360-368, Mar. 2015, doi: https://doi.org/10.1016/j.ultsonch.2014.10.002

[97] N. A. Al-Dhabi, K. Ponmurugan, and P. Maran Jeganathan, "Development and validation of ultrasound-assisted solid-liquid extraction of phenolic compounds from waste spent coffee grounds," Ultrason. Sonochem., vol. 34, pp. 206-213, Jan. 2017, doi: https://doi.org/10.1016/j.ultsonch.2016.05.005

[98] K. Kumar, S. Srivastav, and V. S. Sharanagat, "Ultrasound assisted extraction (UAE) of bioactive compounds from fruit and vegetable processing by-products: A review," Ultrason. Sonochem., vol. 70, art. no. 105325, Jan. 2021, doi: https://doi.org/10.1016/j.ultsonch.2020.105325

[99] C. Wen, J. Zhang, H. Zhang, C. S. Dzah, et al., "Advances in ultrasound assisted extraction of bioactive compounds from cash crops - A review," Ultrason. Sonochem., vol. 48, pp. 538-549, Nov. 2018, doi: https://doi.org/10.1016/j.ultsonch.2018.07.018

[100] C. S. Dzah, Y. Duan, H. Zhang, C. Wen, J. Zhang, G. Chen, H. Ma, "The effects of ultrasound assisted extraction on yield, antioxidant, anticancer and antimicrobial activity of polyphenol extracts: A review," Food Biosci., vol. 35, art. no. 100547, Jun. 2020, doi: https://doi.org/10.1016/j.fbio.2020.100547

[101] I. M. Yusoff, Z. Mat Taher, Z. Rahmat, and L. S. Chua, "A review of ultrasound-assisted extraction for plant bioactive compounds: Phenolics, flavonoids, thymols, saponins and proteins," Food Res. Int., vol. 157, art. no. 111268, Jul. 2022, doi: https://doi.org/10.1016/j.foodres.2022.111268

[102] A. C. Feihrmann, N. M. da Silva, A. R. de Marins, M. Antônio Matiucci, et al., "Ultrasound-assisted extraction and encapsulation by spray drying of bioactive compounds from Tradescantia zebrina leaves," Food Chem. Adv., vol. 4, art. no. 100621, Jun. 2024, doi: https://doi.org/10.1016/j.focha.2024.100621

[103] R. Biswas, A. Sarkar, M. Alam, M. Roy, and M. M. Mahdi Hasan, "Microwave and ultrasound-assisted extraction of bioactive compounds from Papaya: A sustainable green process," Ultrason. Sonochem., vol. 101, art. no. 106677, Dec. 2023, doi: https://doi.org/10.1016/j.ultsonch.2023.106677

[104] A. Olfat, T. Mostaghim, S. Shahriari, and M. Salehifar, "Extraction of bioactive compounds of Hypnea flagelliformis by ultrasound-assisted extraction coupled with natural deep eutectic solvent and enzyme inhibitory activity," Algal Res., vol. 78, art. no. 103388, Mar. 2024, doi: https://doi.org/10.1016/j.algal.2023.103388

[105] A. Palma, M. Ruiz-Montoya, M. J. Díaz, I. Giráldez, and E. Morales, "Optimization of bioactive compounds by ultrasound extraction and gas chromatography - mass spectrometry in fast-growing leaves," Microchem. J., vol. 193, art. no. 109231, Oct. 2023, doi: https://doi.org/10.1016/j.microc.2023.109231

[106] K. S. L. Miki, A. P. Dresch, M. Cavali, A. P. da Silva, et al., "Influence of drying methods in the ultrasound-assisted extraction of bioactive compounds from Byrsonima crassifolia to evaluate their potential antitumor activity," Food Humanity, vol. 2, art. no. 100242, May 2024, doi: https://doi.org/10.1016/j.foohum.2024.100242

[107] P. Petchimuthu, G. B. Sumanth, S. Kunjiappan, S. Kannan, S. R. K. Pandian, and K. Sundar, "Green extraction and optimization of bioactive compounds from Solanum torvum Swartz. using ultrasound-aided solvent extraction method through RSM, ANFIS and machine learning algorithm," Sustain. Chem. Pharm., vol. 36, art. no. 101323, Dec. 2023, doi: https://doi.org/10.1016/j.scp.2023.101323

[108] H. Koraqi, A. Trajkovska Petkoska, W. Khalid, N. Kumar, and S. Pareek, "Optimization of experimental conditions for bioactive compounds recovery from raspberry fruits (Rubus idaeus L.) by using combinations of ultrasound-assisted extraction and deep eutectic solvents," Appl. Food Res., vol. 3, no. 2, art. no. 100346, Dec. 2023, doi: https://doi.org/10.1016/j.afres.2023.100346

[109] S. Albu, E. Joyce, L. Paniwnyk, J. P. Lorimer, and T. J. Mason, "Potential for the use of ultrasound in the extraction of antioxidants from Rosmarinus officinalis for the food and pharmaceutical industry," en Ultrason. Sonochem., vol. 11, no. 3-4, pp. 261-265, May 2004, doi: https://doi.org/10.1016/j.ultsonch.2004.01.015

[110] L. Paniwnyk, H. Cai, S. Albu, T. J. Mason, and R. Cole, "The enhancement and scale up of the extraction of anti-oxidants from Rosmarinus officinalis using ultrasound," Ultrason. Sonochem., vol. 16, no. 2, pp. 287-292, Feb. 2009, doi: https://doi.org/10.1016/j.ultsonch.2008.06.007

[111] M. Nicolai, P. Pereira, R. F. Vitor, C. P. Reis, A. Roberto, and P. Rijo, "Antioxidant activity and rosmarinic acid content of ultrasound-assisted ethanolic extracts of medicinal plants," Meas. J. Int. Meas. Confed., vol. 89, pp. 328-332, Jul. 2016, doi: https://doi.org/10.1016/j.measurement.2016.04.033

[112] X. Zhong, X. Wang, N. Zhou, J. Li, et al., "Chemical characterization of the polar antibacterial fraction of the ethanol extract from Rosmarinus officinalis," Food Chem., vol. 344, art. no. 128674, May 2021, doi: https://doi.org/10.1016/j.foodchem.2020.128674

[113] R. S. Pizani, J. Viganó, L. S. Contieri, M. M. Strieder, et al., "New selective and sustainable ultrasound-assisted extraction procedure to recover carnosic and rosmarinic acids from Rosmarinus officinalis by sequential use of bio-based solvents," Food Chem., vol. 435, art. no. 137540, Mar. 2024, doi: https://doi.org/10.1016/j.foodchem.2023.137540

[114] G. Chisha, C. Li, L. Xiao, B. Wang, Y. Chen, and Z. Cui, "Multiscale mechanism exploration and experimental optimization for rosmarinic acid extraction from Rosmarinus officinalis using natural deep eutectic solvents," Ind. Crops Prod., vol. 188, art. no. 115637, Nov. 2022, doi: https://doi.org/10.1016/j.indcrop.2022.115637

[115] A. Ali, B. L. Chua, Y. H. Chow, and C. H. Chong, "Development and characterisation of novel terpenoid-based hydrophobic deep eutectic solvents for sustainable extraction of bioactive antioxidants from Rosmarinus officinalis L," J. Mol. Liq., vol. 388, art. no. 122792, Oct. 2023, doi: https://doi.org/10.1016/j.molliq.2023.122792

[116] S. S. Ayyildiz, E. Pelvan, and B. Karadeniz, "Optimization of accelerated solvent extraction, ultrasound assisted and supercritical fluid extraction to obtain carnosol, carnosic acid and rosmarinic acid from rosemary," Sustain. Chem. Pharm., vol. 37, art. no. 101422, Feb. 2024, doi: https://doi.org/10.1016/j.scp.2023.101422

[117] C. Caleja, L. Barros, M. A. Prieto, M. F. Barreiro, M. B. P. P. Oliveira, and I. C. F. R. Ferreira, "Extraction of rosmarinic acid from Melissa officinalis L. by heat-, microwave- and ultrasound-assisted extraction techniques: A comparative study through response surface analysis," Sep. Purif. Technol., vol. 186, pp. 297-308, Oct. 2017, doi: https://doi.org/10.1016/j.seppur.2017.06.029

[118] M. Jacotet-Navarro, N. Rombaut, A.-S. Fabiano-Tixier, M. Danguien, A. Bily, and F. Chemat, "Ultrasound versus microwave as green processes for extraction of rosmarinic, carnosic and ursolic acids from rosemary," Ultrason. Sonochem., vol. 27, pp. 102-109, Nov. 2015, doi: https://doi.org/10.1016/j.ultsonch.2015.05.006

[119] M. Bellumori, M. Innocenti, A. Binello, L. Boffa, N. Mulinacci, and G. Cravotto, "Selective recovery of rosmarinic and carnosic acids from rosemary leaves under ultrasound- and microwave-assisted extraction procedures," Comptes Rendus Chim., vol. 19, no. 6, pp. 699-706, Apr. 2016, doi: https://doi.org/10.1016/j.crci.2015.12.013

[120] D. Tungmunnithum, L. Garros, S. Drouet, S. Renouard, E. Lainé, and C. Hano, "Green Ultrasound Assisted Extraction of trans Rosmarinic Acid from Plectranthus scutellarioides (L.) R.Br. Leaves," Plants, vol. 8, no. 3, art. no. 50, Feb. 2019, doi: https://doi.org/10.3390/plants8030050

[121] G. Zu, R. Zhang, L. Yang, C. Ma, Y. Zu, W. Wang, C. Zhao, "Ultrasound-Assisted Extraction of Carnosic Acid and Rosmarinic Acid Using Ionic Liquid Solution from Rosmarinus officinalis," Int. J. Mol. Sci., vol. 13, no. 9, pp. 11027-11043, Sep. 2012, doi: https://doi.org/10.3390/ijms130911027

[122] A. M. Hrebień-Filisińska and G. Tokarczyk, "The Use of Ultrasound-Assisted Maceration for the Extraction of Carnosic Acid and Carnosol from Sage (Salvia officinalis L.) Directly into Fish Oil," Molecules, vol. 28, no. 16, art. no. 6094, Aug. 2023, doi: https://doi.org/10.3390/molecules28166094

[123] N. Dhouibi, S. Manuguerra, R. Arena, C. M. Messina, et al., "Impact of the Extraction Method on the Chemical Composition and Antioxidant Potency of Rosmarinus officinalis L. Extracts," Metabolites, vol. 13, no. 2, art. no. 290, Feb. 2023, doi: https://doi.org/10.3390/metabo13020290

RESEARCH ARTICLE

VOL. 45 | NO. 2 | **MAY-AUGUST 2024** | PP 62-77

Revista Mexicana de Ingeniería Biomédica

dx.doi.org/10.17488/RMIB.45.2.4

E-LOCATION ID: **1419**

Enhancing Multiple Sequence Alignment with Genetic Algorithms: A Bioinformatics Approach in Biomedical Engineering

Una Mejora del Alineamiento Múltiple de Secuencias con Algoritmos Genéticos: Un Enfoque de Bioinformática en la Ingeniería Biomédica

Ernesto Rios-Willars [1], *Jennifer Vélez-Segura* [2], *María Magdalena Delabra-Salinas*[3]

[1] Universidad Autónoma de Coahuila, Facultad de Sistemas Unidad Saltillo - México

[2] Universidad Nacional de Colombia - Colombia

[3] Universidad Autónoma de Coahuila, Facultad de Enfermería Unidad Saltillo - México

ABSTRACT

This study aimed to create a genetic information processing technique for the problem of multiple alignment of genetic sequences in bioinformatics. The objective was to take advantage of the computer hardware's capabilities and analyze the results obtained regarding quality, processing time, and the number of evaluated functions. The methodology was based on developing a genetic algorithm in Java, which resulted in four different versions: Gp1,Gp2,Gp3,and Gp4. A set of genetic sequences were processed, and the results were evaluated by analyzing numerical behavior profiles. The research found that algorithms that maintained diversity in the population produced better quality solutions, and parallel processing reduced processing time. It was observed that the time required to perform the process decreased, according to the generated performance profile. The study concluded that conventional computer equipment can produce excellent results when processing genetic information if algorithms are optimized to exploit hardware resources. The computational effort of the hardware used is directly related to the number of evaluated functions. Additionally, the comparison method based on the determination of the performance profile is highlighted as a strategy for comparing the algorithm results in different metrics of interest, which can guide the development of more efficient genetic information processing techniques.

KEYWORDS: bioinformatics, genetic algorithm, multiple sequence alignment, msa

RESUMEN

El objetivo del presente trabajo es desarrollar una estrategia de procesamiento de información genética para el problema del alineamiento múltiple de secuencias en el área de bioinformática con el propósito de explotar la potencia del hardware y analizar los resultados en términos de calidad de las soluciones obtenidas, así como el tiempo requerido por el sistema de cómputo para realizar el proceso y la determinación del número de funciones evaluadas. Los procedimientos y metodología para dicho trabajo fueron basados en la programación de un Algoritmo Genético en lenguaje Java, del que sucesivamente se obtuvieron cuatro diferentes versiones denominadas Gp1, Gp2, Gp3 y Gp4. Con esto se procesó un conjunto de secuencias genéticas y se evaluaron los resultados a través de la determinación de los perfiles de comportamiento numérico. Entre los hallazgos se encuentra que la diversidad en la población y el procesamiento paralelo tienen influencia en los resultados. A partir del perfil de comportamiento numérico se observa una reducción en el tiempo requerido para realizar el proceso. Se concluye que a) el equipo de cómputo convencional puede generar muy buenos resultados al procesar información genética cuando los algoritmos son preparados para aprovechar al máximo los recursos de hardware. Esto puede guiar al desarrollo de estrategias más eficientes de procesamiento de información genética.

PALABRAS CLAVE: bioinformática, algoritmo genético, alineamiento múltiple de secuencias, msa

Corresponding author

TO: Ernesto Rios-Willars
INSTITUTION: Universidad Autónoma de Coahuila, Facultad de Sistemas Unidad Saltillo - México
ADDRESS: Ciudad Universitaria, Fundadores Km 13, Zona Centro, 25350 Arteaga, Coahuila, México.
EMAIL: riose@uadec.edu.mx

Received:

12 February 2024

Accepted:

1 May 2024

INTRODUCTION

Deoxyribonucleic acid, commonly known as DNA, is a large and complex molecule located in the nucleus of cells in all living organisms. It takes the shape of a double helix structure, where the genetic information unique to each individual and species is stored. All life is based on a code written in DNA molecule, the common denominator among living beings [1]. DNA can exist in a single-stranded form or as higher-order structures, including the canonical double helix and noncanonical duplex, triplex, and quadruplex species [2]. In a DNA molecule, each sugar in the two strands is attached to one of four nitrogenous bases - Adenine (A), Guanine (G), Cytosine (C), and Thymine (T). These bases can bond through hydrogen bonds, and their bonding possibilities differ. Specifically, DNA's double helix structure is attributed to hydrogen bonds between A-T (two) and C-G (three) base pairs[3].

The number of hydrogen bonds determines the specific pairing between nitrogenous bases, but this structure is prone to errors and can sometimes be repaired [4][5].

According to the NCBI database [6], the number of records has doubled approximately every 18 months since 1982[7]. From a computer science perspective, advanced metaheuristic strategies are required to handle such information[8][9].

We developed a genetic algorithm to perform multiple genetic sequence alignments in this work. The objective is to explore the improvement from different parametrization schemas (Gp1, Gp2, Gp3, and Gp4) for the algorithm`s performance in terms of a) the solution quality (fitness) achieved by the algorithm and b) the computational effort ($N\hat{F}E$) with the count of evaluated functions. Since the parameter adjustment is made in the number of processing cores and mutation level, the secondary objective is to describe the impact of such adjustments on the processing time between the four algorithm schemas.

In the field of genetics, the parallelization strategy of processing information has shown significant improvement in the results, especially in reducing the computational time required to solve various problems[10][11][12]. As a validation method, the numerical performance profile measures the relative efficiency of the algorithm in solving the set of problems[13].

Bioinformatics software testing is often complex due to the difficulty in verifying the correctness of output and effectively generating failure-revealing test cases[14]. In this work, we developed four strategies based on a genetic algorithm for the multiple sequence alignment problem and compared their performance to each other. Multiple sequence alignment (MSA) is essential in bioinformatics, aiding in phylogenetic, protein, and genomic analysis, but faces challenges in increasing alignment accuracy[15].

There are several algorithm strategies in the state of the art, such as the "Progressive alignment," which has been one of the most used methods since the 1980s [16]. In addition to improvements in algorithm design, modern hardware technology has increased processing speed and enabled more simultaneous alignment sequences[17]. Furthermore, integrations based on framework processing like Apache Spark can produce promising results and new perspectives [18].

Regarding the processing algorithms, researchers have developed exact, progressive, and iterative algorithms to address the Multiple Sequence Alignment (MSA) problem. Exact algorithms exhaustively search in the space of solutions and calculate the global optimum in sequences of relatively small lengths. However, they cannot guarantee finding the best solution in arrangements of hundreds or thousands of bases. Blast is an example of this type of algorithm [19]. On the other hand, progressive algorithms work by iteratively improving a sequence alignment by adding new sequences. The process involves gradually building upon an initial alignment until an optimal solution is found [20][21]. Dynamic programming algorithms are commonly used to implement strategies that explore solution spaces using a substitution matrix [22]. One example is the ClustalW algorithm [23]. However, errors at the beginning of an alignment can propagate to the rest of the operation, which is a drawback of these algorithms. Furthermore, another strategy to tackle bigger MSA problems is to iteratively perform partial alignments [24][25].

On the other hand, Genetic algorithms are iterative metaheuristic strategies based on bioinspiration. A thorough analysis of the algorithms used in this context can be found in [26]. Due to the metaheuristic origin of Genetic Algorithms, which does not guarantee achieving the optimal solution, we assume no comparison between metaheuristics and/or stochastic strategies vs. progressive or deterministic strategies. However, metaheuristics permit working with more extensive problem instances.

This work presents a bioinformatics breakthrough and builds on fundamentals established by previous papers, such as [27], highlighting the importance of hardware acceleration in DNA sequence alignment. The utility of parallel processing was established by [28], which improves the process at the bit level. This work presents an innovative methodology that combines multiple techniques, including genetic algorithms, to enhance multiple sequence alignment. The methodology also employs the algorithms' performance profile as an efficient comparison method.

Due to the increasing scientific research in medicine-based informatics, the genetic algorithm has been tested using a set of genetic sequences from a group of vegetables of particular interest in medicine, such as *Euphorbia pulcherrima*, which has Anti-Inflammatory, Analgesic, Sedative, and Muscle-Relaxant Activities [29]. Preventing health complications is a significant motivation for studying the properties of vegetables.

MATERIALS AND METHODS

The computational processes in this study were meticulously developed on four identical personal computers (PCs) with a Microsoft Windows operating system. These PCs were equipped with 8 GB of RAM and an Intel core *i5* processor, ensuring the study's robustness and reliability. The algorithms were programmed in Java with Netbeans IDE, a widely recognized and trusted platform for software development.

Genetic Algorithm

In this study, a genetic algorithm (GA) is used to simulate the natural adaptation process of living beings. This computer-based representation was initially proposed by [30]. These are some instances of how GA's are used:[31][32][33][34]. While most search algorithms operate on a single solution, a GA operates on a population of solutions. The classical GA codes a given problem, generating a population of potential solutions. This method involves crossing, leading to mutation, and discovering new and improved solutions. This statement is founded on Darwin's evolutionary theory.

Sequence Alignment

When there are two sequences (*m,n*) that can accommodate a limited number of gap insertions, the number of alignments increases as the length of the sequences increases. The number of potential alignments for a pair of sequences m and n, with 'k' insertions, can be calculated using Equation (1) as stated by Waterman in 1995:

$$f = \sum_{k=0}^{\min(m,n)} \frac{(m+n-k)!}{k!\,(m-k)!\,(n-k)!} \tag{1}$$

When attempting to solve the multiple sequence alignment problem using brute force, the problem becomes NP-complete. In contrast, dynamic programming has a complexity of $O(LN)$, where L is sequence length, and N is the number of sequences. Researchers aim to enhance MSA efficiency via heuristic and metaheuristic approaches and parallel implementations to reduce computational costs [35].

Sum-of-pairs multiple alignments: The given strings, represented by *S1* to *Sk*, are used to create multiple alignment. This alignment consists of strings $T_1 \ldots T_K$, which are the same length as the original strings. The new strings are made by inserting spacing symbols at specific positions in the original strings. However, only columns full of spacing symbols are not allowed.

Given a multiple alignment $T_1 \ldots T_K$ of length m and a scoring function σ for pairs of characters ($\sigma(a,b)$) and pairs of character and spacing symbol ($\sigma(a,\text{-})$ or $\sigma(\text{-},b)$), we define its sum-of-pairs score as described in Equation (2):

$$\sigma(\mathrm{T}_1, \ldots, \mathrm{T}_\mathrm{k}) = \sum_{i<j} \sum_{p=1}^{m} \sigma\left(\mathrm{T}_\mathrm{i}(p), \mathrm{T}_\mathrm{j}(p)\right) = \sum_{i<j} \sigma * \left(\mathrm{T}_\mathrm{i}, \mathrm{T}_\mathrm{j}\right). \tag{2}$$

Compute a multiple alignment of strings S1 to Sk with a given scoring function sigma to find the maximum sum-of-pairs score.

Problem Codification: Text or binary sequences are commonly used for multiple sequence alignment. These sequences include array-like data structures, making handling characters and reordering positions easier. As a result, the computational effort required by the processing machine is reduced. In this work, each alignment matrix *A* represents an individual, and each matrix position contains a single character (*a*). Equation (3) shows the matrix positions where a nucleotide or a gap can be found.

$$A = \begin{pmatrix} a_{11} & a_{12} & a_{13} & \ldots & a_{1n} \\ a_{21} & a_{22} & a_{32} & \ldots & a_{2n} \\ a_{31} & a_{32} & a_{33} & \ldots & a_{3n} \\ \ldots & \ldots & \ldots & \ldots & \ldots & \ldots \\ a_{m1} & a_{m2} & a_{m3} & \ldots & a_{mn} \end{pmatrix} \tag{3}$$

Each row in the alignment represents a sequence of the set to be aligned.

Proposed genetic algorithm: GAAPd

The algorithm starts with an Initial Population (Pi) of 500 individuals, which is later reduced to a fixed number of 100 individuals (Pt) between 100 generations. This helps maintain stability in the algorithm and prevents excessive computational resource usage. The individuals in the initial population are generated by random potential solutions to the problem.

Individuals are evaluated using a parallel process and the widely used Blosum evaluation matrix [36]. This matrix helps measure the quality of the in-turn alignment. There are ongoing efforts to parallelize genetic algorithms either partially or entirely, and these efforts have demonstrated meaningful results in their respective fields of application [37][38][39][40].

To speed up the evaluation process, we divide the workload and assign it to each evaluator instance, which is a component of the evaluation class designed for this process. We avoid double evaluations of union regions to ensure synchronicity among evaluators.

After completing the task, evaluators assign each population member a fitness value (ft) used on their partial results. Figure 1 illustrates the evaluation process described in this work.

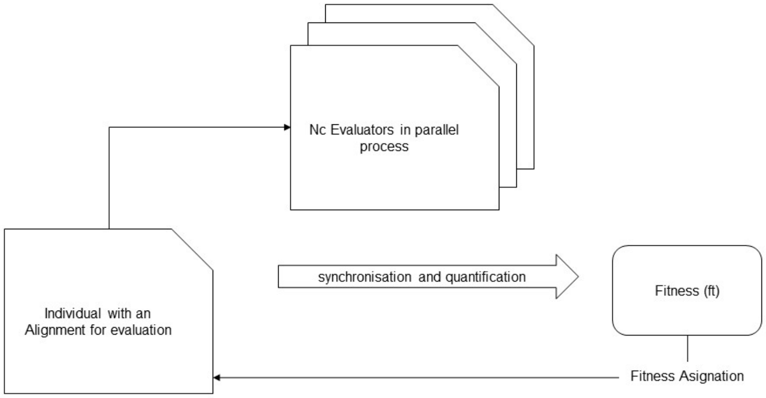

FIGURE 1. **The process of evaluation. Nc refers to the number of evaluator instances created to evaluate everyone. Once the fitness value is assigned, the process is repeated for the following individuals in the population.**

According to theory, there is a direct correlation between the number of cores and the reduction of processing time ($\hat{T}$), stated in Equation (4). However, other intrinsic processes consume resources, such as synchronization and quantification.

$$\hat{T} = N\hat{F}E/Nc \tag{4}$$

Where $N\hat{F}E$ is the number of evaluated functions.

During the crossover process, individuals are randomly selected from the best performers of the evaluation process in the Pt set. In this context, it implies that only the most outstanding individuals proceed to the crossover phase. Their probability of being assigned to another individual is

$Pb = 1/Pt$, equal for all.

A random double-point cut is made (CPA,CPB), and each crossover produces two children integrated into the population. The positions of CPA and CPB in the alignment matrix are also random.

After making the necessary cuts for both individuals, three parts of the father ($P1F,P2F,and\ P3F$) and three of the mothers ($P1M,P2M,and\ P3M$) are obtained.

Child 1 and Child 2 incorporate all six elements shown in Figure 2.

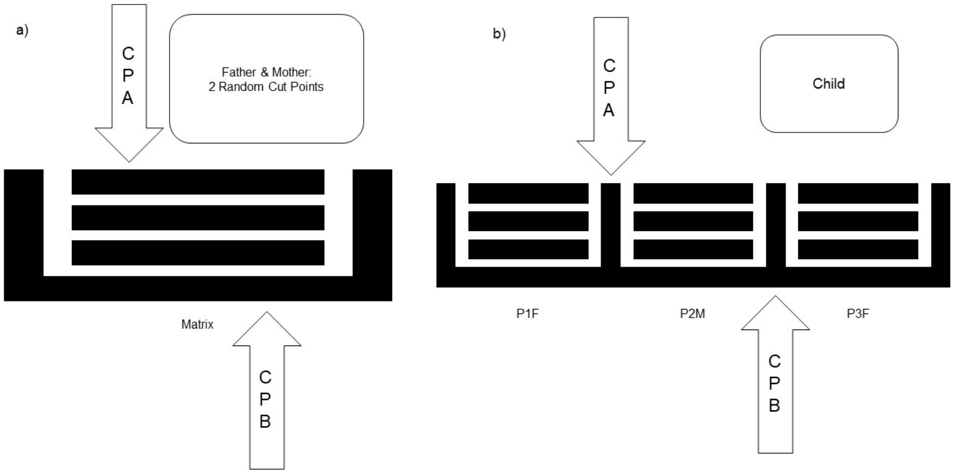

FIGURE 2. **The crossover processes. In this process, two individuals produce three parts each. The resulting child has one part from the mother (P2M) and two from the father (P1F,P3F). Another child has one part from the mother and one from the father.**

The mutation process occurs for progenies [41], which is achieved by inserting or deleting gaps using the hyphen character "-" in various positions within the matrix. This process helps to improve the alignment further. The probability of an individual moving to the mutation process is Pm = 0.2, in which changes are randomly applied to the alignment matrix based on the Pm value.

Various mutation techniques have been documented in the literature, each relying on a specific mutation probability [41][42][43]. We developed four forms of mutation described as follows:

a) One of the sequences is randomly selected for mutation, where a maximum of 200 gaps can be inserted at the beginning.
b) A random point in the matrix is selected for gap insertion. The number of spaces added is randomly determined, up to 300.
c) Insertion of a gap column at a random point. A gap column is inserted at some position in the alignment matrix.
d) Random gaps are deleted. Up to 100 gaps are removed, and the number of gaps removed is randomly determined within a range of 1 to 100.

Algorithm Pseudocode and GitHub Access

The pseudocode of the proposed algorithm is presented as follows. Let Nc be the number of processing cores and Nm the mutation level as a repeating mutation process over a given matrix.

1) Population Initialisation (*P*)
2) Population Evaluation (Blosum Matrix)
    a. Distribute partial work for cores (Nc) and evaluator Instances.
    b. Execute parallel evaluation process.
    c. Once finished, evaluation instances compute the overall fitness value.
3) Worst Individuals Elimination.
4) Crossover.
5) Repeat progeny mutation (*Nm*) Times.
6) Integrate progeny into *P*.

The GitHub project is available for further analysis at https://github.com/riosew/GAAPd-Software.git.

The algorithm is presented as a set of corresponding classes. The different versions designated as Gp1, Gp2, Gp3, and Gp4 can be produced by changing the number of cores (*Nc*) for the parallel process and the mutation level (*Nm*) to change the mutation cycles. Thus, it can be executed with the different *Nc* and *Nm* values in Table 1. It initiates the process with a basic visual interface, where the user can change the indicated values.

TABLE 1. GAAPd versions.

Version	Nc	Nm
Gp1	1	1
Gp2	4	4
Gp3	1	4
Gp4	4	1

Time Complexity Analysis Big O

The evaluation process is divided into the following parts.

Creation of evaluators: This loop runs several times equal to the number of available cores. Inside this loop, another loop runs several times equal to the size of the alignment matrix. Therefore, this part of the algorithm has a complexity of $O(n*m)$, where n is the number of cores and m is the size of the matrix.

Waiting for all evaluators: This loop runs until all evaluators have finished. In the worst case, this could take time proportional to the evaluator, which takes the longest to complete the work.

Traversal of evaluators adding results: This loop runs several times equal to the number of evaluators (equal to the number of cores). Therefore, this part of the algorithm has a complexity of $O(n)$, and the total complexity of the evaluation process is $O(n*m)$, where n is the number of cores and m is the size of the matrix. However, the complexity analysis of the nested cycles in the micro evaluator instance (mE) is worth noticing. The mE instances are as many instances as the core Nc value. The complexity of the mE process is $O(nmp^2)$. Since n and m are the matrix size, and p is the vector size in the Blosum evaluation matrix, which performs a traversing process for n and m. Finally, in big(O) analysis, the worst case of operation establishes the total algorithm complexity.

Experimental Method

This paper's experiment describes a sequence of algorithms and the Performance Profile.

Set of Sequences

The dataset has been expanded by integrating 13 sequence groups, described in Table 2. It is available for future reference on the Galaxy platform [44] at https://usegalaxy.org/u/rioswillars/h/dataset-for-genetic-algorithm. Each group comprises N sequences of varying lengths.

TABLE 2. **Test Sequence Sets.**

Set	Name	*N*
1	*Agave victoriae reginae*	38
2	*Aristida purpurea*	38
3	*Bellucia grossularioides*	42
4	*Bursera simaruba*	35
5	*Cnidoscolus urens*	35
6	*Cordia alliodora*	28
7	*Curatella Americana*	33
8	*Cydista diversifolia*	29
9	*Echinocactus platyacanthus*	38
10	*Ephiphylum hookeri*	31
11	*Erythrina herbacea*	35
12	*Euphorbia pulcherrima*	23
13	*Gossypium arboretum*	29

Algorithms

Four versions of the GAAPd algorithm were created to evaluate the number of evaluated functions ($N\hat{F}E$), and quality of alignment achieved ($Fitness$). The computational processing parameters were adjusted at varying levels and the impact of processing time due to the adjustments was registered for comparison between the four GAAPd versions. The parametters for adjustment are: the number of core decomposition (Nc), and mutation cycles for the children in each generation (Nm). These versions are named Gp1, Gp2, Gp3, and Gp4; their characteristics are listed in Table 1.

Determination of numerical performance profiles

A comparative analysis was conducted to determine the robustness and efficiency of four methods: Gp1, Gp2, Gp3, and Gp4. The study used numerical performance profiles, which define the cumulative distribution function for a numerical performance profile. The metrics of interest were the algorithm's execution time, its ability to reach the global optimum in the objective function, and the number of evaluations performed during the calculation sequence. These factors were compared to analyze the performance and convergence of the optimization method.

This paper aims to compare four different methods based on three metrics. The first metric is the relative distance between the optimal solution found by the optimization method and the known global optimal solution obtained by the ClustalW algorithm. This metric measures the robustness of the process, i.e., its ability to locate the global optimum of the objective function. The second and third metrics are the number of function evaluations $N\hat{F}E$ required during the processing and the time taken ($\hat{T}$) for process.

To evaluate specific metrics, we considered four optimization methods ($ns = 4$) and 13 problems or sets of sequences ($np = 13$). Each case study was solved 30 times, with random initial solutions and different random alignments. The stop condition was stabilized within the 100-generation limit. However, since the stop criterion is based on the generation number, a sensitive tolerance of 1.0E-06 is assumed for the value of the objective function since the optimal solution is uncertain. It was set as the convergence criterion for the four methods for all four optimization methods and sequence sets, the values of $t_{p,s}$ were calculated using the results of the 30 calculations and the following expressions (Equation 5).

$$t_{p,s}^{d} = \frac{\dot{f}_{obj} - \hat{f}_{obj}}{\dot{f}_{obj} - f_{obj}^{w}} \qquad t_{p,s}^{NFE} = N\hat{F}E \quad t_{p,s}^{T} = \hat{T} \tag{5}$$

Being $\hat{f}_{obj}$ the average value of the target function calculated by the optimization method, $\dot{f}_{obj}$ is the global optimum of the objective function, f_{obj} is the maximum value for the objective function found within the calculation sequence, $N\hat{F}E$ and $\hat{T}$ are respectively the average value of the number of functions evaluated and the time to reach the convergence of the optimization method. It is important to note that the values of $\hat{f}_{obj}$, $N\hat{F}E$ y $\hat{T}$ were determined using the 30 numerical experiments performed for the case study. As established in the literature [45], average values are often used for behavioral metrics to describe method performance. Based on the above, this study also employs such an approach. On the other hand, for all three metrics, the numerical performance profile rate $r_{p,s}$ is defined as in Equation (6):

$$r_{p,s} = \frac{t_{p,s}}{min\{t_{p,s}: s \in S\}} \tag{6}$$

Where S corresponds to the set of optimization methods analyzed. This method assigns a value of 1 to the algorithm that performs the best in each problem. Finally, the cumulative probability rate $\rho_s(\tau)$ for the optimization strategy S and the metric in question is defined as in the Equation (7):

$$\rho_s(\tau) = \frac{1}{n_p} cantidad\{p \in P: r_{p,s} \leq \tau\} \tag{7}$$

Where τ is a factor that is defined in $(1, \infty)$. In the graph of the performance profile, for example, the graph of ρ_s *versus* τ, compares the relative performance between optimization methods for the problem group. So far, performance profiles have been used by [46] to compare bioinspired algorithms and *benchmark* functions. However, this concept has not been used to compare the methods described in the MSA problem.

RESULTS AND DISCUSSION

The results of the fitness, $N\hat{F}E$, and time metrics are summarized and described below. As stated, the fitness value represents the algorithm's ability to reach better results, iteratively searching for solutions for a given problem. In this case, there are 13 problems for the performance evaluation; the problem count is presented in Table 3 as a C value. Furthermore, as described before, each problem C represents a set of sequences to be aligned in the multiple sequence alignment problem for the algorithm, and each algorithm $(Gp1, Gp2, Gp3,$ and $Gp4)$ ran 30 times for the calculated performance mean values. Also, the table presents the mean values for the fitness metric on each algorithm and each of the 13 multiple alignment problems.

TABLE 3. **Mean values for the Fitness metric of the Gp1, Gp2, Gp3 and Gp4 algorithms for the 13 multiple sequence alignment problems.**

C	Gp1	Gp2	Gp3	Gp4
1	62723.7	62385.6	63085.2	63105.4
2	59747.1	60072.8	59776.5	59605.0
3	57785.0	58536.2	58413.7	57109.7
4	52653.2	53250.0	53497.3	53526.8
5	16934.0	16463.8	16917.7	17270.7
6	-4932.2	-4724.0	-5529.0	-4903.8
7	-43993.1	-44014.3	-43848.8	-43909.3
8	-33991.1	-33350.3	-33782.7	-33775.6
9	54515.2	54405.9	54311.7	53919.9
10	-99067.2	-98881.0	-98633.5	-98737.2
11	52933.6	53749.8	52805.7	52540.1
12	-4082.1	-4463.7	-4449.5	-4134.2
13	9190.8	8423.8	8997.1	8699.8

The fitness metric shows promising performance results for the Gp2 and Gp3 algorithms since the objective is to increment the most possible fitness value. Also, the negative values describe complicated sequences for the alignment problem for all four algorithms.

For the number of evaluated functions ($N\hat{F}E$) metric, Table 4 shows the better performance of the Gp3 algorithm in problems 1 and 8. Gp1 performed better in sequence set number 2. Furthermore, all four algorithms present similar $N\hat{F}E$ results in sequence set number 12. This shows a significant difference in the algorithms' performance in terms of the different strategies they represent.

TABLE 4. **The $N\hat{F}E$ values for each of the four algorithms on the alignment of the 13 sets of sequences. The results show substantial differences between the four algorithms.**

C	Gp1	Gp2	Gp3	Gp4
1	690.867	684.067	679.600	688.733
2	680.400	693.033	686.433	685.100
3	684.333	690.700	686.233	686.600
4	686.033	693.167	688.867	687.900
5	685.300	687.167	683.233	681.033
6	684.667	689.867	683.633	684.167
7	692.133	683.167	690.233	693.933
8	682.367	690.400	679.600	689.867
9	686.200	689.400	684.533	681.067
10	693.400	685.667	686.733	686.733
11	685.233	680.767	693.333	690.700
12	682.733	683.367	683.867	683.100
13	685.933	681.500	683.967	683.600

The time it takes for the algorithms to process the stated problems is a commonly used metric for comparing the strategies' performance. Table 5 shows the performance in terms of the required time for each of the four algorithms to process the 13 multiple alignment problems. It is worth noting that $Gp3$ took more time than the other algorithms to process the alignment problems. Furthermore, $Gp4$ showed better performance than the different algorithms. The efficiency of an algorithm is not determined by the time it takes to run. Still, in this case, the time comparison helps show the main difference between the algorithms: the number of nuclei for the hardware process.

TABLE 5. The comparative of the mean values in the metric Time for the four algorithms in the 13 sets of sequences for the multiple alignment problem.

C	Gp1	Gp2	Gp3	Gp4
1	4409.033	3943.900	5065.433	3381.000
2	4118.767	3554.400	4849.733	2964.267
3	4582.700	3944.633	5352.100	3268.467
4	3779.267	3289.667	4397.400	2727.467
5	3542.733	3141.700	4128.300	2598.000
6	2649.367	2543.267	3106.400	2061.000
7	3439.833	3138.667	4025.133	2667.833
8	2929.867	2753.867	3396.033	2300.000
9	4546.700	3874.767	5232.233	3361.800
10	5006.133	4514.933	5748.400	3919.100
11	3866.033	3288.933	4525.900	2901.100
12	2501.500	2321.367	2912.000	2032.300
13	4440.800	3894.400	5086.733	3478.067

We present a Microsoft Excel file named results in the provided github link for a detailed description of the tables above.

Figure 3 displays the performance profile for the metric $t^{d}_{p,s}$. This metric is associated with the ability of the algorithm to reach a better solution to a given problem. The figure 3 shows the optimization method's ability to approach the global optimum in the problems considered. $Gp1$ and $Gp3$ maintain remarkable performance and approach convergence. This can be attributed to the fact that they perform single-core processing with maximum and minimum mutation levels of 1 and 4, respectively. It is worth noting that this characteristic is in $Gp1$ and $Gp3$ and contributes to the state of the art of genetic programming, particularly regarding the mutation level for the individuals in the Genetic Algorithms population. In other words, this means that the medium-level mutation had no fitness improvement benefits for this case study.

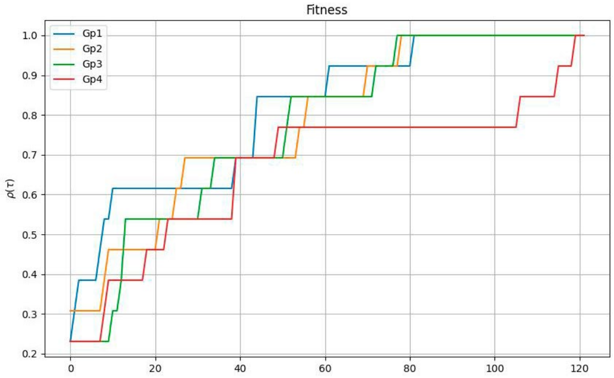

FIGURE 3. Numerical performance profile for fitness metric $t^{d}_{p,s}$ described as fitness value for each of the four algorithms.

Regarding efficiency, the metric $N\hat{F}E$ is associated with the number of evaluated functions and represents the hardware computational effort that the algorithmic strategy performs. Figure 4 is the performance profile, which indicates that $Gp4$ performs remarkably well. This may be because $Gp4$ employs the fewest mutations in the Genetic Algorithm and the highest number of cores in its algorithmic strategy. Similarly, $Gp1$ also demonstrates remarkable performance. It is worth noting that the previously described fitness results are consistent with the performance of $Gp1$ with its algorithmic strategy by using the fewest number of processing cores and the lowest level of mutation.

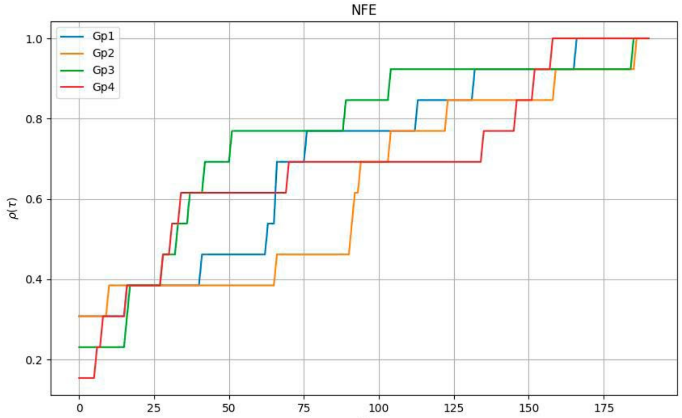

FIGURE 4. **Numerical performance profile for the metric $N\hat{F}E$.**

Figure 5 indicates that the $Gp4$ optimization method outperforms the others in terms of efficiency, as measured by the time spent on optimization $\hat{T}$. This may be because $Gp4$ utilizes greater parallel processing cores and fewer mutation processing than the other methods.

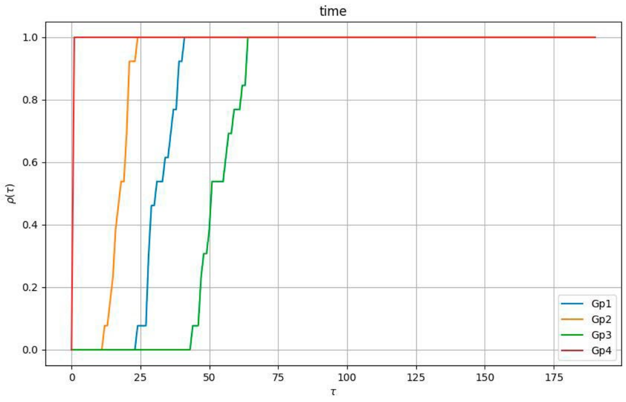

FIGURE 4. **Numerical performance profile for the metric $\hat{T}$.**

However, the Gp4 algorithm did not produce remarkable fitness or $N\hat{F}E$ values results. This shows that ensuring an efficient algorithmic and mutation process is more important than incorporating hardware resources.

CONCLUSIONS

This paper compares and discusses four strategies of the Genetic Algorithm method using the numerical performance profile model [47] in a set of genetic sequences. Based on the findings, the Gp1 approach is the most robust compared to other methods studied in this research. However, the efficiency, measured by the number of functions evaluated and convergence time, varies between the alignment methods. *Gp*4 is the method with the fewest evaluated functions and the highest processing speed. Thus, it can be concluded that the number of cores influences the alignment method's efficiency in parallel processing, and the robustness of the alignment method is related to the number of mutations. However, the *Gp*2 algorithm, with the highest core number and mutation level, did not perform remarkably well compared to the other strategies that varied the mutation level and number of cores.

Increasing the sequences in the data set is recommended to obtain more accurate results. By testing with the data set used in this research, these findings can be compared to other studies on genetic algorithms. Finally, it is essential to note that variations in mutation levels or other parameters can affect the performance of the different strategies.

On the other hand, conventional computer equipment can produce promising results when processing genetic information if the algorithms are specifically designed to make the most of hardware resources. Additionally, the computational effort of the hardware used impacts the number of evaluated functions. The quality of the solution obtained in the case of multiple sequence alignment relies on specific parameters of the genetic algorithm, such as the size of the population, the mutation level, and the crossing method. Moreover, the comparison method based on the determination of the performance profile is recommended as a valuable strategy for contrasting results in different metrics of interest.

ACKNOWLEDGEMENTS

The authors would like to thank the Faculty of Systems Saltillo Unit of the Autonomous University of Coahuila for the facilities in this study.

COMPETING INTERESTS

The authors have no competing interests to declare.

AUTHOR CONTRIBUTION

E.R.W. conceptualization, methodology, software, writing original draft. M. M. D. S. formal analysis, investigation, supervision, validation, writing review and editing. J. V. S. validation.

REFERENCES

[1] N. Mićić and B. Mićić, “God is Dead, Long Live DNA,” Agro-knowledge J., vol. 18, no. 2, pp. 143-146, Dec. 2017, doi: https://doi.org/10.7251/AGREN1702143M

[2] D. Ghoshdastidar and M. Bansal, “Dynamics of physiologically relevant noncanonical DNA structures: an overview from experimental and theoretical studies,” Brief Funct. Genomics, vol. 18, no. 3, pp. 192-204, Jun. 2018, doi: https://doi.org/10.1093/bfgp/ely026

[3] E. Arunan, “One Hundred Years After the Latimer and Rodebush Paper, Hydrogen Bonding Remains an Elephant!,” J. Indian Inst. Sci., vol. 100, no. 1, pp. 249-255, Jan. 2020, doi: https://doi.org/10.1007/s41745-019-00154-4

[4] A. M. Fleming and C. J. Burrows, “Formation and processing of DNA damage substrates for the hNEIL enzymes,” Free Radic. Biol. Med., vol. 107, pp. 35-52, Jun. 2017, doi: https://doi.org/10.1016/j.freeradbiomed.2016.11.030

[5] É. Leroux, C. Brosseau, B. Angers, A. Angers, and S. Breton, “Méthylation de l’ADN mitochondrial,” Med. Sci., vol. 37, no. 3, pp. 258-264, Mar. 2021, doi: https://doi.org/10.1051/medsci/2021011

[6] E. W. Sayers, E. E. Bolton, J. R. Brister, K. Canese, et al., ‘Database resources of the national center for biotechnology information’, Nucleic Acids Res., vol. 50, no. D1, pp. D20-D26, Jan. 2022, doi: https://doi.org/10.1093/nar/gkab1112

[7] GenBank and WGS Statistics, GenBank, 2024. [Online]. Available: https://www.ncbi.nlm.nih.gov/genbank/statistics/

[8] M. Abdel-Basset, L. Abdel-Fatah, and A. K. Sangaiah, "Metaheuristic Algorithms: A Comprehensive Review," in Computational Intelligence for Multimedia Big Data on the Cloud with Engineering Applications, A. K. Sangaiah, M. Sheng, Z. Zhang, Eds., Catalunya, Spain: Academic Press, 2018, pp. 185-231. doi: https://doi.org/10.1016/B978-0-12-813314-9.00010-4

[9] S. M. Almufti, A. Ahmad Shaban, Z. Arif Ali, R. Ismael Ali, and J. A. Dela Fuente, "Overview of Metaheuristic Algorithms," PGSRT, vol. 2, no. 2, pp. 10-32, Apr. 2023, doi: https://doi.org/10.58429/pgjsrt.v2n2a144

[10] D. Rodriguez, D. Gomez, D. Alvarez, and S. Rivera, "A Review of Parallel Heterogeneous Computing Algorithms in Power Systems," Algorithms, vol. 14, no. 10, art. no.. 275, Sep. 2021, doi: https://doi.org/10.3390/a14100275

[11] X. Wang and J. Liu, "Multiscale Parallel Algorithm for Early Detection of Tomato Gray Mold in a Complex Natural Environment," Front. Plant. Sci., vol. 12, art. no. 620273, May 2021, doi: https://doi.org/10.3389/fpls.2021.620273

[12] X. Dong, Y. Wu, Z. Wang, L. Dhulipala, Y. Gu, and Y. Sun, "High-Performance and Flexible Parallel Algorithms for Semisort and Related Problems," in Proceedings of the 35th ACM Symposium on Parallelism in Algorithms and Architectures, New York, NY, USA, 2023, pp. 341-353. doi: https://doi.org/10.1145/3558481.3591071

[13] M. Kimiaei, A. Hassan Ibrahim, and S. Ghaderi, "A subspace inertial method for derivative-free nonlinear monotone equations," Optimization, pp. 1-28, Sep. 2023, doi: https://doi.org/10.1080/02331934.2023.2252849

[14] A. H. Kamali, E. Giannoulatou, T. Y. Chen, M. A. Charleston, A. L. McEwan, and J. W. K. Ho, "How to test bioinformatics software?," Biophys Rev., vol. 7, no. 3, pp. 343-352, Sep. 2015, doi: https://doi.org/10.1007/s12551-015-0177-3

[15] Y. Zhang, Q. Zhang, J. Zhou, and Q. Zou, "A survey on the algorithm and development of multiple sequence alignment," Brief Bioinform., vol. 23, no. 3, art. no. bbac069, May 2022, doi: https://doi.org/10.1093/bib/bbac069

[16] M. Maiolo, X. Zhang, M. Gil, and M. Anisimova, "Progressive multiple sequence alignment with indel evolution," BMC Bioinformatics, vol. 19, no. 1, art. no. 331, Dec. 2018, doi: https://doi.org/10.1186/s12859-018-2357-1

[17] B. Schmidt and A. Hildebrandt, "Dedicated Bioinformatics Analysis Hardware," in Encyclopedia of Bioinformatics and Computational Biology, Sydney, Australia: Elsevier, 2019, pp. 1142-1150. doi: https://doi.org/10.1016/B978-0-12-809633-8.20186-6

[18] R. Guo, Y. Zhao, Q. Zou, X. Fang, and S. Peng, "Bioinformatics applications on Apache Spark," Gigascience, vol. 7, no. 8, art. no. giy098, Aug. 2018, doi: https://doi.org/10.1093/gigascience/giy098

[19] N. A. Stover and A. R. O. Cavalcanti, "Using NCBI BLAST," Curr. Protoc. Essent. Lab. Tech, vol. 14, no. 1, May 2017, doi: https://doi.org/10.1002/cpet.8

[20] S. Iantorno, K. Gori, N. Goldman, M. Gil, and C. Dessimoz, "Who Watches the Watchmen? An Appraisal of Benchmarks for Multiple Sequence Alignment," Methods Mol. Biol., vol. 1079, 2014, pp. 59-73. doi: https://doi.org/10.1007/978-1-62703-646-7_4

[21] A. Löytynoja, "Alignment Methods: Strategies, Challenges, Benchmarking, and Comparative Overview," Methods Mol. Biol., vol. 855, 2012, pp. 203-235. doi: https://doi.org/10.1007/978-1-61779-582-4_7

[22] Y. He, "Research on global double sequence alignment optimization algorithm based on dynamic programming," in Third International Conference on Computer Science and Communication Technology (ICCSCT 2022), Beijing, China, 2022, art. no. 125060L, doi: https://doi.org/10.1117/12.2662630

[23] J.-H. Hung and Z. Weng, "Sequence Alignment and Homology Search with BLAST and ClustalW," Cold Spring Harb. Protoc., vol. 2016, no. 11, art. no. pdb.prot093088, Nov. 2016, doi: https://doi.org/10.1101/pdb.prot093088

[24] Q. Zou, X. Shan, and Y. Jiang, "A Novel Center Star Multiple Sequence Alignment Algorithm Based on Affine Gap Penalty and K-Band," Phys. Procedia, vol. 33, pp. 322-327, 2012, doi: https://doi.org/10.1016/j.phpro.2012.05.069

[25] F. Tang, J. Chao, Y. Wei, F. Yang, Y. Zhai, L. Xu, Q. Zou, "HAlign 3: Fast Multiple Alignment of Ultra-Large Numbers of Similar DNA/RNA Sequences," Mol. Biol. Evol., vol. 39, no. 8, Aug. 2022, doi: https://doi.org/10.1093/molbev/msac166

[26] B. Reddy and R. Fields, "Multiple Sequence Alignment Algorithms in Bioinformatics," in Smart Trends in Computing and Communications. Lecture Notes in Networks and Systems, 2022, pp. 89-98. doi: https://doi.org/10.1007/978-981-16-4016-2_9

[27] D. Pacheco Bautista, M. González Pérez, and I. Algredo Badillo, "From sequencing to hardware acceleration of DNA alignment software: A integral review," Rev. Mex. Ing. Biomed., vol. 36, no. 3, pp. 257-275, Sep. 2015, doi: https://doi.org/10.17488/RMIB.36.3.6

[28] D. Pacheco-Bautista, "ABPSE: Alineador de ADN Basado en Paralelismo a Nivel de Bit y la Estrategia Siembra y Extiende," Rev. Mex. Ing. Biomed., vol. 40, no. 1, pp. 1-13, 2019. doi: https://doi.org/10.17488/RMIB.40.1.4

[29] A. S. M. Aljohani, F. A. Alhumaydhi, A. Rauf, E. M. Hamad, and U. Rashid, "In Vivo Anti-Inflammatory, Analgesic, Sedative, Muscle Relaxant Activities and Molecular Docking Analysis of Phytochemicals from Euphorbia pulcherrima," Evid. Based Complement. Alternat. Med., vol. 2022, art. no. 7495867, Apr. 2022, doi: https://doi.org/10.1155/2022/7495867

[30] J. H. Holland, Adaptation in Natural and Artificial Systems. The MIT Press, 1992, doi: https://doi.org/10.7551/mitpress/1090.001.0001

[31] K. Hao, J. Zhao, K. Yu, C. Li, and C. Wang, "Path Planning of Mobile Robots Based on a Multi-Population Migration Genetic Algorithm," Sensors, vol. 20, no. 20, art. no. 5873, Oct. 2020, doi: https://doi.org/10.3390/s20205873

[32] H. Ahrabian, M. Ganjtabesh, A. N. Dalini, and Z. R. M. Kashani, "Genetic algorithm solution for partial digest problem," Int. J. Bioinform. Res. Appl., vol. 9, no. 6, pp. 584-594, 2013, doi: https://doi.org/10.1504/ijbra.2013.056622

[33] M. Fernandez, J. Caballero, L. Fernandez, and A. Sarai, "Genetic algorithm optimization in drug design QSAR: Bayesian-regularized genetic neural networks (BRGNN) and genetic algorithm-optimized support vectors machines (GA-SVM)," Mol. Divers, vol. 15, no. 1, pp. 269-289, Feb. 2011, doi: https://doi.org/10.1007/s11030-010-9234-9

[34] M. Sale and E. A. Sherer, "A genetic algorithm based global search strategy for population pharmacokinetic/pharmacodynamic model selection," Br. J. Clin. Pharmacol., vol. 79, no. 1, pp. 28-39, Jan. 2015, doi: https://doi.org/10.1111/bcp.12179

[35] S. H. Almanza-Ruiz, A. Chavoya, and H. A. Duran-Limon, "Parallel protein multiple sequence alignment approaches: a systematic literature review," J. Supercomput., vol. 79, no. 2, pp. 1201-1234, Feb. 2023, doi: https://doi.org/10.1007/s11227-022-04697-9

[36] D. Song, J. Chen, G. Chen, N. Li, et al., "Parameterized BLOSUM Matrices for Protein Alignment," IEEE/ACM Trans. Comput. Biol. Bioinform., vol. 12, no. 3, pp. 686-694, May 2015, doi: https://doi.org/10.1109/tcbb.2014.2366126

[37] J. S. Piña, S. Orozco-Arias, N. Tobón-Orozco, L. Camargo-Forero, R. Tabares-Soto, and R. Guyot, "G-SAIP: Graphical Sequence Alignment Through Parallel Programming in the Post-Genomic Era," Evol. Bioinform. Online, vol. 19, art. no. 117693432211505, Jan. 2023, doi: https://doi.org/10.1177/11769343221150585

[38] I. R. and A. Chavoya, "PaMSA: A Parallel Algorithm for the Global Alignment of Multiple Protein Sequences," IJACSA, vol. 8, no. 4, pp. 513-522, 2017, doi: https://dx.doi.org/10.14569/IJACSA.2017.080468

[39] T. Harada and E. Alba, "Parallel Genetic Algorithms," ACM Comput. Surv., vol. 53, no. 4, pp. 1-39, Jul. 2021, doi: https://doi.org/10.1145/3400031

[40] J. Zhu, G. Wang, Y. Li, Z. Duo, and C. Sun, "Optimization of hydrogen liquefaction process based on parallel genetic algorithm," Int. J. Hydrogen Energy, vol. 47, no. 63, pp. 27038-27048, Jul. 2022, doi: https://doi.org/10.1016/j.ijhydene.2022.06.062

[41] J. Xu, L. Pei, and R. Zhu, "Application of a Genetic Algorithm with Random Crossover and Dynamic Mutation on the Travelling Salesman Problem," Procedia Comput. Sci., vol. 131, pp. 937-945, 2018, doi: https://doi.org/10.1016/j.procs.2018.04.230

[42] K. R. Anil Kumar and E. R. Dhas, "Opposition based genetic optimization algorithm with Cauchy mutation for job shop scheduling problem," Mater. Today Proc., vol. 72, pp. 3006-3011, 2023, doi: https://doi.org/10.1016/j.matpr.2022.08.263

[43] T. D. Pham and W.-K. Hong, "Genetic algorithm using probabilistic-based natural selections and dynamic mutation ranges in optimizing precast beams," Comput. Struct., vol. 258, art. no. 106681, Jan. 2022, doi: https://doi.org/10.1016/j.compstruc.2021.106681

[44] Galaxy Community, "The Galaxy platform for accessible, reproducible and collaborative biomedical analyses: 2022 update," Nucleic Acids Res., vol. 50, no. W1, pp. W345-W351, Jul. 2022, doi: https://doi.org/10.1093/nar/gkac247

[45] A. Bonilla-Petriciolet, J. C. Tapia-Picazo, C. Soto-Becerra, and J. G. Zapiain-Salinas, "Perfiles de comportamiento numérico de los métodos estocásticos simulated annealing y very fast simulated annealing en cálculos termodinámicos," Ing. Inv. Tecnolog., vol. 12, no. 1, pp. 51-62, Jan. 2011, doi: https://doi.org/10.22201/fi.25940732e.2011.12n1.006

[46] R.-W. Ernesto, L.-G. Ernesto, B. Rafael, and G.-G. Yolanda, "Perfiles de comportamiento numérico de los métodos de búsqueda immune network algorithm y bacterial foraging optimization algorithm en funciones benchmark," Ing. Inv. Tecnolog., vol. 17, no. 4, pp. 479-490, Oct. 2016, doi: https://doi.org/10.1016/j.riit.2016.11.007

[47] E. D. Dolan and J. J. Moré, "Benchmarking optimization software with performance profiles," Math. Program., vol. 91, no. 2, pp. 201-213, Jan. 2002, doi: https://doi.org/10.1007/s101070100263

ARTÍCULO DE REVISIÓN

VOL. 45 | NO. 2 | **MAYO - AGOSTO 2024** | PP 78-99

Revista Mexicana de Ingeniería Biomédica

dx.doi.org/10.17488/RMIB.45.2.5

E-LOCATION ID: **1414**

Exoesqueletos de Rehabilitación: una Revisión Sistemática de Literatura

Rehabilitation Exoskeletons: a Systematic Literature Review

Jonatan Rivera Robles[1], *Juan Bory Reyes*[1], *Luis Manuel Hernández Simón*[1], *Jesús Ignacio Eduardo Palacios Hernández*[1]

[1] Instituto Politécnico Nacional - México

RESUMEN

La acelerada evolución de la tecnología en la última década, ha permitido grandes avances en campos de la ciencia como la medicina, la robótica, la biónica y la rehabilitación al integrar conocimientos y técnicas de estas áreas.

Los exoesqueletos de rehabilitación constituyen ejemplos de integración multidisciplinaria en el desarrollo de herramientas de intervención fisioterapéutica que han demostrado tener resultados significativos en pacientes con enfermedades neurológicas.

Esta revisión bibliográfica sistemática, presenta los avances, desarrollos y características de estos dispositivos y su situación actual, específicamente aquellos que presentan mayor impacto en su co-citación y co-ocurrencia para que los trabajos integrados a la investigación sean verificables y confiables. Esto mediante la implementación de una metodología para la elaboración del estado del arte del tema de exoesqueletos de rehabilitación, basado en la implementación de bases de datos científicas, herramientas bibliometricas digitales sistematizadas y su integración sistémica.

La literatura científica sobre los exoesqueletos de rehabilitación fue recopilada de trabajos publicados entre enero de 2014 al 30 de noviembre de 2023, los cuales fueron recuperados de la *Web of Science*. Como primera etapa se definen los criterios de inclusión y exclusión para limitar la búsqueda dentro de la base de datos científica, como segunda etapa el procesamiento de la información y los trabajos obtenidos para procesarlos mediante la implementación del software *CiteSpace*, como resultado de esta etapa se obtuvo el análisis de co-ocurrencia, se generó una red gráfica y un análisis de co-citación; Posteriormente con los datos obtenidos de las etapas anteriores se implementó el método PRISMA. Como tercera etapa se presentan los resultados obtenidos de las 1511 publicaciones y 108,512 citas de referencia que tratan sobre exoesqueletos de rehabilitación. Se presenta una discusión sobre las principales características, avances, limitaciones, desafíos y tendencias que presentan estos dispositivos en la actualidad.

PALABRAS CLAVE: análisis, diagnóstico, exoesqueletos, movilidad, rehabilitación

ABSTRACT

The accelerated evolution of technology in the last decade has enabled breakthroughs in fields of science such as medicine, robotics, bionics and rehabilitation by integrating knowledge and techniques from these areas.

Rehabilitation exoskeletons are examples of multidisciplinary integration in the development of physiotherapeutic intervention tools that have shown significant results in patients with neurological diseases.

This systematic literature review presents the advances, developments and characteristics of these devices and their current situation, specifically those that have the greatest impact on their co-citation and co-occurrence so that the works integrated into the research are verifiable and reliable. This is done through the implementation of a methodology for the elaboration of the state of the art on the subject of rehabilitation exoskeletons, based on the implementation of scientific databases, systematised digital bibliometric tools and their systemic integration.

The scientific literature on rehabilitation exoskeletons was compiled from papers published between January 2014 and 30 November 2023, which were retrieved from the *Web of Science*. The first stage was to define the inclusion and exclusion criteria in order to limit the search within the scientific database, and the second stage was to process the information and works obtained in order to process them using the *CiteSpace* software, as a result of this stage, the co-occurrence analysis was obtained, a graphical network was generated and a co-citation analysis, subsequently with the data obtained from the previous stages, the PRISMA method was implemented. As a third step, the results obtained from the 1511 publications and 108,512 reference citations dealing with rehabilitation exoskeletons are presented. A discussion of the main characteristics, advances, limitations, challenges and trends of these devices is presented.

KEYWORDS: analysis, diagnosis, exoskeletons, mobility, rehabilitation

Autor de correspondencia

DESTINATARIO: **Jonatan Rivera Robles**
INSTITUCIÓN: **Instituto Politécnico Nacional**
DOMICILIO: **Av. 100mts, #45, Tlacamaca, Gustavo A. Madero, C.P. 07380. Ciudad de México, México.**
CORREO ELECTRÓNICO: jriverar@ipn.mx

Recibido:

26 Enero 2024

Aceptado:

2 Mayo 2024

INTRODUCCIÓN

El desarrollo tecnológico que se vive actualmente en el siglo XXI, ha permitido desarrollar sistemas muy avanzados en el campo de la robótica, esto a su vez, brinda una contribución significativa en este campo de la medicina para la rehabilitación[1]. Este es el caso de los exoesqueletos utilizados para la rehabilitación de personas con algún problema de movimiento[2] y otras alteraciones físicas; estos son dispositivos que realizan la función de soporte y ayuda de tal manera que son una extensión del cuerpo del paciente que los utiliza, se desarrollan como estructuras externas al cuerpo, las articulaciones del exoesqueleto[3] ayudan al movimiento de las extremidades en el cuerpo. Estos dispositivos integran la destreza del usuario y las potencialidades del dispositivo permitiendo la recuperación de movilidad del individuo[4].

Existen registros que indican los primeros desarrollos alrededor de los exoesqueletos fue en el año de 1960, las primeras aparición de exoesqueletos fueron realizados en los Estados Unidos de América mediante la colaboración de los militares y *General Electric* (GE) con el prototipo denominado "*Hardiman I*". Se desarrolló un exoesqueleto con el objetivo de incrementar la capacidad de carga para el usuario, específicamente para actividades como la descarga y manipulación de materiales. Se construyó con la finalidad de manipular cargas de hasta 25 kilogramos y el usuario solo sintiera la carga correspondiente a un kilogramo de peso. El dispositivo de cuerpo entero no pudo ser implementado en una persona por que presentaba problemas de inestabilidad y peligro. Este dispositivo contaba una extremidad superior capaz de manipular una carga 340 kilogramos de peso[5].

Los exoesqueletos, "*ReWalk*" y "*eLegs*" permiten mejorar la marcha de pacientes con alteraciones de la movilidad para caminar. La órtesis robótica Lokomat ha demostrado una mejoría considerable en personas con problemas para caminar[6]. Estos dispositivos para la rehabilitación, basan su funcionamiento en realizar una serie de movimientos definidos por fisioterapeutas, lo que proporciona a los médicos evaluar el avance y mejoría que los pacientes de una forma automática. Los exoesqueletos son activos, es decir contienen actuadores que permiten la ejecución de funciones previamente definidas[7].

Autores como L. Zhang *et al.*[8] y D. Shi *et al.*[9] han desarrollado estudios de la viabilidad y uso de estos dispositivos en diferentes áreas de la ingeniería, la biomecánica, la medicina y la rehabilitación; han propuesto métodos para su diseño, los cuales ofrecen un área de oportunidad para los investigadores debido a la complejidad del tema y de la solución de los modelos matemáticos que los rigen.

Estas directrices contribuyen al perfeccionamiento de tecnologías que ayudan en la labor de los médicos orientadas al tratamiento de personas con problemas de movilidad[10]. Los exoesqueletos son la herramienta que pretende coadyuvar en el mejoramiento de la calidad de vida de los pacientes.

MATERIALES Y MÉTODOS

Esta investigación presenta una revisión sistemática de toda la investigación disponible relevante respecto de Exoesqueletos de Rehabilitación y en relación con su desarrollo y aplicación, enmarcado en el enfoque sistémico[11]. Para su elaboración, se ha implementado en una primera etapa la *Web of Science Core Collection* un índice de citas confiable para ubicar investigaciones en un conjunto multidisciplinario y seleccionado de revistas, libros y conferencias, en segunda etapa *CiteSpace*[12][13] y tercera etapa el método *Preferred Reporting Items for Systematic Reviews and Meta-Analyses* (PRISMA)[14] que permite estructurar de manera ordenada la información para su análisis (Figura 1).

Seguidamente, se muestra de manera detallada las fases que la componen, con el objetivo de identificar los exoesqueletos más utilizados en el campo de la rehabilitación y su desarrollo e implementación en el campo de la rehabilitación.

En este contexto unos de los dispositivos que pretenden apoyar en el mejoramiento de la movilidad en las personas son los exoesqueletos[15], dispositivos conformados por elementos mecánicos, electrónicos e informáticos diseñados para ser implementados sobre el cuerpo del paciente, de forma que asemeja una prenda de vestir, definido más claramente por el término en inglés "*Wearable robots*"[16] que permite apoyar las extremidades del cuerpo del paciente para su movilidad y/o aumentar sus capacidades físicas. La gran mayoría de los desarrollos en este campo están orientados a la medicina, pensados y diseñados para adaptarse al cuerpo del usuario mediante la implementación de sensores y elementos para el procesamiento de datos para la retroalimentación de conjunto con el usuario para la ejecución de alguna operación o movimiento mediante los motores para realizar tareas predeterminadas.

Búsqueda inicial

Los datos recopilados que integran este estudio provienen de la literatura científica indexada en la *Web of Science* al 21 de noviembre del 2023, se utilizó una estrategia de búsqueda sistemática para cumplir con los requisitos de búsqueda exhaustiva. La estrategia de búsqueda fue desarrollada mediante una combinación de palabras "exoesqueletos" y "aplicaciones médicas" contenidas en las bases de datos *PubMed, ScienceDirect* y *Scopus*. Consecutivamente, se aumentó aplicando otra combinación, usando los operadores booleanos AND y OR[17] dependiendo de cómo acomodaran las palabras "grados de libertad", "pacientes", "exosqueletos robóticos", "usable". Estas búsquedas permitieron obtener un vasto número de datos. Muchos de estos duplicados, otros con poco valor referencial al objetivo de esta revisión, pero permiten una visión más amplia del mundo sobre la temática tratada y esto, permite corroborar que este tema, presenta que anteriormente se había realizado una revisión sistemática.

Algunos resultados arrojados por *Scopus* se encontraron duplicados en *Elsevier,* por tal motivo se excluyeron de la búsqueda.

Búsqueda sistemática

La búsqueda se llevó a cabo en dos etapas la primera en marzo de 2021 y la segunda en marzo de 2023, en *ScienceDirect, Elsevier, PubMed* y *Springer Link*, delimitando los resultados a manuscritos publicados en el periodo comprendido entre 2014 hasta el 2023. La combinación en cuestión de términos que presentan los mejores resultados son los siguientes: *(exoskeletons OR rehabilitation) OR exoskeletons to support rehabilitation) AND (exoskeletons OR degrees of freedom) OR systemic approach) OR systematic review) OR Rehabilitation) OR Physiotherapy) OR Medical applications) OR Sensors) OR Control systems*. Específicamente, se obtuvieron 1511 resultados distribuidos de la siguiente forma: 680 en *ScienceDirect*, 412 *Elsevier,* 380 *PubMed* y 39 en *Springer Link*. Posterior a la recopilación, se procedió a definir los criterios de inclusión y exclusión. El primer criterio para la búsqueda se limitó a "artículo" y "revisión", excluyendo todas las demás opciones. Los documentos integrados en esta investigación incluyen atributos básicos como: fecha de publicación, autor o autores, la institución, el país y las referencias citadas; con estos datos se estructuro la base de datos con la que se desarrolló el análisis posterior. En una segunda etapa del procesamiento de la información se generaron redes de co-ocurrencia y co-citación para analizar sus características, esto mediante la implementación de la herramienta tecnológica *CiteSpace*, una aplicación de Java desarrollada por Chen[18], este método se ha comprobado ampliamente en trabajos de cienciometría [19][20][21]. El sesgo temporal de los documentos integrados dentro de esta investigación fue de año 2014 al 2023 con 1 año por corte, Los tipos de nodos incluían la categoría, la revista citada, las referencias y las palabras clave. El criterio de selección fue que la publicación estuviera entre las 50 primeras por mayor número de citas en cada sesgo temporal.

Criterios de inclusión

1. Que presenten estudios de casos únicos, revisiones, estudios empíricos, estudios de caso único.
2. Que utilicen técnicas de rehabilitación y fisioterapia para tratamientos de problemas en los diferentes miembros del paciente.
3. Que hablen de mejorar la movilidad, entendido dentro del marco del enfoque sistémico.
4. Que el estudio se concentre en la atención de problemas en las extremidades superiores e inferiores.
5. Que se hayan publicado en el periodo comprendido entre 2014 a 2023.

Criterios de exclusión

1. Los estudios que se enfoquen en procedimientos quirúrgicos.
2. Los estudios orientados a exoesqueletos que no presenten aportes verificables.
3. Los que no se refieren a rehabilitación y fisioterapia.
4. Aquellos que se encuentran fuera del contexto del análisis o utilizan métodos de difícil interpretación.

RESULTADOS Y DISCUSIÓN

Por las características de los resultados obtenidos, estos se dividieron en tres secciones. La primera sección contiene la búsqueda sistematizada sobre los exoesqueletos de rehabilitación y el análisis bibliométrico (WoS); la segunda sección presenta los resultados del análisis de la red de co-ocurrencia de publicaciones y el análisis de co-citación (CiteSpace); en la tercera y última sección se muestran los resultados finales obtenidos (PRISMA).

Como resultado de la recopilación, filtrado de duplicación y procesado de datos, se recuperaron un total de 782 publicaciones y 9005 referencias citadas en el campo de la investigación sobre "exoesqueletos de rehabilitación" que se publicaron entre los años 2014 al 2023; En la Figura 1 se muestra el número de artículos publicados y citados que conforma la base de datos de la investigación.

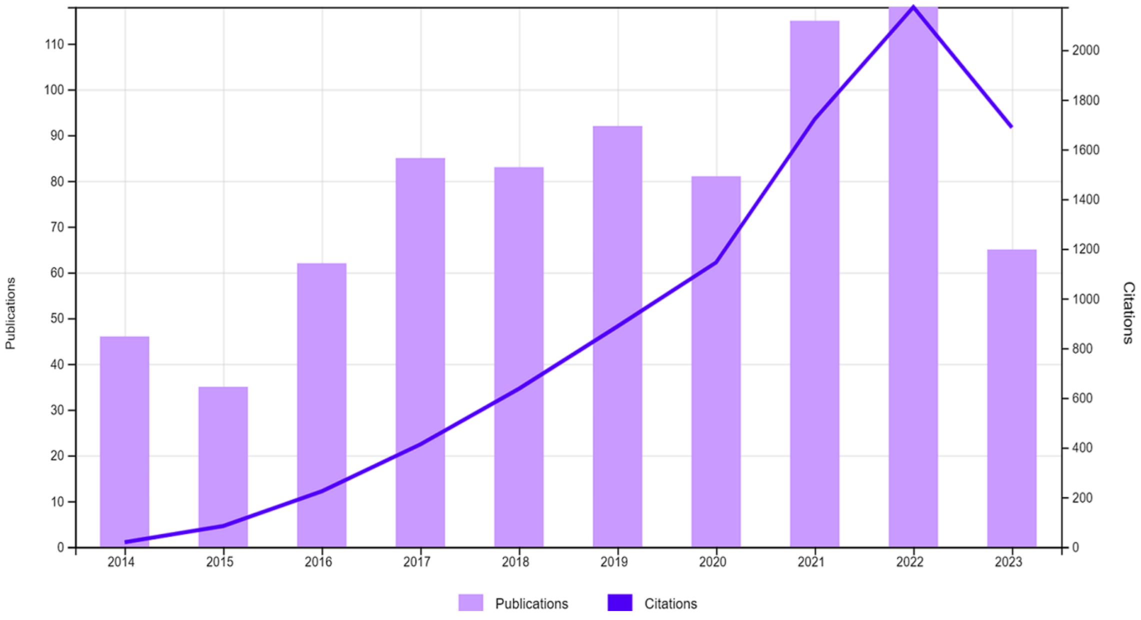

FIGURA 1. Publicaciones indexadas en *Web of Science* (2014 a 2023) sobre exoesqueletos de rehabilitación.

Los resultados muestran que el número de publicaciones relacionadas con los exoesqueletos de rehabilitación presentan una tendencia anual significativamente creciente en la última década (2014-2023). También se destaca la tendencia creciente en el número de citas, el año 2023 presenta una caída tanto en las citas como en número de publicaciones.

Análisis de co-ocurrencias

La *Web of Science* (WoS) implementa la técnica de co-ocurrencia para el manejo de su base de datos, por lo que clasifica las publicaciones en una o más categorías[22], en el caso de las publicaciones de exoesqueletos de rehabilitación se han ordenado en 71 categorías durante los últimos 10 años. En la Tabla 1 se detallan las métricas de co-ocurrencia de categorías en la investigación.

Partiendo de los datos de la Tabla 1, se construyó una red de co-ocurrencias de las conexiones internas entre categorías mediante el uso del software *CiteSpace*, esto permitió revelar temas y patrones en los datos que visualizan las relaciones complejas entre los elementos del estudio (Figura 2). Esta red combinada se basa en una distribución correspondiente a muestras de años consecutivos, resaltando los trabajos más importantes; cada nodo de la red representa un autor y este a su vez una referencia citada, las líneas que conectan los nodos simbolizan los enlaces de citación y el grosor de estas muestran la importancia de la referencia citada. Los resultados arrojan que hay 14 *clusters* de autores predominantes en la red sobre exoesqueletos de rehabilitación.

En la Figura 2 se observan los siguientes datos: la generación de la red se desarrolló con fecha: diciembre 9, 2023 a las 2:57:02 PM, la base de datos procesada corresponde a la *Web of Science* (WoS), Periodo de duración 2014-2023 (Longitud de corte=1). Criterios de selección: g-índex (k=25), Factor de retención de enlaces (LRF) 3.0. Enlace/nodo (L/N) 10. Años de búsqueda (LBY) -1. Equivalencia (e) = 1.0. Red: Nodo (N)= 228, Borde (E)= 777 (Densidad =0.03), Cinco Co-citación más grandes 203 (89 %), modularidad Q= 0.7227, Silueta media ponderada S= 0.8867, Media armónica Q, S = 0.7963.

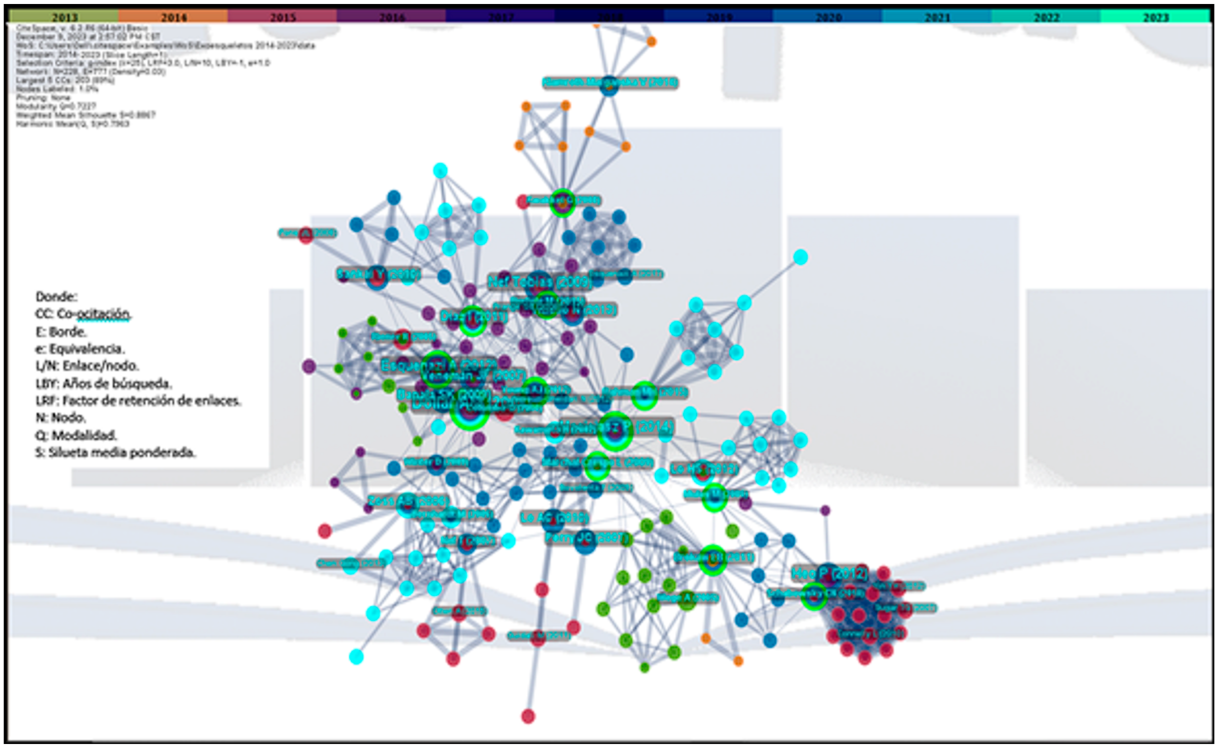

FIGURA 2. **Red de co-ocurrencia de publicaciones sobre exoesqueletos de rehabilitación publicadas de 2014 a 2023.**

TABLA 1. **Categorías de co-ocurrencia en publicaciones relacionadas con exoesqueletos de rehabilitación (2014 a 2023).**

Categorías WoS	Publicaciones	% de 782
Robótica	244	31.202
Ingeniería Eléctrica Electrónica	217	27.749
Ingeniería Biomédica	140	17.903
Sistemas de control de automatización	126	16.113
Informática Inteligencia Artificial	105	13.427
Ingeniería mecánica	90	11.509
Rehabilitación	76	9.719
Ingeniería Multidisciplinar	59	7.545
Neurociencia	59	7.545
Instrumentos Instrumentación	45	5.754
Informática Sistemas de Información	35	4.476
Física aplicada	35	4.476
Ciencia de los materiales Multidisciplinar	33	4.220
Telecomunicaciones	30	3.836
Neurología clínica	24	3.069
Química Analítica	23	2.941
Química Multidisciplinar	23	2.941
Informática Aplicaciones Interdisciplinarias	23	2.941
Ingeniería de fabricación	22	2.813
Teoría y métodos informáticos	21	2.685
Ingeniería Industrial	20	2.558
Informática Cibernética	18	2.302
Ciencias multidisciplinares	18	2.302
Ciencia de los materiales Biomateriales	14	1.790
Mecánica	11	1.407

Análisis de co-citación

Mediante la información obtenida se desarrolló y visualizo la red de agrupaciones de co-citación (Figura 3) que contiene 107 nodos y 308 enlaces. Los nodos representan artículos citados que se han etiquetado con autores respectivos y años de publicación.

Se identificaron y etiquetaron un total de 53 *clusters* de co-citación de publicaciones relacionadas con exoesqueletos de rehabilitación. Las tendencias obtenidas de la investigación se caracterizan por agrupaciones de artículos citados por publicaciones de investigaciones correspondientes. En la red, Q fue de 0.7493 y la media de S fue de 0.9544, lo que indica que la red es fiable y tenía una alta calidad para la estructura de co-citación. En resumen, se identificaron 5 agrupaciones destacadas que representan temas de investigación importante, estas se muestran en detalle en la Tabla 2, que incluyen información sobre el tamaño, el valor S, el año, la duración y la etiqueta de los primeros 5 clúster. El tamaño se refiere al número de artículos citados en el clúster, que determina el volumen del clúster. Un valor alto S denota una buena homogeneización de los nodos en cada clúster.

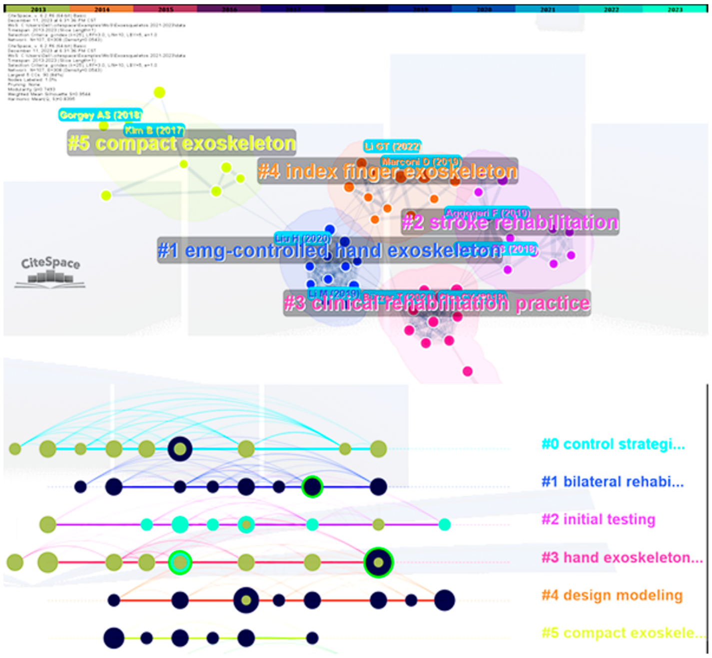

FIGURA 3. Principales grupos de co-citación relacionados con exoesqueletos de rehabilitación en investigaciones publicadas entre 2013 a 2023.

TABLA 2. Principales clusters de co-citación relacionados con exoesqueletos de rehabilitación de investigaciones publicadas en el periodo de 2014 a 2023.

Cluster	Tamaño	Silueta	Año	Duración	Etiquetas
1	27	0.864	2017	2014-2020	Exoesqueleto; robótico dispositivo; rehabilitación robótica; robot exoesqueleto; estudio piloto; rehabilitación de la marcha.
2	23	0.844	2019	2019-2023	Exoesqueleto activo; paciente con ictus crónico; dispositivo rehabilitación; recuperación motora; estudio piloto.
3	25	0.599	2018	2018-2021	Exoesqueleto controlado por electromiografía (EMG); participación activa; neurorehabilitación; sistema de entrenamiento locomotor accionado por cable; lesión medular humana, marcha asistida por exoesqueleto.
4	25	0.92	2019	2018-2023	Exoesqueleto; sistema de rehabilitación; unidad de interacción hombre-máquina amigable con el ser humano; rehabilitación tipo novedoso; lectura eficaz de interacciones.
5	9	0.912	2017	2017-2018	Solicitud de rehabilitación; cinemática articular; entrenamiento de la marcha; algoritmo de control exoesqueleto robótico.

Fundados en los criterios anteriores y aplicando un segundo nivel de tamizado de la información, se implementó del método PRISMA en los grupos 1 y 4 con mayor silueta media ponderada, se seleccionaron cincuenta y dos manuscritos. Se realizó la lectura del resumen y mediante esta, se eliminaron 16, principalmente por orientarse en procedimientos invasivos y sin apoyo (n=10), por estar centrados en estudios médicos o por no incluir las zonas de las lesiones (n=4) y por salirse del contexto de la investigación, dificultando su análisis y procesamiento de datos (n=2). Al final, 36 manuscritos cubrieron los criterios establecidos para su inclusión y realizar la revisión sistemática (Figura 4). La herramienta de Control de Calidad de la Revisión, fue el método PRISMA.

Diagrama de flujo PRISMA 2020 para nuevas revisiones sistemáticas que incluían búsquedas en bases de datos, registros y otras fuentes.

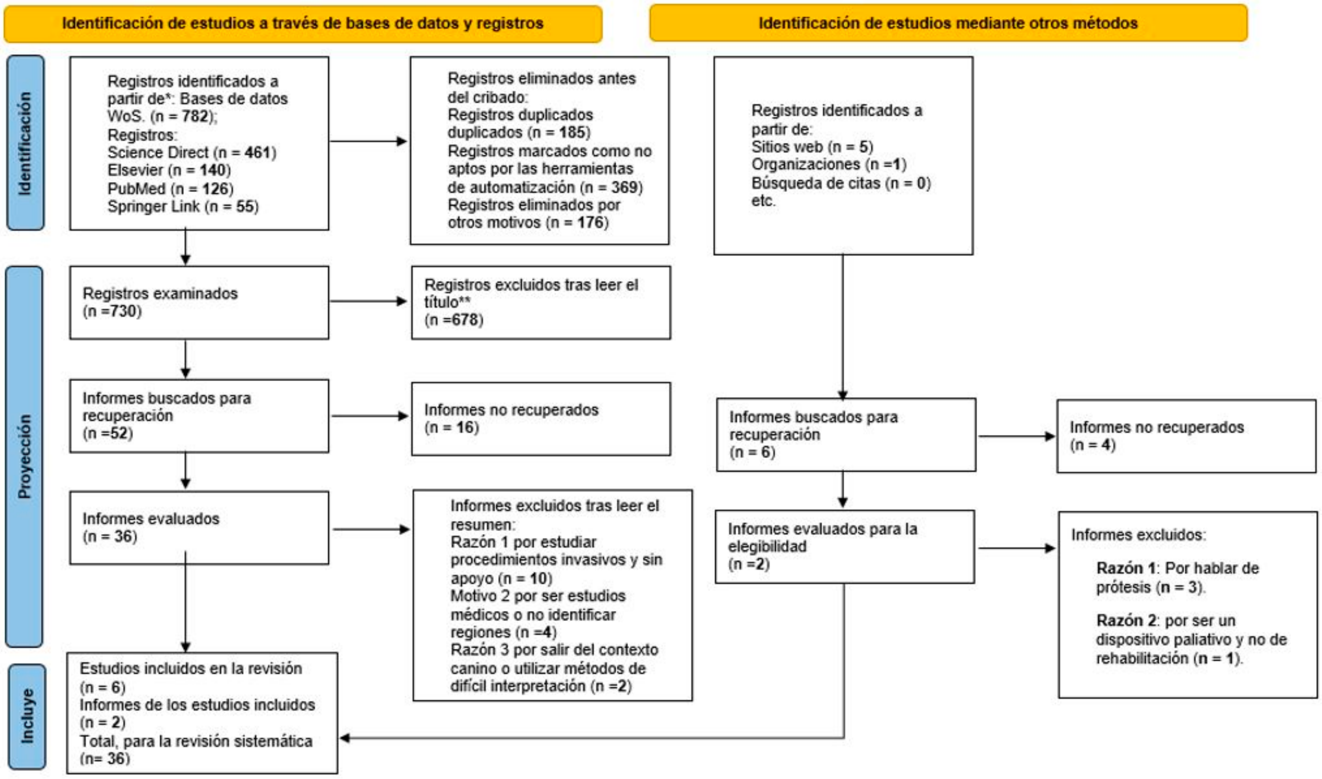

*Considere, si es posible, comunicar el número de registros identificados en cada base de datos o registro consultado (en lugar del número total de todas las bases de datos/registros).
**Si se utilizaron herramientas de automatización, indique cuántos registros fueron excluidos por un humano y cuántos fueron excluidos por herramientas de automatización.
De: Page MJ, McKenzie JE, Bossuyt PM, Boutron I, Hoffmann TC, Mulrow CD, *et al.* La declaración PRISMA 2020: una guía actualizada para informar revisiones sistemáticas. BMJ 2021; 372:n71. doi: https://doi.org/10.1136/bmj.n71. Para más información, visite: http://www.prisma-statement.org/

FIGURA 4. **Diagrama de Flujo PRISMA en cuatro niveles.**

Todos ellos señalaban regiones de miembros inferiores de problemas de movilidad con el enfoque de la Teoría General de Sistemas (TGS)[23] orientados a procedimientos invasivos, la mayoría evaluando tareas motoras y uno enfocado en un análisis neurológico, pero que fue incluido ya que presenta información importante y con relación al resto. El objetivo fue resumir las investigaciones relacionadas exclusivamente exoesqueletos de cuerpo completo, exoesqueletos de miembros inferiores y orientados a la rehabilitación. Varios de los estudios son piloto o prueba, cuyo objetivo es conocer la viabilidad para hacer posteriores estudios con un mayor tamaño de muestra.

Por lo general los estudios consideran un tamaño reducido además de características muy heterogéneas, tanto dentro de un mismo estudio como al comparar unos estudios con otros. Esto puede explicarse por la complejidad de la patología, resulta difícil conseguir un grupo amplio y homogéneo de pacientes. El nivel de las investigaciones incluidas se evaluó a través de la Escala *Oxford Centre for Evidence Based-Medicine* (OCEBM)[24], para valorar el nivel de aportación e impacto.

Publicaciones con métricas elevadas

La centralidad de la interrelación (BC) y la resistencia al estallido (BS) son dos métricas importantes en el análisis de la co-citación. En la Tabla 3 se enumeran los artículos con los 10 mayores índices de BC de todos los nodos de la red. También se muestran 4 artículos (los enumerados del 1 al 4) que deberían ser considerados publicaciones de alto impacto sobre exoesqueletos para la rehabilitación. Una publicación de Kim B. *et al.*[25] está identificado como la que tiene el mayor BC (0.27) y ha sido citada en diversos campos de la investigación, como la robótica (428 citas), ingeniería eléctrica, electrónica (350 citas), ingeniería Biomédica (210 citas) y en la rehabilitación (195 citas).

TABLA 3. **Las 20 publicaciones con mayor fuerza de explosión.**

Rango	Resistencia al estallido	Autor	Año	Título de la publicación
1	0.27	Kim B., *et al.*	2017	*An upper-body rehabilitation exoskeleton Harmony with an anatomical shoulder mechanism: Design, modelling, control, and performance evaluation*[25].
2	0.21	Humanchahua D., *et al.*	2021	*A Robotic Prosthesis as a Functional Upper-Limb Aid: An Innovative Review*[26].
3	0.20	Bützer T., *et al.*	2021	*Fully Wearable Actuated Soft Exoskeleton for Grasping Assistance in Everyday Activities*[27].
4	0.17	Trigili E., *et al.*	2019	*Design and Experimental Characterization of a Shoulder-Elbow Exoskeleton With Compliant Joints for Post-Stroke Rehabilitation*[28].
5	0.14	Hao L., *et al.*	2020	*Human-robot cooperative control based on sEMG for the upper limb exoskeleton robot*[29].
6	0.14	Molteni F., *et al.*	2018	*Exoskeleton and End-Effector Robots for Upper and Lower Limbs Rehabilitation: Narrative Review*[30].
7	0.14	Du Plessis t., *et al.*	2021	*A Review of Active Hand Exoskeletons for Rehabilitation and Assistance*[31].
8	0.13	Chu C. Y., *et al.*	2018	*Soft robotic devices for hand rehabilitation and assistance: a narrative review*[32].
9	0.12	Calabró R. S., *et al.*	2018	*Shaping neuroplasticity by using powered exoskeletons in patients with stroke: a randomized clinical trial*[33].
10	0.10	Chen T.Y., *et al.*	2019	*An Elbow Exoskeleton for Upper Limb Rehabilitation with Series Elastic Actuator and Cable-Driven Differential*[34].
11	0.09	Boser Q. A., *et al.*	2021	*Defining the design requirements for an assistive powered hand exoskeleton: A pilot explorative interview study and case series*[35].
12	0.09	Al Rezage Ghasaq, *et al.*	2016	*Fuzzy PID control of lower limb exoskeleton for elderly mobility*[36].
13	0.09	Amiri M. S,. *et al.*	2019	*Hybrid design of PID controller for four DoF lower limb exoskeleton*[37].
14	0.08	Marconi D., *et al.*	2019	*A novel hand exoskeleton with series elastic actuation for modulated torque transfer*[38].
15	0.07	De la Cruz-Sánchez B.A., *et al.*	2019	*Development of Hand Exoskeleton Prototype for Assisted Rehabilitation: Proceedings of the 4thIFToMM Symposium on Mechanism Design for Robotics*[39].
16	0.07	Donkor E.S., *et al.*	2018	*Stroke in the 21st Century: A Snapshot of the Burden, Epidemiology, and Quality of Life*[40].
17	0.07	Rahaman M. H., *et al.*	2015	*Development of a whole arm wearable robotic exoskeleton for rehabilitation and to assist upper limb movements*[41].
18	0.06	Aggogeri F., *et al.*	2019	*Robotics for rehabilitation of hand movement in stroke survivors*[42].
19	0.06	Ambrosini E., *et al.*	2019	*A Hybrid Robotic System for Arm Training of Stroke Survivors: Concept and First Evaluation*[43].
20	0.04	Al-Fahaam H., *et al.*	2018	*Novel soft bending actuator-based power augmentation hand exoskeleton controlled by human intention*[44].

Discusión

Como principales características en este estudio, cabe resaltar la cantidad de publicaciones encontradas (1511 con 108,512 citas), relacionadas al tema de los exoesqueletos de rehabilitación, A partir de esta muestra se depuraron 782 publicaciones que presentan una citación de 9005 referencias, este cribado permitió realizar los análisis de co-citación y co-ocurrencia para obtener datos significativos en la investigación como son los siguientes: las categorías como han sido clasificados, la cantidad de trabajos contenidos en cada categoría, el porcentaje correspondiente a cada categoría, las 10 categorías predominantes con base en su productividad. Aunado a estos resultados se obtuvo una red de co-ocurrencia que muestra cómo se agrupan las 71 categorías de los trabajos de investigación referentes a exoesqueletos de rehabilitación y que dentro de estas existen 14 categorías predominantes; estas muestras se encuentran en un sesgo temporal de 119 meses (enero 2014 a noviembre 2023).

A partir del análisis de co-citación de los trabajos contenidos en las 14 categorías predominantes se logró construir una red que muestra los principales grupos de co-citación, estos grupos fueron jerarquizados por el grado de conexión entre los *clusters* tomando la métrica de -1 nada de conexión y 1 total conexión. La Figura 3 resalta cinco *clusters*, constituidos de 109 nodos con 308 enlaces, estos representan artículos citados etiquetados mediante autores y años de publicación para construir una línea de tiempo que represente su comportamiento.

Los *cluster* de la Tabla 2 fueron jerarquizados a partir del tamaño de su silueta, de la siguiente forma: El *cluster* con mayor silueta es el cluster 4 con un tamaño de 23 nodos y una silueta de 0.92, después le sigue el cluster 5 con un tamaño de 9 nodos y una silueta de 0.912, el *cluster* 1 se ubica en la tercera posición al presentar un tamaño de 27 nodos y una silueta de 0.864, el *cluster* 2 con un tamaño de 25 nodos y una silueta de 0.844, El *cluster* 1 presenta un tamaño de 27 nodos con una silueta de 0.864, el *cluster* 2 con un tamaño de 25 nodos y una silueta de 0.844, *cluster* 3 un tamaño de 25 nodos con una silueta de 0.599. Estos hallazgos ayudaron a focalizar los trabajos científicos más representativos en cuanto al desarrollo, diseño, aplicación, control y materiales empleados, que aportan interesantes propuestas y datos relevantes dentro del estudio de los exoesqueletos de rehabilitación.

A continuación se presenta una descripción detallada de los contenidos de cada una de las publicaciones resultantes del presente estudio, agrupada de la siguiente forma:

Artículos de Revisión de literatura

La revisión que presentan C. J. Yang, *et al.*[1], resalta las tecnologías clave de los sistemas tipo exoesqueleto, presentan la investigación desde varios puntos de vista del diseño biomecánico, el modelado de la estructura del sistema, la cooperación y la asignación de funciones, la estrategia de control y la evaluación de la seguridad en un marco general. Sin embargo, todavía es necesario mejorar el diseño, el accionamiento y el control de estos dispositivos para que sean rentables en el mercado mundial. En comparación con el trabajo de revisión sistemática de B. Kalita, *et al.*[10]. Sobre dispositivos ortésicos y exoesqueléticos para extremidades inferiores. Los autores plantean que los dispositivos se revisaron a grandes rasgos según los tipos de articulación, los modos de actuación y las estrategias de control. Además, también presentan comparaciones tabulares con los tipos y aplicaciones de estos dispositivos. Por último, analizan las mejoras necesarias para aumentar la eficacia de los dispositivos de rehabilitación de miembros inferiores, así como la fase de desarrollo en la que se encuentran.

La revisión desarrollada por E. Swinnen, *et al.*[6] Tiene por objetivo evaluar la eficacia del entrenamiento de la marcha asistido por robot en pacientes con lesión medular, los estudios se agruparon por resultados (función corporal, actividad, participación y componentes de la Clasificación Internacional del Funcionamiento, de la Discapacidad y de la Salud - CIF) y diseño del estudio y se combinaron en una síntesis narrativa. Los autores concluyeron que no había pruebas disponibles de que el entrenamiento de marcha asistido por robot mejorara la función de la marcha más que otras estrategias de entrenamiento locomotor en pacientes con lesión de la médula espinal. Aunque los métodos de revisión no se informaron en su totalidad, las conclusiones de los autores reflejaron los datos limitados y es probable que sean fiables.

Contrario a la revisión de E. Swinnen, *et al.*, la realizada por D. Shi, *et al.,*[9] evalúa de forma crítica el progreso de la investigación en el análisis de la marcha humana y resume sistemáticamente los avances en el diseño mecánico y el control de los robots exoesqueleto de rehabilitación de extremidades inferiores. Del rendimiento de los prototipos típicos deduce que estos robots pueden conectarse a las extremidades humanas como formas vestibles; además, es posible controlar el movimiento del robot en cada articulación para simular la marcha normal y conducir la extremidad del paciente para realizar entrenamientos de rehabilitación asistidos por robots. Por tanto, la integración humano-robot es una de las líneas de investigación más importantes y, en este contexto, el diseño de estructuras híbridas rígidas-flexibles-blandas, la generación de una marcha personalizada y la fusión de información multimodal son tres tecnologías clave.

El trabajo de Huamanchahua, *et al.*[26] proporciona una visión muy interesante sobre la integración de las señales encefalografías para el control de dispositivos, por lo que también desarrollaron una matriz que incorpora propuestas que consideran de 2 a 15 DoF (grados de libertad), los actuadores utilizados, y la clasificación considerando si son activas, pasivas, eléctricas, mioeléctricas e híbridas. En conclusión, el artículo proporciona información a las personas que quieren crear una extensión superficial por debajo del codo y hacer uso del control de las señales electromiográficas que se extraen de las contracciones musculares.

T. Du Plessis, *et al.*[31] se enfoca en tecnologías de exoesqueletos activos para la rehabilitación, la asistencia, el aumento de los dispositivos hápticos para exoesqueletos de mano, resaltando los retos a los que se enfrentan los ingenieros y desarrolladores e intentan resolverlos. Planteando que cada exoesqueleto de mano tiene ciertos requisitos que cumplir para lograr sus objetivos. Ellos extraen estos requisitos y los clasifican en dos secciones: generales y específicos, con el fin de ofrecer una plataforma común para el desarrollo de futuros dispositivos. Los requisitos que consideran técnicamente son: tamaño, peso, ergonomía, rehabilitación, actuadores y sensores; estos se deben a la anatomía y biomecánica complejas de la mano. Concluyen que, mediante la implantación de sistemas inteligentes, las nuevas técnicas de rehabilitación, las técnicas de detección (electroencefalografía (EEG), electromiografía (EMG), admitancia) y estimación de la asistencia aplicada se pueden generar dispositivos más integrales y de mayor efectividad.

En contraste C. Y. Chu, *et al.*[32] centran su análisis en la detección de los modos de rehabilitación que estos dispositivos pretenden aplicar. Especificando que el Entrenamiento en Tareas Específicas (TST, por sus siglas en inglés) fue la forma más comúnmente discutida, ya que tiene como objetivo permitir que los pacientes comiencen a recuperar la función en su mano. El TST suele ser uno de los primeros ejercicios de rehabilitación y es probable que siga siendo un elemento básico de la rehabilitación robótica. La siguiente modalidad de entrenamiento más común fue el Movimiento Pasivo Continuo (MPC), que probablemente seguirá ganando popularidad debido a su facilidad de aplicación y eficacia funcional. El CPM se centra en la mejora de la amplitud de movimiento y la recuperación de la fuerza, un paso lógico en el proceso de rehabilitación. Por último, la Resistencia Activa (RA) fue el ejercicio menos comúnmente implementado, probablemente porque representa una de las etapas finales de la rehabilitación: el entrenamiento de la fuerza. A medida que más dispositivos avancen hacia sus fases de evaluación, se espera que aumente la popularidad de los ejercicios de resistencia activa.

Gracias a los planteamientos de los diferentes autores se puede visualizar un contexto más integrador de las diferentes características, clasificaciones, aplicaciones, diseños y aspectos a considerar en lo referente a los exoesqueletos en el campo de la rehabilitación y la fisioterapia.

Una característica recurrente en cada uno de éstos es el uso de elementos dinámicos en comparación con los dispositivos estáticos convencionales.

Artículos originales

Hasta la aparición del prototipo denominado Hardiman I (1971)[5], los sistemas de manipulación bilateral solían manipular un máximo de peso de 100 libras, eran pesados con una estructura muy grande en relación con su utilidad y solo permitían una operación remota. El prototipo propuso alternativas de solución a las limitaciones mecánicas de diseño de este tipo de sistemas que existían en esos tiempos, para el desarrollo de este prototipo los investigadores necesitaron lograr avances técnicos substanciales tanto en el diseño y la fabricación de maquinaria que les permitiera la construcción de los sistemas de control, los servosistemas bilaterales de alta carga, nuevos métodos de diseño y análisis de datos.

El Programa Hardiman I, fue decisivo para el desarrollo de nuevos conceptos en la manipulación de carga general para aplicaciones militares y estableció una buena base técnica sobre la que construir.

La *General Electric Company* había desarrollado un sistema servo bilateral hidromecánico que se estaba incorporando a los primeros manipuladores industriales pesados.

En los trabajos previos a la propuesta, la *General Electric Company* había realizado una investigación de los factores humanos y la cinemática con un dispositivo exoesquelético pasivo que proporcionaba un medio para medir los movimientos articulares y determinar el número mínimo de articulaciones necesarias para que un hombre tenga movilidad suficiente. También se había construido un pequeño modelo a escala para ilustrar las características básicas del sistema propuesto.

Los principales supuestos, que iban más allá del estado de la técnica, eran los siguientes:

1. Que la tecnología de servomotores bilaterales podría ser avanzada para satisfacer el aumento de la carga del sistema.
2. Que el sistema podía empaquetarse físicamente.
3. Que se podría conseguir el control del sistema de marcha bípedo.

Cumplir estas premisas significaba hacer cosas que no se habían hecho antes; Se consideró que los riesgos estaban bien equilibrados con el historial de logros técnicos de *General Electric Company*.

Pero se reconoció que existía un riesgo técnico sustancial el cual era el desarrollo de la interfaz hombre-máquina. Esto condujo a la definición de los requisitos específicos del sistema y de los subsistemas.

Posterior al desarrollo de este prototipo los resultados y avances tecnológicos obtenidos, plantearon una visión nueva a los investigadores permitiendo el diseño y construcción de prototipos más robustos para los años venideros.

Orientado a miembros superiores

El exoesqueleto denominado "*Harmony*"[25], desarrollado para rehabilitación de la parte superior del cuerpo, se caracteriza por ser un mecanismo anatómico de hombro con 5 grados de libertad activos accionado por actuadores elásticos en serie y formulado bajo un algoritmo recursivo de Newton-Euler con representación de dinámica espacial.

Otra propuesta de exoesqueleto interesante es el denominado "*Relab tenoexe*" de los autores Bützer, T., Lambercy, O., *et al.*[27] el cual presenta un módulo que genera los cuatro tipos de agarre para la mano, mediante un sistema remoto de sujeción que propone varias opciones en el diseño y control adaptados a las características individuales de cada usuario; esto comprobado mediante las pruebas realizadas en pacientes con accidentes cerebrovasculares y lesiones de la medula espinal.

Continuando con los exoesqueletos orientados a la neurorrehabilitación de extremidades superiores se encuentra el Sistema de Control "NESM" desarrollado por E. Trigili, *et al.*[28]. El cual emplea un mecanismo de auto alineación basado en juntas rotacionales pasivas que permite auto alinear suavemente los ejes de rotación del robot con las articulaciones de los usuarios en respuesta a movimientos repentinos e imprevistos provocados por contracciones espásticas y ayudando a personalizar ejercicios de rehabilitación pasiva, activo-asistido, activo-resistivo y activo-perturbado.

En T. Chen, *et al.*[34] se desarrolla un exoesqueleto de 2 grados de libertad que intenta proporcionar un control de par independiente en la flexión/extensión del codo y la supinación/pronación del antebrazo. Este utiliza dos actuadores elásticos en serie (SEA) idénticos para accionarlo. Los dos SEA están acoplados mediante un novedoso diferencial accionado por cable. El exoesqueleto es compacto y ligero, con una masa de 0,9 kg. Los errores de par RMS aplicados fueron inferiores a 0,19 Nm. Las pruebas de banco demostraron un tiempo de subida del par de aproximadamente 0,1 s, un ancho de banda de control del par de 3,7 Hz y una impedancia inferior a 0,03 Nm/deg a 1 Hz. El controlador puede simular una rigidez de pared máxima estable de 0,45 Nm/deg. El rendimiento global es adecuado para aplicaciones de terapia robótica y se discute la novedad del diseño.

El novedoso exoesqueleto "*HandeXos-Beta*" (HX-β) de dedo índice y pulgar para la rehabilitación de la mano fue desarrollado en D. Marconi, *et al.*[38]. El sistema HX-β presenta una arquitectura cinemática innovadora que permite el accionamiento independiente de la flexión/extensión y circunducción (oposición) del pulgar, permitiendo así una variedad de configuraciones de agarre naturalistas y funcionales. Además, cuenta con una novedosa arquitectura de actuadores elásticos en serie (SEA) que mide directamente el par transferido externamente en tiempo real y, por lo tanto, permite modos de funcionamiento controlados tanto por posición como por par, lo que permite la implementación de paradigmas de ejercicio tanto de robot a cargo como de usuario a cargo. Por último, la órtesis ajustable de HX-β, los grados de libertad pasivos y el esquema de control subactuado permiten una comodidad óptima, la alineación de las articulaciones robot-usuario y un accionamiento flexible para usuarios de distintos tamaños de mano. Además del diseño mecatrónico y las capacidades funcionales resultantes de HX-β, este trabajo presenta una serie de caracterizaciones de rendimiento físico, incluido el rendimiento del sistema de control de posición y par, la respuesta de frecuencia, la fuerza del efector final y la impedancia de salida.

B. A. De la Cruz-Sánchez, *et al.*[39] presenta un exoesqueleto de mano controlado por electromiografía (EMG) para movimientos básicos en terapia bilateral asistida, donde el trabajo bimanual es requerido por el paciente. Los usuarios objetivo son individuos con la mano derecha afectada por un accidente o problemas cerebrovasculares que requieren rehabilitación pasiva o asistida. A través de una GUI de Matlab, el sistema recibe, procesa y clasifica señales electromiográficas del usuario adquiridas por un brazalete MYO obteniendo una precisión del 81,2 % utilizando *k-Nearest Neighbors* (kNN) como algoritmo de clasificación y *Random Subset Feature Selection* (RSFS) como algoritmo de selección de características. Posteriormente, el exoesqueleto reproduce el movimiento detectado en la mano contraria del usuario. El prototipo de exoesqueleto tiene 8 grados de libertad (DOF), se ha construido mediante impresión 3D y tiene movimiento independiente de los dedos. El controlador del movimiento se basa en la lógica difusa. Para el análisis del rendimiento del sistema, se utiliza información cinemática de un sistema de captura de movimiento para comparar las trayectorias en diferentes tareas de agarre de la mano de un usuario con y sin el exoesqueleto con un error máximo del 10,63 % y un mínimo del 3,46 % con la posición final deseada, lo que físicamente representa una diferencia de 1,89° y 0,07° respectivamente.

Con el fin de ayudar a las personas con discapacidades físicas que tienen mermada la función de las extremidades superiores, En M. H. Rahman, *et al.*[41] se desarrolla un nuevo robot de tipo exoesqueleto de 7 grados de libertad denominado *Motion Assistive Robotic-Exoskeleton for Superior Extremity* (ETS-MARSE), para facilitar los movimientos cotidianos de las extremidades superiores y proporcionar una terapia de rehabilitación eficaz para la extremidad superior. El "ETS-MARSE" consta de una parte de apoyo al movimiento del hombro, una parte de apoyo al movimiento del codo y el antebrazo, y una parte de apoyo al movimiento de la muñeca. Está diseñado para llevarlo en la parte lateral de la extremidad superior con el fin de proporcionar movimientos naturalistas del hombro (flexión/extensión vertical y horizontal y rotación interna/externa), codo (flexión/extensión), antebrazo (pronación/supinación) y articulación de la muñeca (desviación radial/cubital y flexión/extensión).

Este artículo se centra en el modelado, diseño, desarrollo y control del "ETS-MARSE". Se realizaron experimentos con sujetos humanos varones sanos en los que se llevó a cabo un seguimiento de trayectorias en forma de ejercicios pasivos de rehabilitación (es decir, trayectorias preprogramadas recomendadas por un terapeuta/clínico). Los resultados experimentales demostraron que el "ETS-MARSE" puede llevar a cabo eficazmente la terapia de rehabilitación pasiva.

Un trabajo que requiere una mención particular, es Q. A. Boser, *et al.*[35] que tiene por objetivo definir las necesidades y expectativas preliminares de los usuarios finales de un exoesqueleto de mano asistivo. Se considera que los exoesqueletos de mano motorizados son una tecnología emergente que ha demostrado ser prometedora para ayudar a las personas con problemas en la función de la mano. En la investigación se describen varios diseños de exoesqueletos de mano; aunque, la mayoría no se han basado en criterios orientados al paciente. Es por esto, que fueron recopilados datos cualitativos y cuantitativos para comprender los requisitos de diseño de los usuarios finales de exoesqueletos de asistencia para las manos. Este trabajo refuerza la importancia de implicar a los usuarios de tecnología de rehabilitación en el proceso de desarrollo de dispositivos, planteando así algunos requerimientos a considerar para futuras investigaciones y desarrollo de prototipos.

Orientado a miembros inferiores

Continuando con los exoesqueletos orientados a miembros inferiores en R. S. Calabrò, *et al.*[33] se considera que el uso de dispositivos neurorobóticos puede mejorar la recuperación de la marcha mediante el entrenamiento de mecanismos específicos de plasticidad cerebral, lo que puede ser clave para el éxito de la rehabilitación con este método. Se evalúa si el exoesqueleto portátil “Ekso™” podía mejorar el rendimiento de la marcha en comparación con el entrenamiento convencional de la marcha sobre el suelo en pacientes con hemiparesia por ictus en fase crónica y si este fomenta la recuperación de mecanismos específicos de plasticidad cerebral. A través de esta investigación se concluye que el entrenamiento de la marcha con “Ekso™” parece prometedor en la rehabilitación de la marcha de pacientes que han sufrido una apoplejía. El estudio propone una base neurofisiológica putativa que respalda los efectos secundarios de “Ekso™”. Este conocimiento puede ser útil para planificar protocolos de rehabilitación de la marcha altamente adaptados al paciente.

Al Rezage, *et al.*[36] presenta investigaciones sobre el desarrollo de un dispositivo de asistencia para la movilidad de personas mayores. Se Diseña un exoesqueleto como dispositivo de asistencia para mejorar la extremidad inferior y proporcionar un par de soporte que aumente el par de la cadera y la rodilla durante el ciclo de la marcha. Consiste en un humanoide y un exoesqueleto accionado en *Solid Works* y que se importan al entorno virtual *Visual Nastran 4D.* Utiliza un algoritmo de control PID difuso para controlar el exoesqueleto accionado. Realizaron tareas de marcha simuladas con un humanoide que porta el exoesqueleto. Se supone que el humanoide representa a una persona mayor, es capaz de proporcionar el 60 % del par total necesario para completar el ciclo de la marcha, y que el dispositivo de asistencia proporciona el 40 % del par total.

ReWalk es un exoesqueleto robótico que tiene por objetivo que las personas con problemas en las extremidades inferiores causadas por la paraplejia puedan realizar movimientos de cadera y rodilla para que puedan ponerse de pie y caminar erguidas. Este es un exoesqueleto corporal. En L. Zhang, *et al.*[8] se realiza un estudio comparativo entre *“ReWalk”*, *“EAW”* y *“Lokomat”*, llevando a cabo un meta-análisis en red de ensayos controlados aleatorios y no aleatorios para evaluar las capacidades locomotoras logradas con dos tipos diferentes de programa de entrenamiento de la marcha asistido por robot (RAGT) en personas con lesión de la médula espinal (LME). El estudio analiza al dispositivo *Lokomat* y la marcha asistida por exoesqueleto vestible (EAW), ya que no se han comparado directamente con anterioridad. Ellos concluyen que el dispositivo *Lokomat* y el EAW portátil tuvieron efectos sobre el rendimiento de las capacidades de locomoción, a saber, la distancia, la velocidad y la función. El EAW portátil podría mejorar la velocidad de la marcha en comparación con el *Lokomat.*

Sistemas de control para exoesqueletos

El artículo presentado por H. Liu, *et al.*[29] propone un método de control cooperativo humano-robot basado en señales sEMG (electromiografía de superficie) para accionar un exoesqueleto neumático de extremidades superiores que actúe de acuerdo con las intenciones de movimiento del usuario. La información sobre la intención de movimiento del humano se estima combinando el método de regresión con el de clasificación. Basándose en el modelo de estimación del par de torsión de la articulación, que se origina a partir del modelo musculo esquelético de tipo Hill, se utiliza el método de regresión para estimar el par de torsión deseado de la articulación mediante la fusión de la señal sEMG con el ángulo de la articulación. Para evitar las sacudidas y mantener las extremidades del robot en estado estático, se desarrolla un método de clasificación con la máquina de vectores de soporte para conocer el estado de la articulación que el humano pretende mantener.

Los autores M. S. Amiri, *et al.*[37] desarrollan un método de ajuste de un controlador proporcional-integral-derivativo para un exoesqueleto de 4 grados de libertad utilizando un híbrido de algoritmo genético y optimización de enjambre de partículas. La función de transferencia de cada eslabón del exoesqueleto de miembro inferior, adquirida a partir de un modelo de péndulo, utiliza un sistema de control proporcional-integral-derivativo de bucle cerrado, mientras que cada eslabón se asumió como un eslabón de 1 grado de libertad. En el sistema de control, aplicaron un algoritmo híbrido para medir los parámetros del controlador de cada articulación y minimizar el error. Además, se simuló un modelo tridimensional del exoesqueleto de miembro inferior para validar el controlador propuesto. La trayectoria del sistema de control con controlador proporcional-integral-derivativo optimizado sigue con precisión la señal de entrada deseada. El resultado del controlador híbrido optimizado se comparó con el algoritmo genético y la optimización por enjambre de partículas basada en estadísticas. El error medio del algoritmo propuesto se determinó mediante análisis numérico.

CONCLUSIONES

Este artículo de revisión examina las principales referencias bibliográficas y de mayor relevancia a tener en cuenta al momento de efectuar un proyecto o prototipo de exoesqueleto, orientando al investigador en la elaboración de su propuesta mejor estructurada y más completa. Durante la revisión bibliográfica se logró constatar la importancia del uso de exoesqueletos como alternativa para la rehabilitación. La evidencia sobre el uso de exoesqueletos portables de miembros superiores e inferiores en personas con alguna patología es ampliamente comprobada y ayuda a corregir los patrones en la caminata en cuanto a velocidad y distancia recorrida, aportando un beneficio psicológico y de satisfacción en los usuarios. Sin embargo, podemos afirmar que los resultados reportados en la literatura considerada en el presente estudio no son concluyentes teniendo en cuenta la heterogeneidad de las muestras consideradas en la mayoría de ellos.

Se evidencia la necesidad de profundizar en estudios metodológicamente bien diseñados y con muestras heterogéneas más amplias. El uso de exoesqueletos está comprobado que funciona en pacientes con problemas de movilidad y sirve como apoyo y asistencia de los movimientos y/o el aumento de las capacidades del paciente.

Después de revisar las publicaciones científicas que presentan mayor co-citación y co-ocurrencia, se encontraron una gran cantidad de investigaciones relacionadas directamente con el tema. Se logra confirmar la clasificación establecida de estos dispositivos según su funcionamiento que deriva en exoesqueletos activos y pasivos. Se identificó una subdivisión que los agrupa según la parte del cuerpo que recibe ayuda: orientado a miembros superior, inferior, cuerpo completo, espalda; para finalmente constatar que también pueden ser clasificados por su uso ya sea médico o para potenciar capacidades de los usuarios.

Como conclusión de esta investigación se puede afirmar que el desarrollo de los exoesqueletos de rehabilitación está orientado a las diferentes causas que provocan la perdida de movilidad en las personas, las que pueden ir desde un trauma o accidente cardiovascular, hasta alguna condición genética.

Brechas y limitaciones detectadas

Un punto de coincidencia en la literatura revisada es la limitante en el diseño de los estudios realizados dependiendo de la heterogeneidad de la muestra de pacientes a tratar, los criterios de selección de la población para realizar las pruebas, la intensidad de los ejercicios con los diferentes dispositivos, el análisis y evaluación de los resultados; principalmente por el número reducido de sujetos de prueba y la complejidad de la evaluación clínica adecuada.

Adicionalmente estas revisiones incorporan una variedad de exoesqueletos dependiendo del objetivo de su diseño, características y aplicaciones. Esto genera una limitante ya que no todas especifican la duración de las sesiones o si fue solo una sesión en su aplicación, el número de repeticiones en los estudios, la intensidad y frecuencia con respecto de los tratamientos convencionales presentando diferencias sistemáticas entre estudios.

Las consideraciones de las revisiones clínicas respecto a esta heterogeneidad en el uso de los exoesqueletos varían por las limitaciones de las metodologías aplicadas en los estudios, lo que ha generado que los resultados de la implementación de estos dispositivos no sean concluyentes en algunos casos. Sin embargo, en el caso de exoesqueletos con mayor avance en su desarrollo se han considerado estas limitaciones y se han enfocado en adaptarlos a las características particulares de cada paciente y reducir esta variabilidad.

Desafíos

Los principales desafíos que presentan los estudios realizados se centran en el desarrollo de protocolos de operación y pruebas estandarizados con muestras heterogéneas de pacientes para diseñar terapias centradas en movimientos bien definidos, con repeticiones acorde a las capacidades del paciente, pero garantizando la efectividad, intensidad, frecuencia e impacto que requiere el paciente para obtener resultados medibles y favorables en su rehabilitación.

Otro desafío que se presenta en algunos dispositivos es la relacionada a los sistemas de control y los sensores que utilizan para la obtención de las señales que controlan la movilidad de las extremidades ya sea de articulaciones, miembros superiores, inferiores o de cuerpo completo, así como también la sensibilidad del paciente ante estos movimientos, otro punto importante a considerar es el tamaño de los dispositivos, en algunos casos la configuración que presentan por la integración de mecanismos los convierte en voluminosos y esta condición limita la sensación de libertad de movimiento en el paciente.

Una condición recurrente es la relacionada a las fuentes de energía eléctrica que requieren los dispositivos para su funcionamiento, la duración de las baterías, el peso que estas tienen y como evitar que este se transmita al paciente.

En general los exoesqueletos por encontrarse en proceso de desarrollo y estar en la fase de prototipos resultan ser de elevado costo de fabricación y venta, mayormente por la necesidad de fabricarlos como trajes a la medida de cada paciente. Otro condicionante es el mantenimiento regular que requieren y el personal especializado que debe realizarlo, así como las refacciones que se requieren para su reparación.

Tendencias

Los exoesqueletos tienen un futuro prometedor dentro del campo de la medicina, específicamente en su implementación como alternativa de rehabilitación; con el creciente avance tecnológico en temas como: Desarrollo de nuevos materiales, la impresión en tercera dimensión, la miniaturización de los componentes electrónicos, sistemas de monitoreo y control de mayor eficiencia, poderosos sistemas de adquisición de datos y baterías de menor tamaño con mayor duración. Todo lo anterior permitirá un desarrollo futuro de dispositivos más robustos, ligeros, eficientes, económicos y ergonómicamente más cómodos para los pacientes.

Con todas estas mejoras se vislumbran exoesqueletos de rehabilitación más variados, con mayor difusión dentro de la población hospitalaria, de menor costo que brinden mayor seguridad al paciente, que presenten mayor portabilidad, facilidad de mantenimiento y operación.

Otra visión prometedora de los exoesqueletos es ampliar su campo de aplicación en la terapia física, apoyo asistencial a las personas de la 3ra edad y que permitan mejorar la vida de personas con discapacidades físicas o genéticas.

En resumen, el potencial de los exoesqueletos va en crecimiento considerando que hace menos de un lustro se consideraban fantasías y ciencia ficción, actualmente en el 2024 son una realidad que tiende a ser parte de la vida cotidiana de las personas, esta idea resulta fascinante y retadora desde el punto de vista de la ciencia para los investigadores. El uso e implementación de estos dispositivos al interactuar con el mundo físico está cambiando la percepción de los pacientes en su calidad de vida.

Los exoesqueletos están revolucionando los tratamientos de rehabilitación y fisioterapia en el campo de la medicina moderna ya que ofrecen una alternativa viable en la asistencia y apoyo a los pacientes, con el objetivo de recuperar la movilidad, la libertad de realizar actividades básicas del día a día y la funcionalidad perdida. Todo ello en asistencia a los tratamientos de enfermedades cerebrovasculares, neuromusculares, relacionadas con la medula espinal, entre otras. Aunado a esto, también desempeñan una alternativa en el tratamiento y prevención de lesiones en pacientes diagnosticados con algún nivel de descalcificación de los huesos, lesiones musculares y afecciones articulares.

Los exoesqueletos *ReWalk, Ekso* y *Lokomat* son los más usados y comerciales. Estos, junto con Indego, están aprobados bajo los estándares de la Administración de Alimentos y Drogas de Estados Unidos (FDA) por sus siglas en ingles. Recientemente se han reportado investigaciones sobre la seguridad y costo de un nuevo diseño de robot llamado *AIDER*.

CONFLICTO DE INTERÉS

Los autores declaran no tener ningún conflicto de interés.

AGRADECIMIENTOS

Los autores quieren agradecer al Instituto Politécnico Nacional, donde este trabajo fue desarrollado, por el soporte financiero.

CONTRIBUCIÓN DE LOS AUTORES

J. R. R. conceptualización, curación de datos, investigación, metolodología, software, escritura del manuscrito original. J. B. R. conceptualización, investigación, metodología, escritura del manuscrito original. L. M. H. S. análisis formal, supervisión, investigación, revisión y edición de manuscrito. J. I. E. P. H. investigación, curación de datos, validación, escritura de manuscrito original.

REFERENCIAS

[1] C. J. Yang, J. F. Zhang, Y. Chen, Y. M. Dong, and Y. Zhang, "A review of exoskeleton-type systems and their key technologies," Proc. Inst. Mech. Eng. C: J. Mech. Eng. Sci., vol. 222, no. 8. pp. 1599-1612, Ago. 2008, doi: **https://doi.org/10.1243/09544062JMES936**

[2] A. Rivera, "Tratamiento de rehabilitación en enfermedades neuromusculares," LUXMED, vol. 18, no. 52, 2023, doi: **https://doi.org/10.33064/52lm20233603**

[3] C. Camilo Rodríguez-Beltrán y D. Andrés Benavides-Cárdenas "Utility and benefits of different exoskeletons for strokes diseases," Vis. Electron., vol. 16, no. 1, 2022. [En línea]. Disponible en: **https://revistas.udistrital.edu.co/index.php/visele/article/view/18684**

[4] N. Robinson, R. Mane, T. Chouhan y C. Guan, "Emerging trends in BCI-robotics for motor control and rehabilitation," Curr. Opin. Biomed. Eng., vol. 20. art. no. 100354, 2021, doi: **https://doi.org/10.1016/j.cobme.2021.100354**

[5] B. R. Fick, J. B. Makinson, Hardiman I Prototype for Machine Augmentation of Human Strength and Endurance. USA: General Electrico Co Schenectady NY Specialty Materials Handling Products Operation, 1971.

[6] E. Swinnen, S. Duerinck, J. P. Baeyens, R. Meeusen y E. Kerckhofs, "Effectiveness of robot-assisted gait training in persons with spinal cord injury: A systematic review," J. Rehabil. Med., vol. 42, no. 6. pp. 520-526, 2010, doi: **https://doi.org/10.2340/16501977-0538**

[7] A. Rodríguez-Fernández, J. Lobo-Prat y J. M. Font-Llagunes, "Systematic review on wearable lower-limb exoskeletons for gait training in neuromuscular impairments," J. Neuroeng. Rehabil., vol. 18, no. 1, art. no. 22, 2021. doi: **https://doi.org/10.1186/s12984-021-00815-5**

[8] L. Zhang, F. Lin, L. Sun, y C. Chen, "Comparison of Efficacy of Lokomat and Wearable Exoskeleton-Assisted Gait Training in People With Spinal Cord Injury: A Systematic Review and Network Meta-Analysis," Front. Neurol., vol. 13, art. no. 772660, 2022. doi: **https://doi.org/10.3389/fneur.2022.772660**

[9] D. Shi, W. Zhang, W. Zhang, y X. Ding, "A Review on Lower Limb Rehabilitation Exoskeleton Robots," Chin. J. Mech. Eng., vol. 32, no. 1, art. no. 74, 2019, doi: **https://doi.org/10.1186/s10033-019-0389-8**

[10] B. Kalita, J. Narayan, y S. K. Dwivedy, "Development of Active Lower Limb Robotic-Based Orthosis and Exoskeleton Devices: A Systematic Review," Int. J. Soc. Robotics, vol. 13, pp. 775-793, 2021, doi: **https://doi.org/10.1007/s12369-020-00662-9**

[11] M. P. Pantoja-Aguilar y J. R. Salazar Garza-Treviño, "Etapas de la administración: hacia un enfoque sistémico," Rev. Esc. Adm. Neg., no. 87, pp. 139-154, 2019, doi: **https://doi.org/10.21158/01208160.n87.2019.2412**

[12] C. Chen y M. Song, "Visualizing a field of research: A methodology of systematic scientometric reviews," PLoS One, vol. 14, no. 10, art. no. e0223994, 2019, doi: **https://doi.org/10.1371/journal.pone.0223994**

[13] Y. Zhang, X. Liu, X. Qiao, y Y. Fan, "Characteristics and Emerging Trends in Research on Rehabilitation Robots from 2001 to 2020: Bibliometric Study," J. Med. Internet Res., vol. 25, art. no. e42901, 2023, doi: **https://doi.org/10.2196/42901**

[14] M. J. Page, J. E. McKenzie, P. M. Bossuyt, I. Boutron, *et al.*, "The PRISMA 2020 statement: An updated guideline for reporting systematic reviews," BMJ, vol. 372, art. no. n71, 2021, doi: **https://doi.org/10.1136/bmj.n71**

[15] L. G. Fernández Álvarez, S. Núñez Nagy y R. Cano de la Cuerda, "Exoesqueletos portables en personas con lesión medular. Revisión sistemática," RIECS, vol. 5, no. 1, pp. 86-105, 2020, doi: **https://doi.org/10.37536/RIECS.2020.5.1.194**

[16] Y. Shi, W. Dong, W. Lin, y Y. Gao, "Soft Wearable Robots: Development Status and Technical Challenges," Sensors, vol. 22, no. 19, art. no. 7584, 2022, doi: **https://doi.org/10.3390/s22197584**

[17] A. C. Picalho, E. Rosangela De Oliveira Lucas, I. S. Amorim, "AtoZ novas práticas em informação e conhecimento Lógica booleana aplicada na construção de expressões de busca Boolean logic applied to the construction of search expressions", AtoZ, vol. 11, pp. 1-12, 2022. [En línea]. Disponible en: **https://revistas.ufpr.br/atoz/article/view/81838/45027**

[18] C. Chen, "CiteSpace II: Detecting and visualizing emerging trends and transient patterns in scientific literature," J. Am. Soc. Inf. Sci. Tec., vol. 57, no. 3, pp. 359-377, 2006, doi: **https://doi.org/10.1002/asi.20317**

[19] S. H. Chang, T. Afzal, J. Berliner, G. E. Francisco, "Exoskeleton-assisted gait training to improve gait in individuals with spinal cord injury: A pilot randomized study," Pilot Feasibility Stud., vol. 4, art. no. 64, 2018, doi: **https://doi.org/10.1186/s40814-018-0247-y**

[20] A. D. Delgado, M. X. Escalon, T. N. Bryce, W. Weinrauch, S. J. Suarez, A. J. Kozlowski, "Safety and feasibility of exoskeleton-assisted walking during acute/sub-acute SCI in an inpatient rehabilitation facility: A single-group preliminary study," J. Spinal Cord Med., vol. 43, no. 5, pp. 657-666, 2020, doi: **https://doi.org/10.1080/10790268.2019.1671076**

[21] A. S. Khan, D. C. Livingstone, C. L. Hurd, J. Duchcherer, *et al.*, "Retraining walking over ground in a powered exoskeleton after spinal cord injury: A prospective cohort study to examine functional gains and neuroplasticity," J. Neuroeng. Rehabil., vol. 16, no. 1, art. no. 145, 2019, doi: **https://doi.org/10.1186/s12984-019-0585-x**

[22] P. T. P. Oliver, "Citation Indexing for Studying Science," Nature, vol. 227, no. 5260, art. no. 870, 1970, doi: **https://doi.org/10.1038/227870b0**

[23] V. A. Domínguez Ríos y M. Ángel López Santillán, "Teoría General de Sistemas, un enfoque práctico: General Systems Theory, a practical approach," Tecnociencia Chih., vol. 10, no. 3, pp. 125-132, 2017, doi: **https://doi.org/10.54167/tch.v10i3.174**

[24] J. Howick, I. Chalmers, P. Glasziou, T. Greenhalgh, et al., Thornton "Explanation of the 2011 Oxford Centre for Evidence-Based Medicine (OCEBM) Levels of Evidence (Background Document)." Oxford Centre for Evidence-Based Medicine. **https://www.cebm.ox.ac.uk/resources/levels-of-evidence/explanation-of-the-2011-ocebm-levels-of-evidence**

[25] B. Kim y A. D. Deshpande, "An upper-body rehabilitation exoskeleton Harmony with an anatomical shoulder mechanism: Design, modeling, control, and performance evaluation," Int. J. Robot. Res., vol. 36, no. 4, pp. 414-435,2017, doi: **https://doi.org/10.1177/0278364917706743**

[26] D. Huamanchahua, D. Rosales-Gurmendi, Y. Taza-Aquino, D. Valverde-Alania, M. Cama-Iriarte, A. Vargas-Martinez, R. A. Ramirez-Mendoza, "A robotic prosthesis as a functional upper-limb aid: An innovative review," en 2021 IEEE International IOT, Electronics and Mechatronics Conference (IEMTRONICS), Toronto, ON, Canada, 2021, pp. 1-8, doi: **https://doi.org/10.1109/IEMTRONICS52119.2021.9422648**

[27] T. Bützer, O. Lambercy, J. Arata, R. Gassert, "Fully Wearable Actuated Soft Exoskeleton for Grasping Assistance in Everyday Activities," Soft Robot., vol. 8, no. 2, pp. 128-143, 2020, doi: **https://doi.org/10.1089/soro.2019.0135**

[28] E. Trigili, S. Crea, M. Moise, A. Baldoni, *et al.*, "Design and experimental characterization of a shoulder-elbow exoskeleton with compliant joints for post-stroke rehabilitation," IEEE/ASME Trans. Mech., vol. 24, no. 4, pp. 1485-1496, 2020, doi: **https://doi.org/10.1109/TMECH.2019.2907465**

[29] H. Liu, J. Tao, P. Lyu, y F. Tian, "Human-robot cooperative control based on sEMG for the upper limb exoskeleton robot," Rob. Auton. Syst., vol. 125, art. no. 103350, 2020, doi: **https://doi.org/10.1016/j.robot.2019.103350**

[30] F. Molteni, G. Gasperini, G. Cannaviello, E. Guanziroli, "Exoskeleton and End-Effector Robots for Upper and Lower Limbs Rehabilitation: Narrative Review," PM R, vol. 10, no. 9, pp. S174-S188, 2018, doi: **https://doi.org/10.1016/j.pmrj.2018.06.005**

[31] T. Du Plessis, K. Djouani, C. Oosthuizen, "A Review of Active Hand Exoskeletons for Rehabilitation and Assistance," Robotics, vol. 10, no. 1, art. no. 40, 2021, doi: **https://doi.org/10.3390/robotics10010040**

[32] C. Y. Chu y R. M. Patterson, "Soft robotic devices for hand rehabilitation and assistance: A narrative review," J. Neuroeng. Rehabil., vol. 15, no. 1, art. no. 9, 2018, doi: **https://doi.org/10.1186/s12984-018-0350-6**

[33] R. S. Calabrò, A. Naro, M. Russo, P. Bramanti, *et al.*, "Shaping neuroplasticity by using powered exoskeletons in patients with stroke: a randomized clinical trial," J. Neuroeng. Rehabil., vol. 15, no. 1, art. no. 35, 2018, doi: **https://doi.org/10.1186/s12984-018-0377-8**

[34] T. Chen, R. Casas, P. S. Lum, "An Elbow Exoskeleton for Upper Limb Rehabilitation with Series Elastic Actuator and Cable-Driven Differential," IEEE Trans. Robot., vol. 35, no. 6, pp. 1464-1474, 2019, doi: **https://doi.org/10.1109%2FTRO.2019.2930915**

[35] Q. A. Boser, M. R. Dawson, J. S. Schofield, G. Y. Dziwenko, J. S. Hebert, "Defining the design requirements for an assistive powered hand exoskeleton: A pilot explorative interview study and case series," Prosthet. Orthot. Int., vol. 45, no. 2, pp. 161-169, 2021, doi: **https://doi.org/10.1177/0309364620963943**

[36] G. Al Rezage, M. O. Tokhi, "Fuzzy PID control of lower limb exoskeleton for elderly mobility," en 2016 IEEE International Conference on Automation, Quality and Testing, Robotics (AQTR), Cluj-Napoca, Romania, 2016, pp. 1-6, doi: **https://doi.org/10.1109/AQTR.2016.7501310**

[37] M. S. Amiri, R. Ramli, y M. F. Ibrahim, "Hybrid design of PID controller for four DoF lower limb exoskeleton," Appl. Math. Model., vol. 72, pp. 17-27, 2019, doi: https://doi.org/10.1016/j.apm.2019.03.002

[38] D. Marconi, A. Baldoni, Z. McKinney, M. Cempini, S. Crea, N. Vitiello, "A novel hand exoskeleton with series elastic actuation for modulated torque transfer," Mechatronics, vol. 61, pp. 69-82, 2019, doi: https://doi.org/10.1016/j.mechatronics.2019.06.001

[39] B. A. De la Cruz-Sánchez, M. Arias-Montiel, E. Lugo-González, "Development of Hand Exoskeleton Prototype for Assisted Rehabilitation," en Mechanism Design for Robotics, A. Gasparetto y M. Ceccarelli, Eds., Cham, Switzerland: Springer International Publishing, 2019, pp. 378-385, doi: https://doi.org/10.1007/978-3-030-00365-4_45

[40] E. S. Donkor, "Stroke in the 21st Century: A Snapshot of the Burden, Epidemiology, and Quality of Life," Stroke Res. Treat., vol. 2018, art. no. 3238165, 2018. doi: https://doi.org/10.1155/2018/3238165

[41] M. H. Rahman, M. J. Rahman, O.L. Cristobal, M. Saad, J.P. Kenné, P.S. Archambault, "Development of a whole arm wearable robotic exoskeleton for rehabilitation and to assist upper limb movements," Robotica, vol. 33, no. 1, pp. 19-39, 2015, doi: https://doi.org/10.1017/S0263574714000034

[42] F. Aggogeri, T. Mikolajczyk, J. O'Kane, "Robotics for rehabilitation of hand movement in stroke survivors," Adv. Mech. Eng., vol. 11, no. 4, doi: https://doi.org/10.1177/1687814019841921

[43] E. Ambrosini, J. Zajc, S. Ferrante, G. Ferrigno, *et al.*, "A Hybrid Robotic System for Arm Training of Stroke Survivors: Concept and First Evaluation," IEEE Trans. Biomed. Eng., vol. 12, pp. 3290-3300, doi: https://doi.org/10.1109/tbme.2019.2900525

[44] H. Al-Fahaam, S. Davis, S. Nefti-Meziani, T. Theodoridis, "Novel soft bending actuator-based power augmentation hand exoskeleton controlled by human intention," Intell. Serv. Robotics, vol. 11, no. 3, pp. 247-268, 2018, doi: https://doi.org/10.1007/s11370-018-0250-4

RESEARCH ARTICLE

VOL. 45 | NO. 2 | **MAY-AUGUST 2024** | PP 100-113

Revista Mexicana de
Ingeniería Biomédica

dx.doi.org/10.17488/RMIB.45.2.6

E-LOCATION ID: **1413**

Predicting the Shelf Life of Dairy Products through Mathematical Modelling and *in silico* Experimentation

Modelado Mecanicista y Experimentación *in silico* para la Predicción de la Vida de Anaquel en Productos Lácteos

Yolocuauhtli Salazar-Muñoz[1], *Paul A. Valle*[2], *Emmanuel Rodríguez*[2], *Manuel F. Alvarado Ontíveros*[1]

[1] Tecnológico Nacional de México/Instituto Tecnológico de Durango - México

[2] Tecnológico Nacional de México/Instituto Tecnológico de Tijuana - México

ABSTRACT

The preservation of foods such as milk, meat, and vegetables through fermentation results in products like yogurt, cheese, pickles, sausages, and silage with an extended shelf life compared to their natural unprocessed counterparts. This work aims to formulate a mathematical model of first-order ordinary differential equations (ODEs) that accounts for both the physicochemical and microbiological parameters affecting biomass kinetics [B(t)], acidity [A(t)], and viscosity [V(t)] as a function of temperature across different yogurt samples. In order to validate the efficacy of the model in predicting yogurt shelf life, we compared its fitting results with commonly employed systems or equations, including the Weibull model, the Reaction Order model, the Arrhenius Equation, and the Q10 Factor. Our evaluation, based on R-squared (R^2) values exceeding 0.95, demonstrates the robustness of the proposed model. Furthermore, all parameters were estimated along with their corresponding 95 % confidence intervals. The mathematical model estimates the dynamic of each of the physicochemical and microbiological parameters which will help to predict the behavior over time of the shelf life of yogurt at different temperatures.

KEYWORDS: experimental data, nonlinear regression, nonlinear time-varying systems, numerical simulations, shelf life

RESUMEN

La conservación de alimentos como la leche, la carne y las verduras mediante la fermentación da como resultado productos como yogur, queso, encurtidos, salchichas y ensilados con una vida útil más prolongada en comparación con sus homólogos naturales sin procesar. El objetivo es formular un modelo matemático de ecuaciones diferenciales ordinarias (EDOs) de primer orden que tengan en cuenta los parámetros fisicoquímicos y microbiológicos que afectan la cinética de la biomasa [B(t)], la acidez [A(t)] y la viscosidad [V(t)] en función de la temperatura en diferentes muestras de yogur. Para validar la eficacia del modelo para predecir la vida útil del yogur, comparamos los resultados de ajuste con métodos comúnmente empleados como el modelo de Weibull, el modelo de orden de reacción, la Ecuación de Arrhenius y el Factor Q10. Nuestra evaluación, basada en valores de R-cuadrada (R^2) mayores a 0.95, demuestra la solidez del modelo propuesto. Además, se estimaron todos los parámetros junto con sus correspondientes intervalos de confianza del 95 %. El modelo matemático estima la dinámica de cada uno de los parámetros microbiológicos y fisicoquímicos los cuales ayudan a predecir el comportamiento sobre la vida de anaquel del yogur a diferentes temperaturas.

PALABRAS CLAVE: datos experimentales, regresión no lineal, simulaciones numéricas, sistemas no lineales variantes en el tiempo, vida de anaquel

Corresponding author

TO: **Paul A. Valle**
INSTITUTION: **Tecnológico Nacional de México/Instituto Tecnológico de Tijuana**
ADDRESS: **Blvd. Alberto Limón Padilla s/n, Tijuana 22454, México**
EMAIL: **paul.valle@tectijuana.edu.mx**

Received:

9 January 2024

Accepted:

13 May 2024

INTRODUCTION

Dairy products are foods with nutritional characteristics that exist in the market, their care in the industry is transcendental since they offer a proportion of high-quality proteins while also providing calcium and vitamins such as A, D, E, and the B set [1]. The preservation of foods such as milk, meat, and vegetables to obtain products such as yogurt, cheese, pickles, sausages, silage, etc., allows them to have a longer shelf life than natural or unprocessed products. The shelf life of dairy products is longer than that of milk, but is still limited; hence, various techniques have been adopted to improve it [2]. The shelf life and quality of yogurt are determined by physical, chemical, and microbiological changes that modify its sensorial properties and decrease the general attributes of the product and therefore, overall consumer approval [3][4]. Now, concerning shelf life prediction, Mataragas *et al.* [5] developed a methodology to formulate a predictive model of yogurt spoilage concluding that shelf life cannot be established with microbiological data alone, as one requires information of other parameters determined by sensory and physicochemical analyses. Shao *et al.* evaluated the Fourier-transform infrared spectroscopy as a rapid and non-invasive analytical technique to assess the quality and shelf life of yogurt during storage [6]. Papadopoulou *et al.* used partial least squares and, support vector machine regression and classification models to determine quantitative estimations of overall yogurt characteristics [7]. Furthermore, a survival analysis methodology was applied to estimate the shelf life of the probiotic yogurt by considering either a 25 % or a 50 % probability of consumer rejection; from the latter, shelf life was estimated at 38 and 53 days, respectively [8]. Artificial Neural Networks (ANN) models can also be applied to predict quality and deterioration during storage, these parameters are important in risk assessment, food safety and quality [9]; single- and double-layer Neural Networks were used to predict food quality in other milk products such as spreadable processed cheese [10], soft cheese [11], Ultra-High Temperature (UHT) soybean milk [12], and regular soy milk [13]. It is worth mentioning that viscoelastic, organoleptic, and microbial characteristics as well as the shelf life of yogurt changed with the addition of fruits and vegetables, however, they are mainly used to improve the nutritional and functional properties of the product [14]. Now, one can see that the most common shelf life estimation methods are by means of probability techniques and mathematical modelling. Probability techniques include the following distributions: normal, logs-normal, Weibull, exponential, and extreme value, among others. Meanwhile, concerning mathematical modelling one can find linear and nonlinear (sigmoidal-type) primary models; the reaction order model; the Arrhenius equation; the Q10 factor; and the survival method [5][14][15][16][17][18][19]. In the latter, shelf life prediction may be performed at either a constant or variable temperature [20].

This work aims to evaluate a proposed nonlinear and time-varying mathematical model of first-order ordinary differential equations (ODEs) that consider the influence of physicochemical and microbiological parameters on biomass kinetics evolution, specifically acidity, and viscosity as functions of temperature. Further, we compare the fitness capabilities of our model with those well-established in the literature for shelf life estimation.

MATERIALS AND METHODS

This section describes the origin of the experimental data, the procedure to fit our proposed model, the biostatistics around the estimation of all parameters, and the description of each equation.

Experimental data

Experimental data was extracted from Zhi *et al.* [1] where they discuss the evaluation of yogurt shelf life using physicochemical, microbiological, and sensory parameters. Values for the time-evolution were extracted with the open-source software Graph Grabber v2 plot digitizing from Quintessa Ltd. This application allows us to manually extract data points from the original figures as a comma separated value (cvs) file. The data corresponds to two yogurt samples identified as S_0^1 and S_0^2 for two temperatures, 5 °C and 15 °C. In each sample, the following three variables were extracted: biomass [B(t)], acidity [A(t)], and viscosity [V(t)], as it is illustrated in Figure 1.

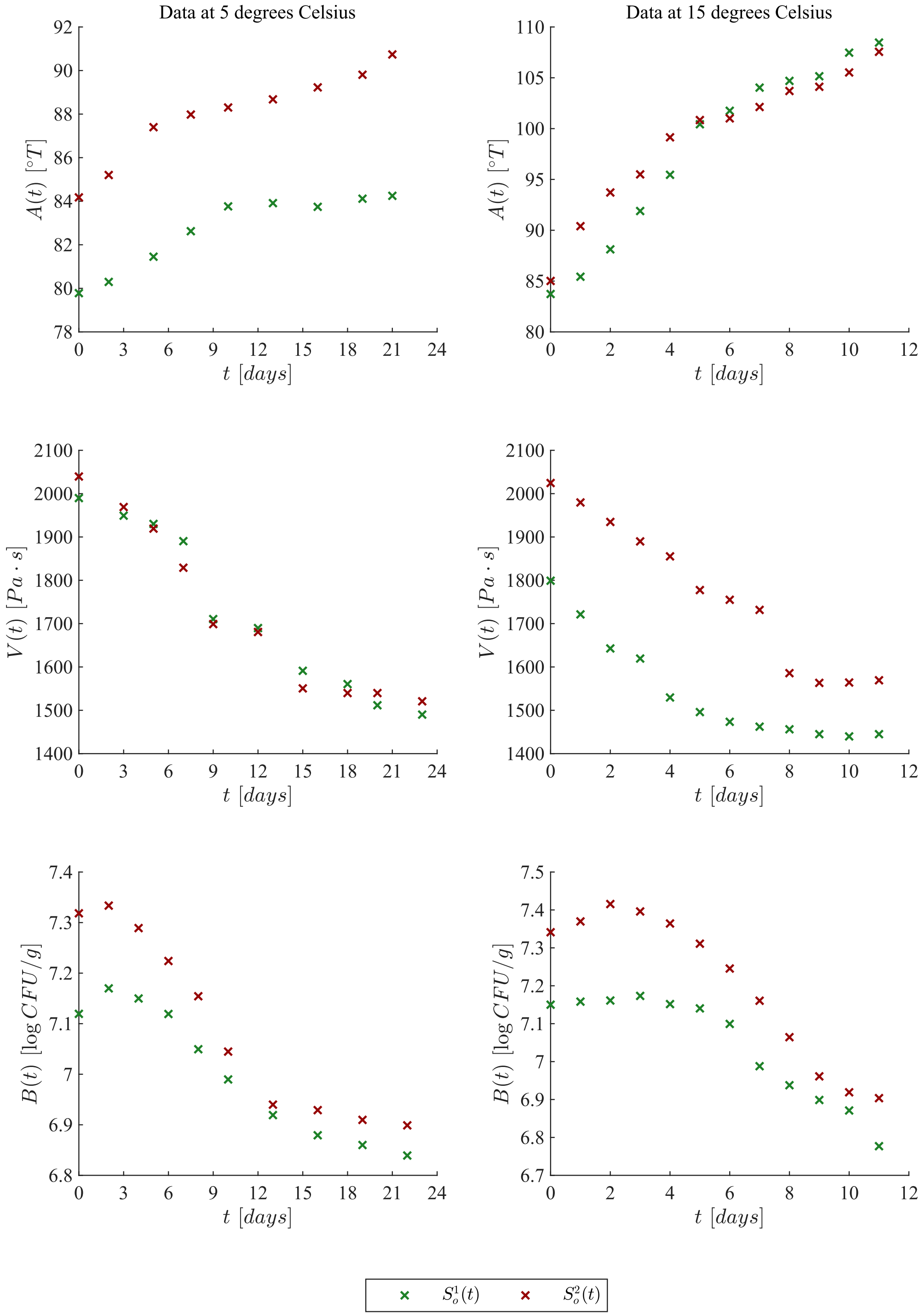

FIGURE 1. Experimental data extracted from Zhi *et al.* [1] with the Graph Grabber software. Each point corresponds to the shelf life of two samples of yogurt (S_0^1 and S_0^2) observed at 5°C for over 20 days and at 15°C for over 10 days. Panels from top to bottom are for acidity [A(t)], viscosity [V(t)], and biomass kinetics [B(t)]; where *logx=log$_{10}$ x*.

Mathematical modelling and data fitting

The dynamics of physicochemical and microbiological parameters of yogurt at two different shelf temperatures were modelled through a set of three first-order ODEs describing acidity in Titratable acidity units (°T), viscosity in pascal-second (Pa·s), and biomass in colony-forming units (CFU) per gram. Further, each equation considers the temperature (T) as follows:

$$\dot{A} = \alpha_1 A(1 - \alpha_2 A)t^{1/T} \tag{1}$$

$$\dot{V} = \beta_1 V(1 - \beta_2 V)tT \tag{2}$$

$$\dot{B} = \frac{\gamma_1 B}{B + T} + \gamma_2 B(1 - \gamma_3 B)\frac{t}{T} \tag{3}$$

It is evident that Equations (1), (2), (3) are non-linear and nonautonomous. Further, based on the positivity of dynamical systems theory, positive half-trajectories with nonnegative initial conditions $[A(0),V(0),B(0) \geq 0]$, will be located within the following domain:

$$\boldsymbol{R}^3_{+,0} = \{A(t), B(t), V(t) \geq 0\}$$

The latter implies that all solutions will always have nonnegative values, which corresponds with the biological meaning of each variable. Now, let us describe the biological assumptions on which our mechanistic model (1)-(3) was formulated. Equation (1) describes the increase in Acidity [A(t)] by the logistic law, where α_1 is the growth rate and α_2 the limited rate capacity. Equation (2) describes the decrease in Viscosity [V(t)] where the parameter β_1 denotes the decrease rate and the lower value is given by $1/\beta_2$. Equation (3) describes Biomass [B(t)] dynamics with an initial growth phase formulated by the Michaelis-Menten term with rate γ_1; then, the latter is followed by a death phase after the maximum concentration measured in the samples by the logistic law where γ_2 is the decrease rate with lower bound given by $1/\gamma_3$. Further, it should be noted that we found that both time (t) and temperature (T) needed to be considered in the modelling process; in Equation (1), these parameters are included as a radical term $[t^{1/T}]$, in Equation (2) as a product of both parameters $[tT]$, and in Equation (3) as a rational term $[t/T]$.

Now, in order to fit Equations (1)(2)(3) to the experimental data of Figure 1, we developed an algorithm in Matlab 2023a based on the *fitnlm* function from the Statistics and Machine Learning Toolbox. Further, equations were numerically solved by using the improved Euler's method (Heun's method) with an integration step (Δ_t) of 1×10^{-3}. Initial values for the *fitnlm* function were set as follows for both 5 °C and 15°C data of acidity and viscosity:

$$Acidity: P_0 = [1 \times 10^{-2}, 1 \times 10^{-2}]$$

$$Viscosity: P_0 = [1 \times 10^{-3}, 1 \times 10^{-3}]$$

whilst for biomass, the following were set for 5 °C:

$$Biomass: P_0 = [1 \times 10^{-1}, 1 \times 10^{-1}, 1 \times 10^{-1}]$$

and the next for 15 °C:

$$Biomass: P_0 = [1 \times 10^{-1}, 1 \times 10^{-2}, 1]$$

Fitting results from the *fitnlm* function include the estimated value for each parameter as well as common biostatistics such as the t-value, degrees of freedom (dof), standard error (SE); 95 % confidence intervals (95CI), and p-value. A measure of the goodness of fit is provided by means of the R-squared (R^2). Results are shown in Tables 1-4 and illustrated in Figures 2-3 and will be discussed in the next section. Now, let us briefly explain the most common models used for shelf life prediction as results from our model will be compared with those determined with the Weibull Model, the Reaction Order, the Arrhenius Equation, and the Q10 Factor. Furthermore, the threshold for yogurt feasibility is already established by the NOM-181-SCFI/SAGARPA-2018, which specifies that the product must contain at least 10^7 *CFU/g* of viable biomass concentration.

Weibull Model

The Weibull Model has been used to estimate the shelf life of several foods, including yogurt [16] by the next Equation 4:

$$E = \alpha\gamma\left(1 + \frac{1}{\beta}\right) \tag{4}$$

where α and β are known parameters as they define the shape and scale of the study to be carried out, meanwhile, γ represents the gamma function. Results were computed by means of statistical software using the data illustrated in Figure 1.

Reaction Order

The Reaction Order is mainly based on the principles of chemical kinetics with the following structure in Equation 5:

$$t = \frac{A - A_0}{K} \tag{5}$$

where A is the final half-life value, A_0 is the initial quality and K is the reaction rate. Values were determined from a linear equation, where A_0 is the intercept and K its slope.

Arrhenius Equation

The Arrhenius equation, also known as activation energy, focuses on the rate of chemical reactions as their temperature increases as indicated below Equation 6:

$$ln\, k = ln\, A - E_a RT \tag{6}$$

Where the zero-crossing points can be used to estimate shelf life by considering the effect of temperature on the kinetics of the product [21][22]. Therefore, the equation to determine the shelf life according to [23] is given by next Equation 7:

$$Q_e = Q_0 - kt_s \tag{7}$$

where Q_0 is the value of the quality characteristic at the start of the experiment and Q_e is the value reached at the time t_s, *i.e.,* the estimated shelf life, and k is the speed of the reaction, *i.e.,* the slope of the straight line.

Q10 Factor

The Q_{10} factor states that the rate of degradation is affected by a constant rate when temperature changes with time [18]. This makes it possible to determine the shelf life of foods by the following Equation 8:

$$t_1 = t(Q_{10})^{(T_2 - T_1)/10} \tag{8}$$

where t is the service lifetime, Q_{10} is the acceleration factor, and T_1 and T_2 represent the changes in temperature in degree Celsius (°C).

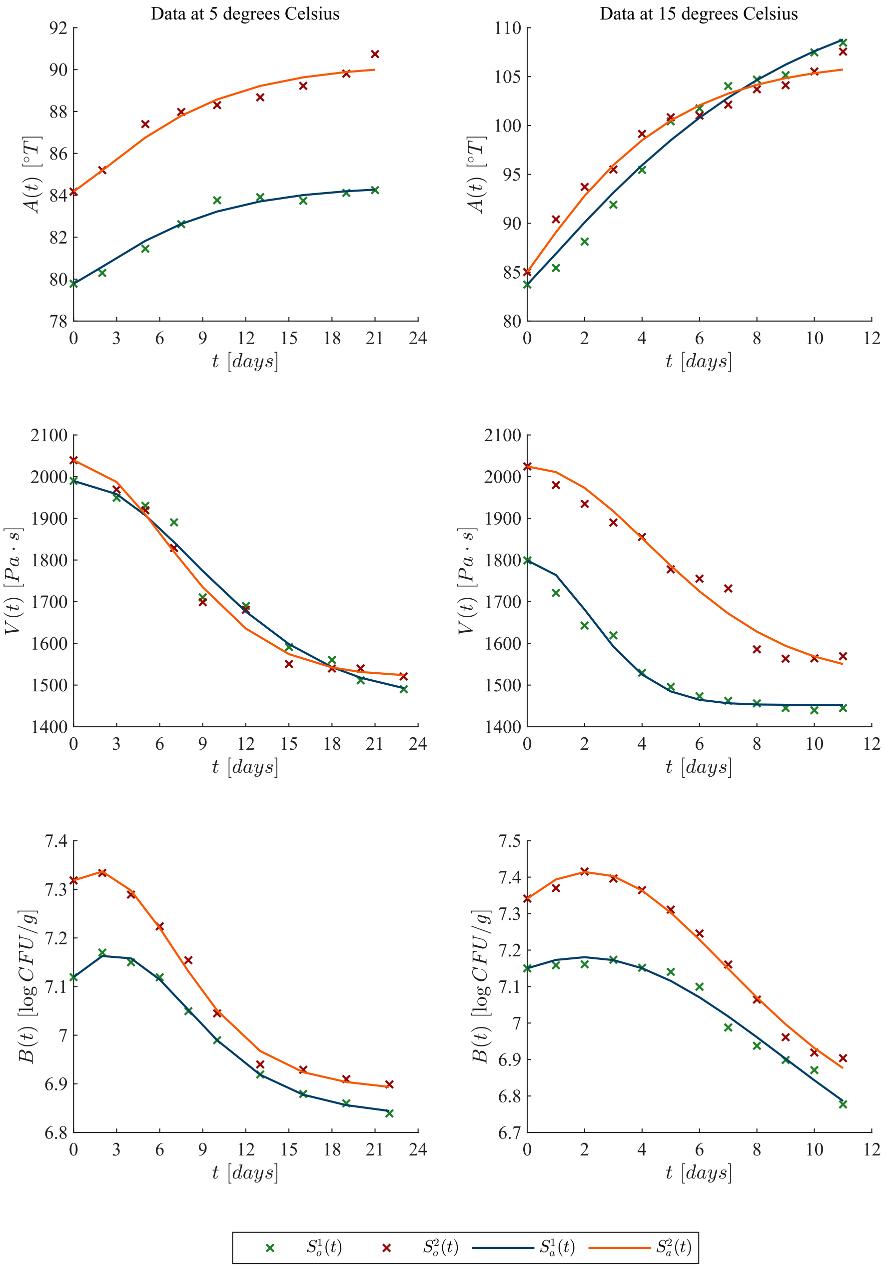

FIGURE 2. **Fitting results of Equations (1)(2)(3) to the observed data corresponding to the two samples of acidity [A(t)], viscosity [V(t)], and biomass at 5 °C and 15 °C. The × marker represents the observed data where green is for sample 1 [$S_o^1(t)$] and red for sample 2 [$S_o^2(t)$]; the solid lines are for the approximated data from our mathematical model.**

RESULTS AND DISCUSSION

Nonlinear regression was performed for all variables [A(t), V(t) and B(t)] at two temperatures [5 °C and 15 °C] for the two samples of yogurt [$S_o^1(t)$ and $S_o^2(t)$]. The fitting results of our model are illustrated by means of *in silico* experimentation in Figure 2. Estimated values of parameters and biostatistics for Equations (1)(2)(3) are shown, respectively in Tables 1-3, where we present the corresponding standard error (SE), 95 % confidence intervals (95CI), and the p-value for each estimate. The latter implies that the significance value (α) was predefined as 0.05. These statistics allow us to conclude on the statistical significance of our results.

One can see that all lower bounds of the 95CI in Table 1 and Table 2 are positive, and that p-values are lower than α. Hence, Equations (1) and (2) are able to describe with a high level of confidence the dynamics of both Acidity [A(t)] and Viscosity [V(t)]. Further, as it is shown in Table 4, the coefficient of determination for the two samples at both temperatures is higher than 0.95. Now, regarding results for Equation (3) shown in Table 3, we found that our proposed model can accurately describe the dynamics of biomass [B(t)] as all estimated values but one was statistically significant. Further, the coefficient of determination for the two samples at both temperatures is higher than 0.98 (see Table 4). Following the latter, the estimated value of parameter γ_2 in[1] Equation (3) had a negative lower bound in the 95CI due to the non-steep slope of the growth phase in sample 1 [$S_o(t)$] of biomass at 15 °C, as it is illustrated in the right lower panel of Figure 1. Therefore, results from the nonlinear regression algorithm indicated that only parameter γ_1 had a significant influence on the observed growth phase as there was nearly zero growth of biomass in the first three days. Additionally, it is important to disclose the following information regarding the fitting process of our mathematical model. Nonlinear regression of Equations (1)(2)(3) at 5 °C is performed, respectively, at 7, 8, and 7 dof, with t-values of 2.3646, 2.3060, and 2.3646. Meanwhile, at 15 °C we have the following: 10, 10, and 9 dof, with t-values of 2.2281, 2.2281, and 2.2622. It is evident that as more data is available the value of the dof is higher and the t-value is lower. The latter is used to compute the margin of error (MoE) for the estimated values of parameters (MoE = t-value·SE), and the estimate ± MoE gives us the bounds of the 95CI.

Now, let us apply Equations (1)(2)(3) to observe overall changes in the dynamics of each variable at 5 °C and 15 °C for 60 days (2 months). Results are illustrated in Figure 3, where the base 10 logarithm of the threshold 10^7 *CFU/g* is indicated in both panels of biomass evolution in the two lower panels of the *in silico* experimentation.

Concerning acidity, this variable converges to a lower level at 5 °C compared to 15 °C samples. The latter implies that a higher temperature increases acidity values in yogurt, this relationship is further elucidated in Table 1, where values for α_1 are higher at 15 °C than at 5 °C. However, viscosity values remain consistent at both temperatures, converging to ~1460 Pa·s for sample 1 and ~1520 Pa·s for sample 2, but it should be noted that values for β_1 are different across samples and temperatures, as documented in Table 2. Returning to biomass dynamics, is evident that the final predicted concentration is inversely proportional to temperature as it is higher at 5 °C and lower at 15 °C. Samples 1 and 2 reach a value of 6.809 and 6.867 logCFU/g, respectively, at 5 °C. Meanwhile, at 15 °C the model estimates a concentration of 6.377 and 6.614 *logCFU/g* in samples 1 and 2, respectively. Therefore, at lower temperatures, the biomass concentration remains above the established threshold for more days. These differences are also reflected in the estimated values of γ_1 and γ_2 documented in Table 3.

Yogurt in optimal conditions adheres to the defined standards of the NOM-181-SCFI/SAGARPA-2018. The experimental data and the in *silico* experimentation indicate that the observed variables are affected by the storage temperature as well as the initial biomass concentration [B(0)]. Higher temperatures lead to changes in the microbiological characteristics that ultimately reduce the shelf life of the product; for samples 1 and 2 at 5 °C we have results of 9.6 and 11.6 days, whilst at 15 °C results for samples 1 and 2 are estimated at 7.3 and 8.9 days. The latter implies a reduction in shelf life of 2.3 and 2.7 days, respectively. Furthermore, initial concentrations of biomasses were measured at 7.119 and 7.318 *logCFU/g* for samples at 5 °C, and 7.150 and 7.341 *logCFU/g* for samples at 15 °C, respectively, by Zhi *et al.* [1].

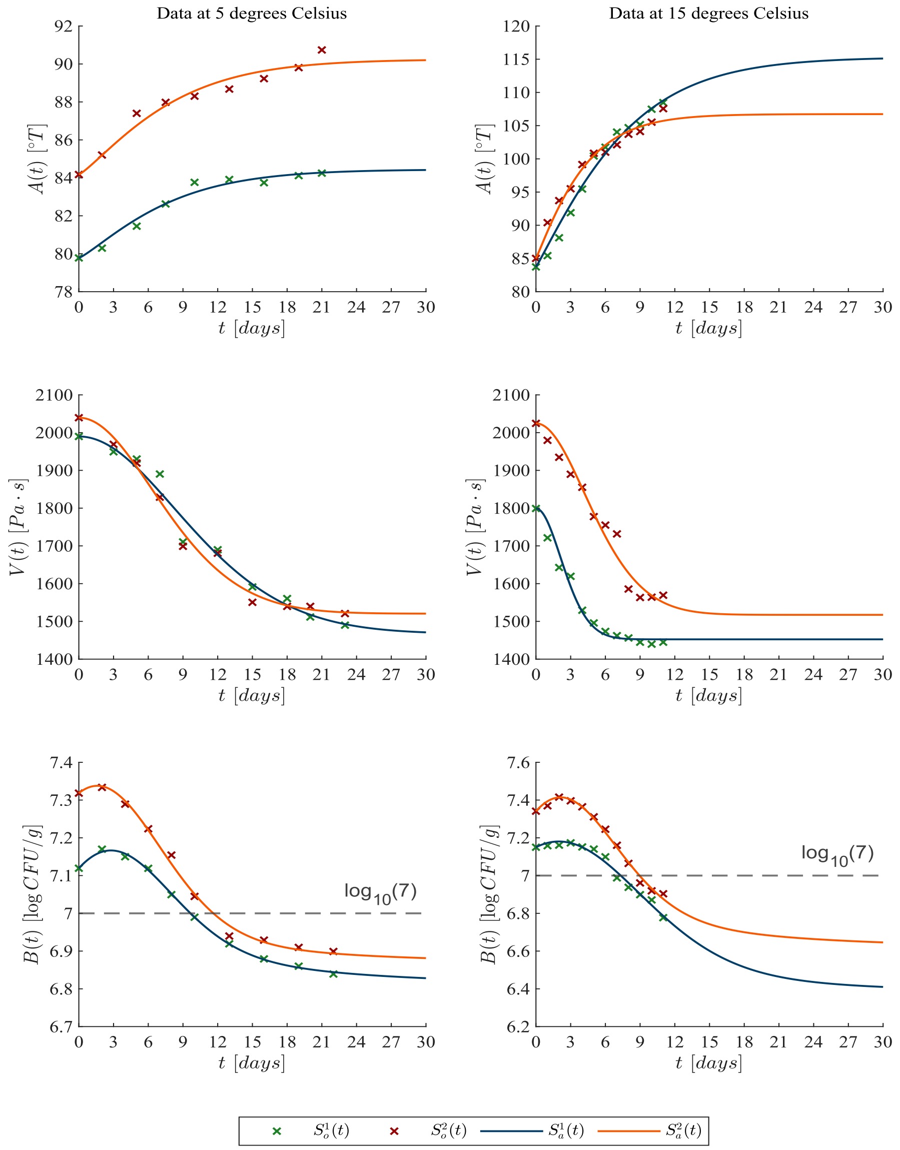

FIGURE 3. **Prediction results of 30 days for the two samples of acidity, viscosity, and biomass, at 5 °C and 15 °C. It should be highlighted that all solutions *[A(t), V(t), B(t)]* are bounded and dissipative. Boundedness ensures that concentrations of substances stay within physiologically acceptable ranges. Dissipativity is linked to the energy balance of the system and is often associated with the metabolic and thermodynamic aspects of biological processes. The × marker represents the observed data where green is for sample 1 [$S_o^1(t)$] and red for sample 2 [$S_o^2(t)$]; the solid lines are for the approximated data from our mathematical model.**

Now, let us discuss the results of the estimated shelf life of yogurt with the Weibull Model, the Reaction Order, the Arrhenius Equation, and the Q_{10} factor. First, it should be noted that these models should be applied to each data set of each variable. Hence, in Figures 4, Figure 5 and Figure 6 we present the different results estimated for the shelf life of the sample 1 of yogurt at the two observed temperatures. Furthermore, the exact shelf life estimation in days is presented in Table 5 for sample 1. When analyzing acidity, the longest shelf life was estimated at 5 °C with a result of 569 days by the Reaction Order. Meanwhile, the shortest time was obtained with the Weibull model at 15 °C with 78.5 days as shown in Figure 4. Concerning viscosity, both the Weibull Model and the Reaction Order estimated a longer shelf life at a higher temperature, 294.4 and 81 days, respectively. However, both the Arrhenius Equation and the Q10 factor estimated a longer shelf life for the lower temperature data as illustrated in Figure 5. Now, when applying all models to the biomass data sets of sample 1, the longer shelf life was estimated for the temperature at 5 °C, which is to be expected in real-life scenarios of yogurt storage. Nonetheless, it is evident that all these models overestimate the shelf life of a product such as yogurt. Additionally, these models do not consider the threshold that has been stablished for yogurt feasibility by the NOM-181-SCFI/SAGARPA-2018 for the biomass concentration of at least 10^7 *CFU/g* in the product.

TABLE 1. **Acidity [A(t)]: Estimation of parameters and biostatistics for 5°C 15°C for both samples S_o^1 and S_o^2. The values describe the estimate value (Estimate), the standard error (SE), the confidence interval (95CI) and the *p-value*.**

Temperature	Sample	Parameters	Estimate	SE	95CI		*p*-value
5 °C	$S_o^1(t)$	α_1	1.052×10^{-1}	1.722×10^{-2}	6.445×10^{-2}	1.4589×10^{-1}	4.874×10^{-4}
		α_2	1.184×10^{-2}	3.853×10^{-5}	1.175×10^{-2}	1.1934×10^{-2}	1.019×10^{-15}
	$S_o^2(t)$	α_1	1.017×10^{-1}	2.015×10^{-2}	5.406×10^{-2}	1.494×10^{-1}	1.484×10^{-3}
		α_2	1.108×10^{-2}	5.478×10^{-5}	1.095×10^{-2}	1.121×10^{-2}	1.904×10^{-14}
15 °C	$S_o^1(t)$	α_1	1.519×10^{-1}	2.158×10^{-2}	1.039×10^{-1}	2.000×10^{-1}	3.534×10^{-5}
		α_2	8.672×10^{-3}	2.280×10^{-4}	8.1645×10^{-3}	9.180×10^{-3}	3.753×10^{-12}
	$S_o^2(t)$	α_1	2.715×10^{-1}	2.655×10^{-2}	2.123×10^{-1}	3.306×10^{-1}	1.295×10^{-6}
		α_2	9.369×10^{-3}	7.693×10^{-5}	9.198×10^{-3}	9.540×10^{-3}	3.418×10^{-17}

TABLE 2. **Viscosity [V(t)]: Estimation of parameters and biostatistics for 5°C 15°C for both samples S_o^1 and S_o^2. The values describe the estimate value (Estimate), the standard error (SE), the confidence interval (95CI) and the p-value.**

Temperature	Sample	Parameters	Estimate	SE	95CI		*p*-value
5 °C	$S_o^1(t)$	β_1	2.070×10^{-3}	3.876×10^{-4}	1.176×10^{-3}	2.9637×10^{-3}	6.938×10^{-4}
		β_2	6.815×10^{-4}	1.583×10^{-5}	6.450×10^{-4}	7.1801×10^{-4}	9.341×10^{-11}
	$S_o^2(t)$	β_1	3.569×10^{-3}	3.884×10^{-4}	2.673×10^{-3}	4.4648×10^{-3}	1.592×10^{-5}
		β_2	6.577×10^{-4}	6.903×10^{-6}	6.418×10^{-4}	6.7363×10^{-4}	1.643×10^{-13}
15 °C	$S_o^1(t)$	β_1	1.163×10^{-2}	1.470×10^{-3}	8.351×10^{-3}	1.4901×10^{-2}	1.301×10^{-5}
		β_2	6.885×10^{-4}	4.350×10^{-6}	6.788×10^{-4}	6.9819×10^{-4}	2.488×10^{-18}
	$S_o^2(t)$	β_1	2.717×10^{-3}	5.607×10^{-4}	1.467×10^{-3}	3.9662×10^{-3}	6.764×10^{-4}
		β_2	6.590×10^{-4}	1.692×10^{-5}	6.214×10^{-4}	6.9672×10^{-4}	2.962×10^{-12}

TABLE 3. Biomass [B(t)]: Estimation of parameters and biostatistics for 5°C and 15°C for both samples S_o^1 and S_o^2. The values describe the estimate value (Estimate), the standard error (SE), the confidence interval (95CI) and the *p*-value.

Temperature	Sample	Parameters	Estimate	SE	95CI		*p* value
5 °C	$S_o^1(t)$	γ_1	5.640×10^{-2}	3.565×10^{-3}	4.797×10^{-2}	6.483×10^{-2}	9.767×10^{-7}
		γ_2	1.510×10^{-1}	8.117×10^{-3}	1.318×10^{-1}	1.702×10^{-1}	3.215×10^{-7}
		γ_3	1.473×10^{-1}	9.815×10^{-5}	1.470×10^{-1}	1.475×10^{-1}	1.543×10^{-20}
	$S_o^2(t)$	γ_1	4.059×10^{-2}	1.135×10^{-2}	1.376×10^{-2}	6.743×10^{-2}	9.0134×10^{-3}
		γ_2	1.461×10^{-1}	2.028×10^{-2}	9.811×10^{-2}	1.940×10^{-1}	1.770×10^{-4}
		γ_3	1.459×10^{-1}	2.470×10^{-4}	1.453×10^{-1}	1.465×10^{-1}	1.051×10^{-17}
15 °C	$S_o^1(t)$	γ_1	9.465×10^{-2}	2.632×10^{-2}	3.511×10^{-2}	1.542×10^{-1}	5.7819×10^{-3}
		γ_2	2.467×10^{-1}	1.363×10^{-1}	-6.159×10^{-2}	5.550×10^{-1}	1.037×10^{-1}
		γ_3	1.575×10^{-1}	6.666×10^{-3}	1.425×10^{-1}	1.726×10^{-1}	2.076×10^{-9}
	$S_o^2(t)$	γ_1	2.054×10^{-1}	2.525×10^{-2}	1.483×10^{-1}	2.626×10^{-1}	1.935×10^{-5}
		γ_2	5.109×10^{-1}	9.235×10^{-2}	3.020×10^{-1}	7.198×10^{-1}	3.644×10^{-4}
		γ_3	1.519×10^{-1}	1.545×10^{-3}	1.484×10^{-1}	1.554×10^{-1}	5.898×10^{-15}

TABLE 4. The R^2 provides a measure of the goodness of fit of our proposed mathematical model (1)-(3) to the observed data of each variable.

T	Sample	Acidity [A(t)]	Viscosity [V(t)]	Biomass [B(t)]
5°C	$S_o^1(t)$	0.973	0.978	0.999
	$S_o^2(t)$	0.957	0.987	0.995
15°C	$S_o^1(t)$	0.982	0.972	0.980
	$S_o^2(t)$	0.980	0.966	0.992

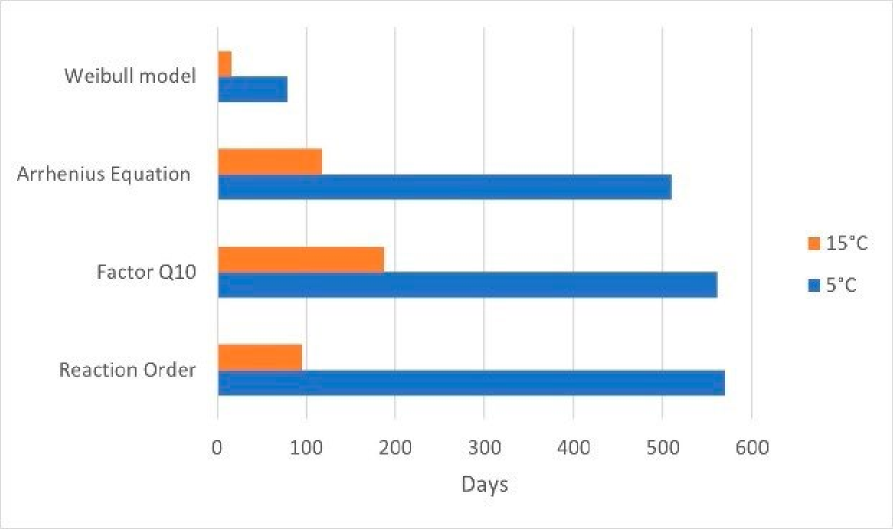

FIGURE 4. **Shelf life estimation for sample 1 of yogurt when analyzing the data sets of the observed acidity [A(t)] at 5°C and 15°C.**

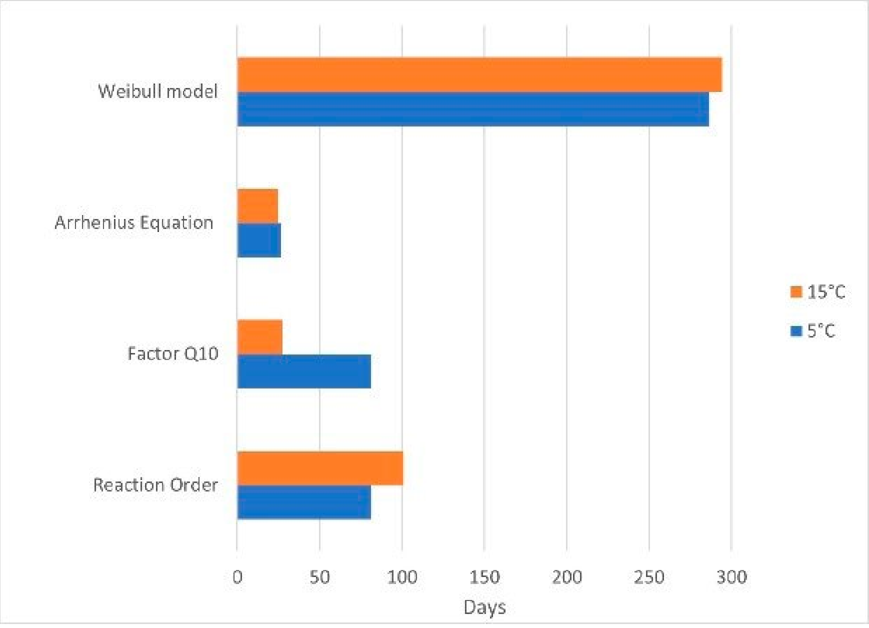

FIGURE 5. **Shelf life estimation for sample 1 of yogurt when analyzing the data sets of the observed viscosity [V(t)] at 5°C and 15°C.**

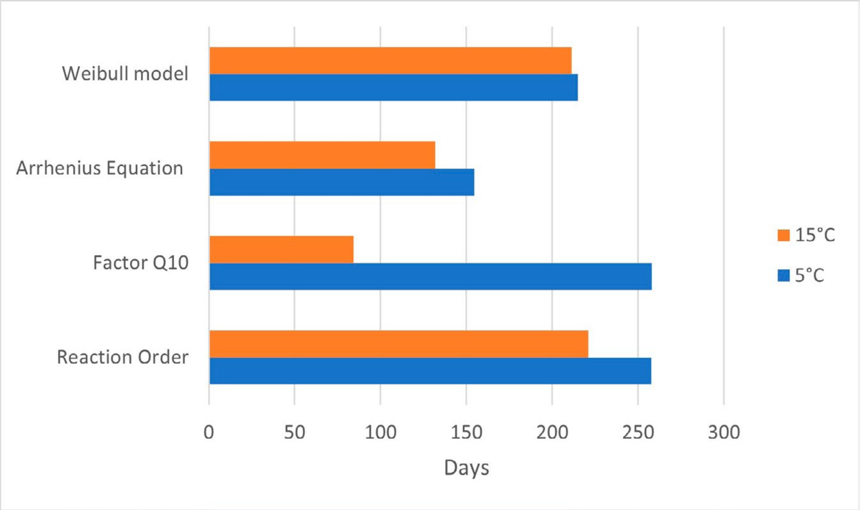

FIGURE 6. **Shelf life estimation for sample 1 of yogurt when analyzing the data sets of the observed biomass dynamics [B(t)] at 5°C and 15°C.**

TABLE 4. **Summarized results for the shelf life estimation of sample 1 [$S_o^1(t)$] with the Weibull Model, the Reaction Order, the Arrhenius Equation, and the Q_{10} factor. Results for the shelf life are given in days.**

T	Sample	Acidity [A(t)]	Viscosity [V(t)]	Biomass [B(t)]
5°C	$S_o^1(t)$	0.973	0.978	0.999
	$S_o^2(t)$	0.957	0.987	0.995
15°C	$S_o^1(t)$	0.982	0.972	0.980
	$S_o^2(t)$	0.980	0.966	0.992

CONCLUSIONS

As large quantities are wasted in expired dairy products, the industry requires processes to reduce yogurt waste by improving quality and extending shelf life. Although there are several methods based on the chemical reaction rate to determine the shelf life of yogurt, these give different values for the same experimental data of the product. Hence, a mathematical model using first-order ODEs is better suited to determine the overall shelf life based on the physicochemical and microbiological properties of the product.

As mentioned before, yogurt reaches the end of its shelf life due to the values established by food standards. Therefore, it can be concluded that by modelling the shelf life of each of the samples analyzed, it would be possible to better estimate the shelf life based on changes of the different variables analyzed by each food productor.

Therefore, our proposed mathematical model (1)-(3) is able to accurately approximate the changes of each of the physicochemical and microbiological variables such as biomass, acidity and viscosity at different storage temperatures. Then, by following the already established thresholds one can estimate the total number of days that the product will be suitable for human consumption. Further, when comparing results is easy to determine that a lower temperature will increase shelf life and reduce waste in the short-term

One limitation of our model is that it does not consider biomass death rate as it was formulated by means of a combination of growth laws, a Michaelis-Menten kinetics, and the logistic law. Therefore, the in silico experimentation of Figure 3 illustrates that once this variable reaches the plateau, then the predicted values do not tend to zero as time increases. It is left as future work to validate the model with yogurt samples at different temperatures and determine the relationship between the variables, which may allow us to better estimate the shelf life of yogurt by considering the dynamics among these different variables.

ACKNOWLEDGEMENTS

This research was fulfilled within the TecNM projects “Estrategias in silico integradas con biomatemáticas y sistemas dinámicos no lineales para el modelizado, análisis y control de sistemas biológicos 19377.24-P ”; “Modelizado de sistemas no lineales para procesos de fermentación basados en la dinámica de crecimiento de microorganismos: parte 2 19805.24-P”. The professor Y. Salazar and P. A. Valle are members of the RICCA “Red Internacional de Control y Cómputo Aplicados”.

AUTHOR CONTRIBUTIONS

Y. S. M. conceptualization, methodology, validation, formal analysis, investigation, resources, writing original draft, writing review and editing, and project administration. P. A. V. conceptualization, methodology, software, validation, resources, writing original draft, writing review and editing, and visualization. E. R. T. Software and formal analysis. M. F. A. O. Data curation and investigation. All authors have read and agreed to the published version of the manuscript.

REFERENCES

[1] N.-N. Zhi, K. Zong, K. Thakur, J. Qu, et al., “Development of a dynamic prediction model for shelf life evaluation of yogurt by using physicochemical, microbiological and sensory parameters,” CyTA - J. Food, vol. 16, no. 1, pp. 42-49, Jan. 2018, doi: https://doi.org/10.1080/19476337.2017.133657

[2] S. Sarkar, “Shelf-life extension of cultured milk products,” Nutr. Food Sci., vol. 36, no. 1, pp. 24-31, Jan. 2006, doi: : https://doi.org/10.1108/00346650610642160

[3] C. Paulo Vieira, M. Pereira da Costa, B. da Silva Frasão, V. L. de Melo Silva, R. Vilela de Barros Pinto Moreira, Y. E. Chifarelli de Oliveira Nunes, C. A. Conte-Junior, “Nondestructive prediction of the overall quality of cow milk yogurt by correlating a biogenic amine index with traditional quality parameters using validated nonlinear models,” J. Food Compos. Anal., vol. 84, art. no. 103328, Dec. 2019, doi: https://doi.org/10.1016/j.jfca.2019.103328

[4] F. Al-Rimawi, M. Alayoubi, c. Elama, M. Jazzar, and A. Çakıcı, “Use of cinnamon, wheat germ, and eucalyptus oils to improve quality and shelf life of concentrated yogurt (Labneh),” Cogent Food Agric., vol. 6, no. 1, art. no. 1807810, 2020, doi: https://doi.org/10.1080/23311932.2020.1807810

[5] M. Mataragas, V. Dimitriou, P. N. Skandamis, and E. H. Drosinos, “Quantifying the spoilage and shelf-life of yogurt with fruits,” Food Microbiol., vol. 28, no. 3, pp. 611-616, May 2011, doi: https://doi.org/10.1016/j.fm.2010.11.009

[6] Y. Shao, Y. He, and S. Feng, “Measurement of yogurt internal quality through using Vis/NIR spectroscopy,” Food Res. Int., vol. 40, no. 7, pp. 835-841, Aug. 2007, doi: https://doi.org/10.1016/j.foodres.2007.01.014

[7] O. S. Papadopoulou, A. A. Argyri, V. Kounani, C. C. Tassou, and N. Chorianopoulos, “Use of Fourier Transform Infrared Spectroscopy for Monitoring the Shelf Life and Safety of Yogurts Supplemented With a Lactobacillus plantarum Strain With Probiotic Potential,” Front. Microbiol., vol. 12, art. no. 678356, Jun. 2021, doi: https://doi.org/10.3389/fmicb.2021.678356

[8] A. G. Cruz, E. H. M. Walter, R. Silva Cadena, J. A. F. Faria, H. M. A. Bolini, H. P. Pinheiro, A. S. Sant’Ana, “Survival analysis methodology to predict the shelf-life of probiotic flavored yogurt,” Food Res. Int., vol. 43, no. 5, pp. 1444-1448, Jun. 2010, doi: https://doi.org/10.1016/j.foodres.2010.04.028

[9] J. Stangierski, D. Weiss, and A. Kaczmarek, “Multiple regression models and Artificial Neural Network (ANN) as prediction tools of changes in overall quality during the storage of spreadable processed Gouda cheese,” Eur. Food Res. Technol., vol. 245, no. 11, pp. 2539-2547, Nov. 2019, doi: https://doi.org/10.1007/s00217-019-03369-y

[10] S. Goyal and G. K. Goyal, “Shelf Life Estimation of Processed Cheese by Artificial Neural Network Expert Systems,” J. Adv. Comput. Sci. Technol., vol. 1, no. 1, pp. 32-41, 2012. [Online]. Available: https://www.sciencepubco.com/index.php/JACST/article/view/10/439

[11] J. F. Oblitas-Cruz and J. A. Sánchez-González, “Application of Weibull analysis and artificial neural networks to predict the useful life of the vacuum packed soft cheese,” Rev. Fac. Ing. Univ. Antioquia, no. 82, pp. 53-59, Mar. 2017, doi: https://doi.org/10.17533/udea.redin.n82a07

[12] R. R. B. Singh, A. P. Ruhil, D. K. Jain, A. A. Patel, and G. R. Patil, “Prediction of sensory quality of UHT milk - A comparison of kinetic and neural network approaches,” J. Food Eng., vol. 92, no. 2, pp. 146-151, May 2009, doi: https://doi.org/10.1016/j.jfoodeng.2008.10.032

[13] X. Dong, Q. Li, D. Sun, X. Chen, and X. Yu, “Direct FTIR Analysis of Free Fatty Acids in Edible Oils Using Disposable Polyethylene Films,” Food Anal. Methods, vol. 8, no. 4, pp. 857-863, 2015, doi: https://doi.org/10.1007/s12161-014-9963-y

[14] I. Ahmad, M. Hao, Y. Li, J. Zhang, Y. Ding, and F. Lyu, “Fortification of yogurt with bioactive functional foods and ingredients and associated challenges - A review,” Trends Food Sci. Technol., vol. 129, pp. 558-580, Nov. 2022, doi: https://doi.org/10.1016/j.tifs.2022.11.003

[15] W. F. Castro, A. G. Cruz, M. S. Bisinotto, L. M. R. Guerreiro, et al., “Development of probiotic dairy beverages: Rheological properties and application of mathematical models in sensory evaluation,” J. Dairy Sci., vol. 96, no. 1, pp. 16-25, 2013, doi: https://doi.org/10.3168/jds.2012-5590

[16] E. Al-Kadamany, M. Khattar, T. Haddad, and I. Toufeili, “Estimation of shelf-life of concentrated yogurt by monitoring selected microbiological and physicochemical changes during storage,” LWT - Food, Sci. Techol., vol. 36, no. 4, pp. 407-414, 2003, doi: https://doi.org/10.1016/S0023-6438(03)00018-5

[17] E. Al-Kadamany, I. Toufeili, M. Khattar, Y. Abou-Jawdeh, S. Harakeh, and T. Haddad, “Determination of shelf life of concentrated yogurt (labneh) produced by in-bag straining of set yogurt using hazard analysis,” J. Dairy Sci., vol. 85, no. 5, pp. 1023-1030, 2002, doi: https://doi.org/10.1016/B978-0-12-809633-8.20186-6

[18] R. Arboretti, E. Barzizza, L. Salmaso, R. Ceccato, et al., “Shelf-life prediction: A comparison of methods,” Electron. J. Appl. Stat. Anal., vol. 15, no. 3, pp. 527-552, 2022, doi: https://doi.org/10.1285/i20705948v15n3p527

[19] M. Mahendradattal, F. Bastianl, Kasmiati, and N. Amaliah, “Shelf-life prediction of seasoning powder made from whole fermented fish (peda) by using Arrhenius method,” in Procc. of International Seminar Current Issues and Challenges in Food Safety, 2007, pp. 222-232.

[20] R. Sánchez, F. Cerrón, J. Canchuricra, and M. Aquino, “Vida util del yogur bionatural usando el metodo del valor Q10 y analisis de supervivencia,” Tecnol. Alimentos, pp. 1-9, 2013.

[21] I. Saguy and M. Karel, “Modelling of quality deterioration during food processing and storage,” Food Technol., vol. 34, no. 2, pp. 78-85, 1980.

[22] P. S. Taoukis, T. P. Labuza, and I. S. Saguy, “Kinetics of Food Deterioration and Shelf-Life Prediction,” in Handbook of food engineering practice, United State of America: CRC Press, 1997, pp. 367-407.

[23] R. M. Salinas-Hernández, G. A. González-Aguilar, and M. E. Tiznado-Hernández, “Utilization of physicochemical variables developed from changes in sensory attributes and consumer acceptability to predict the shelf life of fresh-cut mango fruit,” J. Food Sci. Technol., vol. 52, no. 1, pp. 63-77, 2015, doi: https://doi.org/10.1007/s13197-013-0992-0

ÁRTICULO DE REVISIÓN

VOL. 45 | NO. 2 |**MAYO - AGOSTO 2024** | PP 115-139

Revista Mexicana de Ingeniería Biomédica

dx.doi.org/10.17488/RMIB.45.2.7

E-LOCATION ID: **1415**

Técnicas de Imagenología Óptica Aplicadas a Dermatología

Optical Imaging Techniques Applied to Dermatology

Erick Enrique Amezcua-López[1], *Luis Francisco Corral-Martínez* [1], *Gerardo Trujillo-Schiaffino*[1], *Didia Patricia Salas-Peimbert*[1], *Marcelino Anguiano-Morales*[1]

[1]Tecnológico Nacional de México/Instituto Tecnológico de Chihuahua, División de Estudios de Posgrado e Investigación, Chihuahua - México

RESUMEN

El uso de tecnologías de imagen ópticas ha permitido en años recientes mejorar el diagnóstico en área de la dermatología. Entre las técnicas se pueden nombrar, tomografía de coherencia óptica, la espectroscopia de Raman, la imagenología optoacústica, entre otras. Cada una de estas técnicas tiene aplicaciones tanto en la medicina general como en la dermatología, pero con sus respectivas limitaciones y enfoques. Este trabajo revisa las técnicas de imagenología de manera general, dándole prioridad al análisis teórico que permite la operación de la técnica, para luego mostrar un ejemplo de imagen obtenida con la técnica correspondiente. Después, se hace una extensiva revisión en las técnicas de imagen hiperespectral y dermatoscopios hiperespectrales polarizados. Finalmente, se habla del futuro hacia la cual se dirige la tecnología de la imagenología óptica.

PALABRAS CLAVE: dermatología, imagenología, óptica

ABSTRACT

The use of optical imaging technology in recent years has improved diagnostics in the dermatology area. The techniques that can be named are optical coherence tomography, Raman spectroscopy, and optoacoustic imaging. Each technique has applications in general medicine and dermatology but with their respective limitations and focus. This work reviews the imaging techniques in general, prioritizing the theoretical background that allows the technique to operate, and then an image example obtained with the technique is shown. Then, an extensive review of the techniques of hyperspectral imaging and hyperspectral polarized dermatoscope is made. Finally, we talk about new trends in optical imaging future.

KEYWORDS: dermatology, imaging, optic

Autor de correspondencia

DESTINATARIO: **Erick Enrique Amezcua-López**
INSTITUCIÓN: **Tecnológico Nacional de México/Instituto Tecnológico de Chihuahua, División de Estudios de Posgrado e Investigación, Chihuahua**
DOMICILIO: **Av. Tecnológico #2909, Chihuahua, Chih. México, CP 31310**
CORREO ELECTRÓNICO: D20060683@chihuahua.tecnm.mx

Recibido:

26 Enero 2024

Aceptado:

10 Junio 2024

INTRODUCCIÓN

La dermatoscopia, también conocida como dermoscopia o microscopía de epiluminiscencia[1] es una técnica desarrollada en años recientes con el objetivo de permitir un estudio más detallado de enfermedades que afectan la piel, permitiendo un análisis *in vivo* y por debajo de algunas capas de la piel. Un dermatoscopio por lo general se construye en su forma más simple de una fuente de luz y un lente magnificador[2]. Entre los dermatoscopios se encuentra los de contacto y no contacto, así como de luz polarizada y luz no polarizada, cada uno con sus ventajas y desventajas[3]. Entre las ventajas de los dermatoscopios polarizados esta su capacidad de permitir visualizar estructuras más profundas de la piel, sin necesidad de una interfaz o que exista contacto directo con la piel, ya que un dermatoscopio no polarizado requiere de esta interfaz para poder reducir la luz que se refleja y que se refracta. Otra diferencia importante es que los colores marrón y azul parecen más oscuros al analizarlos bajo un dermatoscopio polarizado[3].

El dermatoscopio no es la única herramienta para el diagnóstico en dermatología, ya que a lo largo de los años ha cambiado las necesidades de diagnóstico y están han requerido el uso de diferentes técnicas, por lo que en este artículo se explorarán varias de estas técnicas y su fundamento teórico, con el fin de comprender mejor su funcionamiento y utilidad.

MATERIALES Y MÉTODOS

Se realizó una búsqueda sistemática de la literatura con el fin de identificar las técnicas ópticas más importantes usadas en el área de la dermatología.

La búsqueda se enfocó en artículos de investigación, artículos de revisión, artículos de congreso y libros relacionados con las técnicas de imagenología óptica, dándole mayor importancia a la técnica de imagen hiperpesctral polarizada, para ello se utilizaron las palabras claves *“Hyperspectral imaging”, “Dermatoscopy”, “Hyperspectral Medical Imaging”, “Hyperspectral Dermatoscopy”, “Hyperspectral Polarization”, “Polarization Image”, “Hyperspectral Dermatology”, “Polarized Medical Imaging”,* y se utilizaron bases de datos como Scholar Google, IEEE Xplore, PubMed y CONRICyT.

Los criterios de exclusión fueron que los artículos no tuvieran más de 10 años de antigüedad, a menos que fueran de gran relevancia para el área de estudio y que fueran publicados en revistas revisadas por pares.

Imagenología óptica

La imagenología óptica es una técnica que emplea fuentes de luz visible, infrarroja y ultravioleta que permiten producir imágenes para uso clínico, en esta técnica se aprovecha la interacción de este tipo de radiación de baja energía con los tejidos biológicos para generar imágenes de la superficie del tejido o de capas subsuperficiales. La imagenología óptica complementa a las técnicas tradicionales que emplean el ultrasonido, rayos X o resonancia magnética como principios de funcionamiento. El uso de radiación no ionizante permite someter al paciente de manera segura a procesos de monitoreo prolongados o repetitivos[4].

Interacción radiación-tejido

Desde el punto de vista de la óptica, la piel es considerada un medio turbio por la forma en que interactúa con la luz. La propagación en ella no se da de manera uniforme debido a su composición heterogénea, su textura irregular, su contenido de melanina y los procesos dinámicos de circulación sanguínea. A continuación, se describen los procesos físicos más relevantes de la interacción de la radiación con el tejido biológico.

Absorción

La absorción en un tejido es el proceso de aniquilación de la energía fotónica cuando ésta interactúa con las moléculas y se transforma en otro tipo de energía, como sonido, calor e incluso fotones con una menor energía, como en el caso de la fluorescencia o la fosforescencia[5]. Los principales elementos de la absorción en el tejido son los cromóforos. La absorción se puede caracterizar por medio de la ecuación de Beer-Lambert (Ecuación 1):

$$I(d) = I_0 e^{-\mu_a d} \tag{1}$$

donde $I(d)$ es la intensidad de la luz trasmitida, I_0 es la intensidad incidente, d es el grosor de la capa de tejido y μ_a es el coeficiente de absorción[4].

Esparcimiento elástico

El esparcimiento elástico es el fenómeno por el cual los fotones son absorbidos por las moléculas y después reemitidos en diferentes direcciones, debido a que las moléculas están orientadas al azar, esto implica que no exista pérdida de energía en el proceso. Es de mencionar que los fotones se reemiten conservando su frecuencia y longitud de onda[6].

El esparcimiento en los tejidos se puede determinar a través de la siguiente ecuación (Ecuación 2)[4]:

$$I(d) = I_0 e^{-\mu_s d} \tag{2}$$

donde μ_s es el coeficiente de esparcimiento.

Existen dos tipos de esparcimiento elástico: el esparcimiento Rayleigh y el esparcimiento Mie.

Esparcimiento Rayleigh

Este esparcimiento se da cuando la partícula es mucho más pequeña que la longitud de onda del haz incidente. La partícula absorbe todos los fotones y luego los reemite de forma aleatoria dada la distribución aleatoria de las partículas. Por esto último es que se obtiene un haz incoherente del esparcimiento Rayleigh[7].

Esparcimiento Mie

Para la situación en la que la partícula es más grande que la longitud de onda de la luz incidente, el esparcimiento Rayleigh es inadecuado para describir el fenómeno. En este caso lo que se presentará es que la luz esparcida por la partícula interferirá de distintas formas con la luz que también fue esparcida por otra partícula cercana a ella, esta interferencia bien puede ser constructiva o destructiva. Por lo anterior, lo que se obtiene de este esparcimiento es una superposición de las ondas esparcidas por cada fracción de las partículas[7]. Sin embargo, la diferencia de fase entre las ondas secundarias tiende a ser pequeña, lo que provoca que la irradiancia sea grande.

Tomografía de coherencia óptica

La tomografía de coherencia óptica [OCT, por su acrónimo en inglés] es un arreglo interferométrico que consiste en irradiar la piel con una fuente de luz de banda ancha como puede ser un láser ajustable o un diodo súper luminoso. Después la luz reflejada de la muestra interferirá con la luz del brazo de referencia[8].

Si el largo del camino del brazo de referencia es cambiado a una velocidad constante lineal v, entonces la señal que saldrá de la interferencia entre la luz esparcida en dirección hacia atrás (reflejada) desde la muestra y la luz en el brazo de referencia serán moduladas por la frecuencia Doppler (Ecuación 3)[4]:

$$F_D = \frac{2v}{\lambda} \tag{3}$$

donde F_D es la frecuencia de Doppler, v es la velocidad de cambio lineal y λ es la longitud de onda.

Esta técnica provee imágenes en tiempo real de la piel con una penetración de 1 a 1.5 mm y una resolución de menos de 10 µm[9].

El arreglo fundamental consiste en una fuente de luz de banda ancha, un divisor de haz, dos brazos ópticos, uno de ellos con la muestra y el otro como referencia y finalmente un detector, esto se muestra en la Figura 1.

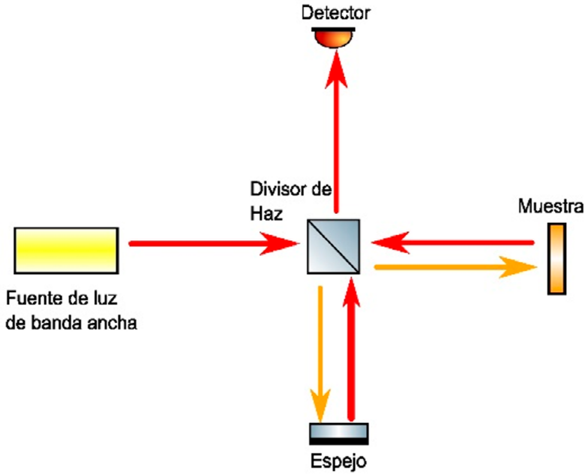

FIGURA 1. **Arreglo experimental para la técnica de tomografía de coherencia óptica (elaboración propia).**

La forma en que trabaja el arreglo es la siguiente: La luz de banda ancha incide en el divisor de haz y esto divide el haz en 2 partes, una de ellas se refleja en el espejo sin que este provoque ningún cambio en ella (haz de referencia), mientras que el haz que interactúa con la muestra sufre de un cambio en su fase (haz de muestra), lo cual es medido por el detector al comparar la superposición de las ondas de ambos brazos[5].

Entre los usos de la OCT está la detección de melanomas, tumores, diagnóstico de enfermedades inflamatorias, biopsias, cardiología, urología, enfermedades de las uñas (como la onicomicosis), fibrosis de la piel malformaciones y demás estudios de la piel[10][11][12][13][14][15]. Una imagen obtenida por medio de OCT se muestra en la Figura 2.

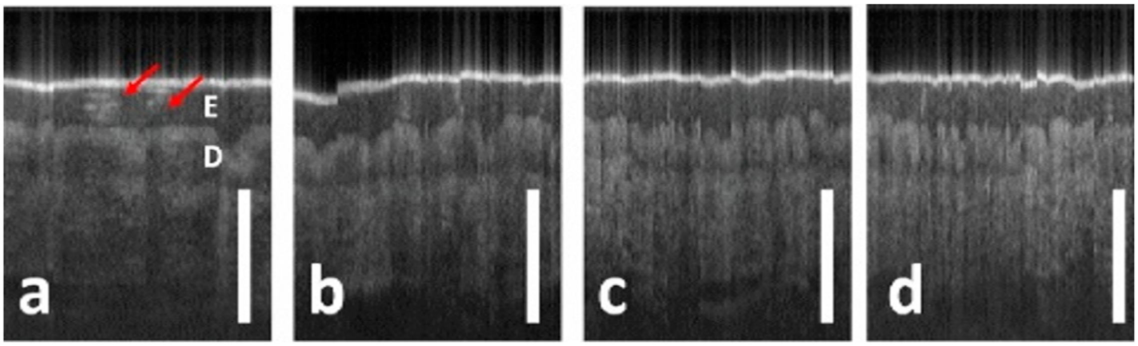

FIGURA 2. **Tomografías de coherencia óptica tomadas a diferentes intervalos. a) 10 µm, b) 20 µm, c) 30 µm, y d) 30 µm. E) indica la epidermis y D) la dermis (imagen tomada de *"Manually scanned single fiber optical coherence tomography for skin cancer characterization"* de Chuchvara *et al.*)[12].**

Imagenología optoacústica

Es una técnica reciente en la cual pulsos cortos de láser son usados para provocar una expansión termoelástica, esta expansión genera un aumento de ondas de ultrasonido que pueden ser registradas con un detector[4], como se muestra en la Figura 3. El patrón de la onda de sonido es convertido en una imagen de tres dimensiones de alta resolución[9]. La intensidad de la señal obtenida con esta técnica depende de la cantidad de energía absorbida y transformada en calor y de las propiedades termoelásticas de la muestra.

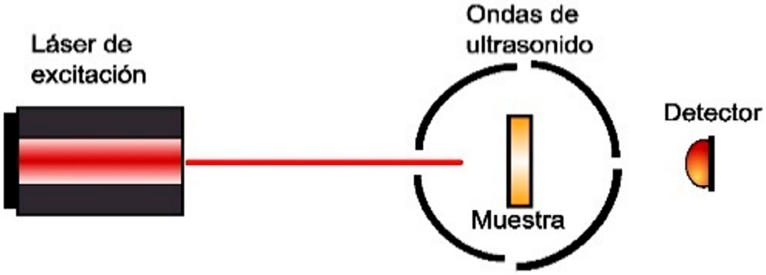

FIGURA 3. **Arreglo experimental para la técnica de imagenología optoacústica (elaboración propia).**

Esta absorción causa un incremento en la temperatura local, la cual es definida por la relación (Ecuación 4)[4]:

$$\Delta T = \frac{E_T}{cp\ V\rho} \cong \frac{E\,\mu_a\,d}{cp\ V\rho} \tag{4}$$

donde cp es la capacidad de calor específica para una presión constante, $V = \pi\omega^2 d$ es el volumen iluminado, ω es el radio del haz del láser y ρ es la densidad del medio. Asumiendo una expansión adiabática de un volumen iluminado a una presión constante, se puede calcular el cambio de volumen como (Ecuación 5):

$$\Delta V = \pi(\omega+\Delta\omega)^2 d - \pi\omega^2 d = \beta\ V\,\Delta \cong \frac{\beta\,E\,\mu_a\,d}{cp\,\rho} \tag{5}$$

Entre las aplicaciones de esta técnica está la detección de tumores y visualización en venas[16], un ejemplo de esto se muestra en la Figura 4. Filtros con este principio pueden ser usados para obtener imágenes espectrales de tejido y obtener la reflectancia difusa de las lesiones[17][18][19].

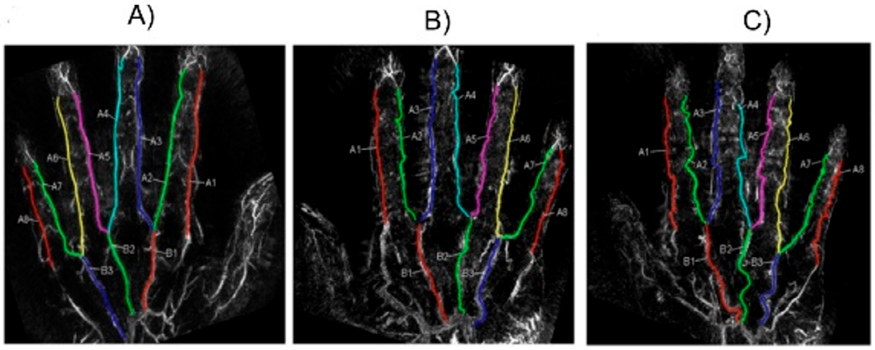

FIGURA 4. **Ejemplos de venas de sangre con diferente curvatura, vistas por medio de imagen optoacústica. a) Venas con pequeña curvatura, b) venas con curvatura media, c) venas con una larga curvatura curvatura (imagen tomada de *"Label-free photoacoustic imaging of human palmar vessels: A structural morphological analysis"* de Y. Matsumoto *et al.*)[19].**

Imagenología de fluorescencia

Los electrones y los átomos pueden estar en distintos estados de energía, el estado fundamental (baja energía) y el estado de excitación (alta energía), en complemento con los estados rotacionales y vibracionales. Antes de la excitación, la configuración de los electrones de la molécula es el estado fundamental. Durante la excitación por una particular longitud de onda los electrones pueden ser elevados a un estado de mayor energía. Cuando los electrones absorben energía, estos son excitados un estado vibración y electrónico de energía superior. En la fluorescencia, los electrones pierden algo de energía vibracional y regresan al más bajo nivel de excitación. Además, los electrones caen al estado fundamental y de manera simultánea emiten luz fluorescente. El regreso al estado fundamental ocurre con pérdida de energía en diversas formas[5].

1. Emisión de luz (fluorescencia).
2. Generación de calor.
3. La molécula puede sufrir una reacción química como polimerización o descomposición.

La luz emitida siempre será de una longitud de onda mayor que la luz de excitación.

Por lo general, las moléculas absorben la energía siguiendo la teoría cuántica que se define con la siguiente ecuación (Ecuación 6):

$$\Delta E = h\nu = \frac{hc}{\lambda} \tag{6}$$

donde ΔE es el cambio energético, ν es la frecuencia del fotón, h es la constante de Planck, c es la velocidad de luz y λ es la longitud de onda de la luz.

El arreglo de fluorescencia consiste en una fuente de luz de banda ancha, filtros tanto de excitación como de emisión, un lente objetivo, un espejo dicroico, un espécimen a estudiar y un detector, todo esto se observa en la Figura 5.

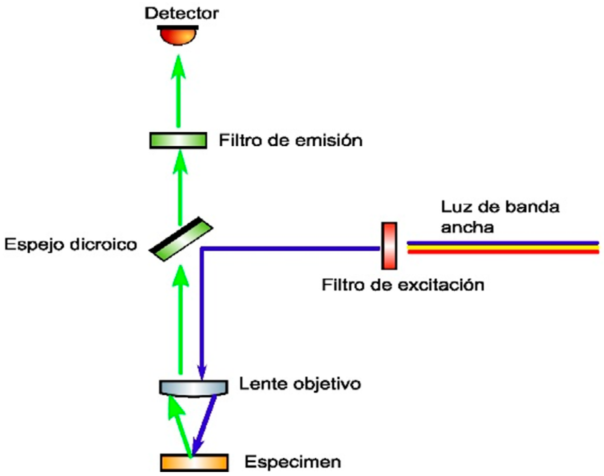

FIGURA 5. **Arreglo experimental para la técnica de imagen de fluorescencia (elaboración propia).**

Este arreglo trabaja de la siguiente manera: un haz de luz de banda ancha pasa por el filtro de excitación, quedando únicamente una longitud de onda de alta energía, como lo son las cercanas al ultravioleta, este haz incide en el espejo dicroico y se refleja hacia un lente objetivo, que centra la energía en el espécimen, este último absorbe la energía y la reemite con una longitud de onda distinta. El haz resultante viaja de nueva cuenta por el arreglo, se transmite a través del filtro dicroico y se realiza una selección muy específica de longitud de onda mediante el filtro de emisión, para luego incidir en el detector[5].

Entre las aplicaciones se puede mencionar el mapeo de la oxihemoglobina y los cromóforos de la melanina, la detección de cáncer, la mejor visualización de heridas y el diagnostico de onicomicosis[20][21][22][23][24][25]. Un ejemplo de imagen obtenida con esta técnica se observa en la Figura 6.

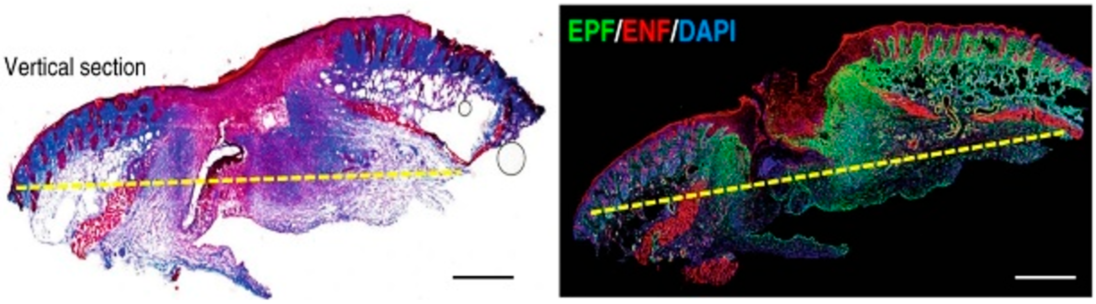

FIGURA 6. **Tinción de una tricromía de Masson, con su vista vertical y una imagen por medio de fluorescencia (imagen tomada de *"Injury triggers fascia fibroblast collective cell migration to drive scar formation through N-cadherin"* de D. Jiang *et al.*)[22].**

Espectroscopia Raman

El efecto Raman es un fenómeno que se presenta cuando los fotones son esparcidos de manera inelástica por las moléculas de la materia con la que interactúan, esto produce un cambio en la energía de los fotones y por lo tanto en su longitud de onda, estos fotones son reemitidos tanto a longitudes de onda mayores (transición de Stokes) como a longitudes de onda menores (transición anti-Stokes). Los cambios de energía producidos están determinados por los estados de vibración y rotación de la molécula con la cual interactuaron. Este fenómeno es utilizado en aplicaciones biomédicas e industriales[26][27].

La espectroscopía de Raman es una técnica basada en el efecto Raman y se enfoca en medir el cambio de energía en el fotón que es esparcido, lo que permite determinar la composición química de las moléculas con las que interactúan los fotones[5]. El espectrómetro de Raman consta de una fuente de luz monocromática, lentes ópticas, un objetivo de microscopio, la muestra, un espejo dicroico y un analizador de espectro. Por lo regular, este instrumento detecta vibraciones en el rango de 3200-200 cm^{-1}[28]. La forma en que opera este arreglo es en hacer incidir la luz monocromática de láser en la muestra para que ésta por esparcimiento reemita la luz y retorne a través de un espejo dicroico, con el fin de solo permitir pasar una porción deseada de la energía de la onda, la cual es finalmente detectada por un espectrómetro. El arreglo óptico se ilustra en la Figura 7, mientras que un ejemplo de uso se observa en la Figura 8.

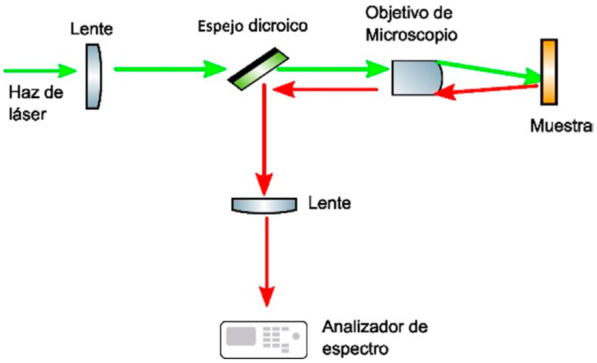

FIGURA 7. **Arreglo experimental para la técnica de espectroscopia de Raman (elaboración propia).**

Esta técnica es muy versátil y se usan en aplicaciones tan diversas como el análisis de materiales, detección de material tóxico, diagnóstico de cáncer, monitoreo de tratamientos en la piel, inmunología, el diagnostico de onicomicosis y detección de hidroquinona[29][30][31][32][33][23][34].

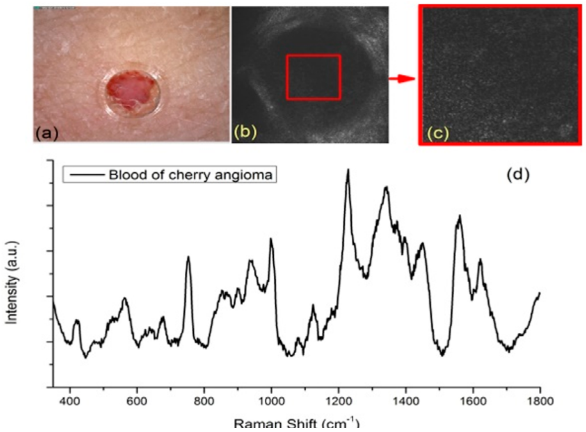

FIGURA 8. **a) Imagen con un dermatoscopio de un angioma b) imagen de una vena con microscopia confocal de reflectancia, c) imagen extraída de la región de interés de la imagen b), y d) Espectro de Raman extraído de la región analizada en el inciso c) (imagen tomada de *"A Method for accurate in vivo micro-Raman spectroscopic measurements under guidance of advanced microscopy imaging"* H. Wang *et al.*)[31].**

Microscopía confocal

Es una técnica de microscopía la cual permite una alta resolución y una imagen en tiempo real de la epidermis y la parte superior de la dermis con resolución a nivel celular. La resolución lateral de este tipo de microscopios es inversamente proporcional a la apertura numérica (NA) del lente objetivo del microscopio (Ecuación 7):

$$\Delta x = \frac{0.46\,\lambda}{NA} \tag{7}$$

La resolución prevista Δx es 0.4 µm con una NA = 1.2 con el lente objetivo inmerso en agua y a una longitud de onda λ = 1064 nm. La resolución axial es más sensible a la apertura numérica del lente objetivo del microscopio. Dado lo anterior, para obtener la máxima resolución axial (y con ello el mejor grado de seccionamiento óptico), es preferible usar objetivos de microscopio con la mayor apertura numérica posible. El ancho máximo al medio máximo de la distribución de la irradiancia axial define la resolución axial o el grosor de la sección óptica (Ecuación 8)[4]:

$$\Delta z = \frac{1.4n\,\lambda}{NA^2} \tag{8}$$

donde n es el índice de refracción del medio en el que está inmerso el lente objetivo. La resolución axial prevista Δz es de 1.4 µm con una NA = 1.2 de la lente inmersa en agua a una longitud de onda λ = 1064 nm y n = 1.35

La técnica consiste en iluminar por encima el tejido, esta iluminación se concentrará en un solo punto, para que luego esta información sea filtrada por una barrera física llamada *“pinhole”*, la cual solo permitirá que la luz del plano de interés incida en el detector. El contraste de la técnica es gracias a la diferencia en la intensidad de la reflexión. Gracias a esto la queratina y la melanina muestran una alta reflectancia por lo que las células pigmentadas serán muy brillantes en las imágenes[9].

El arreglo de un microscopio confocal básico consiste en una fuente de luz, un divisor de haz, un lente objetivo, un espécimen a estudiar, un *“pinhole”* y un detector, como se muestra en la Figura 9[4].

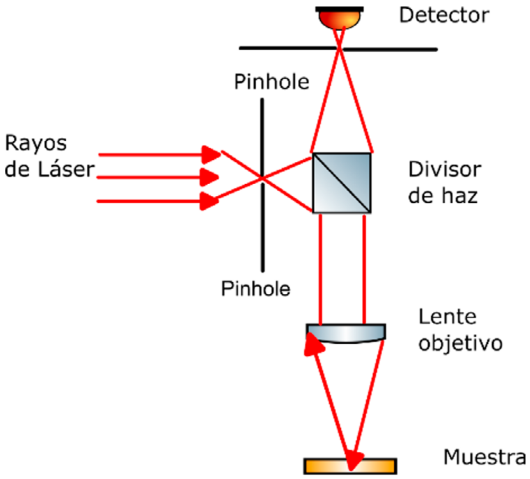

FIGURA 9. Arreglo experimental para la técnica de microscopía confocal (elaboración propia).

La microscopia confocal se usa principalmente en diagnóstico diferencial de lesiones pigmentadas, el análisis de tejido ex vivo y análisis de la piel[35][36][37]. En la Figura 10 se muestra una imagen obtenida con la técnica.

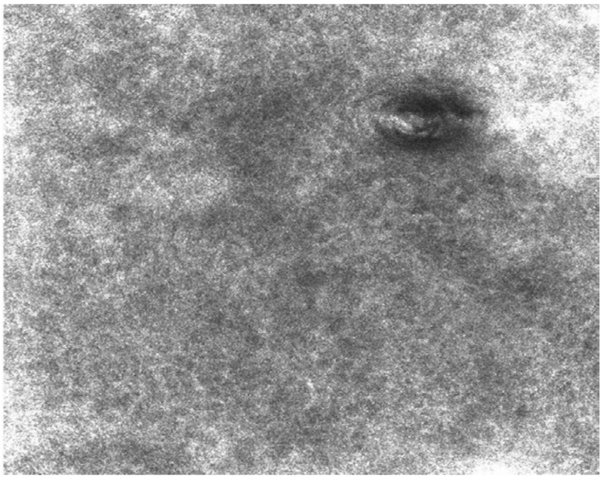

FIGURA 10. Microscopía confocal del estrato espinoso de la cara a 24 μm de profundidad profundidad (imagen tomada de *"Visualizing the in-vivo application of zinc in sensitive skin using reflectance confocal microscopy"* de H. J. Ahn *et al.*)[36].

Polarización

La luz es una onda electromagnética transversal que tiene una componente eléctrica y magnética, las cuales interactúan entre sí. Por lo que la polarización de la luz depende estas 2 componentes. La luz polarizada es aquella en la que la luz mantiene fija la orientación del campo eléctrico, aunque su magnitud y signo varíe. En este caso el campo eléctrico reside en lo que se conoce como plano de vibración[6].

Las componentes del campo eléctrico pueden ser escritas de la forma (Ecuación 9):

$$E_x\ (z,\ t) = i\ E_{0x} cos\ (kz - \omega t) \tag{9}$$

y (Ecuación 10)

$$E_y\ (z,t) = j\ E_{0y} cos\ (kz - \omega t + \varepsilon) \tag{10}$$

donde E_{0x} y E_{0y} son las amplitudes de campo eléctricos de cada componente, k es el número de onda, z es la dirección de propagación la onda, ω es la frecuencia angular, t es el tiempo y finalmente ε es el desfasamiento relativo entre ambas ondas. Como se puede observar, el agregar ε a la ecuación 10, hace que el coseno de esta no pueda alcanzar el mismo valor del coseno de la ecuación 9. Dado lo anterior es posible escribir la radiación polarizada de la forma (Ecuación 11):

$$E = E_x(z,\ t) + E_y(z,\ t) \tag{11}$$

Dependiendo del valor de desfasamiento, es posible obtener varios casos de polarización: luz linealmente polarizada, circularmente polarizada y elípticamente polarizada[38]. Mediante la eliminación o la detección de este campo eléctrico se pueden detectar o hacer más visibles características que las entregadas por una imagen de luz no polarizada. Un esquema para detectar imágenes porlarizadas se muestra en la Figura 11.

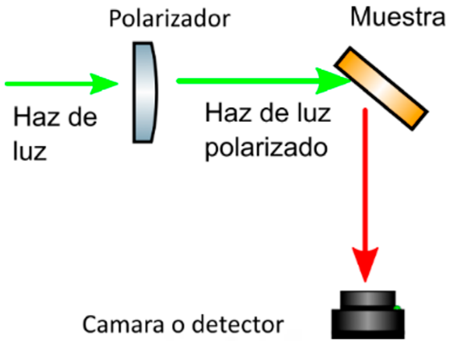

FIGURA 11. Esquema para la detección de una imagen polarizada (elaboración propia).

La polarización se utiliza en área como la detección de melanomas[20], análisis de la piel[39], cuantificación de melanina y hemoglobina[40] y análisis del nevus melanocítico[41]. Una imagen de piel bajo luz polarizada se observa en la Figura 12.

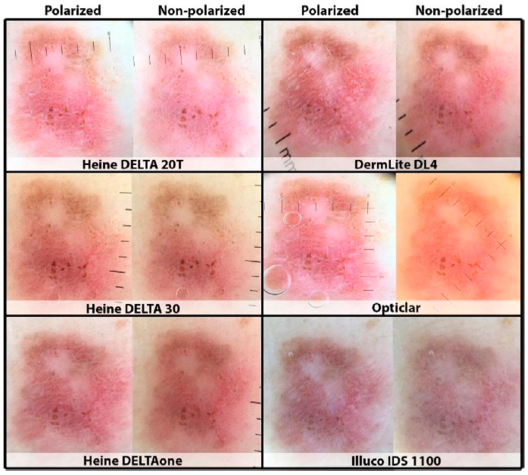

FIGURA 12. Piel analizada bajo luz polarizada y no polarizada, con distinto dermatoscopios comerciales (imagen tomada de *"Not All Polarized-light Dermatoscopes May Display Diagnostically Critical Polarizing-specific Features"* de C. Whybrew *et al.*)[39].

Imagen hiperespectral

La imagen hiperespectral o imagen espectrométrica es aquella en la que se obtienen imágenes en distintas longitudes de onda, lo cual proporciona información espectral de los elementos que existen en las imágenes[42]. Una imagen común suele estar representada en el espacio RGB como se muestra en la Figura 13.

Los ejes X y Y representan la información espacial en la imagen y los colores RGB la información espectral de la imagen. Esto quiere decir que la información espectral solamente será representada por 3 bandas espectrales, Mientras que una imagen hiperespectral suele contener más bandas espectrales, como se muestra en la Figura 13.

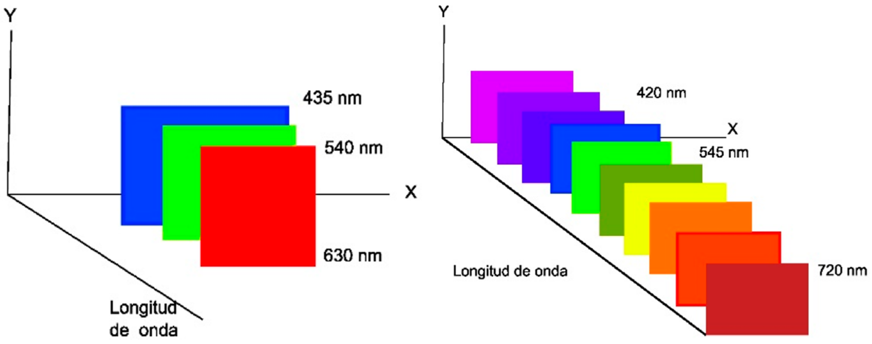

FIGURA 13. **Bandas espectrales de: una imagen RGB (*Red Green Blue)* y una hiperespectral (elaboración propia).**

Esto le da la capacidad a esta técnica de recuperar información del tejido del cuerpo, que se relaciona a longitudes de onda más específicas y que con una imagen RGB es imposible de detectar[42]. En la Figura 14 se muestra tejido a distintas longitudes de onda.

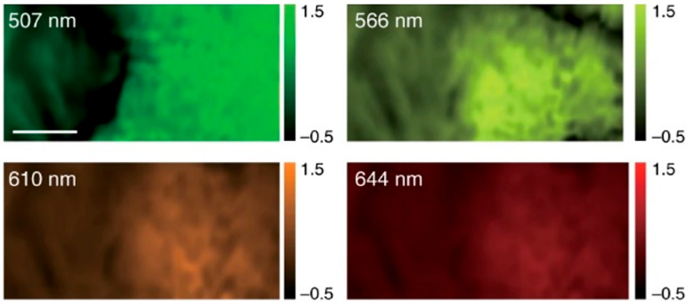

FIGURA 14. **Imágenes de tejido a distintas longitudes de onda (imagen tomada de *"A clinically translatable hyperspectral endoscopy (HySE) system for imaging the gastrointestinal tract"* de J. Yoon *et al.*)[43].**

Aplicaciones de las técnicas de imagenología óptica

Melanomas

En el área de los estudios de los melanomas existen diversos trabajos. El *Melanoma Advanced Imaging Dermatoscope* (mAID) el cual cuenta con 32 longitudes de onda ubicadas entre 350 nm (ultravioleta) y 900 nm (infrarrojo cercano)[44]. El sistema toma varias imágenes con el fin de extraer distintas características para con ello obtener biomarcadores que permitan al sistema de clasificación definir si la lesión es un melanoma. Otra técnica es el utilizar un sistema hiperespectral en el infrarrojo extendido con una franja de 900 nm a 1600[45], Figura 15. Después las imágenes se procesan mediante una inteligencia artificial y que esta emita la decisión de si es o no un melanoma. También es posible el uso de equipos comerciales para delimitar lentigo maligno del lentigo maligno melanoma para una cirugía mediante el uso de sistema hiperespectral Dermlite® DL3, logrando mejores resultados que los obtenidos con dermatoscopios normales o también el obtenido por la luz de Wood[46]. Usando cámaras hiperespectrales como la CUBERT UHD 185, se puede realizar un dermatoscopio en el rango de 450 a 950 y dado el paso de 4 nm de la cámara, se obtiene 125 bandas espectrales con la cual se obtiene la firma espectral para diferentes tipos de lesiones como lo son los nevus normales, la queratosis seborreica, el carcinoma de célula basal y el melanoma[47]. Este mismo trabajo se realizó un banco de imágenes con pacientes y para clasificarlos, los autores prueban distintos esquemas de inteligencia artificial llegando a obtener una precisión del 98.61 % al diferenciar los distintos padecimientos.

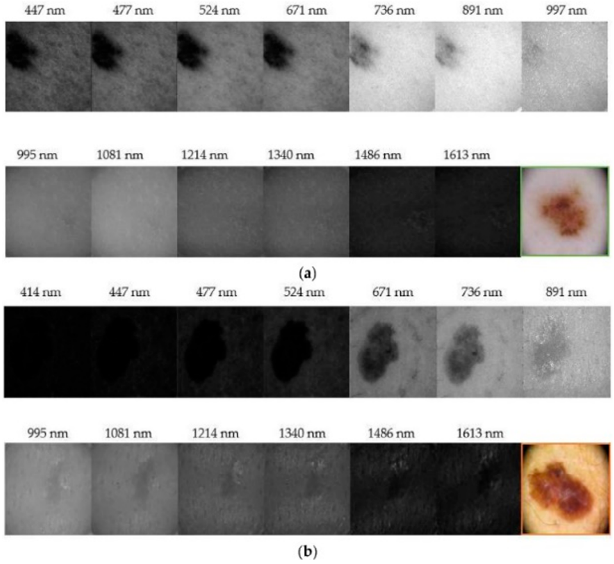

FIGURA 15. Imágenes de reflectancia de un melanoma, a distintas longitudes de onda (imagen tomada de *"Visible and extended near-infrared multispectral imaging for skin cancer diagnosis"* de L. Rey-Barroso *et al.*)[45].

Cáncer

En el área de la detección de cáncer se han desarrollado diversos dermatoscopios hiperespectrales. Se puede mencionar el que haciendo uso de una cámara Ximea MQ022, luz LED blanca y una raspberry como una tarjeta de control y de datos. Este sistema es sensible a 16 bandas comprendidas entre 450 y 630[48]. Este trabajo obtiene un set de 330 imágenes en colaboración con una clínica local de cáncer, para después evaluar la extracción de características que se pueden extraer con una imagen RGB en comparación a una hiperespectral. Otra forma de diagnóstico es por medio de la fluorescencia en combinación con un conjunto de imágenes capturadas entre 390 y 450 nm, mediante un microscopio invertido de fluorescencia, para distinguir elementos que permitan el diagnóstico de cáncer de colon. Se logran obtener curvas de intensidad, de transmitancia y de absorbancia, las cuales demuestran la diferencia entre el tejido sano y el enfermo, lo cual demuestra la factibilidad de desarrollar más esta técnica[21]. Es posible también hacer una distinción del cáncer en tejido colorrectal capturando imágenes de tejido ex vivo con dos cámaras hiperespectrales, la primera de ella en el rango visual de 400 a 1000 nm y la segunda en el infrarrojo de 900 a 1700 nm[49], Figura 16. También se han desarrollado métodos para la extracción de características del cáncer de mama mediante imágenes hiperespectrales, para lo cual primero se obtienen imágenes de muestras *ex vivo* de tejido, tanto con una cámara RGB como con una cámara hiperespectral (Hyperspec VNIR A-Series) en conjunto con un microscopio. Finalmente se usa una red neuronal convolucional para la clasificación de las imágenes[50]. También es posible usar luz blanca con filtro para la detección de tumores malignos y benignos en el rango visible para ello se hace uso de un LED blanco para la iluminación y un modulador optoacústico con el fin de filtrar con una resolución espectral de 2.3 nm dentro los 450-750nm, de esta manera se analiza la reflectancia difusa de las lesiones y se logra separarlas del tejido sano con una efectividad de hasta el 88 %[17].

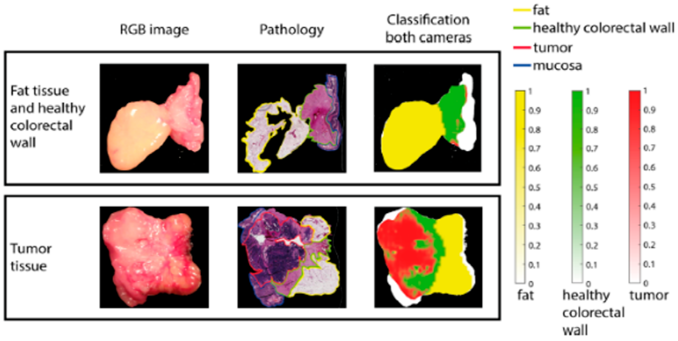

FIGURA 16. Clasificación de tejido sano con respecto a tejido canceroso (imagen tomada de *"Hyperspectral imaging for tissue classification, a way toward smart laparoscopic colorectal surgery"* de E. J. M. Baltussen *et al.*)[49].

Niveles de oxigenación

Otro tema recurrente es el de la medición de niveles de oxigenación en la sangre. Con un sistema hiperespectral es posible la detección cromóforos y del nivel de oxigenación de la sangre[51]. Para ello se usa interferometría de Fabry-Perot, que permite tener una resolución de 6-10 nm en un rango de 500-900 nm. Para la detección, se emplea una red neuronal que determina parámetros como la melanina o el volumen de sangre. Finalmente, se obtienen las imágenes de saturación de oxígeno y de volumen de oxígeno, ambas antes, durante y después de una oclusión en un dedo. El uso de los teléfonos inteligentes también se ha vuelto una propuesta interesante con el fin de reducir los costos de los instrumentos, como sistemas de imagen hiperespectral de bajo costo con un *smartphone*[52]. El instrumento obtiene mapas de oxigenación, hemoglobina y melanina y además determina el pulso cardiaco y oclusiones vasculares. También es posible hacer un sistema compacto de imágenes hiperespectrales utilizando la cámara TIVITA™ Tissue, la cual tiene un rango de 500-1000 nm con un paso de 5nm[53]. Con este instrumento se pueden hacer mediciones in vivo de perfusiones en un trasplante y en lesiones permanentes, demostrado su utilidad en detectar lesiones como un tejido necrótico. También se han desarrollado sistemas hiperespectrales portables para la obtención de mapas de oxigenación de la sangre y de volumen en la sangre, todo esto procesado de manera automática por una red neuronal[54], ver Figura 17.

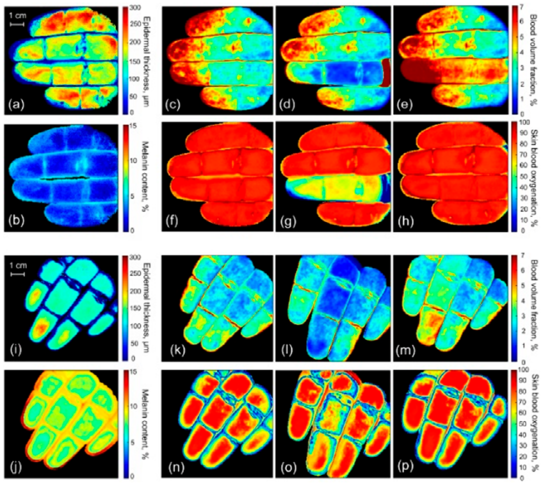

FIGURA 17. Niveles de oxigenación con imagen hiperespectral (imagen tomada de *"Hyperspectral imaging of human skin aided by artificial neural networks"* de E. Zherebtsov *et al.*)[54].

Lesiones

Otra aplicación es hacer uso de estos instrumentos para diagnosticar lesiones, usando imagen optoacústica a 800 nm se pueden analizar lesiones en el pecho de pacientes, se analizan patrones definidos en las imagines que ayudan a determinar si la lesión en el tejido es maligna o benigna[55], ver Figura 18. También con tomografía optoacústica de pocos pulsos de energía se plantea un sistema de diagnóstico no invasivo de cáncer de piel de alta resolución[56]. Existen también sistemas portátiles de imagen optoacústica, en el que su principal ventaja es que mejora la limitación del ángulo de visión de los equipos comerciales, elevando la resolución y el contraste en las imágenes. Estos equipos logran una muy alta resolución que permite distinguir características tanto benignas como malignas del cáncer de mama[57].

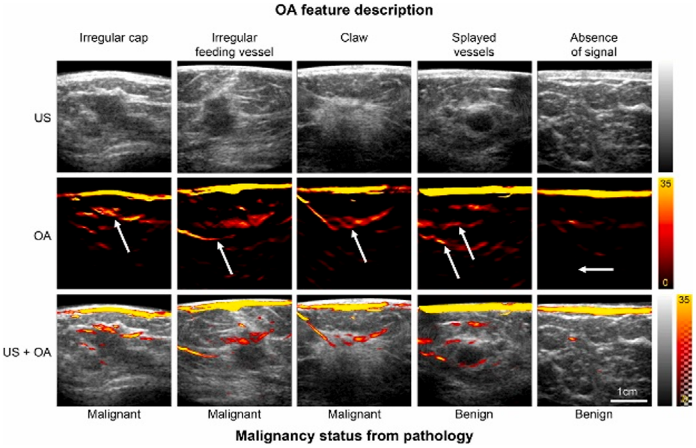

FIGURA 18. Comparativa entre ondas de ultrasonido, imagen optoacústica y la combinación de ambas (imagen tomada de *"An optoacoustic imaging feature set to characterise blood vessels surrounding benign and malignant breast lesions"* de O. Abeyakoon *et al.*)[55].

La dermatitis atópica es la enfermedad inflamatoria crónica más común del mundo y se han demostrado que puede ser diagnosticada con mesoscopía optoacústica de barrido ya que esta permite una imagen tridimensional del proceso de inflamación de la piel que permite identificar algunas de las características más importantes del padecimiento[58].

Innovaciones

Entre las innovaciones en los sistemas hiperespectrales podemos mencionar un sensor para tomar una fotopletismografía, el instrumento se compone de un arreglo multiespectral (525, 590, 650 y 870 nm) y un sistema de control para iluminar con cada longitud de onda la piel bajo diferentes condiciones como ejercicio o reposo[59]. Este instrumento muestra buenos resultados comparado con un electrocardiograma. Otra innovación es lograr obtener una imagen totalmente a color partiendo de información obtenida de imágenes hiperespectrales[60]. El sistema se compone de una cámara D3 (*VRmagic*), un sensor hiperespectral, y 16 filtros de *Fabry Perot* y se logra reconstruir una imagen a color.

Se han explorado las posibilidades de visión con imágenes hiperespectrales en las regiones del infrarrojo cercano (650-950 nm) y el infrarrojo de onda corta (950-1600 nm). Esto se analiza con un sistema con una guía líquida de luz y el uso de 2 sensores refrigerados para la detección de los distintos tipos de infrarrojo[61]. El equipo logra obtener mediciones de contraste de Michelson a distintas longitudes de onda, sin embargo, a grandes profundidades del tejido, solo el rango 1200 a 1350 nm logran un contraste suficiente. Otra metodología es el de un sistema de imagen hiperespectral de transformada de Fourier con dos lentes liquidas para crear el retraso en las ondas[62]. Este sistema ofrece una alta resolución espectral y son interesantes dando que ofrecen toda esta información por medio de la interferometría. Se han modificado sistemas hiperespectrales para darles la capacidad de hacer adquisición de objetos en movimiento, en un rango espectral de 475-925 nm[63]. El instrumento permite con sus modos, capturar elementos estáticos y en movimiento con un tiempo menor a un segundo, lo cual no lo hace totalmente un equipo en tiempo real, pero que en un futuro este tiempo de procesamiento se pueda reducir. También se han presentado una propuesta en el que su innovación radica en el uso de una máscara de amplitud con el cual logran un filtrado espacial adicional al espectral, lo cual le permite recuperar información visual de fase[64], ver Figura 19.

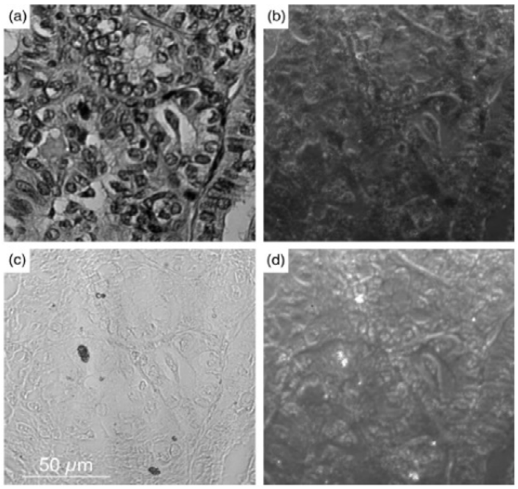

FIGURA 19. **Micrófagos de una sección histológica siendo a) y c) son imágenes espectrales comunes y b) y d) imágenes espectrales con un filtro espacial (imagen tomada de *"Hyperspectral imaging acousto-optic system with spatial filtering for optical phase visualization"* de K. B. Yushkov y V. Ya. Molchanov)[64].**

Dermatoscopios hiperespectrales polarizados

El uso combinado de las tecnologías de imagen hiperespectral y polarización es un tema de bastante interés en el área de las ciencias biomédicas, ya que el uso de ambas técnicas permite recuperar más información en las muestras y tejidos, de la que se obtiene usando estas técnicas de manera individual. Además, ofrece una interesante área de oportunidad en el estudio de diversos campos.

Se puede analizar con este tipo de instrumentos el carcinoma de células basales nodular, el cual es un tipo de cáncer y además la neoplasia más común en el ser humano. Las estructuras parecidas a un arcoíris bajo la luz polarizada, luego de una biopsia, resultan ser células cancerígenas que se infiltraron en la dermis y en tejidos subcutáneos[65].

Una enfermedad dermatológica y que afecta alrededor del 3 % de la población es la psoriasis, ya que esta enfermedad puede degenerar en otras como la hipertensión y la diabetes. Por lo que se han desarrollado un dermatoscopio multiespectral polarizado con tres longitudes de onda (470 nm, 530 nm y 625 nm) y un microscopio de multifotón, los cuales trabajando en conjunto obtienen características de las lesiones psoriásicas, como lo son las venas con sangre y lesiones de color rojo[66], ver Figura 20. También se ha buscado mejorar las imágenes para la evaluación de la escala de las lesiones psoriásicas, ya que esto ayuda a determinar la gravedad de la enfermedad y el tratamiento, por lo que usa un sistema polarizado con tres longitudes de onda (430nm, 530nm y luz blanca de banda ancha) y además usa la segmentación de Otsu, con el fin de resaltar el área de estudio y obtener mejores resultados[67].

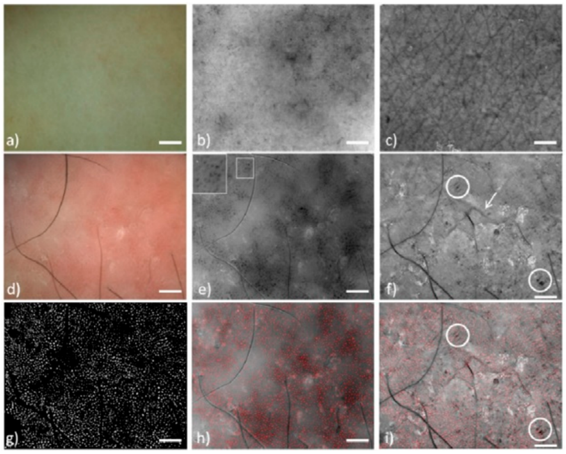

FIGURA 20. **Imágenes bajo un dermatoscopio hiperespectral polarizado (imagen tomada de *"In-vivo imaging of psoriatic lesions with polarization multispectral dermoscopy and multiphoton microscopy"* de D. Kapsokalyvas *et al.*)[66].**

Normalmente un sistema con polarización usa solo un haz polarizado, pero hay propuesta de usar dos haces como el sistema que proponen Abdtlay *et al.* comprendido entre los 450-800 nm, con una resolución de 1.5 a 4.4 nm, El utilizar dos haces le permite aumentar la potencia de salida hasta en un 68 %. También se presenta una caracterización de la salida óptica, de la respuesta espectral y de la respuesta espacial del instrumento. Finalmente comparan estos parámetros cambiando el filtro optoacústico por uno de cristal líquido, siendo este último superior en la respuesta espacial, pero superando en las demás por el filtro optoacústico[18].

También se puede diagnosticar melanomas con esta técnica, utilizando un dermatoscopio hiperespectral polarizado con cuatro longitudes de onda (365nm, 470nm, 530nm y 620nm), que combinado con un preprocesamiento de la imagen y un sistema para extraer características como lo son color y textura, es capaz de clasificar si la lesión es o no un melanoma con una sensibilidad del 83 %[68]. Otro instrumento explora el uso de la región UV para el análisis de melanomas con un rango hiperespectral desde los 350nm hasta los 630nm con luz polarizada, lo cual permite un análisis de fluorescencia lo que, combinado con el espectro visible, permite obtener una mapeado de la oxihemoglobina y los cromóforos de la melanina. El sistema también cuenta un software para la detección automática de los melanomas basado en la textura, específicamente en la extracción de características llegando a una sensibilidad del 0.96 cuando las imágenes no tienen corrección de color[20].

Analizar la melanina es muy importante para los estudios dermatológicos. El sistema *SkinSpect* es un sistema de dermatoscopia hiperespectral desarrollado en 2014 por SMI Inc., con el objetivo de desarrollar un sistema que pudiera obtener de manera precisa el mapa de distribución espacial de la melanina y el oxígeno en la piel[41]. El rango de longitudes de onda de este sistema es de 33 longitudes de onda de luz polarizada desde los 468 nm a los 857 nm. Otro equipo de este estilo es el SpectraCam® el cual es un sistema hiperespectral en el visible (400 nm - 700 nm) que toma una imagen cada 10nm usando un filtro óptico, proporcionando un total de 31 imágenes polarizadas con el fin de reducir la reflexión especular en el tejido. Todo lo anterior le permite cuantificar in vivo la melanina, la hemoglobina y el total de la saturación de oxígeno[40].

Una característica de utilidad es usar varios estados de polarización, como el sistema multiespectral con tres longitudes de onda (470 nm, 530 nm y 625 nm) con polarizadores, utilizando un motor para girar estos últimos. El equipo toma cinco imágenes (B0, B90, R90, G90 Y W90) esta última, combinando los 3 leds para simular una fuente de iluminación blanca. el trabajo obtiene distintas imágenes como el contraste de melanina, contraste de sangre, contraste de esparcimiento, contraste de melanina superficial y contraste de melanina con sangre corregido (con el objetivo de hacer más visibles las venas)[69]. He y Wang proponen de un sistema hiperespectral polarizado que emplea una lampara blanca, una cámara instantánea y una lente de 35 mm que trabaja en conjunto a un filtro de Fabry-Perot para proveer al sistema con 16 bandas espectrales en el visible. Se hace un estudio morfológico de la piel, la absorción de la sangre, la absorción del nevus melanocítico, medición del ritmo cardiaco, recuperación de ejercicio y oclusión vascular[70], ver Figura 21.

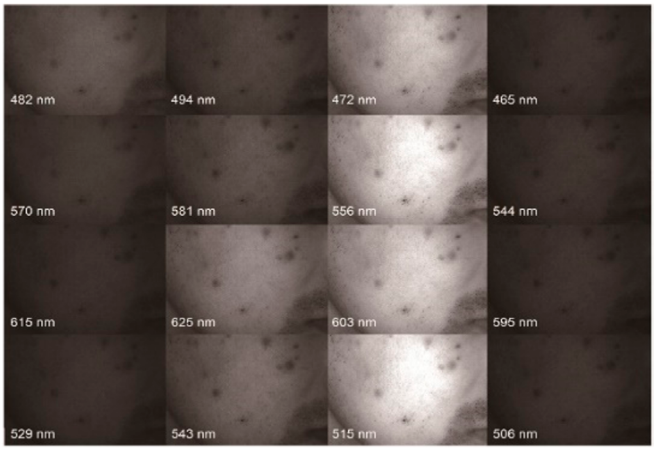

FIGURA 21. **Imágenes en 16 canales espectrales de la piel (imagen tomada de *"Analysis of skin morphological features and real-time monitoring using snapshot hyperspectral imaging"* de Q. He y R. K. Wang[70].**

Debido a la versatilidad los dermatoscopios hiperespectrales polarizados se han utilizado para abordar varios padecimientos que regularmente no son tratadas con dermatoscopia. Usando un sistema hiperespectral polarizado se miden cambios en la pigmentación de la piel, relacionados a la edad y la diabetes. Para ello calcula la polarización residual por medio de una relación entre dos estados de polarización ortogonales, lo que logran relacionar de manera correcta con la edad del paciente, demostrando que esta técnica in vivo es poco invasiva y tiene potencial para futuros estudio[71].

Estas tecnologías también han demostrado su versatilidad al permitir recuperar las matrices de Mueller de muestras biológicas, lo que puede ser auxiliar en el diagnóstico de enfermedades dermatológicas. Se han construido dermatoscopios que se complementan con un polarímetro de Mueller, ya que muchos padecimientos de la piel se basan en parámetros ópticos para su diagnóstico como lo es la regla ABCD para los melanomas o el PASI en la psoriasis, sin embargo, al ser muchos dermatoscopios de contacto, hay problemas como la supresión de perfusiones, por lo que se propone que su diseño sea de no contacto. Este equipo logra recuperar información adicional en las muestras al obtener la matriz de Mueller de esta, lo que es de utilidad en enfermedades como la morfea, donde la molécula quiral del colágeno es importante. También este mismo instrumento se usa para medir la orientación del colágeno y de elementos gelatinosos en una muestra mediante el uso de las matrices de Mueller[72][73].

Como un complemento y muestra de la variedad de aplicaciones de esta técnica, está un prototipo de un sistema de imagen hiperespectral polarizado. El sistema es relativamente sencillo ya que se compone de un filtro optoacústico sintonizable con un rango de 550-1000 nm, un polarizador lineal, un sistema de lentes y un sensor CCD, el cual cuenta con una eficiente resolución espectral apto para múltiples aplicaciones biomédicas[73].

El último trabajo para mencionar en el que se describe un sistema de imagen hiperespectral para hacer la medición y predicción de sustancias como colorantes en matrices con un alto esparcimiento. Se trabaja con un sistema de 400-800 nm con una resolución de 3.6 nm y utiliza como medio arena y colorante, finalmente obtiene mapas con las imágenes hiperespectrales a distintas concentraciones y de ahí hace una regresión numérica con el fin de estimar la concentración de las sustancias en la muestra. El uso de polarizadores es de gran ayuda para discriminar la información superficial de la que está a mayor profundidad[74].

RESULTADOS Y DISCUSIÓN

Después de revisar las técnicas de imagenología más empleadas en dermatología, así como las más novedosas y prometedoras, se construye la Tabla 1, en la cual se hace un resumen y comparativa entre las distintas técnicas, mencionando su uso más común dentro de la medicina y su función en el área de la dermatología.

TABLA 1. **Comparación de técnicas de imagenología.**

Técnica	Uso principal	Uso en dermatología	Resolución espacial	Profundidad	Tiempo de adquisición	Costo
Tomografía de coherencia óptica	Biopsias, cardiología, urología[11]	Diagnostico en tumores, enfermedades inflamatorias, padecimientos en las uñas[8][13][14][75]	3 a 15 μm[8]	0.4 a 2 mm[8]	Bajo[9]	Alto[9]
Imagenología optoacústica	Imágenes espectrales de tejido[17]	Análisis de lesiones mediante la reflectancia difusa de lesiones[18]	>1 mm[76]	~1 μ[76]	Bajo[76]	Bajo[76]
Imagenología de fluorescencia	Detección de melanomas[9]	Mapas de oxihemoglobina y los cromóforos de la melanina y cáncer[20]	Cercana a 1 mm[77]	Hasta 500 μm[77]	Bajo[77]	Medio[77]
Imagen multiespectral e hiperespectral	Patologías circulatorias y del corazón, enfermedades de la retina[70]	Diagnóstico de cáncer de piel[70]	Variable, dependiendo de la aplicación	Desde 1 mm[78]	Bajo[79]	Bajo[79]
Espectroscopía Raman	Análisis de biomoléculas, tejido y materiales[29]	Inmunología, control en tratamientos de la piel y en uñas[28][33][80]	Variable, dependiendo de la aplicación	Hasta 5 μm[32]	Medio[80]	Bajo[81]
Microscopía confocal	Diagnóstico diferencial de lesiones pigmentadas[9][35]	Análisis de tejido ex vivo[35]	1 a 3 μm[9]	1-3 μm[9]	Alto[9]	Medio[82]
Polarización	Detección de melanomas[20]	Mejoramiento en las imágenes de dermatoscopio[40]	Variable, dependiendo de la aplicación	Hasta 150 μm[83]	Bajo[40]	Medio[18]

CONCLUSIONES

El uso de técnicas de imagenología tiene muchos años de existencia y se ha usado para el diagnóstico, tratamiento y control de diversas enfermedades dermatológicas, por lo que es de importancia conocer más a fondo cuales son los fundamentos teóricos que permiten la operación de cada una de las técnicas revisadas en este artículo, ya que esto da la posibilidad de tener en cuenta cuales son las limitantes y el alcance de los instrumentos de uso dermatológico.

Por otra parte, los equipos dermatológicos cada vez son más avanzados y muestra de ello es el uso de tecnologías como la imagen hiperespectral y optoacústica. También en años recientes estos instrumentos han empezado a incorporar tecnologías de áreas que son ajenas a la dermatología como lo es la inteligencia artificial, con lo cual se busca realizar un diagnóstico automático de imágenes dermatológicas. Un ejemplo de esto es la extracción de características en imágenes hiperespectrales con el fin de detectar cáncer de mama, lo cual da un panorama de cómo diferentes tecnologías se han ido incorporando para la mejora del diagnóstico en la dermatología.

Otra vertiente de innovación es la portabilidad de los instrumentos, dada la capacidad de procesamiento que tienen equipos modernos como los teléfonos celulares, los cuales se han usado para plantear instrumentos dermatológicos de bajo costo y que puedan combinarse con software o conectividad directa con el especialista para emitir un diagnóstico.

Con todo lo anterior podemos concluir que la dinámica de los instrumentos de dermatología es incorporar más elementos con el fin de hacer un diagnóstico más preciso y que de manera gradual vayan cubriendo las deficiencias que presentan los instrumentos actuales, como lo pueden ser el costo elevado o la baja portabilidad.

DECLARACIÓN ÉTICA

Las imágenes que fueron tomadas de otros artículos fueron bajo las licencias *Creative Commons Attribution 3.0 International License, Creative Commons Attribution 4.0 International License y la Golden Open Access* que permiten copiar y redistribuir el material en cualquier medio o formato para cualquier propósito, incluso comercial y adaptar el material, siempre y cuando se otorgue el crédito apropiado.

CONFLICTO DE INTERÉS

Los autores declaran no tener conflictos de interés relacionados al contenido de este artículo.

AGRADECIMIENTOS

Los autores agradecen al Tecnológico Nacional de México (TecNM) por el financiamiento del proyecto 18649.23-P. E.E.A.L agradece al Consejo Nacional de Humanidades, Ciencia y Tecnologías (CONAHCYT) por la beca de doctorado 700871.

CONTRIBUCIÓN DE LOS AUTORES

E. E. A. L. conceptualización, diseño y desarrollo de la metodología, curación de datos, análisis formal, escritura del manuscrito original. L. F. C. M. conceptualización, financiamiento, diseño y desarrollo de la metodología, supervisión, revisión y edición del manuscrito. M. A. M. conceptualización, supervisión, revisión y edición del manuscrito. G. T. S. conceptualización, supervisión, revisición y edición del manuscrito. D. P. S. P. conceptualización, supervisión, revisión y edición del manuscrito. Todos los autores revisaron y aprobaron la versión final del manuscrito.

REFERENCIAS

[1] G. Micali, F. Lacarrubba, D. Massimino, R. A. Schwartz, “Dermatoscopy: Alternative uses in daily clinical practice,” J. Am. Acad. Dermatol., vol. 64, no. 6. pp. 1135-1146, 2011, doi: https://doi.org/10.1016/j.jaad.2010.03.010

[2] D. Hirokawa y J. B. Lee, “Dermatoscopy: An overview of subsurface morphology,” Clin. Dermatol., vol. 29, no. 5, pp. 557-565, 2011, doi: https://doi.org/10.1016/j.clindermatol.2010.12.002

[3] C. Benvenuto-Andrade, S. W. Dusza, A. L. Agero, A. Scope, M. Rajadhyaksha, A. C. Halpern, A. A. Marghoob, “Differences Between Polarized Light Dermoscopy and Immersion Contact Dermoscopy for the Evaluation of Skin Lesions,” Arch. Dermatol., vol. 143, no. 3, pp. 329-338, 2007, doi: https://doi.org/10.1001/archderm.143.3.329

[4] V. Tuchyn, Tissue Optics, Bellingham, Estados Unidos: Society of Photo-Optical Instrumentation Engineers, 2015.

[5] R. Splinter, B. A. Hooper, An Introduction to Biomedical Optics, Estados Unidos, CRC Press, 2006.

[6] E. Hecht, Optics, Estados Unidos: Pearson Education, 2017.

[7] D. Malacara, Óptica básica, México: Fondo de Cultura Económica, 2015.

[8] J. Olsen, J. Holmes, G. B. E. Jemec, “Advances in optical coherence tomography in dermatology—a review,” J. Biomed. Opt., vol. 23, no. 04, pp. 1-10, 2018, doi: https://doi.org/10.1117/1.jbo.23.4.040901

[9] J. Welzel, S. Schuh, “Noninvasive diagnosis in dermatology,” J. Dtsch. Dermatol. Ges., vol. 15, no. 10, pp. 999-1016, 2017, doi: https://doi.org/10.1111/ddg.13347

[10] E. Sattler, R. Kästle, y J. Welzel, “Optical coherence tomography in dermatology”, J. Biomed. Opt., vol. 18, no. 6, 2013, art. no. 061224, doi: https://doi.org/10.1117/1.jbo.18.6.061224

[11] X. Shu, L. Beckmann, y H. F. Zhang, “Visible-light optical coherence tomography: a review,” J. Biomed. Opt., vol. 22, no. 12, pp. 1-14, 2017, doi: https://doi.org/10.1117/1.jbo.22.12.121707

[12] N. Chuchvara, B. Rao, y X. Liu, “Manually scanned single fiber optical coherence tomography for skin cancer characterization,” Sci. Rep., vol. 11, no. 1, 2021, art. no. 15570, doi: https://doi.org/10.1038/s41598-021-95118-z

[13] C. E. Psomadakis, N. Marghoob, B. Bleicher, y O. Markowitz, “Optical coherence tomography,” Clin. Dermatol., vol. 39, no. 4, pp. 624-634, 2021, doi: https://doi.org/10.1016/j.clindermatol.2021.03.008

[14] T. Gambichler, A. Pljakic, y L. Schmitz, “Recent advances in clinical application of optical coherence tomography of human skin,” Clin. Cosmet. Investig. Dermatol., vol. 8., pp. 345-354, 2015, doi: https://doi.org/10.2147/CCID.S69119

[15] L. M. C. Vasquez-Pinto, E. P. Maldonado, M. P. Raele, M. M. Amaral, y A. Z. de Freitas, “Optical coherence tomography applied to tests of skin care products in humans - a case study,” Skin Res. Technol., vol. 21, no. 1, pp. 90-93, 2015, doi: https://doi.org/10.1111/srt.12161

[16] A. Taruttis y V. Ntziachristos, “Advances in real-time multispectral optoacoustic imaging and its applications,” Nat. Photon., vol. 9, no. 4, pp. 219-227, 2015, doi: https://doi.org/10.1038/nphoton.2015.29

[17] I. A. Bratchenko, V. P. Sherendak, O. O. Myakinin, D. N. Artemuev, et al., “In vivo hyperspectral imaging of skin malignant and benign tumors in visible spectrum,” J. Biomed. Photonics Eng., vol. 4, no. 1, 2018, art. no. 010301, doi: http://dx.doi.org/10.18287/JBPE17.04.010301

[18] R. Abdlaty, J. Orepoulos, P. Sinclair, R. Berman, y Q. Fang, “High throughput AOTF hyperspectral imager for randomly polarized light,” Photonics, vol. 5, no. 1, 2018, art. no. 3, doi: https://doi.org/10.3390/photonics5010003

[19] Y. Matsumoto, Y, Asao, A. Yoshikawa, H, Sekiguchi, et al., “Label-free photoacoustic imaging of human palmar vessels: A structural morphological analysis,” Sci. Rep., vol. 8, no. 1, 2018, art. no. 786, doi: https://doi.org/10.1038/s41598-018-19161-z

[20] O. A. Melsitov, V. P. Sherendak, S. G. Konovalov, y O. O. Myakinin, “Automatic Malignant Melanoma recognition using a Dermatoscopy Imaging Tool,” presentado en IV Conferencia de Conferencias y Escuelas de Modificaciones «Información sobre tecnologías y nanotecnologías» (ИТНТ-2018), Samara, Rusia, 2018. http://repo.ssau.ru/bitstream/Informacionnye-tehnologii-i-nanotehnologii/Automatic-Malignant-Melanoma-recognition-using-a-Dermatoscopy-Imaging-Tool-69115/1/paper_125.pdf

[21] S. J. Leavesley, M. Walters, C. Lopez, T. Baker, et al., “Hyperspectral imaging fluorescence excitation scanning for colon cancer detection,” J. Biomed. Opt., vol. 21, no. 10, 2016, art. no. 104003, doi: https://doi.org/10.1117/1.jbo.21.10.104003

[22] D. Jiang, S. Christ, D. Correa-Gallegos, P. Ramesh, et al., "Injury triggers fascia fibroblast collective cell migration to drive scar formation through N-cadherin," Nat. Commun., vol. 11, no. 1, 2020, art. no. 5653, doi: **https://doi.org/10.1038/s41467-020-19425-1**

[23] C. Petrokilidou, G. Gaitanis, I. D. Bassukas, A. Velegraki, E. Guevara, M. Z. Vardaki, N. Kourkoumelis, "Emerging optical techniques for the diagnosis of onychomycosis," Appl. Sci., vol. 10, no. 7, 2020, art. no. 2340, doi: **https://doi.org/10.3390/app10072340**

[24] V. K. Ortner, W. Franco, M. Haedersdal, y P. A. Philipsen, "Noninvasive Assessment of Mycotic Nail Tissue Using an Ultraviolet Fluorescence Excitation Imaging System," Lasers Surg. Med., vol. 53, no. 2, pp. 245-251, 2021, doi: **https://doi.org/10.1002/lsm.23285**

[25] A. P. da Silva, T. C. Fortunato, M. D. Stringasci, C. Kurachi, V. S. Bagnato, y N. M. Inada, "Onychomycosis diagnosis using fluorescence and infrared imaging systems", presentado en Biophotonics South America, Rio de Janeiro, Brasil, 2015, doi: **https://doi.org/10.1117/12.2180998**

[26] J. Zhao, H. Zeng, S. Kalia, y H. Lui, "Using Raman Spectroscopy to Detect and Diagnose Skin Cancer In Vivo," Dermatol. Clin., vol. 35, no. 4, pp. 495-504, 2017, doi: **https://doi.org/10.1016/j.det.2017.06.010**

[27] F. Martelli, S. del Bianco, A. Ismaelli, G. Zaccanti, Light propagation through biological tissue and other diffusive media: theory, solutions, and software. Estados Unidos: SPIE - The International Society for Optical Engineering, 2009.

[28] D. Lunter, V. Klang, D. Kocsis, Z. Varga-Medveczky, S. Berkó, y F. Erdő, "Novel aspects of Raman spectroscopy in skin research," Exp. Dermatol., vol. 31, no. 9, pp. 1311-1329, 2022, doi: **https://doi.org/10.1111/exd.14645**

[29] P. Rostron, S. Gaber, D. Gaber, "Raman Spectroscopy, a review," Int. J. Eng. Technical Res., vol. 6, no. 1, pp. 2454-4698, 2016.

[30] N. Kuhar, S. Sil, T. Verma, y S. Umapathy, "Challenges in application of Raman spectroscopy to biology and materials," RSC Adv., vol. 8, no. 46, pp. 25888-25908, 2018, doi: **https://doi.org/10.1039/c8ra04491k**

[31] H. Wang, A. M. D. Lee, H. Lui, D. I. McLean, y H. Zeng, "A Method for accurate in vivo micro-Raman spectroscopic measurements under guidance of advanced microscopy imaging," Sci. Rep., vol. 3, 2013, art. no. 1890, doi: **https://doi.org/10.1038/srep01890**

[32] A. Azan, P. J. Caspers, T. C. Bakker Schut, S. Roy, et al., "A novel spectroscopically determined pharmacodynamic biomarker for skin toxicity in cancer patients treated with targeted agents," Cancer Res., vol. 77, no. 2, pp. 557-565, 2017, doi: **https://doi.org/10.1158/0008-5472.can-16-1733**

[33] N. Chaudhary, C. Wynne, y A. D. Meade, "A review of applications of Raman spectroscopy in immunology," Biomed. Spectrosc. Imaging, vol. 9, no. 1-2, pp. 23-31, 2020, doi: **https://doi.org/10.3233/BSI-200198**

[34] R. Cabrera-Alonso, E. Guevara, M. G. Ramírez-Elías, B. Moncada, y F. J. González, "Detection of hydroquinone by Raman spectroscopy in patients with melasma before and after treatment," Skin Res. Technol., vol. 25, no. 1, pp. 20-24, 2019, doi: **https://doi.org/10.1111/srt.12589**

[35] E. Cinotti, J. L. Perrot, B. Labeille, F. Cambazard, y P. Rubegni, "Ex vivo confocal microscopy: an emerging technique in dermatology," Dermatol. Pract. Concept., vol. 8, no. 2, pp. 109-119, 2018, doi: **https://doi.org/10.5826/dpc.0802a08**

[36] H. J. Ahn, H. J. Kim, H. Ham, J. H. Baek, et al., "Visualizing the in-vivo application of zinc in sensitive skin using reflectance confocal microscopy," Sci. Rep., vol. 11, no. 1, 2021, art. no. 7738, doi: **https://doi.org/10.1038/s41598-021-87346-0**

[37] E. Guevara, J. Manuel Gutierrez-Hernandez, A. Castonguay, F. Lesage, B. Moncada, y F. J. González, "Morphological and molecular imaging of skin simples," Biomed. Res., vol. 28, núm. 4, 2017. [En línea]. Disponible en: **https://www.alliedacademies.org/articles/morphological-and-molecular-imaging-of-skin-samples.html**

[38] D. H. Goldstein, Polarized light, 3ra ed. Estados Unidos: CRC press, 2017.

[39] C. Whybrew, P. Pietkiewicz, I. Kohut, J. C. Chia, B. N. Akay, y C. Rosendahl, "Not All Polarized-light Dermatoscopes May Display Diagnostically Critical Polarizing-specific Features," Dermatol. Pract. Concept., vol. 12, no. 4, 2022, art. no. e2022250, doi: **https://doi.org/10.5826/dpc.1204a250**

[40] A. Nkengne, J. Robic, P. Seroul, S. Gueheunneux, M. Jomier, y K. Vie, "SpectraCam®: A new polarized hyperspectral imaging system for repeatable and reproducible in vivo skin quantification of melanin, total hemoglobin, and oxygen saturation," Skin Res. Technol., vol. 24, núm. 1, pp. 99-107, 2018, doi: **https://doi.org/10.1111/srt.12396**

[41] F. Vasefi, N. MacKinnon, R. Saager, K. M. Kelly, et al., "Multimode optical dermoscopy (SkinSpect) analysis for skin with melanocytic nevus," presentado en Imaging, Manipulation, and Analysis of Biomolecules, Cells, and Tissues IX, SPIE, San Francisco, California, Estados Unidos, 2016, art. no. 971110. doi: **https://doi.org/10.1117/12.2214288**

[42] M. J. Khan, H. S. Khan, A. Yousaf, K. Khurshid, y A. Abbas, "Modern Trends in Hyperspectral Image Analysis: A Review," IEEE Access, vol. 6, pp. 14118-14129, 2018, doi: **https://doi.org/10.1109/ACCESS.2018.2812999**

[43] J. Yoon, J. Joseph, D. J. Waterhouse, A. S. Luthman, et al., "A clinically translatable hyperspectral endoscopy (HySE) system for imaging the gastrointestinal tract," Nat. Commun., vol. 10, no. 1, 2019, art. no. 1902, doi: **https://doi.org/10.1038/s41467-019-09484-4**

[44] A. M. Hosking, B. J. Coakley, D. Chang, F. Talebi-Liasi, et al., "Hyperspectral imaging in automated digital dermoscopy screening for melanoma," Lasers Surg. Med., vol. 51, no. 3, pp. 214-222, 2019, doi: **https://doi.org/10.1002/lsm.23055**

[45] L. Rey-Barroso, F. J. Burgos-Fernández, X. Delpueyo, M. Ares, et al., "Visible and extended near-infrared multispectral imaging for skin cancer diagnosis," Sensors, vol. 18, no. 5, 2018, art. no. 1441, doi: https://doi.org/10.3390/s18051441

[46] N. Neittaanmäki-Perttu, M. Grönroos, L. Jeskanen, I. Pölönen, A. Ranki, O. Saksela, E. Snellman, "Delineating margins of lentigo maligna using a hyperspectral imaging system," Acta Derm. Venereol., vol. 95, no. 5, pp. 549-552, 2015, doi: https://doi.org/10.2340/00015555-2010

[47] H. Fabelo, V. Melián, B. Martínez, P. Beltrán, et al., "Dermatologic Hyperspectral Imaging System for Skin Cancer Diagnosis Assistance," presentado en 2019 XXXIV Conference on Design of Circuits and Integrated Systems (DCIS), Bilbao, España, 2019, pp. 1-6, doi: https://doi.org/10.1109/DCIS201949030.2019.8959869

[48] Y. Gu, Y.-P. Partridge, y J. Zhou, "A Hyperspectral Dermoscopy Dataset for Melanoma Detection," presentado en OR 2.0 Context-Aware Operating Theaters, Computer Assisted Robotic Endoscopy, Clinical Image-Based Procedures, and Skin Image Analysis, Granada, España, 2018, pp. 268-276, doi: https://doi.org/10.1007/978-3-030-01201-4_29

[49] E. J. M. Baltussen, E. N. D. Kok, S. G. Brouwer de Koning, J. Sanders, et al., "Hyperspectral imaging for tissue classification, a way toward smart laparoscopic colorectal surgery," J. Biomed. Opt., vol. 24, no. 1, pp. 1-9, 2019, doi: https://doi.org/10.1117/1.jbo.24.1.016002

[50] S. Ortega, M. Halicek, H. Fabelo, R. Guerra, et al., "Hyperspectral imaging and deep learning for the detection of breast cancer cells in digitized histological images," Proc. SPIE Int. Soc. Opt. Eng., 2020, art. no. 113200V, doi: https://doi.org/10.1117/12.2548609

[51] E. Zherebtsov, A. Popov, A. Doronin, I. Meglinski, y A. Bykov, "Hyperspectral system for imaging of skin chromophores and blood oxygenation," presentado en Diffuse Optical Spectroscopy and Imaging VI 2017, Munich, Alemania, 2017, doi: https://doi.org/10.1117/12.2280779

[52] Q. He y R. Wang, "Hyperspectral imaging enabled by an unmodified smartphone for analyzing skin morphological features and monitoring hemodynamics," Biomed. Opt. Express, vol. 11, no. 2, pp. 895-910, 2020, doi: https://doi.org/10.1364/boe.378470

[53] A. Kulcke, A. Holmer, P. Wahl, F. Siemers, T. Wild, y G. Daeschlein, "A compact hyperspectral camera for measurement of perfusion parameters in medicin,e" Biomed. Tech., vol. 63, no. 5, pp. 547-556, 2018, doi: https://doi.org/10.1515/bmt-2017-0145

[54] E. Zherebtsov, V. Dremin, A. Popov, A. Doronin, et al., "Hyperspectral imaging of human skin aided by artificial neural networks," Biomed. Opt. Express, vol. 10, no. 7, pp. 3545-3559, 2019, doi: https://doi.org/10.1364/boe.10.003545

[55] O. Abeyakoon, R. Woitek, M. G. Wallis, P. L. Moyle, et al., "An optoacoustic imaging feature set to characterise blood vessels surrounding benign and malignant breast lesions," Photoacoustics, vol. 27, 2022, art. no. 100383, doi: https://doi.org/10.1016/j.pacs.2022.100383

[56] A. F. Kukk, F. Scheling, R. Panzer, S. Emmert, y B. Roth, "Combined ultrasound and photoacoustic C-mode imaging system for skin lesion assessment," Sci. Rep., vol. 13, no. 1, 2023, art. no. 17947, doi: https://doi.org/10.1038/s41598-023-44919-5

[57] J. Kukačka, S. Metz, C. Dehner, A. Muckenhuber, et al., "Image processing improvements afford second-generation handheld optoacoustic imaging of breast cancer patients," Photoacoustics, vol. 26, 2022, art. no. 100343 doi: https://doi.org/10.1016/j.pacs.2022.100343

[58] T. Nau, C. Schönmann, B. Hindelang, L. Riobo, et al., "Raster-scanning optoacoustic mesoscopy biomarkers for atopic dermatitis skin lesions," Photoacoustics, vol. 31, 2023, art. no. 100513, doi: https://doi.org/10.1016/j.pacs.2023.100513

[59] L. Yan, S. Hu, A. Alzahrani, S. Alharbi, y P. Blanos, "A multi-wavelength opto-electronic patch sensor to effectively detect physiological changes against human skin types," Biosensors, vol. 7, no. 2, 2017, art. no. 22, doi: https://doi.org/10.3390/bios7020022

[60] F. Tanriverdi, D. Schuldt, y J. Thiem, "Hyperspectral Imaging: Color Reconstruction Based on Medical Data," presentado en 2018 IEEE-EMBS Conference on Biomedical Engineering and Sciences (IECBES), Sarawak, Malaysia, 2018, pp. 194-199, doi: https://doi.org/10.1109/IECBES.2018.8626614

[61] D. Salo, H. Zhang, D. M. Kim, M. Y. Berezin, "Multispectral measurement of contrast in tissue-mimicking phantoms in near-infrared spectral range of 650 to 1600 nm," J. Biomed. Opt., vol. 19, no.8, 2014, art. no. 086008, doi: https://doi.org/10.1117/1.jbo.19.8.086008

[62] A. Jullien, R. Pascal, U. Bortolozzo, N. Forget, y S. Residori, "High-resolution hyperspectral imaging with cascaded liquid crystal cells," Optica, vol. 4, no. 4, pp. 400-405, 2017, doi: https://doi.org/10.1364/OPTICA.4.000400

[63] J. Pichette, W. Charle, y A. Lambrechts, "Fast and compact internal scanning CMOS-based hyperspectral camera: the Snapscan," presentado en Photonic Instrumentation Engineering IV, San Francisco California, Estados Unidos, 2017, art. no. 1011014, doi: https://doi.org/10.1117/12.2253614

[64] K. B. Yushkov y V. Ya. Molchanov, "Hyperspectral imaging acousto-optic system with spatial filtering for optical phase visualization," J. Biomed. Opt., vol. 22, no. 6, 2017, art. no. 066017, 2017, doi: https://doi.org/10.1117/1.jbo.22.6.066017

[65] B. Nirmal, A. Krishnaram, y R. Sudhagar, "Rainbow sign in dermatoscopy of nodular basal cell carcinoma," Indian J. Dermatopathol. Diagn. Dermatol., vol. 6, no. 2, pp. 107-108, 2019, doi: https://doi.org/10.4103/ijdpdd.ijdpdd_27_19

[66] D. Kapsokalyvas, R. Cicchi, N. Bruscino, D. Alfieri, et al., "In-vivo imaging of psoriatic lesions with polarization multispectral dermoscopy and multiphoton microscopy," Biomed. Opt. Express, vol. 5, no. 7, pp. 2405-2419, 2014, doi: https://doi.org/10.1364/boe.5.002405

[67] T. Van Tien, N. Hoang Ohuc, L. Quang Nhien, T. Thi Thu Trang, et al., “Evaluation of scaly levels in psoriasis using multispectral polarized imaging,” presentado en 6th International Conference on the Development of Biomedical Engineering in Vietnam (BME6), Vietnam, 2018, pp. 97-101, doi: https://doi.org/10.1007/978-981-10-4361-1_16

[68] S. G. Konovalov, O. A. Melsitov, O. O. Myakinin, I. A. Bratchenko, A. A. Moryatov, S. V. Kozlov, V. P Zakharov, “Dermatoscopy software tool for in vivo automatic malignant lesions detection,” J. Biomed. Photonics, Eng., vol. 4, no. 4, pp. 105-118, 2018, doi: http://dx.doi.org/10.18287/JBPE18.04.040302

[69] D. Kapsokalyvas, N. Bruscino, D. Alfieri, V. de Giorgi, et al., “Spectral morphological analysis of skin lesions with a polarization multispectral dermoscope,” Opt. Express, vol. 21, no. 4, pp. 4826-4840, 2013, doi: https://doi.org/10.1364/oe.21.004826

[70] Q. He y R. K. Wang, “Analysis of skin morphological features and real-time monitoring using snapshot hyperspectral imaging,” Biomed. Opt. Express, vol. 10, no. 11, pp. 5625-5638, 2019, doi: https://doi.org/10.1364/boe.10.005625

[71] V. Dremin, A. Bykov, Z. Marcinkevics, A. Grabovskis, E. Zherebtsov, A. Popov, I. Meglinski, “Assessment of Age-related Skin Changes Using Hyperspectral Polarization Imaging,” presentado en Medical Laser Applications and Laser-Tissue Interactions IX, Munich, Alemania, 2019, art. no. 110718, doi: https://doi.org/10.1117/12.2526359

[72] D. Fricke, M. Wollweber, y B. Roth, “Mueller Matrix Measurement System for Skin Polarimetry as Additional Module for Non-Contact Dermatoscopy,” presentado en 2019 Conference on Lasers and Electro-Optics Europe & European Quantum Electronics Conference (CLEO/Europe-EQEC), Muchich, Alemania, 2019, pp. 1-1, doi: https://doi.org/10.1109/CLEOE-EQEC.2019.8872705

[73] Q. Wang, J. Shi, J. Wang, D. Zhao, y Y. Liu, “Design and Characterization of an AOTF Hyper-Spectral Polarization Imaging System,” J. Mod. Opt., vol. 64, no. 1, pp. 1-7, 2017, doi: https://doi.org/10.1080/09500340.2016.1200682

[74] J. L. Xu, A. Gobrecht, N. Gorretta, D. Héran, A. A. Gowen, y R. Bendoula, “Development of a polarized hyperspectral imaging system for investigation of absorption and scattering properties,” J. Near Infrared Spectrosc., vol. 27, no. 4, pp. 314-329, 2019, doi: https://doi.org/10.1177/0967033519857732

[75] J. Olsen, P. Lindsø Andersen, L. Themstrup, G. B. E. Jemec, y D. M. L. Saunte, “Optical coherence tomography of onychomycosis: proposed terminology and a suggestion of practical usage,” Arch. Dermatol. Res., vol. 312, no. 1, pp. 51-58, 2020, doi: https://doi.org/10.1007/s00403-019-01989-8

[76] I. Steinberg, D. M. Huland, O. Vermesh, H. E. Frostig, W. S. Tummers, y S. S. Gambhir, “Photoacoustic clinical imaging,” Photoacoustics, vol. 14, pp. 77-98, 2019, doi: https://doi.org/10.1016/j.pacs.2019.05.001

[77] D. R. Miller, J. W. Jarrett, A. M. Hassan, y A. K. Dunn, “Deep tissue imaging with multiphoton fluorescence microscopy,” Curr. Opin. Biomed. Eng., vol. 4, pp. 32-39, 2017, doi: https://doi.org/10.1016/j.cobme.2017.09.004

[78] S. L. P. Aggarwal y F. A. Papay, “Applications of multispectral and hyperspectral imaging in dermatology,” Exp. Dermatol., vol. 31, no. 8, pp. 1128-1135, 2022, doi: https://doi.org/10.1111/exd.14624

[79] J. Yoon, “Hyperspectral Imaging for Clinical Applications,” Biochip J., vol. 16, no. 1, 2022, doi: https://doi.org/10.1007/s13206-021-00041-0

[80] A. Orlando, F. Frranceschini, C. Muscas, S. Pidkova, M. Bartolini, M. Rovere, A. Tagliaferro, “A comprehensive review on Raman spectroscopy applications,” Chemosensors, vol. 9, no. 9, 2021, art. no. 262, doi: https://doi.org/10.3390/chemosensors9090262

[81] S. Duraipandian, M. Sylvest Bergholt, W. Zheng, K. Yu Ho, M. Teh, K. Guan Yeoh, J. Bok Yan So, A. Shabbir, Z. Huang, “Real-time Raman spectroscopy for in vivo, online gastric cancer diagnosis during clinical endoscopic examination,” J. Biomed. Opt., no. 8, 2012, art. no. 081418, doi: https://doi.org/10.1117/1.jbo.17.8.081418

[82] A. D. Elliott, “Confocal Microscopy: Principles and Modern Practices,” Curr. Protoc. Cytom., vol. 92, no. 1, 2020, e68, doi: https://doi.org/10.1002/cpcy.68

[83] S. Y. Chen, Z.-T. Su, D.-J. Lin, M.-X. Lee, et al., “Optimizing imaging depth of anisotropic scattering tissues with polarization engineered second harmonic generation microscopy,” Results Phys., vol. 28, 2021, art. no. 104653, doi: https://doi.org/10.1016/j.rinp.2021.104653

ÁRTICULO DE REVISIÓN

VOL. 45 | NO. 2 | **MAYO - AGOSTO 2024** | PP 140-150

Revista Mexicana de Ingeniería Biomédica

dx.doi.org/10.17488/RMIB.45.2.8

E-LOCATION ID: **1427**

Electroquímica en Medicina: Grafeno y Electroestimulación Celular

Electrochemistry in Medicine: Graphene and Celular Electrostimulation

Griselda Patricia Villareal Valdiviezo[1], *Elia Martha Múzquiz Ramos*[1], *Marisol Gallardo Heredia*[1], *Jorge Carlos Ríos Hurtado*[1]

[1]Universidad Autónoma de Coahuila, Coahuila - México

RESUMEN

El uso de la electroestimulación celular en medicina ha sido un área de interés creciente, y el grafeno ha emergido como un material prometedor en este campo. Este artículo explora cómo la electroestimulación celular puede influir en procesos biológicos clave y cómo el grafeno, con sus propiedades únicas, puede potenciar esta técnica. Se investigaron los aspectos electroquímicos de la interacción grafeno-célula y su impacto en la regulación de la actividad celular. Además, se examinaron diversas aplicaciones del grafeno en la electroestimulación celular, desde la ingeniería de tejidos hasta el tratamiento de enfermedades. Este artículo ofrece una visión integral de cómo la combinación de electroquímica y grafeno está transformando el campo de la medicina regenerativa.

PALABRAS CLAVE: electroestimulación, electroquímica, grafeno

ABSTRACT

The use of cellular electrostimulation in medicine has been an increasingly growing area of interest, and graphene has emerged as a promising material in this field. This article explores how cellular electrostimulation can influence key biological processes and how graphene, with its unique properties, can enhance this technique. The electrochemical aspects of the graphene-cell interaction and its impact on cellular activity regulation were investigated. Additionally, various applications of graphene in cellular electrostimulation, from tissue engineering to disease treatment were examined. This article provides a comprehensive insight into how the combination of electrochemistry and graphene is transforming the field of regenerative medicine.

KEYWORDS: electrostimulation, electrochemistry, graphene

Autor de correspondencia

DESTINATARIO: **Elia Martha Múzquiz Ramos**
INSTITUCIÓN: **Universidad Autónoma de Coahuila**
DOMICILIO: **Blvd. Venustiano Carranza y José Cárdenas Valdés. Saltillo, Coahuila. México. CP 25280**
CORREO ELECTRÓNICO: emuzquiz@uadec.edu.mx

Recibido:

11 Abril 2024

Aceptado:

15 Junio 2024

INTRODUCCIÓN

La electroestimulación celular ha surgido como una técnica destacada en el campo de la medicina regenerativa y la ingeniería de tejidos, ofreciendo soluciones para el tratamiento de enfermedades y lesiones crónicas que anteriormente tenían opciones de tratamiento limitadas. Este método aprovecha la capacidad intrínseca de las células para responder a estímulos eléctricos y modula su comportamiento y función en el entorno biológico[1][2].

La electroestimulación celular implica la aplicación de corrientes eléctricas controladas a las células o tejidos, con el objetivo de influir en su comportamiento y promover la regeneración de tejidos dañados o la reparación de lesiones. Este proceso puede tener efectos diversos y beneficiosos, como la mejora de la proliferación celular, la diferenciación celular hacia linajes específicos, la migración celular dirigida y la síntesis de matriz extracelular[1][3][4].

Esta estimulación destaca por su capacidad para promover la regeneración de tejidos complejos, como el hueso, el cartílago y el tejido nervioso, que normalmente tienen una capacidad limitada para recuperarse después de lesiones o enfermedades[5][6]. Al aplicar corrientes eléctricas específicas a las células y tejidos, es posible desencadenar respuestas biológicas específicas que conducen a la formación de nuevo tejido funcional y la restauración de la función normal del órgano o sistema afectado[7][8].

Los materiales conductores son un elemento importante de esta técnica, ya que estos permiten la transmisión eficiente de electricidad hacia las células y tejidos. Estos materiales, como los polímeros conductores, los metales nobles o los materiales base carbono, actúan como electrodos para llevar la electricidad al entorno celular. En este contexto, el grafeno está ganando interés debido a sus propiedades de alta conductividad y biocompatibilidad.

El grafeno es una forma de carbono puro dispuesto en una sola capa de átomos, colocados en una estructura hexagonal bidimensional, como se muestra en la Figura 1. Es conocido por su excelente conductividad eléctrica la cual lo hace ideal para aplicaciones en dispositivos electrónicos y bioelectrónicos, así como en electroquímica y electroestimulación celular. Además, el grafeno tiene una superficie grande en relación con su volumen, lo que le confiere una gran área superficial. Esto es beneficioso para la adsorción de moléculas y la interacción con células en aplicaciones biomédicas. También, el grafeno es muy resistente y flexible, lo que lo hace adecuado para aplicaciones en dispositivos implantables que requieren materiales duraderos y de baja densidad[4][9].

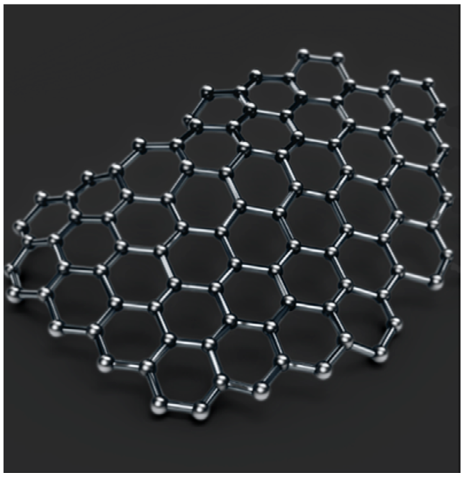

FIGURA 1. **Lámina de grafeno simulada.**

El óxido de grafeno (OG) es un derivado del grafeno que se produce mediante oxidación controlada. Este proceso introduce grupos funcionales en la estructura del grafeno, como grupos hidroxilo y epóxido. Estos grupos funcionales hacen que el OG sea más soluble en agua y más compatible con sistemas biológicos que el grafeno puro, lo que lo hace útil en aplicaciones biológicas y biomédicas. También conserva algunas propiedades del grafeno, como su alta área superficial y estructura bidimensional, pero puede exhibir propiedades adicionales debido a los grupos funcionales[7].

Existen diferentes métodos de obtención para el grafeno y el óxido de grafeno. Algunos de los más comunes para la obtención de grafeno incluyen la exfoliación mecánica, la deposición química de vapor (CVD por sus siglas en inglés) y la reducción química de óxido de grafeno. La exfoliación mecánica es un método simple que produce grafeno de alta calidad, aunque es laborioso y de baja escalabilidad. La CVD permite la producción a gran escala con control preciso sobre la calidad, pero requiere equipos especializados y puede ser costoso. La reducción química de óxido de grafeno es versátil y rentable, pero la calidad del grafeno puede variar según las condiciones de reducción[10][11][12][13].

En cuanto al óxido de grafeno, el método de Hummers es ampliamente utilizado debido a su simplicidad y alta eficiencia en la oxidación del grafito. Sin embargo, utiliza reactivos peligrosos y produce subproductos tóxicos. Los métodos de oxidación química alternativos ofrecen más versatilidad y control, pero pueden requerir condiciones específicas y pueden ser menos eficientes. Por otro lado, los métodos electroquímicos son más respetuosos con el medio ambiente, pero pueden necesitar equipos especializados y tener una eficiencia ligeramente menor[11][14].

En el campo de la medicina regenerativa y la ingeniería de tejidos, el grafeno y el OG encuentra diversas aplicaciones debido a sus propiedades y su capacidad para interactuar con sistemas biológicos. Algunos ejemplos de estas aplicaciones son la fabricación de andamios que pueden promover el crecimiento celular y la diferenciación, dispositivos de liberación de fármacos y biosensores, entre otros[15][16][17].

La aplicación del grafeno en la electroestimulación celular se ha convertido en un campo de investigación prometedor en la medicina regenerativa y la ingeniería de tejidos. Este material de carbono tiene características particulares que lo hacen adecuado para mejorar las terapias de regeneración tisular. Gracias a su excelente conductividad eléctrica y su capacidad para transmitir señales eléctricas a las células, el grafeno proporciona un entorno favorable para la electroestimulación celular[7][9]. En términos de capacidad de carga eléctrica, el grafeno puede manejar densidades de corriente extremadamente altas, llegando hasta 106 $\Omega^{-1}\cdot m^{-1}$, lo cual es significativamente superior a los metales tradicionales como el cobre y la plata[18]. El grafeno ha demostrado capacidades específicas de almacenamiento de carga del orden de 200-300 F/g cuando se utiliza en supercondensadores, lo que varía dependiendo de las condiciones experimentales y la forma específica del grafeno utilizado. También presenta una alta resistencia al daño por electro-migración, haciéndolo ideal para aplicaciones que requieren alta durabilidad bajo condiciones de alta corriente[10][14][19].

El comportamiento del grafeno como conductor eléctrico se basa en su estructura cristalina altamente ordenada, que permite un transporte eficiente de electrones a través de la red de carbono. Cuando se aplica un potencial eléctrico al grafeno, los electrones pueden moverse con facilidad a lo largo de su superficie, generando una corriente eléctrica que puede influir en el comportamiento de las células adyacentes[12].

Además, el grafeno también exhibe propiedades electroquímicas interesantes. Por ejemplo, su estructura de capa única confiere una gran área superficial y una alta densidad de estados electrónicos, lo que facilita la interacción con especies químicas en su entorno. Esta capacidad para adsorber y desorber moléculas orgánicas e inorgánicas le otorga al grafeno un potencial único para influir en procesos electroquímicos celulares[20].

El grafeno actúa como un sustrato conductor que puede transmitir eficientemente los pulsos eléctricos a las células circundantes. Este proceso electroquímico puede desencadenar una serie de respuestas celulares, incluida la migración, proliferación y diferenciación celular, que son fundamentales para la regeneración tisular[8].

En este artículo, exploraremos en detalle el desempeño de la electroquímica en la electroestimulación celular y cómo el uso de materiales avanzados, como el grafeno, está impulsando aún más el campo hacia nuevas fronteras de investigación y aplicación clínica.

MATERIALES Y MÉTODOS

Se llevó a cabo una revisión de la literatura científica para recopilar información relevante sobre el uso del grafeno y el óxido de grafeno en la electroestimulación celular y sus aplicaciones. Se consultaron bases de datos como ScienceDirect, American Chemical Society, SpringerLink y Google Scholar utilizando una combinación de palabras clave que incluyeron *'cellular electrostimulation'*, *'graphene'*, *'graphene oxide'*, *'carbon nanomaterials'*, *'tissue engineering'*, *'neural stimulation'*, *'deep brain stimulation'* y *'electrochemistry'*. Los artículos seleccionados para esta revisión fueron publicados a partir del año 2019, excluyendo libros de texto y artículos utilizados para sustentar fundamentos y definiciones. Se examinó el título, resumen, resultados y conclusiones de las publicaciones y se seleccionaron de acuerdo al siguiente criterio: 1) La investigación debe abordar el uso del grafeno y/o el óxido de grafeno en la electroestimulación celular; 2) Los estudios deben presentar avances significativos en el desarrollo o aplicación de materiales conductores en electroestimulación celular; 3) Se requiere que los artículos incluyan información relevante sobre los aspectos electroquímicos de la interacción electrodo-célula y sus efectos en la actividad celular. Estos artículos seleccionados proporcionaron evidencia directa para respaldar los conceptos fundamentales relacionados con la electroestimulación celular y el uso del grafeno en aplicaciones biomédicas.

RESULTADOS Y DISCUSIÓN

La electroestimulación celular es una técnica que implica la aplicación de corrientes eléctricas para modular la actividad celular y promover procesos regenerativos en tejidos y órganos. Este proceso induce cambios en las células al alterar su potencial de membrana y activar canales iónicos y otras proteínas sensibles al voltaje, lo que puede llevar a la permeabilización de la membrana celular y al flujo de diferentes iones a través de ella. Estos cambios iónicos resultan en la estimulación de diversos procesos celulares, como la activación de genes, la producción y liberación de factores de crecimiento y transcripción, así como la interacción entre células y la adhesión celular[1][2]. En este contexto, los aspectos electroquímicos desempeñan un papel crucial en la comprensión y optimización de la respuesta celular a los estímulos eléctricos.

La interfaz entre el electrodo y la célula es un punto crítico en la transmisión de señales eléctricas y la respuesta celular. En esta interfaz, se producen reacciones electroquímicas que pueden afectar la viabilidad y la funcionalidad celular. La elección del material del electrodo y su composición superficial es muy importante en la estabilidad electroquímica y la compatibilidad celular. Durante la aplicación de corrientes eléctricas, se produce la transferencia de cargas entre el electrodo y el electrolito celular. Esta transferencia de cargas puede generar especies electroactivas, como radicales libres y productos de oxidación, que pueden influir en la fisiología celular y desencadenar respuestas biológicas específicas. La electroestimulación celular conlleva cambios en el potencial de membrana y la permeabilidad iónica de las células, lo que afecta la dinámica de iones como el calcio, el sodio y el potasio. Estos cambios iónicos son mediados por canales iónicos y transportadores de membrana, los cuales son muy importantes en la excitabilidad celular y la transducción de señales. La aplicación de campos eléctricos intensos puede inducir la formación de poros en la membrana celular, un fenómeno conocido como electroporación. Esta alteración temporal de la permeabilidad de la membrana celular permite la entrada de moléculas y biomarcadores extracelulares, lo que puede ser aprovechado en aplicaciones de entrega de fármacos y terapia génica[5][21][22].

Aplicaciones clínicas del grafeno en electroestimulación celular

Las aplicaciones clínicas de la electroestimulación celular con grafeno son variadas y abarcan una amplia gama de áreas médicas. El grafeno se emplea como parte de materiales compuestos o recubrimientos junto con otros materiales, como polímeros, metales o cerámicos, para mejorar sus propiedades mecánicas, eléctricas o biocompatibles. La combinación del grafeno con otros materiales puede ofrecer beneficios adicionales, como mayor resistencia o durabilidad, lo que lo hace más adecuado para su uso en dispositivos biomédicos[23]. Estas aplicaciones están respaldadas por una creciente cantidad de investigaciones que demuestran la eficacia y seguridad de esta técnica en diferentes contextos clínicos.

En el campo de la rehabilitación musculoesquelética, la electroestimulación celular se utiliza para promover la regeneración de tejidos como el hueso y el cartílago, acelerar la recuperación de lesiones deportivas y mejorar la función muscular en pacientes con condiciones crónicas o lesiones traumáticas. Los dispositivos de electroestimulación celular, basados en grafeno, ofrecen una herramienta terapéutica de bajo riesgo para mejorar la calidad de vida de los pacientes con trastornos musculoesqueléticos[9][24][25].

Los andamios de grafeno proporcionan un soporte estructural para el crecimiento celular, permitiendo al mismo tiempo la transmisión de estímulos eléctricos para promover la diferenciación celular hacia el linaje osteogénico. Estudios han demostrado que el grafeno mejora la conductividad eléctrica del andamio, lo que resulta en una mejor respuesta celular y una mayor producción de matriz extracelular. En la Tabla 1 se presentan algunos de estos estudios.

Además, el grafeno puede ser utilizado en la estimulación eléctrica de células nerviosas para tratar lesiones de la médula espinal y los nervios periféricos. Los electrodos de grafeno implantables ofrecen una interfaz biocompatible para la estimulación eléctrica de las células nerviosas. La alta conductividad eléctrica del grafeno mejora la eficacia de estos electrodos y promueve la regeneración de las conexiones neuronales en el sistema nervioso central y periférico[31][32].

TABLA 1. **Investigaciones sobre la aplicación del grafeno en electroestimulación celular en ingeniería de tejidos.**

Autor	Trabajo realizado	Objetivo	Resultados obtenidos
(Wang *et al.*, 2019)[26]	Se evaluaron andamios de poli(ε-caprolactona) (PCL)/grafenos impresos en 3D	Para uso potencial en la mejora de proliferación celular.	Los resultados de pruebas *in vivo* con ratas mostraron que los andamios indujeron una respuesta inmunológica aceptable y promovieron la formación de nuevo tejido y la remodelación ósea cuando se aplicó estimulación eléctrica.
(Li *et al.*, 2020)[27]	Presentaron un dispositivo que utiliza un andamio de grafeno-celulosa para aplicar estimulación eléctrica.	Favorecer la diferenciación celular de células madre adiposas humanas.	Después de 28 días se encontró que la viabilidad celular es alta y que no hay signos visibles de degradación del andamio.
(Dong *et al.*, 2020)[28]	Probaron un andamio fibroso conductor a base de grafeno (GCFS) y estimulación eléctrica (ES).	Reparar lesiones en nervios periféricos.	La ES aceleró la migración de células madre mesenquimales y promovió la secreción de factores neurotróficos in vitro. Además, en estudios *in vivo* en ratas, se observó que la ES mejoró significativamente la regeneración del nervio ciático y la recuperación funcional.
(Zheng *et al.*, 2020)[29]	El estudio desarrolló un hidrogel compuesto por quitosano/oxietilcelulosa hidroxilada (CS/OHEC), liposomas de asiaticósido y óxido de grafeno reducido (rGO).	Mejorar la regeneración de nervios periféricos.	Se demostró que el hidrogel era no tóxico y promovía la adhesión y proliferación de células nerviosas *in vitro*. Además, la ES después de la adición de rGO favoreció la diferenciación y proliferación de células nerviosas.
(Kamalov *et al.*, 2022)[30]	Obtuvieron un composite eléctricamente conductor basado en poliimida termoplástica y grafeno, el cual fue utilizado como bioelectrodo.	Para la estimulación eléctrica de fibroblastos dérmicos humanos.	Se demostró que las películas compuestas tienen buena biocompatibilidad y no son tóxicas para las células de fibroblastos. Además, se observó que la ES preliminar aumenta la actividad proliferativa de las células.

En el ámbito de la neurología, existe una práctica llamada estimulación cerebral profunda (DBS, por sus siglas en inglés), la cual es un procedimiento neurológico en el que se implantan electrodos en áreas específicas del cerebro para modular la actividad neuronal. Estos electrodos están conectados a un dispositivo generador de impulsos, similar a un marcapasos, que se implanta bajo la piel en el pecho o el abdomen. Este dispositivo genera pulsos eléctricos suaves que estimulan las regiones cerebrales específicas, ayudando a controlar los síntomas de ciertos trastornos neurológicos[33]. La electroestimulación celular se investiga como una estrategia terapéutica para el tratamiento de enfermedades neurodegenerativas como el Parkinson[34], el Alzheimer[35], la distonía[36] y la esclerosis lateral amiotrófica (ELA)[33][37].

La DBS se ha convertido en una opción importante en el tratamiento de la enfermedad de Parkinson, especialmente en pacientes cuyos síntomas no responden adecuadamente a la medicación. En el Parkinson, los electrodos se suelen implantar en áreas del cerebro como el núcleo subtalámico (STN) o el globo pálido interno (GPi). La estimulación de estas áreas ayuda a reducir los síntomas motores, como temblores, rigidez y bradicinesia (lentitud de movimiento). La DBS no cura el Parkinson, pero puede mejorar significativamente la calidad de vida de los pacientes al reducir los síntomas y permitir una menor dependencia de la medicación[33][38][39][40].

El uso de DBS en el tratamiento del Alzheimer está en etapas más experimentales en comparación con su aplicación en Parkinson. Investigaciones recientes han explorado la posibilidad de que la estimulación de ciertas áreas del cerebro, como el fornix, pueda mejorar la memoria y la función cognitiva en pacientes con Alzheimer. Aunque los resultados iniciales son prometedores, se necesita más investigación para establecer la eficacia y seguridad de DBS en el tratamiento del Alzheimer[33]. El grafeno está siendo utilizado como material en electrodos neuronales debido a sus características. Su estructura delgada y flexible se adapta bien a las estructuras neuronales del cerebro sin dañarlas, mientras que su alta conductividad eléctrica permite la transmisión eficiente de señales eléctricas entre los electrodos y las neuronas, facilitando una estimulación precisa y controlada del tejido cerebral[41]. Además, su biocompatibilidad garantiza que pueda integrarse de manera segura en el cerebro sin desencadenar reacciones adversas en los tejidos circundantes[13] lo que convierte en un material idóneo para el desarrollo de dispositivos de estimulación cerebral profunda y terapias de neuromodulación[9][35][42][43]. En la Tabla 2 se presentan algunas investigaciones realizadas en este ámbito.

TABLA 2. **Investigaciones sobre la aplicación del grafeno en electroestimulación celular en ingeniería de tejidos.**

Autor	Trabajo realizado	Objetivo	Resultados obtenidos
(Fu *et al.*, 2019)[9]	Se preparó una membrana compuesta conductora de poli(L-ácido lácti-coglicólico) (PLGA)/GO combinados con estimulación eléctrica (ES).	Para reparación de células madre neurales (NSCs).	Se obtuvo que la membrana tenía buena hidrofilicidad, resistencia mecánica y adsorción de proteínas. También promovió significativamente la proliferación de NSC y la diferenciación neuronal en la superficie del material, así como una elongación significativa de las neuritas.
(Lee *et al.*, 2019)[20]	Se construyeron composites híbridos de poli(3,4-etilendioxitiofeno):poli(estireno sulfonato) (PEDOT:PSS)/óxidos de grafeno (GO).	Como material para electrodos implantables.	Estos composites mostraron mejoras significativas en el desempeño electroquímico y la suavidad mecánica. Además, se observaron expresiones proteicas favorables en células neuronales.
(Dybowska-Sarapuk *et al.*, 2022)[44]	Crearon una tinta de nanopartículas de grafeno (GNPs). Luego, se utilizó corriente alterna sinusoidal para electroestimular las células.	Para aplicar recubrimientos de nanopartículas de grafeno (GNPs) en las células madre neuronales.	Se observó que una amplitud de voltaje de estimulación más baja (5V) tuvo el efecto más favorable en el recuento de células madre.
(Maughan *et al.*, 2022)[45]	Desarrollaron un material compuesto con un 60 % en peso de grafeno prístino (pG) y colágeno tipo I.	Para mejorar la estimulación eléctrica eficiente.	Demostraron que el material compuesto promueve el crecimiento robusto de neuronas y células gliales, mejora el crecimiento de neuritas y la viabilidad celular bajo estimulación eléctrica.
(Mendes *et al.*, 2023)[46]	Crearon hidrogeles combinación de gelatina metacrilatada (GelMA) y óxido de grafeno (GO).	Para ingeniería de tejido neural usando la línea celular de feocromocitoma de rata, PC12s.	Se observó que las células proliferaron más en presencia de corrientes eléctricas más altas, y la adición de grafeno al hidrogel mejoró la actividad celular.
(Viana *et al.*, 2024)[47]	Desarrollaron una película delgada de grafeno nanoporoso para su aplicación en la fabricación de interfaces neurales flexibles.	Dicha película permite la creación de microelectrodos pequeños (diámetro de 25 μm)	Obtuvieron microelectrodos con características óptimas para la comunicación eléctrica con tejido neural, grabaciones cerebrales de alta fidelidad en roedores y estimulación neural eficaz con alta selectividad. Además, demostraron que estos dispositivos son biocompatibles con el tejido durante periodos de implantación prolongados.

Además de estas aplicaciones clínicas establecidas, existe un amplio potencial futuro para la electroestimulación celular en áreas emergentes de la medicina regenerativa y la terapia celular. La combinación de grafeno en dispositivos implantables y sistemas de administración de fármacos podría revolucionar el tratamiento de enfermedades crónicas y lesiones agudas al proporcionar terapias específicas y personalizadas que maximicen la eficacia terapéutica y minimicen los efectos adversos[48][49].

CONCLUSIONES

En conclusión, el presente estudio destaca el potencial innovador de la electroestimulación celular utilizando grafeno en una variedad de aplicaciones biomédicas, desde la regeneración tisular hasta el tratamiento de enfermedades neurológicas. A través de una comprensión más profunda de los aspectos electroquímicos y de las interfaces celulares, se ha demostrado que el grafeno y sus derivados pueden desempeñar un papel crucial en la mejora de la eficacia terapéutica y la calidad de vida de los pacientes. Además, el desarrollo de nuevos materiales compuestos y tecnologías de fabricación ofrece nuevas perspectivas para el futuro de la medicina regenerativa y la ingeniería de tejidos. En conjunto, estos avances prometen abrir nuevas fronteras en la investigación biomédica y el tratamiento de enfermedades, ofreciendo soluciones más efectivas y personalizadas para las necesidades clínicas actuales.

CONFLICTO DE INTERÉS

Declaramos que no existe ningún conflicto de intereses en relación con este artículo. No hemos recibido financiamiento ni hemos participado en ninguna organización o entidad con un interés financiero o personal que pueda influir en el trabajo presentado en este artículo.

CONTRIBUCIÓN DE LOS AUTORES

G. P. V. V. Conceptualización, metodología, investigación, análisis formal, escritura del manuscrito original, revisión y edición de manuscrito. E. M. M. R. Conceptualización, metodología, investigación, validación, análisis formal, escritura de manuscrito original, revisión y edición de manuscrito, administración del proyecto y adquisición de fondos. M. G. H. Análisis formal, validación, revisión y edición de manuscrito. J. C. R. H. Análisis formal, validación, revisión y edición de manuscrito.

REFERENCIAS

[1] C. Chen, X. Bai, Y. Ding, I.-S. Lee, “Electrical stimulation as a novel tool for regulating cell behavior in tissue engineering,” Biomater. Res., vol. 23, 2019, art. no. 25, doi: **https://doi.org/10.1186/s40824-019-0176-8**

[2] R. Vaiciuleviciute, I. Uzieliene, P. Bernotas, V. Novickij, A. Alaburda, E. Bernotiene, “Electrical Stimulation in Cartilage Tissue Engineering,” Bioengineering, vol. 10, no. 4, 2023, art. no. 454, doi: **https://doi.org/10.3390/bioengineering10040454**

[3] A. Diamant, J. P. Reilly, Electrostimulation: theory, applications and computational model. Norwood, MA, Estados Unidos: Artech House, 2011.

[4] B. C. Thompson, E. Murray, G. G. Wallace, “Graphite Oxide to Graphene. Biomaterials to Bionics,” Adv. Mater., vol. 27, no. 46, pp. 7563-7582, 2015, doi: **https://doi.org/10.1002/adma.201500411**

[5] L. Leppik, K. M. C. Oliveira, M. B. Bhavsar, J. H. Barker, “Electrical stimulation in bone tissue engineering treatments,” Eur. J. Trauma Emerg. Surg., vol. 46, no. 2, pp. 231-244, 2020, doi: **https://doi.org/10.1007/s00068-020-01324-1**

[6] Z. Zhou, J. Zheng, X. Meng, F. Wang, “Effects of Electrical Stimulation on Articular Cartilage Regeneration with a Focus on Piezoelectric Biomaterials for Articular Cartilage Tissue Repair and Engineering,” Int. J. Mol. Sci., vol. 24, no. 3, 2023, art. no. 1836, doi: **https://doi.org/10.3390/ijms24031836**

[7] Z. Du, C. Wang, R. Zhang, X. Wang, X. Li, "Applications of Graphene and Its Derivatives in Bone Repair: Advantages for Promoting Bone Formation and Providing Real-Time Detection, Challenges and Future Prospects," Int. J. Nanomedicine, vol. 15, pp. 7523-7551, 2020, doi: https://doi.org/10.2147/ijn.s271917

[8] N. Jalilinejad, M. Rabiee, N. Baheiraei, R. Ghahremanzadeh, et al., "Electrically conductive carbon-based (bio)-nanomaterials for cardiac tissue engineering," Bioeng. Transl. Med., vol. 8, no. 1, 2023, art. no. e10347, doi: https://doi.org/10.1002/btm2.10347

[9] C. Fu, S. Pan, Y. Ma, W. Kong, Z. Qi, X. Yang, "Effect of electrical stimulation combined with graphene-oxide-based membranes on neural stem cell proliferation and differentiation," Artif. Cells Nanomed. Biotechnol., vol. 47, no. 1, pp. 1867-1876, 2019, doi: https://doi.org/10.1080/21691401.2019.1613422

[10] K. S. Novoselov, V. I. Fal'ko, L. Colombo, P. R. Gellert, M. G. Schwab, K. Kim, "A roadmap for graphene," Nature, vol. 490, no. 7419, pp. 192-200, 2012, doi: https://doi.org/10.1038/nature11458

[11] D. G. Papageorgiou, I. A. Kinloch, R. J. Young, "Mechanical properties of graphene and graphene-based nanocomposites," Prog. Mater. Sci., vol. 90, pp. 75-127, 2017, doi: https://doi.org/10.1016/j.pmatsci.2017.07.004

[12] A. Ambrosi, C. K. Chua, A. Bonanni, M. Pumera, "Electrochemistry of Graphene and Related Materials," Chem. Rev., vol. 114, no. 14, pp. 7150-7188, 2014, doi: https://doi.org/10.1021/cr500023c

[13] M.-H. Tran, I. Booth, A. Azarakhshi, P. Berrang, J. Wulff, A. G. Brolo, "Synthesis of Graphene and Graphene Films with Minimal Structural Defects," ACS Omega, vol. 8, no. 43, pp. 40387-40395, 2023, doi: https://doi.org/10.1021/acsomega.3c04788

[14] D. A. C. Brownson, C. E. Banks, The Handbook of Graphene Electrochemistry. London: Springer London, 2014. doi: https://doi.org/10.1007/978-1-4471-6428-9

[15] A. Raslan, L. Saenz del Burgo, J. Ciriza, J. L. Pedraz, "Graphene oxide and reduced graphene oxide-based scaffolds in regenerative medicine," Int. J. Pharm., vol. 580, 2020, art. no. 119226, doi: https://doi.org/10.1016/j.ijpharm.2020.119226

[16] M. Hoseini-Ghahfarokhi, S. Mirkiana, N. Mozaffari, M. A. Abdolahi Sadatu, et al., "Applications of Graphene and Graphene Oxide in Smart Drug/Gene Delivery: Is the World Still Flat?," Int. J. Nanomedicine, vol. 15, pp. 9469-9496, 2020, doi: https://doi.org/10.2147/ijn.s265876

[17] P. Zare, M. Aleemardani, A. Seifalian, Z. Bagher, A. M. Seifalian, "Graphene Oxide: Opportunities and Challenges in Biomedicine," Nanomaterials, vol. 11, no. 5, 2021, art. no. 1083, doi: https://doi.org/10.3390/nano11051083

[18] Y. Wu, K. A. Jenkins, A. Valdes-Garcia, D. B. Farmer, et al., "State-of-the-Art Graphene High-Frequency Electronics," Nano Lett., vol. 12, no. 6, pp. 3062-3067, 2012, doi: https://doi.org/10.1021/nl300904k

[19] J. Yang, A. A. Papaderakis, J. S. Keerthi, R. W. Adams, et al., "Measuring the Capacitance of Carbon in Ionic Liquids: From Graphite to Graphene," J. Phys. Chem. C Nanomater. Interfaces, vol. 128, no. 9, pp. 3674-3684, 2024, doi: https://doi.org/10.1021/acs.jpcc.3c08269

[20] S. Lee, T. Eom, M.-K. Kim, S.-G. Yang, B. S. Shim, "Durable soft neural micro-electrode coating by an electrochemical synthesis of PEDOT:PSS / graphene oxide composites," Electrochim. Acta, vol. 313, pp. 79-90, 2019, doi: https://doi.org/10.1016/j.electacta.2019.04.099

[21] X. Zhang, T. Wang, Z. Zhang, H. Liu, L. Li, et al., "Electrical stimulation system based on electroactive biomaterials for bone tissue engineering," Mater. Today, vol. 68, pp. 177-203, 2023, doi: https://doi.org/10.1016/j.mattod.2023.06.011

[22] A.-R. Siddiqui, J. N'Diaye, K. Martin, A. Baby, J. Dawlaty, V. Augustyn, J. Rodríguez-López, "Monitoring SEIRAS on a Graphitic Electrode for Surface-Sensitive Electrochemistry: Real-Time Electrografting," Anal. Chem., vol. 96, no. 6, pp. 2435-2444, 2024, doi: https://doi.org/10.1021/acs.analchem.3c04407

[23] H. Park, S. Zhang, A. Steinman, Z. Chen, H. Lee, "Graphene prevents neurostimulation-induced platinum dissolution in fractal microelectrodes," 2D Mater., vol. 6, no. 3, 2019, art. no. 035037, doi: https://doi.org/10.1088/2053-1583/ab2268

[24] V. Palmieri, F. Sciandra, M. Bozzi, M. De Spirito, M. Papi, "3D Graphene Scaffolds for Skeletal Muscle Regeneration: Future Perspectives," Front. Bioeng. Biotechnol., vol. 8, 2020, art. no. 383, doi: https://doi.org/10.3389/fbioe.2020.00383

[25] X. Xu, H. Zhang, Y. Yan, J. Wang, L. Guo, "Effects of electrical stimulation on skin surface," Acta Mech. Sin., vol. 37, no. 12, pp. 1843-1871, 2021, doi: https://doi.org/10.1007/s10409-020-01026-2

[26] W. Wang, J. R. Passarini Junior, P. R. Lopes Nalesso, D. Musson, et al., "Engineered 3D printed poly(ɛ-caprolactone)/graphene scaffolds for bone tissue engineering," Mater. Sci. Eng. C, vol. 100, pp. 759-770, 2019, doi: https://doi.org/10.1016/j.msec.2019.03.047

[27] J. Li, X. Liu, J. M. Crook, G. G. Wallace, "Electrical stimulation-induced osteogenesis of human adipose derived stem cells using a conductive graphene-cellulose scaffold," Mater. Sci. Eng. C, vol. 107, 2020, art. no. 110312, doi: https://doi.org/10.1016/j.msec.2019.110312

[28] C. Dong, F. Qiao, W. Hou, L. Yang, Y. Lv, "Graphene-based conductive fibrous scaffold boosts sciatic nerve regeneration and functional recovery upon electrical stimulation," Appl. Mater. Today, vol. 21, 2020, art. no. 100870, doi: https://doi.org/10.1016/j.apmt.2020.100870

[29] F. Zheng, R. Li, Q. He, K. Koral, et al., “The electrostimulation and scar inhibition effect of chitosan/oxidized hydroxyethyl cellulose/reduced graphene oxide/asiaticoside liposome based hydrogel on peripheral nerve regeneration in vitro,” Mater. Sci. Eng. C Mater. Biol. Appl., vol. 109, 2020, art. no. 110560, doi: https://doi.org/10.1016/j.msec.2019.110560

[30] A. Kamalov, M. Shishov, N. Smirnova, V. Kodolova-Chukhontseva, et al., “Influence of Electric Field on Proliferation Activity of Human Dermal Fibroblasts,” J. Funct. Biomater., vol. 13, no. 3, 2022, art. no. 89, doi: https://doi.org/10.3390/jfb13030089

[31] H. Bei, Y. Yang, Q. Zhang, Y. Tian, X. Luo, M. Yang, X. Zhao, “Graphene-Based Nanocomposites for Neural Tissue Engineering,” Molecules, vol. 24, no. 4, 2019, art. no. 658, doi: https://doi.org/10.3390/molecules24040658

[32] M. Aleemardani, P. Zare, A. Seifalian, Z. Bagher, A. M. Seifalian, “Graphene-Based Materials Prove to Be a Promising Candidate for Nerve Regeneration Following Peripheral Nerve Injury,” Biomedicines, vol. 10, no. 1, 2021, art. no. 73, doi: https://doi.org/10.3390/biomedicines10010073

[33] A. M. Lozano, N. Lipsman, H. Bergman, P. Brown, et al., “Deep brain stimulation: current challenges and future directions,” Nat. Rev. Neurol., vol. 15, no. 3, pp. 148-160, 2019, doi: https://doi.org/10.1038/s41582-018-0128-2

[34] T. Oz, A. K. Kaushik, M. Kujawska, “Advances in graphene-based nanoplatforms and their application in Parkinson’s disease,” Mater. Adv., vol. 4, no. 24, pp. 6464-6477, 2023, doi: https://doi.org/10.1039/D3MA00623A

[35] R. Fabbri, E. Saracino, E. Treossi, R. Zamboni, V. Palermo, V. Benfenati, “Graphene glial-interfaces: challenges and perspectives,” Nanoscale, vol. 13, no. 8, pp. 4390-4407, 2021, doi: https://doi.org/10.1039/D0NR07824G

[36] F. B. Rodrigues, G. S. Duarte, D. Prescott, J. Ferreira, J. Costa, “Deep brain stimulation for dystonia,” Cochrane Database Syst. Rev., no. 1, 2019, art. no. CD012405, doi: https://doi.org/10.1002/14651858.cd012405.pub2

[37] T. Ha, S. Park, M. Shin, J.-Y. Lee, J.-H. Choi, J.-W. Choi, “Biosensing system for drug evaluation of amyotrophic lateral sclerosis based on muscle bundle and nano-biohybrid hydrogel composed of multiple motor neuron spheroids and carbon nanotubes,” Chem. Eng. J., vol. 463, 2023, art. no. 142284, doi: https://doi.org/10.1016/j.cej.2023.142284

[38] P. Limousin, T. Foltynie, “Long-term outcomes of deep brain stimulation in Parkinson disease,” Nat. Rev. Neurol., vol. 15, no. 4, pp. 234-242, 2019, doi: https://doi.org/10.1038/s41582-019-0145-9

[39] G. Xiao, Y. Song, Y. Zhang, H. Zhao, et al., “Microelectrode Arrays Modified with Nanocomposites for Monitoring Dopamine and Spike Firings under Deep Brain Stimulation in Rat Models of Parkinson’s Disease,” ACS Sensors, vol. 4, no. 8, pp. 1992-2000, 2019, doi: https://doi.org/10.1021/acssensors.9b00182

[40] S. Zhao, G. Li, C. Tong, W. Chen, et al., “Full activation pattern mapping by simultaneous deep brain stimulation and fMRI with graphene fiber electrodes,” Nat. Commun., vol. 11, no. 1, 2020, art. no. 1788, doi: https://doi.org/10.1038/s41467-020-15570-9

[41] S. Nimbalkar, S. Sameji,a, V. Dang, T. Hunt, O. Nunez, C. Moritz, S. Kassegne, “Graphene on glassy carbon microelectrodes demonstrate long-term structural and functional stability in neurophysiological recording and stimulation,” J. Neural Eng., vol. 18, no. 5, 2021, art. no. 056035, doi: https://doi.org/10.1088/1741-2552/ac245a

[42] B. Xu, J. Pei, L. Feng, X.-D. Zhang, “Graphene and graphene-related materials as brain electrodes,” J. Mater. Chem. B, vol. 9, no. 46, pp. 9485-9496, 2021, doi: https://doi.org/10.1039/D1TB01795K

[43] R. Kumar, R. Rauti, D. Scaini, M. Antman-Passig, et al., “Graphene-Based Nanomaterials for Neuroengineering: Recent Advances and Future Prospective,” Adv. Funct. Mater., vol. 31, no. 46, 2021, art. no. 2104887, doi: https://doi.org/10.1002/adfm.202104887

[44] Ł. Dybowska-Sarapuk, W. Sosnowicz, A. Grzeczkowicz, J. Krzemiński, and M. Jakubowska, “Ultrasonication effects on graphene composites in neural cell cultures,” Front. Mol. Neurosci., vol. 15, 2022, art. no. 992494, doi: https://doi.org/10.3389/fnmol.2022.992494

[45] J. Maughan, P. J. Gouveia, J. Gutierrez Gonzalez, L. M. Leahy, et al., “Collagen/pristine graphene as an electroconductive interface material for neuronal medical device applications,” Appl. Mater. Today, vol. 29, 2022, art. no. 101629, doi: https://doi.org/10.1016/j.apmt.2022.101629

[46] A. X. Mendes, A. Teixeira do Nascimento, S. Duchi, A. F. Quigley, et al., “The impact of electrical stimulation protocols on neuronal cell survival and proliferation using cell-laden GelMA/graphene oxide hydrogels,” J. Mater. Chem. B, vol. 11, no. 3, pp. 581-593, 2023, doi: https://doi.org/10.1039/D2TB02387C

[47] D. Viana, S. T. Watson, E. Masvidal-Codina, X. Illa, et al., “Nanoporous graphene-based thin-film microelectrodes for in vivo high-resolution neural recording and stimulation,” Nat. Nanotechnol., no. 4, pp. 514-523, 2024, doi: https://doi.org/10.1038/s41565-023-01570-5

[48] L. Dybowska-Sarapuk, W. Sosnowicz, J. Krzeminski, A. Grzeczkowicz, L. H. Granicka, A. Kotela, M. Jakubowska, “Printed Graphene Layer as a Base for Cell Electrostimulation—Preliminary Results,” Int. J. Mol. Sci., vol. 21, no. 21, 2020, art. no. 7865, doi: https://doi.org/10.3390/ijms21217865

[49] A. F. Rodrigues, A. P. M. Tavares, S. Simões, R. P. F. F. Silva, et al., “Engineering graphene-based electrodes for optical neural stimulation,” Nanoscale, vol. 15, no. 2, pp. 687-706, 2023, doi: https://doi.org/10.1039/D2NR05256C

RESEARCH ARTICLE
VOL. 45 | NO. 2 | **MAY-AUGUST 2024** | PP 151 - 171

Revista Mexicana de Ingeniería Biomédica

dx.doi.org/10.17488/RMIB.45.2.9

E-LOCATION ID: **1418**

Optimizing infection trajectories: Innovation in Controllability of Nonlinear SIR Model

Omar Zakary[1], *Sara Bidah*[1], *Mostafa Rachik*[1]
[1] Hassan II university of Casablanca. Faculty of sciences Ben M'Sick. Casablanca - Morocco

ABSTRACT

Managing infections within populations poses significant challenges, particularly in achieving controllability over nonlinear models within epidemiological systems. In this study, the challenge is addressed by introducing a novel control function tailored to enhance the management of infections. The approach revolves around leveraging a nonlinear SIR epidemiological model, enabling the derivation of explicit solutions and fine-tuning of control parameters to align with predefined objectives. Specifically, the focus lies on guiding the number of infected individuals towards a predetermined threshold at a specified time for all initial values. Through rigorous numerical simulations, the effectiveness of the proposed control strategy in achieving greater controllability and regulating the spread of infection over time is depicted, For example, our simulations show that starting with an initial infected population of 150 individuals in a population of 25,150, the control strategy can reduce the number of infected individuals to below 40 within 30 days. The quantitative results presented underscore the efficacy of the approach, highlighting its potential to significantly impact disease management strategies.

KEYWORDS: controllability, control theory, infectious diseases, nonlinear models, SIR model

Corresponding author

TO: **Omar Zakary**
INSTITUTION: **Hassan II university of Casablanca, Faculty of sciences Ben M'Sick**
ADDRESS: **Bd Commandant Driss Al Harti, Casablanca 20670, Morocco**
EMAIL: **zakaryma@gmail.com**

Received:

9 February 2024

Accepted:

30 June 2024

INTRODUCTION

Controllability stands as a cornerstone concept within mathematical control theory, constituting a qualitative property essential for understanding dynamical control systems. At its core, controllability signifies the capacity to guide a dynamical system from any starting point to a specified end state utilizing admissible controls. However, it's worth noting the diverse range of definitions attributed to controllability in the literature. These definitions vary depending on the class of dynamical systems considered and the characteristics of the admissible controls involved [1][2].

Addressing controllability across different dynamical systems demands the application of various mathematical tools and theories. These encompass principles drawn from a variety of mathematical disciplines, such as functional analysis, matrix analysis, differential geometry, topology, ordinary and partial differential equations, and difference equations [3][4]. Despite the breadth of methods available, there remain numerous unresolved challenges in controllability analysis, particularly concerning nonlinear types of dynamical systems [1][5].

For instance, much of the existing literature on controllability has predominantly focused on unconstrained controls without delays in either the state variables or the controls themselves. This emphasis underscores the need for further exploration and development of controllability concepts tailored to address more intricate dynamical systems with constrained controls and temporal delays [6].

Nonlinear models play in epidemiology a vital role for comprehending the dynamics of disease transmission within populations. By translating biological principles and epidemiological data into mathematical equations, models can simulate the spread of diseases, predict future trends, and evaluate the potential impact of interventions [7][8][9][10]. Epidemiological models often incorporate factors such as transmission rates, population demographics, immunity levels, and behavioral patterns to capture the complexities of disease transmission. These models can help public health authorities develop effective strategies for disease control and prevention, such as vaccination campaigns, quarantine measures, and social distancing policies [11][12][13][14]. Additionally, mathematical modeling enables researchers to assess the effectiveness of various intervention strategies under different scenarios, providing valuable insights for decision-making in public health emergencies [11][13][14].

The SIR model, which stands for Susceptible-Infectious-Recovered, is a fundamental mathematical framework used in epidemiology to understand and forecast the dissemination of infectious diseases within populations. In this model, the individuals are classified into three compartments: (S) susceptible, (I) infectious, and (R) recovered. Susceptible persons (S) are those who are at risk of contracting the disease but have not been infected yet. Infectious individuals (I) are those who are presently infected and capable of transmitting the disease to susceptible individuals. Recovered individuals (R) are those who have recovered from the infection and gained immunity, thus they cannot be infected again and do not contribute to disease transmission [15][16][17][18].

The dynamics of the SIR model are governed by a system of ordinary differential equations (ODEs) that describe how the number of individuals in each compartment changes over time. These equations capture the flow of individuals between compartments based on the rates of infection and recovery. Specifically, susceptible individuals become infected at a rate proportional to the number of susceptible individuals and infectious individuals, while infectious individuals recover at a certain rate.

By solving these differential equations, the SIR model can provide insights into the dynamics of disease spread, such as the peak of the epidemic, the total number of infections, and the effectiveness of interventions such as vaccination or social distancing measures [18].

While the basic SIR model assumes certain simplifications and does not account for demographic factors like births and deaths, it remains a valuable tool for understanding the fundamental principles of infectious disease dynamics and informing public health decision-making. Here, we focus on diseases characterized by the SIR model, especially in situations with large populations or limited demographic data availability, which is described by the following set of equations (Equation 1, Equation 2, and Equation 3):

$$S'(t) = -\frac{\beta S(t)I(t)}{N} \tag{1}$$

$$I'(t) = \frac{\beta S(t)I(t)}{N} - gI(t) - u(t)I(t) \tag{2}$$

$$R'(t) = gI(t) + u(t)I(t) \tag{3}$$

Where β represents the transmission rate, denoting the speed at which susceptible individuals contract the infection upon exposure to infectious individuals, g is the recovery rate, denoting the rate at which infectious persons recover from the disease and become immune. u is the control variable representing the treatment or intervention applied to infectious individuals. N is the population size given by $N=S+I+R$ which is constant.

In many disease control strategies, the primary objective is to minimize the number of infected individuals over time, aiming for the long-term eradication of the disease. However, in certain scenarios, achieving this goal may take an extended period [11], rendering it insufficient for immediate containment. In our work, we address this challenge by focusing on the design of a control mechanism that not only aims to reduce the overall number of infections but also ensures that the number of infected individuals falls below a predetermined threshold within a specific desired time-frame. This approach is particularly crucial in situations where rapid containment is necessary to prevent further transmission and mitigate the impact of the disease outbreak.

MATERIALS AND METHODS

Proposal

The ability to exert control over complex systems, particularly nonlinear ones, holds paramount importance across various fields [2][6], with epidemiology being no exception [19]. Within the domain of epidemiological models, achieving controllability assumes a pivotal role, signifying the capability to effectively manage and manipulate the dynamics of infectious diseases within populations.

An essential aim of infectious disease epidemiology is to comprehend and measure the effort necessary to control or manage outbreaks effectively. This encompasses not only the identification of strategies to curb the spread of diseases but also the quantification of resources, interventions, and policies needed to achieve containment. Moreover, assessing the efficacy of these efforts plays a crucial role in informing public health decisions and policies aimed at minimizing the impact of infectious diseases on populations [19].

During disease outbreaks, authorities often implement a range of control measures, including quarantine, social distancing, and vaccination campaigns, for predefined durations to curtail the spread of the disease and mitigate its adverse effects on public health [19]. These measures' durations (days or months) are typically predetermined based on comprehensive epidemiological projections, modeling studies, and expert recommendations, ensuring a coordinated and efficient response to the outbreak. Additionally, institutions such as the World Health Organization (WHO) may establish thresholds for specific infectious diseases, considering factors like transmission characteristics, severity, and healthcare resource availability [20][21]. These thresholds serve as vital benchmarks for assessing the risk level of disease transmission within a population.

In this study, we investigate the concept of epidemiological controllability, focusing on the development of control strategies to steer the dynamics of infection within populations. Our objective is to design control mechanisms capable of guiding the number of infected individuals toward predetermined thresholds at specified times. This approach aims to enhance our ability to manage and contain infectious outbreaks effectively.

Then, we propose the following novel control law in Equation 4:

$$u(t) = \frac{\beta S_0}{N} e^{\frac{\beta I_0(1+a)}{a(\epsilon+g)N} \times ln\left(\frac{a+e^{t(\epsilon+g)}}{(1+a)e^{t(\epsilon+g)}}\right)} - g + \frac{(g+\epsilon)e^{(g+\epsilon)t}}{e^{(g+\epsilon)t}+a} \tag{4}$$

or, using the laws of exponents, we get the Equation 5:

$$u(t) = \frac{\beta S_0}{N}\left(\frac{a+e^{t(\epsilon+g)}}{(1+a)e^{t(\epsilon+g)}}\right)^{\frac{\beta I_0(1+a)}{a(\epsilon+g)N}} - g + \frac{(g+\epsilon)e^{(g+\epsilon)t}}{e^{(g+\epsilon)t}+a} \tag{5}$$

where S_0 denotes the initial number of susceptible individuals in the population at the onset of the control intervention, and N is the population size. The parameters a and ϵ, both positive constants, play pivotal roles in shaping the effectiveness of our control, with their specific values determined in accordance with the objectives of the control strategy. These constants are carefully selected to optimize the performance of the control mechanism and achieve the desired outcomes in disease containment and prevention.

This control law, tailored for the SIR model (1)-(3), aims at reducing the number of infected individuals over time and ensuring that the number of infections reaches the predefined threshold denoted I_d at a specified time denoted T. The control is designed to address various real-world scenarios and public health challenges, offering proactive measures to mitigate the impact of infectious diseases.

Sufficient condition for admissibility of the control

Theorem 1. If $ga - \frac{\beta S_0}{N} < \epsilon < 1 - \frac{\beta S_0}{N}$, then the proposed control (4) is admissible, i.e

$$\forall t > 0 : 0 < u(t) < 1$$

Proof. Recall that from (5) we have:

$$u(t) = \tfrac{\beta S_0}{N} u_1(t) - g + u_2(t),$$

where $u_1 = \left(\dfrac{a + e^{t(\epsilon+g)}}{(1+a)e^{t(\epsilon+g)}}\right)^{\frac{\beta I_0(1+a)}{a(\epsilon+g)N}}$ and

$u_2(t) = \dfrac{(g+\epsilon)e^{(g+\epsilon)t}}{e^{(g+\epsilon)t} + a}$. We have

$$u_1'(t) = -\frac{I_0\beta(ae^{-t(\epsilon+g)} + 1)^{\frac{I_0\beta(a+1)}{Na(\epsilon+g)}}(a+1)}{N(a + e^{t(\epsilon+g)})(a+1)^{\frac{I_0\beta(a+1)}{Na(\epsilon+g)}}} < 0$$

Then u_1 is a decreasing function, and since

$u_1(0) = 1$ and $\lim\limits_{t\to+\infty} u_1(t) = \left(\dfrac{1}{1+a}\right)^{\frac{\beta I_0(1+a)}{a(\epsilon+g)N}}$, it follows that

$$\forall t > 0: \left(\frac{1}{1+a}\right)^{\frac{\beta I_0(1+a)}{a(\epsilon+g)N}} < u_1(t) < 1$$

On the other hand, we have

$$u_2'(t) = \frac{ae^{t(\epsilon+g)}(\epsilon+g)^2}{(a + e^{t(\epsilon+g)})^2} > 0$$

Then, u_2 is an increasing function, and since $u_2(0) = \dfrac{g+\epsilon}{1+a}$ and $\lim\limits_{t\to+\infty} u_2(t) = g + \epsilon$, thus

$$\forall t > 0: \frac{g+\epsilon}{1+a} < u_2(t) < g + \epsilon.$$

Therefore,

$$\frac{\beta S_0}{N}\left(\frac{1}{1+a}\right)^{\frac{\beta I_0(1+a)}{a(\epsilon+g)N}} - g + \frac{g+\epsilon}{1+a} < u(t) < \frac{\beta S_0}{N} u_1(t) + \epsilon < \frac{\beta S_0}{N} + \epsilon < 1.$$

And for a reasonable population size $(N > \dfrac{\beta I_0(1+a)}{a(\epsilon+g)}$ we get $\dfrac{\beta I_0(1+a)}{a(\epsilon+g)N} < 1$ and since $\frac{1}{1+a} < 1,$ thus

$$\frac{1}{1+a} < \left(\frac{1}{1+a}\right)^{\frac{\beta I_0(1+a)}{a(\epsilon+g)N}}$$

then

$$\begin{aligned} u(t) &> \frac{\beta S_0}{N}\left(\frac{1}{1+a}\right) - g + \frac{g+\epsilon}{1+a} \\ &= \frac{\frac{\beta S_0}{N} + \epsilon - ga}{1+a} > 0 \end{aligned}$$

Remark 1. It's important to note that the conditions outlined in the preceding theorem are sufficient but not necessarily required. In certain scenarios, ϵ may not satisfy these conditions, yet the control remains admissible.

Explicit solutions of the epidemiological model

Theorem 2. If the proposed control (4) is used, then the solutions of the system (1)-(3) are:

$$S^*(t) = S_0 e^{\frac{\beta I_0(1+a)}{a(\epsilon+g)N} \times ln(\frac{a+e^{t(\epsilon+g)}}{(a+1)e^{t(\epsilon+g)}})}$$

and

$$I^*(t) = I_0 \frac{1+a}{e^{(g+\epsilon)t}+a},$$

and $\quad R^*(t) = N - S^*(t) - I^*(t)$

Proof. We have from equation (1):

$$\begin{aligned} S^{*'}(t) \quad &= S_0(\frac{\beta I_0(1+a)}{a(\epsilon+g)N} \times ln(\frac{a+e^{t(\epsilon+g)}}{(a+1)e^{t(\epsilon+g)}}))' e^{\frac{\beta I_0(1+a)}{a(\epsilon+g)N} \times ln(\frac{a+e^{t(\epsilon+g)}}{(a+1)e^{t(\epsilon+g)}})} \\ &= -S_0 \frac{\beta I_0(1+a)}{a(\epsilon+g)N} \times \frac{a(\epsilon+g)}{a+e^{t(\epsilon+g)}} e^{\frac{\beta I_0(1+a)}{a(\epsilon+g)N} \times ln(\frac{a+e^{t(\epsilon+g)}}{(a+1)e^{t(\epsilon+g)}})} \\ &= -S_0 \frac{\beta I_0(1+a)}{N} \times \frac{1}{a+e^{t(\epsilon+g)}} e^{\frac{\beta I_0(1+a)}{a(\epsilon+g)N} \times ln(\frac{a+e^{t(\epsilon+g)}}{(a+1)e^{t(\epsilon+g)}})} \\ &= -\frac{\beta}{N}(\frac{I_0(1+a)}{a+e^{t(\epsilon+g)}})(S_0 e^{\frac{\beta I_0(1+a)}{a(\epsilon+g)N} \times ln(\frac{a+e^{t(\epsilon+g)}}{(a+1)e^{t(\epsilon+g)}})}) \\ &= -\frac{\beta}{N} I^*(t) S^*(t) \end{aligned}$$

And from Equation (2) we have:

$$\begin{aligned} \frac{\beta S^*(t) I^*(t)}{N} - gI^*(t) - u(t)I^*(t) \quad &= \frac{\beta}{N}(\frac{I_0(1+a)}{a+e^{t(\epsilon+g)}})(S_0 e^{\frac{\beta I_0(1+a)}{a(\epsilon+g)N} \times ln(\frac{a+e^{t(\epsilon+g)}}{(a+1)e^{t(\epsilon+g)}})}) \\ &\quad -g\frac{I_0(1+a)}{a+e^{t(\epsilon+g)}} - (\frac{\beta S_0}{N} e^{\frac{\beta I_0(1+a)}{a(\epsilon+g)N} \times ln(\frac{a+e^{t(\epsilon+g)}}{(1+a)e^{t(\epsilon+g)}})} - g + \frac{(g+\epsilon)e^{(g+\epsilon)t}}{e^{(g+\epsilon)t}+a}) \frac{I_0(1+a)}{a+e^{t(\epsilon+g)}} \\ &= \frac{\beta S_0}{N} \frac{I_0(1+a)}{a+e^{t(\epsilon+g)}} e^{\frac{\beta I_0(1+a)}{a(\epsilon+g)N} \times ln(\frac{a+e^{t(\epsilon+g)}}{(a+1)e^{t(\epsilon+g)}})} \\ &\quad -\frac{\beta S_0}{N} e^{\frac{\beta I_0(1+a)}{a(\epsilon+g)N} \times ln(\frac{a+e^{t(\epsilon+g)}}{(1+a)e^{t(\epsilon+g)}})} \frac{I_0(1+a)}{a+e^{t(\epsilon+g)}} - \frac{(g+\epsilon)e^{(g+\epsilon)t}}{e^{(g+\epsilon)t}+a} \times \frac{I_0(1+a)}{a+e^{t(\epsilon+g)}} \\ &= -\frac{I_0(1+a)(g+\epsilon)e^{(g+\epsilon)t}}{(e^{(g+\epsilon)t}+a)^2} \\ &= I^{*'}(t) \end{aligned}$$

Which completes the proof.

Corollary 1. If the proposed control (4) is used, then the number of infected people tends towards zero.

Proof. Based on the result of theorem 2, we have $I^*(t) = I_0 \frac{1+a}{e^{(g+\epsilon)t}+a}$ which is a decreasing function of time and $\lim\limits_{t\to+\infty} I^*(t) = 0$

This result underscores the efficacy of the proposed control strategy, as it effectively drives the number of infected individuals towards zero. It demonstrates the effectiveness of implementing the control mechanism, particularly in its ability to initiate a decline in the number of infections from the outset of its application. Additionally, the theorem 2 provides explicit solutions for the model, which are essential for understanding the dynamics of the infection under the proposed control. Our control strategy includes parameters that significantly influence the speed of convergence to zero. These parameters allow us to adjust and optimize the control measures to achieve desired outcomes more effectively.

On the Controllability of the epidemiological model

Suppose there exists a predefined infection threshold I_d established by the World Health Organization (WHO), and the key objective of the control approach is to ensure that the number of infected persons falls below this threshold I_d at a predetermined time *T*. In accordance with this objective, the following theorem elucidates the critical role of parameter a in achieving this target:

Theorem 3. If the parameter a is chosen to be $a = \frac{I_d e^{(\epsilon+g)T} - I_0}{I_0 - I_d}$, then at time *T*, the number of infected individuals precisely attains the threshol I_d, i.e $I^*(T)=I_d$. Furthermore:

$$(\forall t > T): I^*(t) < I_d.$$

Proof. Let $a = \frac{I_d e^{(\epsilon+g)T} - I_0}{I_0 - I_d}$, then at time T we have

$$\begin{aligned} I^*(T) \qquad &= I_0 \frac{1 + \frac{I_d e^{(\epsilon+g)T} - I_0}{I_0 - I_d}}{e^{(g+\epsilon)T} + \frac{I_d e^{(\epsilon+g)T} - I_0}{I_0 - I_d}} \\ &= I_0 \frac{I_0 - I_d + I_d e^{(\epsilon+g)T} - I_0}{I_0 e^{(\epsilon+g)T} - I_d e^{(\epsilon+g)T} + I_d e^{(\epsilon+g)T} - I_0} \\ &= I_0 \frac{I_d (e^{(\epsilon+g)T} - 1)}{I_0 (e^{(\epsilon+g)T} - 1)} \\ &= I_d. \end{aligned}$$

And since I^* is a decreasing function, $(\forall t > T): I^*(t) < I_d$, which completes the proof.

RESULTS AND DISCUSSION

In this section, computational techniques are employed to evaluate the effectiveness and performance of the proposed control strategies within the SIR model, which is solved using the fourth-order Runge-Kutta method. Using numerical simulations, we explore various scenarios and parameters to assess the impact of the control mechanisms on disease dynamics. By simulating the spread of infectious diseases under different conditions, we aim to gain insights into the efficacy of the proposed strategies in containing outbreaks, reducing the number of infections, and achieving predefined control objectives.

In these simulations, our population consists of N=25150 individuals, with S_0=25000 initially susceptible, I_0=150 initially infected, and R_0=0 initially recovered individuals. The transmission rate is set to β=0.41 (Rate of new infections per day) and the recovery rate to g=0.005 (Rate of recoveries per day). All parameters chosen for these simulations are intended as academic examples. The primary goal in choosing these values was to depict a significant peak of infection, allowing a comprehensive comparison of outcomes with and without control measures.

Figure 1 depicts the progression of the epidemic within the population. We observe a peak in the number of infections, reaching approximately 2.4×10^4 individuals before gradually declining to around 1.5×10^4 by the end of the simulation. Concurrently, the number of susceptible individuals experiences a sharp decrease, approaching zero around t=30 in the simulation. Conversely, the number of recovered individuals exhibits a slow but steady increase, reaching approximately 10^4 by the simulation's conclusion.

The decline in infections coincides with a significant decrease in the number of susceptible individuals, indicating the depletion of the susceptible population due to infection.

After using the proposed control (4) with a=1.3522×10^3 and $\epsilon = 0.1$, it can be seen in figure 2b that despite ϵ not satisfying the conditions outlined in theorem (1), the control remains admissible, where $ag - \frac{\beta S_0}{N} = 6.3532 > \epsilon$, and $ag - \frac{\beta S_0}{N} = 6.3532 > 1 - \frac{\beta S_0}{N} = 0.5924$.

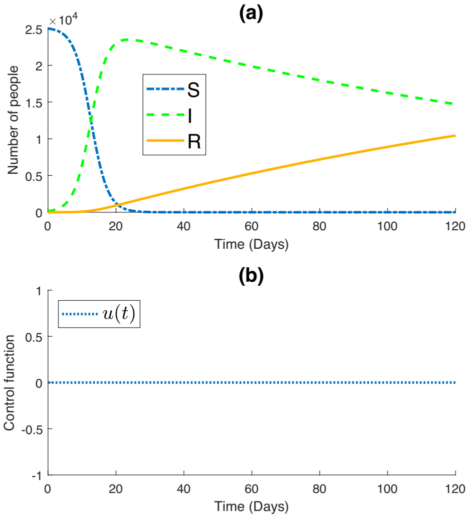

FIGURE 1. **(a) S, I and R functions. (b) The control function u.**

Figure 2a illustrates the impact of implementing the control law on epidemic dynamics. Notably, the control strategy effectively reduces the number of infected individuals compared to the scenario without control. A gradual and stable decline in the number of susceptible individuals is observed, converging to approximately 2×10^4 by the end of the simulation. This contrasts with the rapid decline observed in the absence of control measures.

Additionally, the number of removed individuals exhibits a slow but steady increase, reaching approximately 0.4×10^4 by the end of the simulation. This contrasts with the scenario without control, where a larger number of individuals are removed due to the uncontrolled spread of the disease.

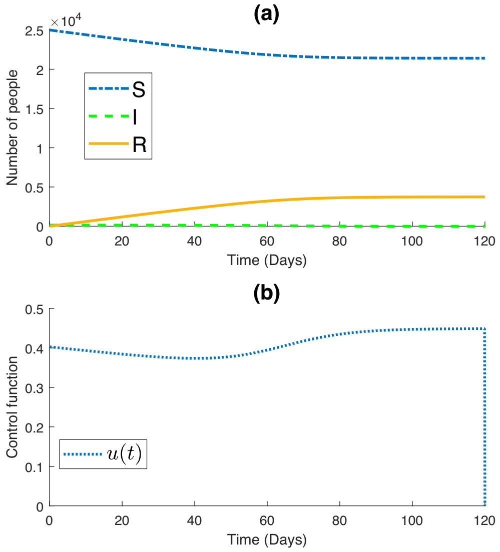

FIGURE 2. (a) S, I and R functions. (b) The control function u.

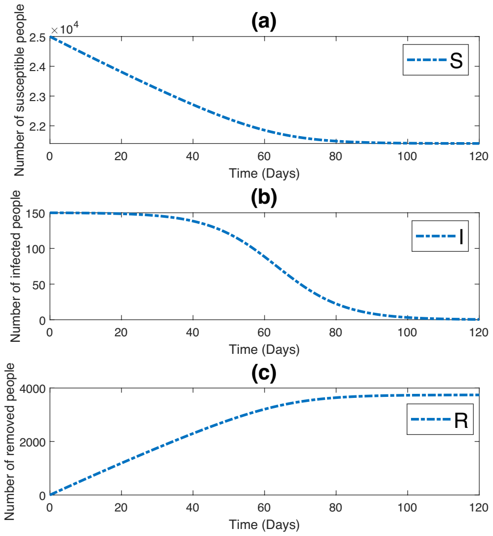

FIGURE 3. (a) Susceptible, (b) Infected, (c) Removed individuals.

In Figure 3, three subplots are presented, each providing insight into the dynamics of the epidemic. Figure 3a illustrates the evolution of the susceptible population, while figure 3b depicts the progression of the infected population. Figure 3c showcases the trend of the removed population over time. Figure 3 enables a clearer understanding of each population's dynamics on different scales. Specifically, smaller numbers, such as the initial infections starting at 150 and gradually declining towards zero, are more easily discernible.

In the Figure 4, the control function is plotted for different values of ϵ, in order to underscore the pivotal role of the parameter ϵ in shaping the behavior of the control function and highlights its significance in designing effective strategies to mitigate the impact of infectious diseases. It can be seen in figure 4 the effect of the parameter ϵ on the control function when a is held constant at 1. Each curve in the plot corresponds to a different value of ϵ, ranging from larger values to smaller ones. As ϵ changes, the control function undergoes noticeable changes in its shape and magnitude.

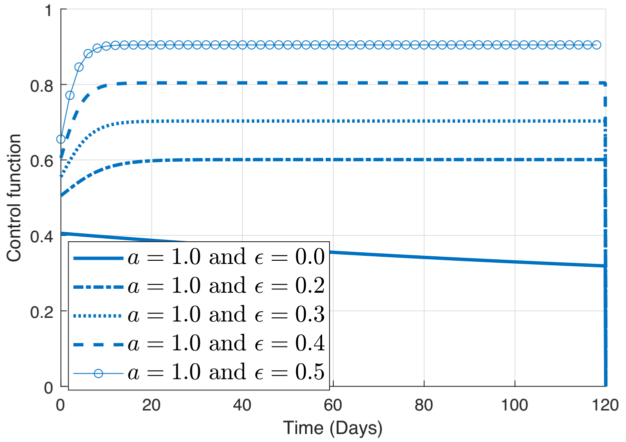

FIGURE 4. The impact of Parameter ϵ on the Control Function.

For larger values of ϵ, the control function exhibits relatively higher amplitude, indicative of a more aggressive intervention approach. However, as ϵ decreases, the amplitude of the control function diminishes, reflecting a milder intervention strategy. Notably, for very small values of ϵ, such as 0.001, the control function demonstrates a significant decrease, suggesting a minimal intervention effort.

The Figure 5 is presented to highlight the sensitivity of the control function to variations in the parameter a and emphasize the significance of meticulously selecting parameter values to optimize the effectiveness of intervention strategies in combating infectious diseases. Figure 5 presents the influence of the parameter a on the control function where ϵ is set to 0.2. Each curve in the plot corresponds to a different value of a, ranging from smaller to larger values. Notably, all curves exhibit the same shape, demonstrating that the general form of the control function remains consistent across varying values of a.

However, closer examination reveals notable differences in the behavior of the control function as a varies. For smaller values of a, such as 100 or 300, the control function demonstrates a rapid increase, indicating a swift implementation of intervention measures to curb the spread of infection. In contrast, for larger values of a, such as 600, 900, or 1500, there is a noticeable delay in the rate of increase of the control function. This delay suggests a slower response to the increasing number of infections, potentially leading to a longer duration before reaching peak intervention levels.

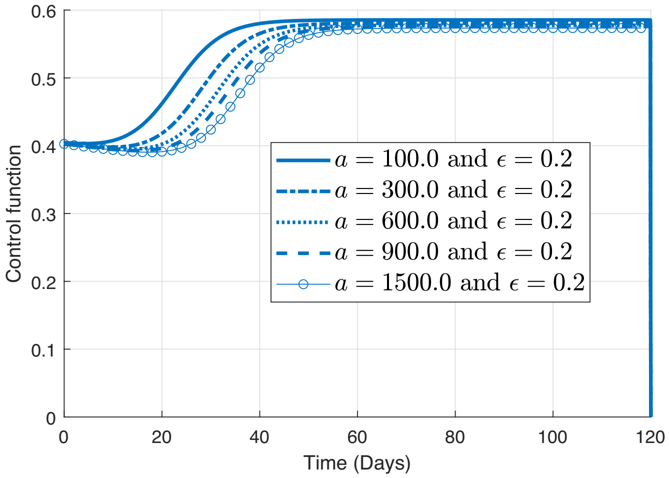

FIGURE 5. **The impact of a on the control function.**

When comparing the effects of ϵ and a on the control function, it becomes apparent that small variations in ϵ lead to significant changes in the control strategy. Even subtle adjustments in ϵ result in noticeable alterations in the shape and magnitude of the control function, highlighting the sensitivity of the intervention approach to this parameter. Conversely, when considering the parameter a, it becomes evident that larger differences between values are required to observe discernible changes in the control function. Unlike ϵ, where small values induce notable shifts in the control, variations in a necessitate much greater disparities to elicit observable differences in the behavior of the intervention strategy. This implies that the system exhibits lower sensitivity to the parameter a compared to ϵ, with substantial differences needed in a to produce discernible changes in the control function.

In the three subplots presented in Figure 6, the impact of varying the parameter ϵ on the different states of the model is observed: susceptible *(S)*, infected *(I)*, and removed *(R)* individuals.

In Figure 6a depicting the susceptibles, it can be seen that as ϵ decreases from 0.5 to 0.1, the rate of decrease in the number of susceptibles accelerates. While in Figure 6b that represents the infected population, we observe the opposite trend. As ϵ increases from 0.1 to 0.5, the rate of decrease in the number of infected individuals becomes more pronounced. This finding is consistent with the dynamics of infectious diseases, where higher values of ϵ indicate a faster recovery or removal of infected individuals from the population. Finally, in Figure 6c illustrating the removed individuals, we observe that all curves exhibit a similar increasing trend over time. However, for larger values of ϵ (0.5 and 0.4), the curve stabilizes around 300 individuals, indicating a slower accumulation of removed individuals. In contrast, for smaller values of ϵ (0.3, 0.2, and 0.1), the curve continues to rise steadily, eventually stabilizing at a higher value of around 950 individuals. This difference suggests that lower values of ϵ lead to a more prolonged period of recovery or removal, resulting in a higher overall number of removed individuals by the end of the simulation.

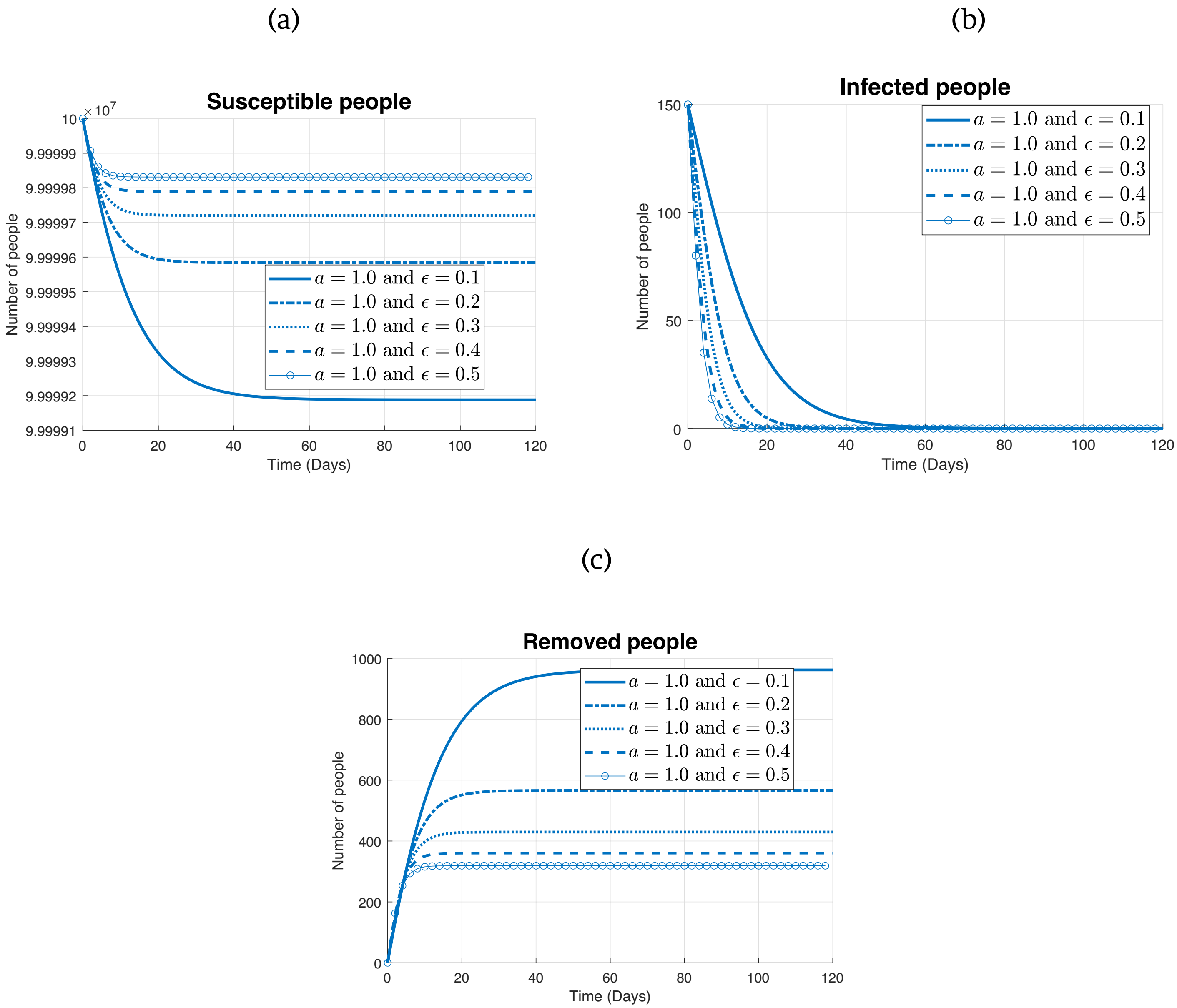

FIGURE 6. **The impact of ϵ on (a) Susceptible (b) Infected (c) Removed people.**

Figure 7 examines the impact of varying the parameter a on the different states of the model: susceptible *(S)*, infected *(I)*, and removed *(R)* individuals.

In Figure 7a illustrating the susceptibles, it can be seen that as the parameter a increases from 100 to 1500, the rate of decrease in the number of susceptibles accelerates.

While in Figure 7b representing the infected population, it noticed that regardless of the value of a, all curves exhibit a similar shape. However, as a increases, the rate of decrease in the number of infected individuals slows down. This finding suggests that while higher values of a may still effectively control the spread of the disease, they may lead to a longer duration of infection within the population.

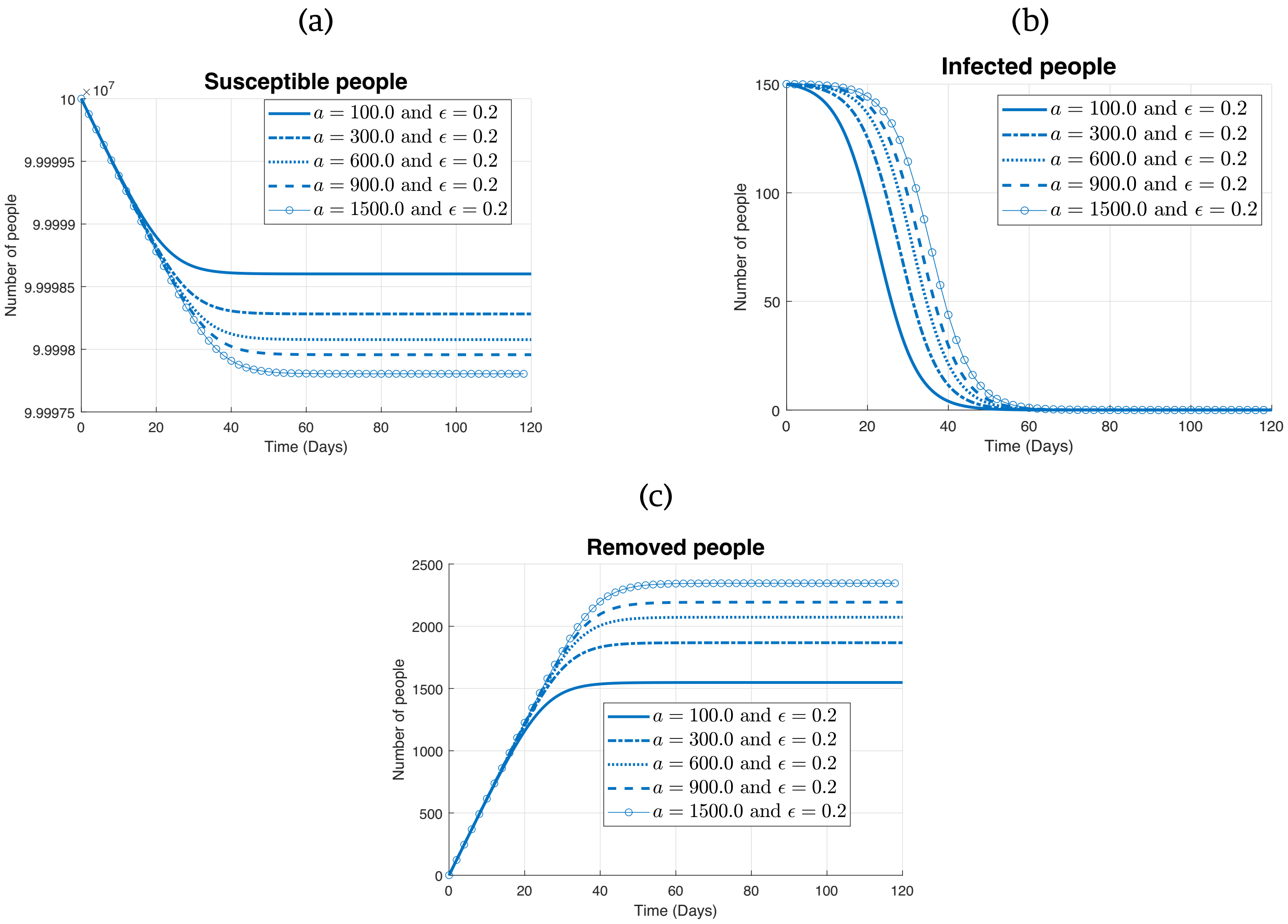

FIGURE 7. The impact of a on (a) Susceptible (b) Infected (c) Removed people.

Finally, in Figure 7c depicting the removed individuals, it can be seen that all curves follow a similar increasing trend over time. However, for smaller values of a (100 and 300), the curve stabilizes around 1600 individuals, indicating a slower accumulation of removed individuals. Conversely, for larger values of a (600, 900, and 1500), the curve continues to rise steadily, eventually stabilizing at a higher value of around 2300 individuals by the end of the simulation.

In Figure 8, the impact of different values of the parameter ϵ on the infection dynamics is explored, with a fixed threshold I_d=15 and predefined time T=40. Each curve represents the evolution of the infected population I over time, ranging from ϵ=0.1 to ϵ=0.5.

The key observation from this plot is the efficacy of the proposed control approach in containing the infection within the desired threshold. Across all curves, it can be seen that the number of infections falls below the threshold I_d=15 precisely at the predefined time T=40. This shows the precise controllability achieved by the proposed intervention, regardless of the specific value of ϵ.

However, we notice differences in the shapes of the decreasing curves for varying values of ϵ. For smaller values of ϵ, such as ϵ=0.1 and ϵ=0.2, the infection decreases rapidly. This rapid decline suggests that smaller perturbations in the control parameter ϵ lead to more pronounced effects on infection containment. In contrast, for larger values of ϵ, such as ϵ=0.4 and ϵ=0.5, the infection decreases at a slower rate. This slower decline indicates that larger values of ϵ result in less effective control measures, requiring more time to begin decreasing towards the predefined threshold.

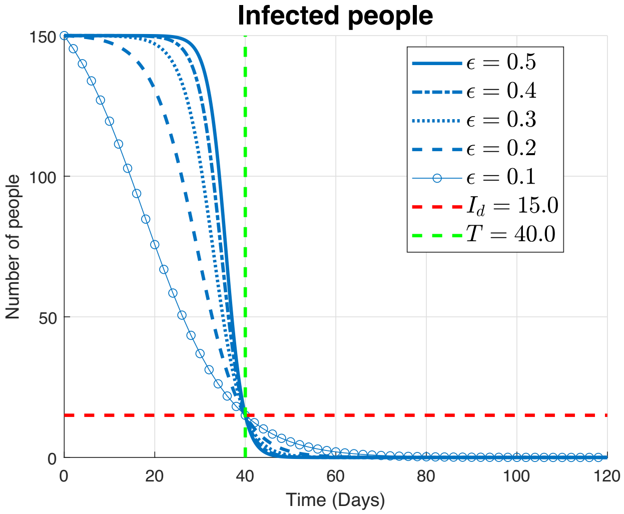

FIGURE 8. **The impact of ϵ on the controllability effectiveness.**

In Figure 9, six subplots are presented illustrating the infection dynamics *(I)* for various combinations of the threshold I_d and the predefined time *T*. Each subplot corresponds to a specific pair of values (I_d in individuals and *T* is time unit) : (a) I_d=15 and *T*=20, (b) *Id*=15 and *T*=30, (c) I_d=15 and *T*=60, (d) I_d=30 and *T*=40, (e) I_d=40 and *T*=40, and (f) I_d=50 and *T*=40.

Across all subplots, it can be seen that the number of infected individuals precisely reaches the desired threshold I_d exactly at the designated time *T*. This outcome underscores the remarkable effectiveness of our proposed control law in managing the rate of infection spread within the population.

In Figure 9a where I_d=15 and *T*=20, we observe the infection curve intersecting the threshold line at *T*=20, indicating successful containment of the infection within the desired time. Subsequent subplots (b) and (c) exhibit similar trends, with the infection curve intersecting the threshold line at the designated times *T*=30 and *T*= 60, respectively.

In Figure 9 (d), (e), and (f), scenarios with higher threshold values of I_d are explored, while maintaining *T*=40. Despite the varying threshold levels, it can be observed that the infection curve intersecting the threshold line at the predefined time T=40, highlighting the robustness of our control strategy across different infection severity levels.

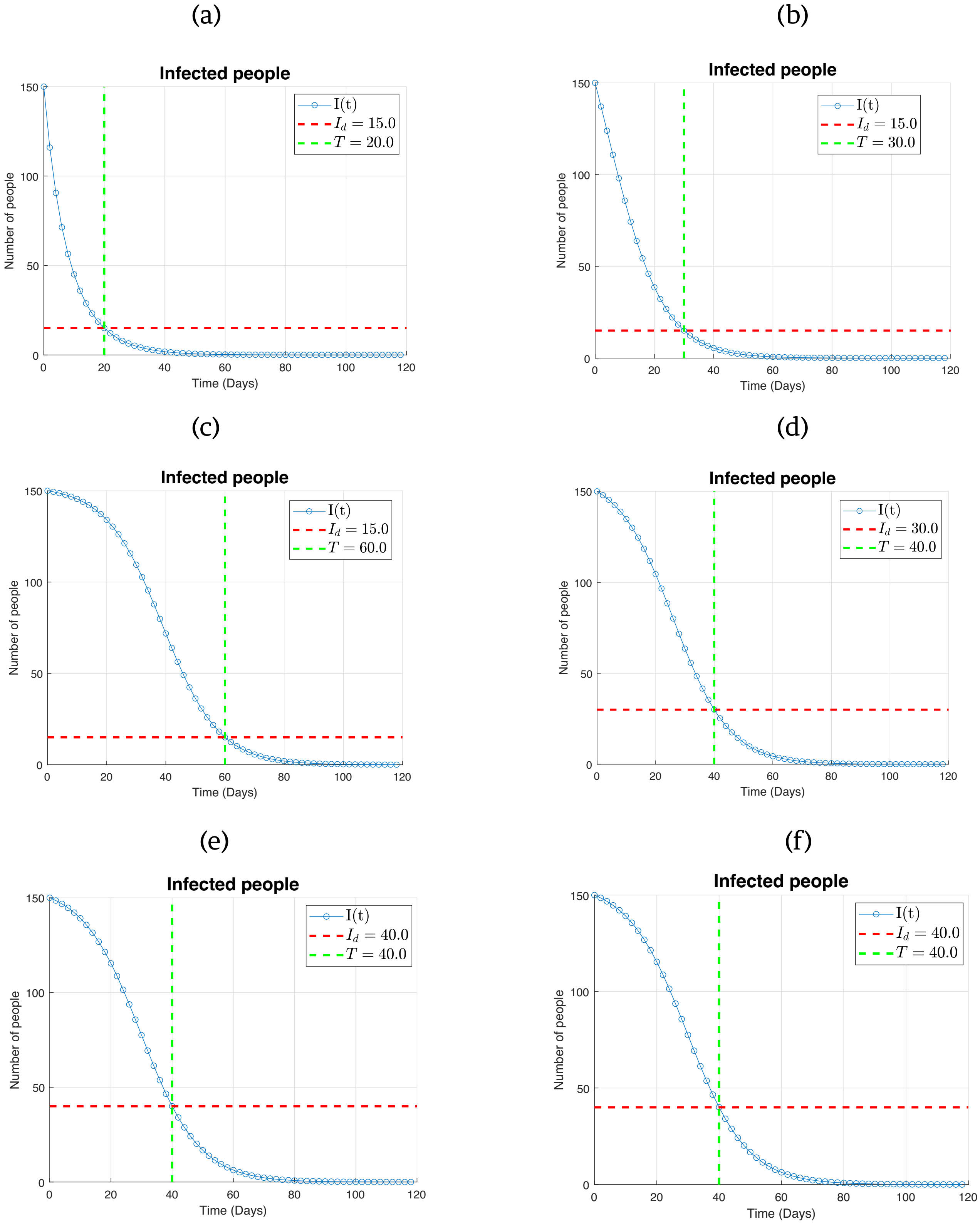

FIGURE 9. **The controllability effectiveness.**

Figure 10 explores the influence of varying initial infected populations (I_0) on the effectiveness of the controllability. Through three subplots representing the susceptible (a), infected (b), and removed (c) populations, we investigate the impact of different initial conditions on the trajectory of the epidemic, where I_d=40, T=40, S_0=10^8 and R_0=0

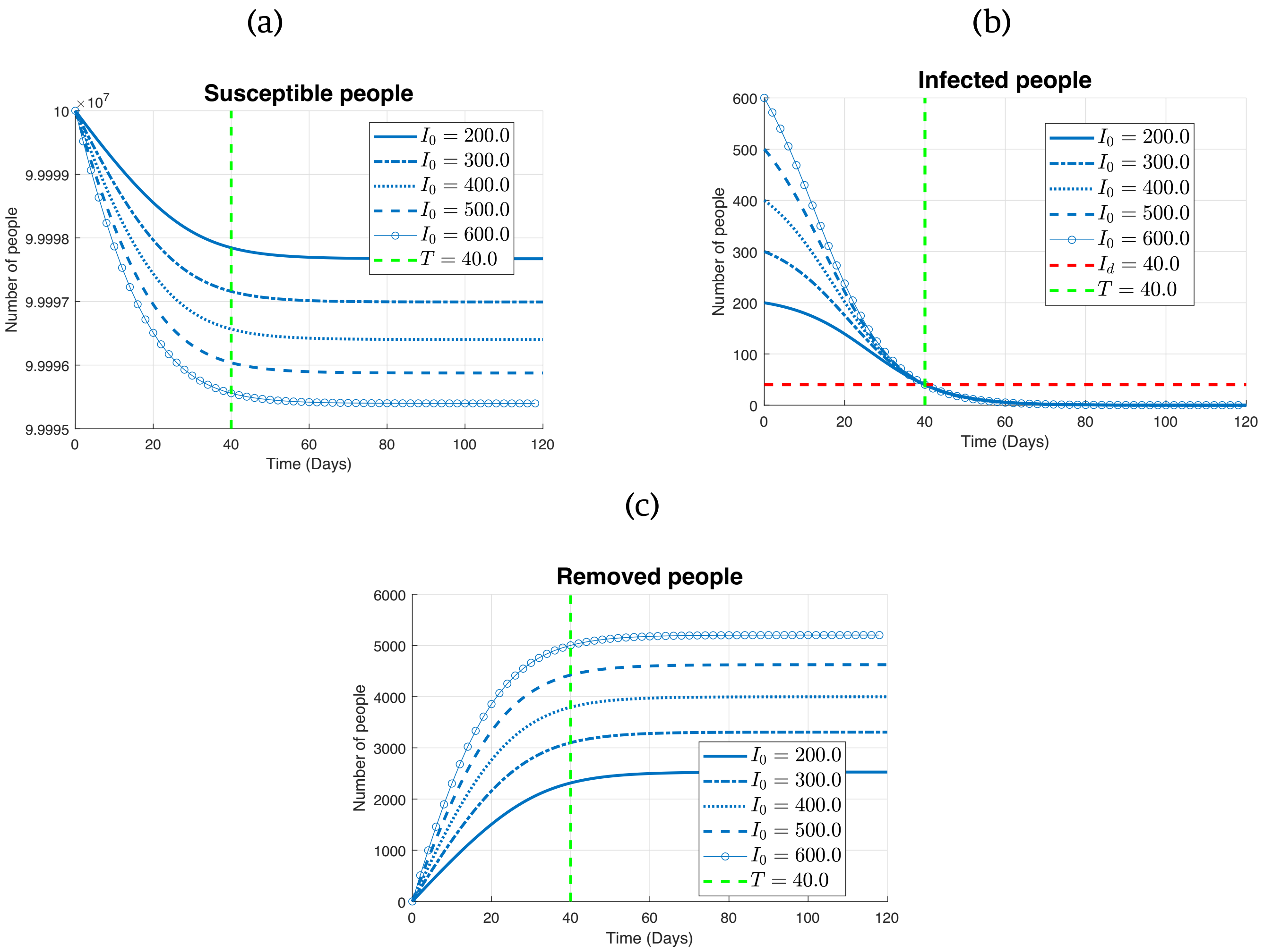

FIGURE 10. **The impact of I_0 on the controllability effectiveness (a) Susceptible individuals, (b) Infected individuals and (c) Removed individuals.**

Firstly, focusing on the infected population (Figure 10b), it can be observed that all curves intersect the predefined threshold line (I_d) at the designated time (T), indicating the successful implementation of the control strategy. This demonstrates the ability of the control measures to achieve the desired containment objective regardless of the initial outbreak size.

For the susceptible population (Figure 10a), we note a discernible trend: for larger initial infected populations (I_0), the decline in susceptible individuals is more pronounced. This suggests that higher levels of infection exert greater pressure on the susceptible population, leading to a more rapid depletion of susceptible individuals.

In contrast, when examining the removed population (Figure 10c), a contrasting pattern is observed. Here, larger initial infected populations result in a more substantial increase in removed individuals over time. This observation highlights the effectiveness of the control strategy in transitioning infected individuals to the removed category.

When the initial infected population is large, there is a higher probability of interactions between infected and susceptible individuals, resulting in increased transmission of the disease.

Consequently, more individuals become infected over time. However, with the implementation of effective control measures, such as vaccination campaigns, quarantine measures, or other interventions, the transmission dynamics are disrupted.

The impact of varying the initial values of S_o and R_o on the effectiveness of controllability is also investigated. However, it found that regardless of the initial values of S_o, the function I showed no changes. Similarly, variations in the initial values of R_o did not affect the dynamics of the infection. These observations suggest that the controllability of the system remains robust and relatively unaffected by changes in the initial states of susceptible and recovered individuals.

Figure 11 investigates the impact of varying initial values of infected individuals (I_o) in the absence of control measures where $S_o = 10^8$ and $R_o = 0$. Through this analysis, it was observed that without control, there is a substantial increase in the number of removed individuals, indicating the natural progression of the infection. Conversely, when implementing control measures, such as those outlined in figure 10c, the number of infections remains relatively low, resulting in a smaller number of individuals transitioning to the removed category. This clear contrast underscores the effectiveness of the control strategy in mitigating the spread of infection and minimizing the number of individuals affected.

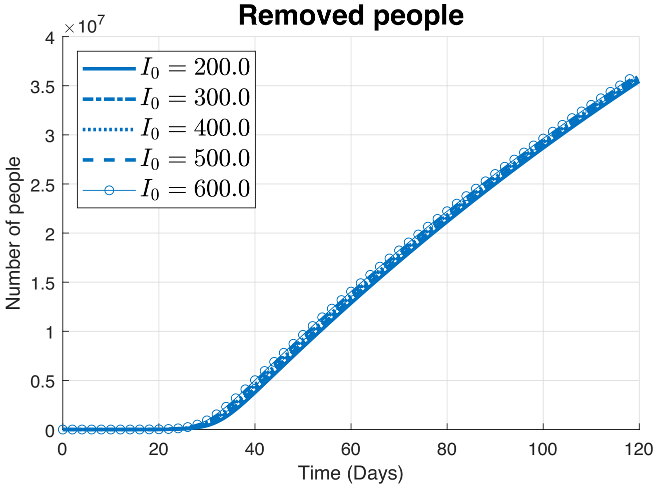

FIGURE 11. **Impact of I_o on removed people without the control.**

Figure 12 illustrates a parameter space analysis of the maximum intensity of the control function *u(t)* across varying combinations of parameters a and ϵ. Each point in the parameter space grid represents a unique combination of parameter values. The color intensity represents the maximum value of the control function achieved for each parameter combination. This analysis provides insights into how changes in parameters a and ϵ influence the effectiveness of the control strategy. This figure illustrates the admissibility the control for a wide range of parameters.

Our proposed control strategy, tailored for the SIR model, offers distinct advantages over existing approaches [22][23][24]. While these papers provide valuable insights into controlling infectious diseases and focus on generic control methods, our proposed control stands out in terms of precision and adaptability.

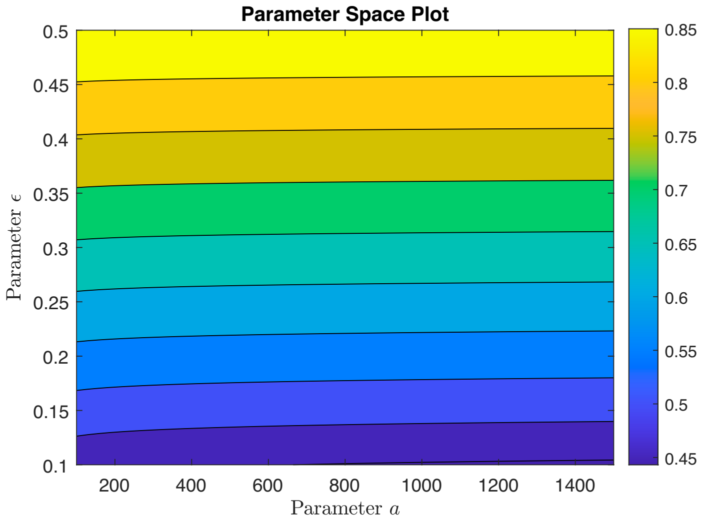

FIGURE 12. **Impact of I_0 on removed people without the control.**

One key advantage of our proposed control is its ability to ensure the total controllability of the number of infections. The infection dynamics can be guided to a desired state from any initial condition, at a desired time. This level of precision is unparalleled and represents a significant advancement in epidemic control strategies. In contrast to the methods discussed in [22][23][24], which rely on Pontryagin's principle to reduce the number of infections, our approach offers greater control over the infection dynamics. While Pontryagin's principle is effective in minimizing infections, it lacks the precision and flexibility inherent in our proposed control strategy.

CONCLUSIONS

This study addresses the formidable challenge of controllability in nonlinear models, with a specific focus on designing a control strategy to manage infection dynamics within the SIR framework. By tackling this complex task, our research contributes significantly to the field of epidemiology, offering policymakers and public health authorities invaluable insights for implementing targeted interventions and resource allocation strategies.

Our novel control law, tailored specifically for SIR models, represents a significant advancement in infectious disease control.

By providing explicit solutions to the model, our approach effectively mitigates the spread of infection and guides the number of infected individuals towards predetermined thresholds at specified times.

This precision in controlling infection dynamics is essential for effective epidemic management and containment efforts. Through comprehensive numerical simulations, the remarkable efficacy of our proposed control law is depicted. The results unequivocally show that our approach enables precise regulation of the pace of infection decline, aligning with predefined targets with remarkable accuracy. For instance, by employing the proposed control function, a gradual decrease in the infection rate is ensured, ultimately leading it towards zero. Moreover, the approach guarantees that the number of infections will dip below a predetermined threshold at a specified time.

This level of precision represents a novel contribution compared to existing studies in the field [22][23][24][25][26], where control functions primarily focus on minimizing the number of infections using Pontryagin's maximum principle.

In [22], the authors presented a model for the transmission dynamics of influenza and considered two optimal control strategies involving preventive measures (such as awareness campaigns, hand washing, using hand sanitizer, and wearing masks) and treatment. These strategies were used to minimize the total number of infected individuals and the associated costs of implementing these controls. The objective function was designed to reduce both the infection rate and the cost of interventions. The optimal control analysis and numerical simulations revealed that these interventions effectively reduced the number of exposed and infected individuals.

Similarly, in [24], within the framework of a basic susceptible-infected-removed (SIR) model, an Erlang distribution for the infectious period was considered, and optimal isolation strategies were explored. The objective functional to be minimized included the cost of isolation efforts per time unit and the sanitary costs due to the incidence of the epidemic outbreak. The simulations demonstrated that the shape of the optimal solutions was influenced by different distributions of the infectious period, the relative weight of the two cost components, and the initial conditions.

These control strategies did not ensure the convergence of the number of infected individuals to zero. Additionally, they did not provide a mechanism for precisely steering the number of infections toward a predetermined threshold at a specific time, as proposed by our control strategy. Our approach not only aims to reduce the number of infections but also ensures that the number of infected individuals reaches a specific target at a designated time, providing a more precise and effective method of controlling the spread of the infection.

During the early stages of the COVID-19 pandemic, many countries implemented stringent control measures, such as closing borders and enforcing lockdowns, to curb the spread of the virus [26]. These measures aimed primarily at reducing the infection rate within a specific time frame, often without considering the significant economic impacts. Such control measures effectively reduced the number of new infections by limiting cross-border movement and preventing the importation of new cases. However, these measures also resulted in considerable economic disruptions, affecting trade, tourism, and overall economic activity.

Our control strategy represents a severe control approach that prioritizes the reduction of infections within a predetermined time frame without any constraints. This strategy is highly effective in significantly reducing the number of infections within the predetermined time T.

However, while the optimal control methods provided by Pontryagin's Maximum Principle are still effective in reducing infections [22][23][24][26], they lack precision in terms of controlling the exact timing and magnitude of infection reduction. The optimal control strategy aims to minimize the infections while simultaneously considering other factors, such as economic costs and social impacts, by incorporating constraints within the objective function. As a result, the optimal control can achieve infection reduction but may not provide precise control over the specific timeframe or the exact number of infections reduced.

This finding highlights the versatility and adaptability of our control strategy, positioning it as a promising tool for epidemic management across diverse settings and scenarios.

AUTHOR CONTRIBUTIONS

O. Z. Conceptualization, formal analysis, writing original draft. S. B. Methodology, formal analysis, and writing review and editing. M. R. Supervision, validation, and writing review and editing.

REFERENCES

[1] J. Klamka, “Controllability of dynamical systems. a survey,” Bull. Pol. Acad. Sci. Tech. Sci., vol. 61, no. 2, pp. 335-342, 2013, doi: http://dx.doi.org/10.2478/bpasts-2013-0031

[2] H. J. Sussmann and V. Jurdjevic, “Controllability of nonlinear systems,” J. Differ. Equ., vol. 12, no. 1, pp. 95-116, 1972, doi: http://dx.doi.org/10.1016/0022-0396(72)90007-1

[3] L.-Z.Wang, R.-Q. Su, Z.-G. Huang, X.Wang, W.-X.Wang, C. Grebogi, and Y.-C. Lai, “A geometrical approach to control and controllability of nonlinear dynamical networks,” Nat. Commun., vol. 7, no. 1, 2016, art. no. 11323, doi: http://dx.doi.org/10.1038/ncomms11323

[4] R. Sakthivel, R. Ganesh, Y. Ren, and S. M. Anthoni, “Approximate controllability of nonlinear fractional dynamical systems,” Commun. Nonlinear Sci. Numer. Simul., vol. 18, no. 12, pp. 3498-3508, 2013, doi: http://dx.doi.org/10.1016/j.cnsns.2013.05.015

[5] K. Beauchard and C. Laurent, “Local controllability of 1d linear and nonlinear schrödinger equations with bilinear control,” J. Math. Pures Appl., vol. 94, no. 5, pp. 520-554, 2010, doi: http://dx.doi.org/10.1016/j.matpur.2010.04.001

[6] X.-L. Ding and J. J. Nieto Roig, “Controllability of nonlinear fractional delay dynamical systems with prescribed controls,” NAMC, vol. 23, no. 1, pp. 1-18, 2018, doi: http://dx.doi.org/10.15388/NA.2018.1.1

[7] O. Zakary, A. Larrache, M. Rachik, and I. Elmouki, “Effect of awareness programs and travel-blocking operations in the control of hiv/aids outbreaks: a multi-domains sir model,” Adv. Differ. Equ., vol. 2016, no. 1, 2016, art. no. 169, doi: http://dx.doi.org/10.1186/s13662-016-0900-9

[8] O. Zakary, S. Bidah, M. Rachik, and H. Ferjouchia, “Mathematical model to estimate and predict the covid-19 infections in morocco: Optimal control strategy,” J. Appl. Math., vol. 2020, pp. 1-13, 2020, doi: http://dx.doi.org/10.1155/2020/9813926

[9] K. O. Kwok, A. Tang, V. W. Wei, W. H. Park, E. K. Yeoh, and S. Riley, “Epidemic models of contact tracing: systematic review of transmission studies of severe acute respiratory syndrome and middle east respiratory syndrome,” Comput. Struct. Biotechnol. J., vol. 17, pp. 186-194, 2019, doi: http://dx.doi.org/10.1016/j.csbj.2019.01.003

[10] M. Moustafa, M. H. Mohd, A. I. Ismail, and F. A. Abdullah, “Dynamical analysis of a fractional-order ecoepidemiological model with disease in prey population,” Adv. Differ. Equ., vol. 2020, 2020, art. no. 48, doi: https://doi.org/10.1186/s13662-020-2522-5

[11] X. Wang, H. Peng, B. Shi, D. Jiang, S. Zhang, and B. Chen, “Optimal vaccination strategy of a constrained time-varying seir epidemic model,” Commun. Nonlinear Sci. Numer. Simul., vol. 67, pp. 37-48, 2019, doi: http://dx.doi.org/10.1016/j.cnsns.2018.07.003

[12] P. C. Jentsch, M. Anand, and C. T. Bauch, “Prioritising covid-19 vaccination in changing social and epidemiological landscapes: a mathematical modelling study,” Lancet Infect. Dis., vol. 21, no. 8, pp. 1097-1106, 2021, doi: http://dx.doi.org/10.1016/S1473-3099(21)00057-8

[13] M. Lhous, O. Zakary, M. Rachik, E. M. Magri, and A. Tridane, “Optimal containment control strategy of the second phase of the covid-19 lockdown in morocco,” Appl. Sci., vol. 10, no. 21, 2020, art. no. 7559, doi: http://dx.doi.org/10.3390/app10217559

[14] Z. Omar, B. Sara, and R. Mostafa, “The impact of staying at home on controlling the spread of covid-19: Strategy of control,” Rev. Mex. Ing. Biomed. vol. 42, no. 1, 2021. https://doi.org/10.17488/rmib.42.1.2

[15] O. Zakary, M. Rachik, and I. Elmouki, “On the analysis of a multi-regions discrete sir epidemic model: an optimal control approach,” Int. J. Dynam. Control, vol. 5, pp. 917-930, 2017, doi: http://dx.doi.org/10.1007/s40435-016-0233-2

[16] Z. Omar, M. Rachik, and I. Elmouki, “A new analysis of infection dynamics: multi-regions discrete epidemic model with an extended optimal control approach,” Int. J. Dynam. Control, vol. 5, pp. 1010-1019, 2017, doi: http://dx.doi.org/10.1007/s40435-016-0264-8

[17] D. Osthus, K. S. Hickmann, P. C. Caragea, D. Higdon, and S. Y. Del Valle, “Forecasting seasonal influenza with a state-space sir model,” Ann. Appl. Stat., vol. 11, no. 1, pp. 202-224, 2017, doi: http://dx.doi.org/10.1214/16-AOAS1000

[18] M. Kröger and R. Schlickeiser, “Analytical solution of the sir-model for the temporal evolution of epidemics. part a: time-independent reproduction factor,” J. Phys. A Math. Theor., vol. 53, 2020, art. no. 505601, doi: http://dx.doi.org/10.1088/1751-8121/abc65d

[19] C. Fraser, S. Riley, R. M. Anderson, and N. M. Ferguson, “Factors that make an infectious disease outbreak controllable,” Proc. Natl. Acad. Sci., vol. 101, no. 16, pp. 6146-6151, 2004, doi: http://dx.doi.org/10.1073/pnas.0307506101

[20] X. Zhao, K. Siegel, M. I.-C. Chen, and A. R. Cook, “Rethinking thresholds for serological evidence of influenza virus infection,” Influenza Other Respir. Viruses, vol. 11, no. 3, pp. 202-210, 2017, doi: http://dx.doi.org/10.1111/irv.12452

[21] F. D. Sahneh, F. N. Chowdhury, and C. M. Scoglio, “On the existence of a threshold for preventive behavioral responses to suppress epidemic spreading,” Sci. Rep., vol. 2, 2012, art. no. 632, doi: http://dx.doi.org/10.1038/srep00632

[22] F. Khondaker, "Optimal control analysis of Influenza epidemic model," App. Math., vol. 13, no. 10, pp. 845-857, 2022, doi: **https://doi.org/10.4236/am.2022.1310053**

[23] D. I. Ketcheson, "Optimal control of an SIR epidemic through finite-time non-pharmaceutical intervention," J. Math. Biol., vol. 83, 2021, art. no. 7, doi: **https://doi.org/10.1007/s00285-021-01628-9**

[24] L. Bolzoni, R. Della Marca, and M. Groppi, "On the optimal control of SIR model with Erlang-distributed infectious period: isolation strategies," J. Math. Biol., vol. 83, 2021, art. no. 36, doi: **https://doi.org/10.1007/s00285-021-01668-1**

[25] E. V. Grigorieva, E. N. Khailov, and A. Korobeinikov. "Optimal control for a SIR epidemic model with nonlinear incidence rate," Math. Model. Nat. Phenom., vol. 11, no. 4, pp. 89-104, 2016, doi: **https://doi.org/10.1051/mmnp/201611407**

[26] Fatmawati, C. W. Chukwu, R. T. Algahtani, C. Alfiniyah, F. F. Herdicho, Tasmi, "A pontryagin's maximum principle and optimal control model with cost-effectiveness analysis of the COVID-19 epidemic," Decis. Anal. J., vol. 8, 2023, art. no. 100273, doi: **https://doi.org/10.1016/j.dajour.2023.100273**